SCUOLA DI DOTTORATO
UNIVERSITÀ DEGLI STUDI DI MILANO-BICOCCA

Department of Biotechnology and Biosciences

PhD program in Translational and Molecular Medicine (DIMET)
Cycle XXXIV

Activatory CRISPR/dCas9 as a therapeutic strategy in Dravet Syndrome

Surname Ricci Name Raffaele

Registration number 849618

Tutore / Tutor: Dr Vania Broccoli

Cotutore / Co-tutor: Dr Gaia Colasante

Coordinatore / Coordinator: Prof Andrea Biondi

ANNO ACCADEMICO / ACADEMIC YEAR 2020/2021

TABLE OF CONTENTS

Acronyms and abbreviations III

CHAPTER 1:

GENERAL INTRODUCTION

1. Excitation and inhibition in the Central Nervous System 1
   - 1.1 Neuronal excitability and voltage-gated Na^+ channels 2
   - 1.2 The cerebral cortex organization and development 8
   - 1.3 Importance of excitatory-inhibitory balance in neural circuits 14
   - 1.4 Epilepsy 16
2. Dravet Syndrome (DS) 19
   - 2.1 Clinical features 20
   - 2.2 *SCN1A* mutations 21
   - 2.3 Mouse models of DS 24
   - 2.4 Current treatments and Gene therapy on DS 26
3. Patient-derived Induced pluripotent stem cells (iPSCs): a new tool to model human pathologies 29
   - 3.1 2D neuronal differentiation 30
   - 3.2 *In vitro* human modelling for neurodevelopmental disorders 34
   - 3.3 Human DS modeling 37

AIM OF THE THESIS 42
References 43

CHAPTER 2:
Human induced pluripotent stem cells differentiation in neuronal subtypes to model Dravet Syndrome 63

CHAPTER 3:
dCas9-based *Scn1a* gene activation restores inhibitory interneuron excitability and attenuates seizures in Dravet Syndrome mice 167

CHAPTER 4:
CRISPR/dCas9 as a Therapeutic Approach for Neurodevelopmental Disorders: Innovations and Limitations Compared to Traditional Strategies (Mini review) 246

CHAPTER 5:
SUMMARY, CONCLUSIONS AND FUTURE PERSPECTIVES 278

Acronyms and abbreviations

AAVs: adeno-associated viruses

AP: action potential

ASOs: antisense oligonucleotides

AIS: axonal initial segment

BDNF: brain-derived neurotrophic factor

BMP: bone morphogenetic protein

CNS: central nervous system

CRISPR: clustered regularly interspaced short palindromic repeats

dbcAMP: dibutyryl cyclic adenosine monophosphate

DS: Dravet Syndrome

EBs: embryoid bodies

EEG: electroencephalogram

ExNs: excitatory neurons

GE: ganglionic eminence

GEFS+: genetic epilepsy with febrile seizure plus

GINs: GABAergic interneurons

ILAE: International League Against Epilepsy

iPSCs: induced pluripotent stem cells

LGE: lateral ganglionic eminence

LV: lentivirus

MGE: medial ganglionic eminence

NGS: next generation sequencing

NMD: nonsense-mediated decay

NPC: neural progenitor cells

PMDS: Phelan–McDermid syndrome

PV: parvalbumin

RTT: Rett syndrome

SHH: Sonic Hedgehog

SMA: spinal muscular atrophy

SMEI: severe myoclonic epilepsy of infancy

SST: somatostatin

SVZ: subventricular zone

TALEN: transcription activator-like effector nuclease

VIP: vasoactive intestinal peptide

VZ: ventricular zone

ZFN: zinc finger nuclease

CHAPTER 1
GENERAL INTRODUCTION

1. Excitation and inhibition in the Central Nervous System

The most important functional component of the central nervous system (CNS) is the brain, and its activity is fundamental to process the information coming from the external environment, and to organize all activities of an organism. It displays a very complex structure which includes a heterogeneous cellular population. Among all cells, the neuronal percentage is the highest. The other cells making up the brain are called glial cells and they can be divided into three groups: astrocytes, which generate blood-brain barrier and support neurons in their activity, in synapse formation, and nutrition; oligodendrocytes, important for neurons' axons myelination; microglia, the immune system component of the brain. The functional units of the brain are neurons, excitable cells specialized in the transmission of electrical signals. Neuronal activity is well organized in circuitries, in which each neuron establishes different contacts with the others. In this manner it is possible to generate responses to all received stimuli. Circuitries which analize similar information can be grouped together, forming three macro-circuits: the sensory system, which processes all stimuli coming from the outside, the associative system, which integrate information, and motor system, fundamental to generate a response to the stimuli.

1.1 Neuronal excitability and voltage-gated Na^+ channels

Neuronal communication is based on transmission of electrical inputs from a neuron to another, thanks to the generation of specific contact points, the synapses, compartments formed by three components, a pre-synaptic neuron, a post-synaptic neuron, and astrocytes (tripartite synapse), which can release gliotransmitters to modulate neurons activity (Halassa, Fellin, and Haydon 2007). It is in this compartment, that pre-synaptic neuron releases a neurotransmitter that can bind its receptor, placed on post-synaptic neuron membrane, inducing its hyper- or de-polarization. This mechanism can involve two kinds of receptors: ionotropics, which are channels themselves, or metabotropics, which interact through G protein with channels regulating their activity. Hundreds of genes encoding for ion channels can be found in the mammalian genome. Channels conduct ions, inside and outside of cells, allowing communication between intra- and extracellular compartments maintaining internal homeostasis, and playing an important role in the signal transduction. Among all channels several categories can be distinguished basing on their specific capability to be permeable to different ions, Na^+, K^+, Ca^{2+}, Cl^-, and their structure is strictly associated with their mechanisms of action.

Voltage-gated ion channels are among the most important ion channels in neurons. This category of channels, which mainly includes sodium (Na_v) and potassium (K_v) channels, can open or close in response to local changes in membrane potential,

allowing to the cell to respond to different inputs and to generate currents through the membrane. The entry of cations or the exit of anions can induce depolarization of membrane potential, while the exit of positive ions or the entry of negative ions induces hyperpolarization.

Considering the relevance of Na_V channels for neuronal activity, several studies have been conducted on these proteins. The first studies date back to 1952, when Hodgkin and Huxley, performed the first experiments to record Na^+ currents, using voltage clamp, and discovering for the first time some properties of these channels, like their voltage-dependent activation, rapid inactivation and their specific conductance for Na^+ ions (Hodgkin and Huxley 1952). Only in 1980, through the usage of several biochemical approaches, the Na^+ channel protein was isolated (William A. Catterall 1980). Later other purification studies helped to identify more in detail Na^+ channel structure from mammalian brain: a complex formed by an α subunit (260 kDa), associated with four auxiliary β subunits (33-36 kDa) (William A. Catterall 2000). Finally, once cDNA encoding for the entire channel was isolated, Noda and colleagues (Noda et al. 1984) deduced its amino acids sequence. The protein was discovered to comprise four internally homologous domains formed by α-helical transmembrane segments (Figure 1).

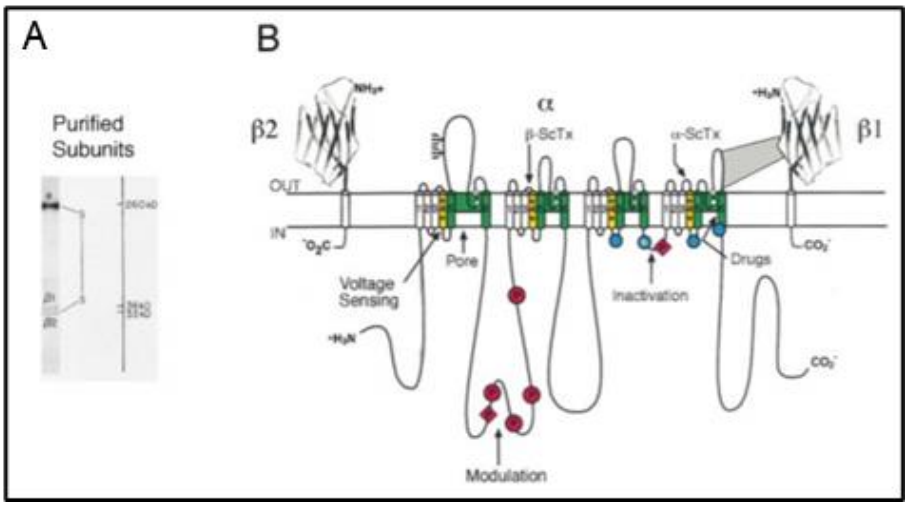

Figure 1. Subunit Structure of the Voltage-Gated Sodium Channels. (A) Sodium channel purified from rat brain showing the α, β1, and β2 subunits and their molecular weights. (B) The primary structures of the subunits of the voltage-gated ion channels (adapted from Catterall 2000).

Subsequently, α-subunit sodium channel cDNA was extracted from rat brain and expressed in Xenopus oocytes, to study its functionality (Goldin et al. 1986; Noda et al. 1986). It was also demonstrated that β subunits were essential for the kinetics and voltage dependence of gating (A. L. L. Isom et al. 1992; L. L. Isom et al. 1995). Sodium channel molecular modeling led to a more detailed 2D folding pattern of the α-subunit: each homologous domain contains six α-helical transmembrane segments (S1-6) and a further loop dipped into the transmembrane region between S5 and S6 forming the outer pore. Also, other loops were reported in this predicted structure

controlling channel activity, one localized outside the cell between S5 and S6, and the others inside the cell at the N-term, C-term, and connecting all homologous domains (Costa and Catterall 1984; Eaholtz, Scheuer, and Catterall 1994).

Later, studying different point mutations, and using pore blockers tetrodotoxin and saxitoxin, it was possible to identify some amino acids, in the membrane-reentrant loop (domain I), as essential for tetrodotoxin binding or to generate outer and inner rings, important for ion selectivity filter (William A. Catterall 2000).

S4 segments of all homologous domains were reported to be enriched in positively charged amino acids and for this reason they have been soon hypothesised to be associated with the voltage dependence activation of the channel. Considering the negative internal electrical field, and the negatively charged amino acids in adjacent transmembrane segments, which can create ion pairs with S4 positive amino acids, the S4 segments in basal condition, were thought to be placed inward to close the pore. When cell depolarization occurs, this balance can be interrupted, and the S4 segments can move outward, inducing conformational changes opening the pore of the channel (Figure 2). This hypothetical mechanism known as sliding helix (W. A. Catterall 1986) or helical screw (Guy and Seetharamulu 1986) model, was confirmed later with the first mutagenesis studies of sodium channels, in which neutralization of the positively charged amino acids in S4 segments was found to alter the

voltage-dependent gating, shifting the voltage dependence to higher values (Stühmer et al. 1989).

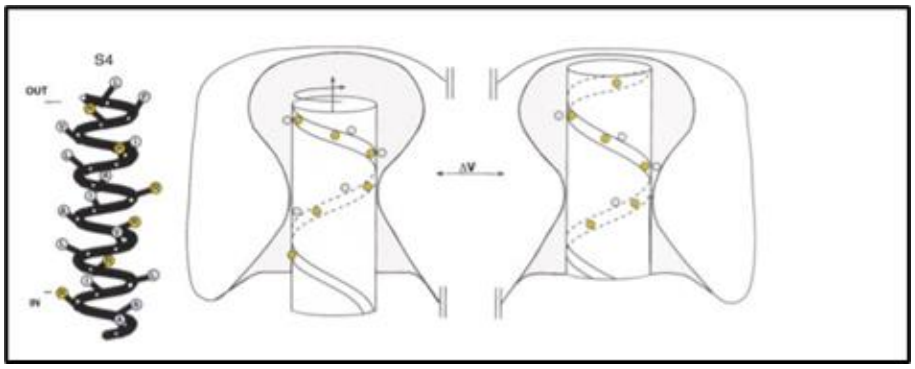

Figure 2. Voltage-Dependent Activation by Outward Movement of the S4 Voltage Sensors. The S4 segment in a single domain is illustrated as a rigid cylinder within a channel with a narrow. Upon depolarization, the segment moves outward and rotates to place the positively charged residues in more outward positions but is still neutralized by interactions with negative residues in the transmembrane part of the protein (adapted from Catterall 2000).

Mammals can express nine different voltage gated Na^+ channels α subunits, which can be distinguished for tissue expression and biophysical properties. $Na_v1.1$, $Na_v1.2$, $Na_v1.3$ and $Na_v1.6$ (encoded by the *SCN1A*, *SCN2A*, *SCN3A* and *SCN8A* gene, respectively), are the most important Na^+ channel subtypes expressed in the CNS. Considering their fundamental function in generating action potential (AP), they accumulate at high density in the axonal initial segment (AIS), which is the first tract of axons in which APs arise (Leterrier 2018). Inside this sub-structure

$Na_v1.1$, $Na_v1.2$ and $Na_v1.6$ isoforms, can occupy different places depending on the stage of development and the different cellular subtypes. In particular, $Na_v1.1$ and $Na_v1.2$ channels are fundamental for the generation of both somatodendritic and axonal APs (Hu et al. 2009; William A. Catterall, Kalume, and Oakley 2010).

On the other hand, also K_v channels play a very important role in neuronal activity.

K_v channels are encoded by 40 genes and are divided into 12 subfamilies. Similarly to Na_v channels, they are formed by four α-subunits each one containing six transmembrane α-helical segments, S1-S6, and an internal P-loop, all organized circumferentially around a central pore (Wulff, Castle, and Pardo 2009). The S1-S4 segments act as voltage sensor domain and can close the pore by pulling on the S4-S5 linker (Swartz 2004; Bezanilla 2008a; 2008b). Fundamental for K_v channels is the interaction between α and β subunits, given that β subunits can modify the gating of the channel. Furthermore, even other modifications can change channel properties, as phosphorylation, dephosphorylation, ubiquitylation, sumoylation and palmitoylation.

Considering the concentration gradient of K^+ across the cell membrane, K_v channels main activity results in an efflux of cations, with the aim to repolarize or hyperpolarize the membrane. Indeed, when AP arises, Na_v channels open for a short period, letting Na^+ ions to enter inside the cell, to allow

depolarization; after that, Na_v channels undergo inactivation and in a short while, K_v channels activated and remain open for a longer period letting the cell to repolarize.

Among all Kv channels, $K_v1.1$, $K_v1.2$ and $K_v2.1$ are fundamental in controlling neuronal excitability, indeed, knockout mice for genes encoding these channels, *Kcna1*, *Kcna2 and Kcnb1*, display seizures (Smart et al. 1998; Brew et al. 2007; Speca et al. 2008). Also in humans, loss of function mutations on *KCNA1* have been linked to partial seizures, episodic ataxia and myokymia disorders (Zuberi et al. 1999). Furthermore, the activation range and fast deactivation kinetics of K_v3 channels help neurons to fire repetitively at high frequencies (Wulff, Castle, and Pardo 2009), fundamental prerogative belonging to those neurons called “fast-spiking”, as parvalbumin (PV) interneurons, which can fire AP up to 1000 Hz, playing key roles in vital functions such as sound location, motor coordination and cognition.

1.2 The cerebral cortex organization and development

The cerebral cortex is one of the most important regions of the brain. It is composed by numerous folds which allow it to reach a surface area of 250.000 mm^2, all contained into the skull. Among neurons forming cortex it is possible to distinguish two major subpopulations: excitatory, or projection, neurons, which can be distinguished for the capability to release glutamate, and to display long axons that can reach distant targets, both

intracortical and sub-cerebral; inhibitory interneurons, which establish local connections with modulatory function, by using the neurotransmitter gamma-aminobutyric acid (GABA).

During development, in different region of the brain, excitatory and inhibitory neurons are generated. After the generation, they migrate and organize in different layers, giving the cerebral cortex a characteristic laminar structure. The mechanisms regulating these processes are very complex and based on the activity of several signaling centers which secrete diffusible molecules that form overlapping gradients and act as morphogens (Hoch et al. 2009). Different members of the Wnt and bone morphogenetic proteins (BMP) families are secreted from medial and caudal regions of the cortex (Hoch et al. 2009). These extracellular factors can induce a regionalization of the progenitor cells by leading them to activate the expression of homeodomain and helix–loop–helix transcription factors, which are subsequently refined by cross-repressive interactions. In this manner, the telencephalic vesicles could be divided into a dorsal or pallial and a ventral or subpallial region (Campbell 2003). These patterning transcription factors, in turn, induce another group of transcription factors defining progenitor identities and contributing to the selection of specific neuronal phenotypes (Figure 3) (Guillemot 2005; Hoch et al. 2009).

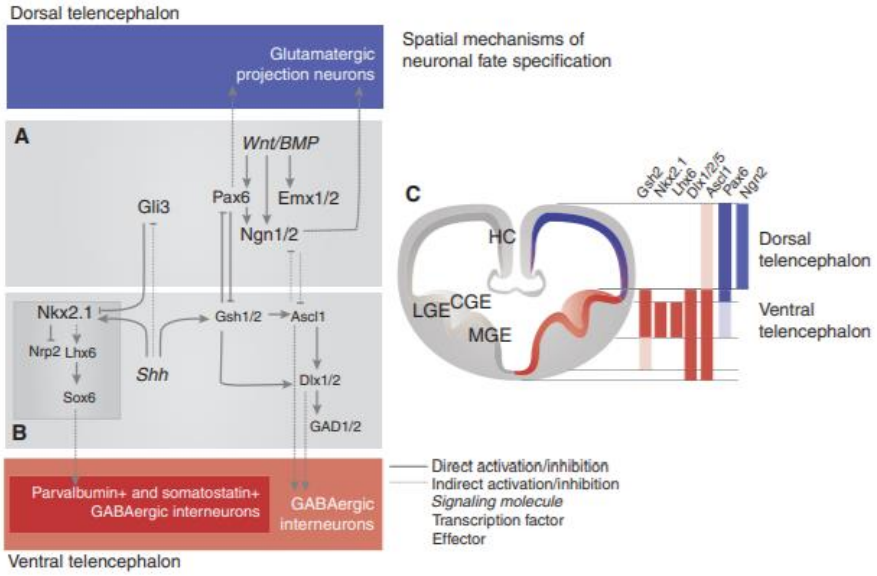

Figure 3. Spatial mechanisms of neuronal fate specification. (A) BMP and Wnt signals, diffusing from the dorsal midline of the telencephalon, induce expression of important transcriptional regulators of dorsal telencephalic fates (Emx1/2, Pax6, Ngn1/2). Pax6 and Ngn1/2 promote glutamatergic neuron generation. (B) The morphogen Sonic Hedgehog (Shh) secreted by the ventral midline of the telencephalon, represses Gli3 and induces the expression of ventral transcriptional factors, as Nkx2.1 and Gsh1/2. Gsh1/2 induce expression of the pro-neural gene Ascl1, which activate Dlx1/2 promoting GABAergic interneurons (GINs) generation. Nkx2.1, through induction of Lhx6 and Sox6, further specifies subpopulations of cortical interneurons defined by the expression of PV and somatostatin (SST). (C) Dorsally or ventrally restricted expression of transcriptional factors is established by cross-repression (shown in A and B) (adapted from (Martynoga, Drechsel, and Guillemot 2012)).

On the other hand, Shh establishes ventral identities in the telencephalon (Rallu et al. 2002) by inhibiting the Gli3 dorsalising factor and inducing the expression of the homeodomain proteins Gsh1 and Gsh2 in the entire ventral telencephalon and Nkx2.1 in the medial part of the ventral telencephalon (Rallu et al. 2002). Then, Nkx2.1 and Gsh1/2 can work independently by inducing the expression of other transcriptional factors, including the LIM homeobox protein Lhx6 by Nkx2.1, and of Ascl1, Dlx1 and Dlx2 by Gsh1/2 (Toresson et al. 2000; Du et al. 2008; Wang et al. 2009). Furthermore, Ascl1 and Dlx1/2, are essential to initiate the neuronal differentiation of ventral telencephalic progenitors (Casarosa et al. 1999; Yun et al. 2002; Long et al. 2009).

Concurrently, Wnt acts in a similar way in the dorsal telencephalon, inducing the expression of Pax6 and the pro-neural proteins Ngn1, while Pax6 forces the expression of Ngn2, (Gunhaga et al. 2003; Scardigli et al. 2003; Hirabayashi et al. 2004). Thanks to the activity of Ngn1/2 and Pax6 neurogenesis can occur in the cerebral cortex (Nieto et al. 2001; Heins et al. 2002; Schuurmans et al. 2004).

Furthermore, as demonstration that the dorsal and ventral transcriptional cascades are mutually repressive, deletion of dorsal transcription factors, leads to expansion of ventral morphogens into the pallial region, and vice versa. So, Gli3 represses Shh target genes and Pax6 represses Gsh2, while Ngn1/2 repress Ascl1 (Figure 2) (Fode et al. 2000; Toresson et al. 2000; Rallu et al. 2002).

Furthermore, it is important to mention that the dorsal pro-neural factors Ngn1 and Ngn2 and the ventral Ascl1, display two distinct roles in the generation of neurons from neural progenitors (Bertrand et al. 2002). Firstly, they activate neurogenesis, by forcing the exit from the cell cycle, selecting the neuronal respect to the astroglial fate, initiating the migration of the new neurons to their locations, and inducing the growth of axon and dendrites to allow the terminal differentiation of the neurons. Secondly, they specify the morphology and the regional identity of the new neurons, together with the neurotransmitter they will have to use to communicate with other neurons. In particular, Ngn1/2 induces the glutamatergic and pyramidal neurons generation, while Ascl1 specifically promotes the GINs generation (Fode et al. 2000; Parras et al. 2002; Hand et al. 2005).

Hence, following the different morphogens concentrations along the dorso-ventral and antero-posterior axis, boundaries between specific progenitor zones are generated (Wilson and Rubenstein 2000; Marín and Rubenstein 2003). Once cell specification has been concluded, cells are ready for migration. Two types of neural progenitor cells (NPCs) migration have been reported into the brain: radial migration, which interests excitatory neurons (ExNs) progenitors, characterized by a movement from ventricular zone to cortical plate, with the help of radial glial cells, and tangential migration, which provides inhibitory neurons progenitors movement orthogonally to the direction of radial migration, from lateral (LGE) and medial ganglionic eminences

(MGE) to the cortex layers (Figure 4) (Marín and Rubenstein 2003).

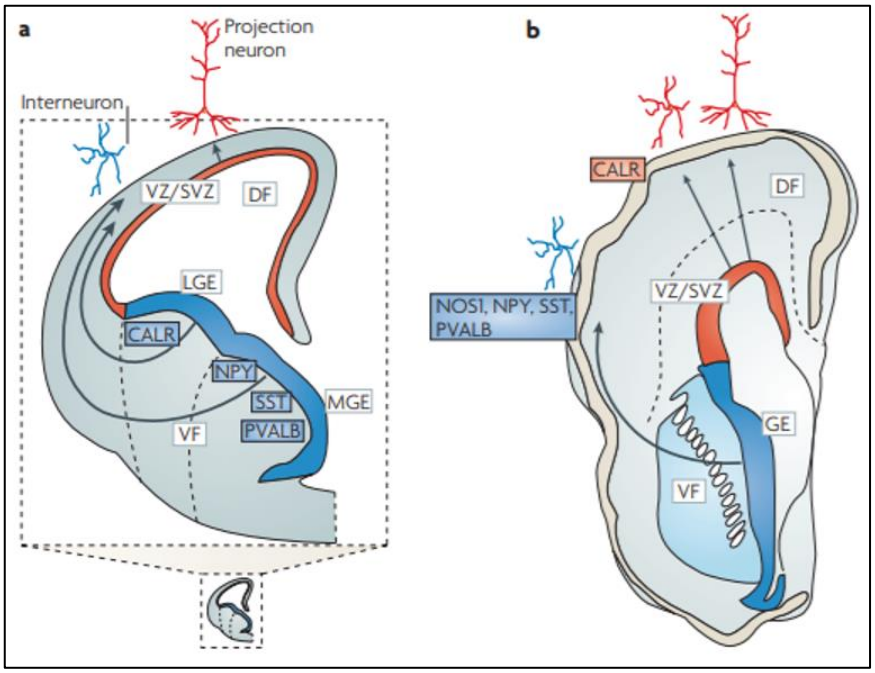

Figure 4. Rodent and human fetal forebrains during corticogenesis. Cross sections of half of a rodent (A) and a human fetal forebrain (B). In rodents, interneurons generate mainly from ganglionic eminence (GE), while in humans originate both in the GE as well as locally in the ventricular and subventricular zones (VZ/SVZ) of the dorsal telencephalon (adapted from (Rakic 2009)).

At the end of the migration, in the early fetal stage, GINs start to contact ExNs forming synapses to regulate their activity and generate the first neuronal circuits. This phenomenon will continue during all life displaying plasticity, considering that some

circuits could be re-adapted or pruned even after long time from the generation (Kostović and Judaš 2015).

1.3 Importance of excitatory-inhibitory balance in neural circuits

Each neuron has the possibility to establish numerous connections with other neurons, forming complex neural networks or circuits. Four types of functional microcircuits can be recognized in the cortex considering the type of interaction between excitatory and inhibitory neurons: local excitatory circuits, anterograde and retrograde inhibitory circuits (Figure 5) and counter-inhibitory circuits (Isaacson and Scanziani 2011). The functionality of these circuits always depends on the activity of both excitatory and inhibitory neurons.

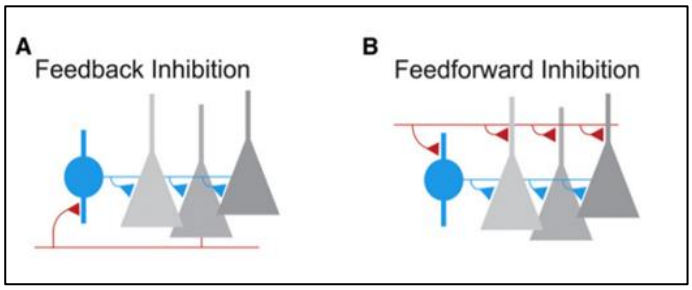

Figure 5. (A) Feedback and (B) feedforward circuits are fundamental building blocks of cortical inhibition (adapted from Isaacson and Scanzani 2011).

Afferent excitatory inputs diffuse in the superficial and deep layers of the cortex through principal neurons, but this process is always controlled by the anterograde (or feedforward) inhibitory circuit, mainly mediated by PV+ fast-spiking interneurons. It is clear that principal neurons also innervate PV+ interneurons, generating a powerful inhibition of neuronal networks, that however is delayed compared to the excitatory stimulus.

The retrograde (or feedback) inhibitory circuit is always mediated by Martinotti cells. They receive synapses mostly from layer V pyramidal neurons and thanks to their ascending axons reaching the layer I, they could establish inhibitory synapses on the dendrites of the same pyramidal neurons that have stimulated them, establishing a feedback mechanism. Hence, inhibition generated is proportional to incoming excitation. Therefore, Martinotti cells activity is essential to limit excessive activation of cortical circuits, preventing the development of epileptic seizures.

Finally, the counter-inhibitory circuit is characterized by local connections between inhibitory neurons, with the aim of disinhibiting downstream excitatory neurons.

Through these types of interactions, increases in excitation are always followed by increases in inhibition (Haider et al. 2006; Okun and Lampl 2008; Atallah and Scanziani 2009). Furthermore, alterations in inhibition/excitation mechanisms or in their relationship can shift cortical activity to a hyperexcitable (epileptiform) or silent (comatose) state (Dudek and Sutula 2007). As response to the alteration, compensatory effects can

occur to preserve the normal excitability of cortical networks (Turrigiano 2011).

1.4 Epilepsy

Epilepsies are heterogeneous neurological disorders characterized by recurrent seizures and related cognitive, psychological, and social impairments (Devinsky et al. 2018). Epileptic patients can also develop different comorbidities as learning difficulties and psychiatric disorders (depression or autism spectrum disorder). With a prevalence of 6.4 cases per 1.000 persons and an annual incidence of 67.8 cases per 100,000 person-years, around 65 million people worldwide are affected by epilepsy, and present stress of living with a continuous fear to have an unpredictable seizure, that can lead to loss of autonomy for all daily activities. Epilepsy can also lead to death for a direct effect of seizures (sudden unexpected death in epilepsy, status epilepticus, motor vehicle accidents, falls, etc) or for indirect effect (aspiration pneumonia, suicide, adverse effects of drugs, etc)(Devinsky et al. 2018).

In 2005, the International League Against Epilepsy (ILAE) defined a seizure as “a transient occurrence of signs and/or symptoms due to abnormal excessive or synchronous neuronal activity in the brain” (Fisher et al. 2005).

The onset of a seizure can be focal (localized precisely in one or more brain regions, “seizure focus”), generalized (with

widespread distribution in the brain), or of unknown onset. A focal seizure is characterized by symptoms related to the region affected in the brain. Instead, among generalized seizures, there are motor (tonic-clonic, tonic, clonic-myoclonic and atonic seizures) and non-motor seizures.

The generation of a seizure, ictogenesis, can be detected and recorded using neurophysiology tools and electrodes that can measure the activity of one specific neuron, or the activity related to multiple neurons. This neuronal activity can be studied by combining electrophysiology and functional or molecular imaging with optogenetics (Devinsky et al. 2018). Ictogenesis can be a response to a distortion of the normal balance between excitation and inhibition in the brain (Stafstrom and Carmant 2016). This imbalance can be the consequence of an alteration affecting brain functions at many levels, from intracellular signaling cascades to neuronal circuits. Although in most cases the cause of this disease cannot be defined, epileptogenesis can be related to different insults altered brain functions, like infectious diseases, autoimmune diseases, structural or metabolic alterations, and genetic mutations. Genetic epilepsies can include patients showing abnormal synaptic connectivity in cortical dysplasia, patients presenting mutations on genes encoding for specific neurotransmitters receptors or, the most diffused, patients with mutations on genes encoding for ion channels, which provide alteration related to their functionality.

Only in some cases patients can use the surgery to cure the pathology. For the rest of them, different anti-seizure drugs are available, even if not always they work properly. For these reasons, lots of patients are looking for neurostimulation devices, dietary therapies, or clinical trials of new drugs as alternative options.

Patients presenting suspected epilepsy should perform periodic electroencephalography (EEG), to classify seizure types and epilepsy syndromes, where the term “epilepsy syndrome” refers to specific clinical characteristics according to the type of seizures, age of onset, EEG findings, genetics, prognosis, and response to antiepileptic drugs. Basing on all these information, different epileptic syndromes have been recognized, and Dravet Syndrome is one of them.

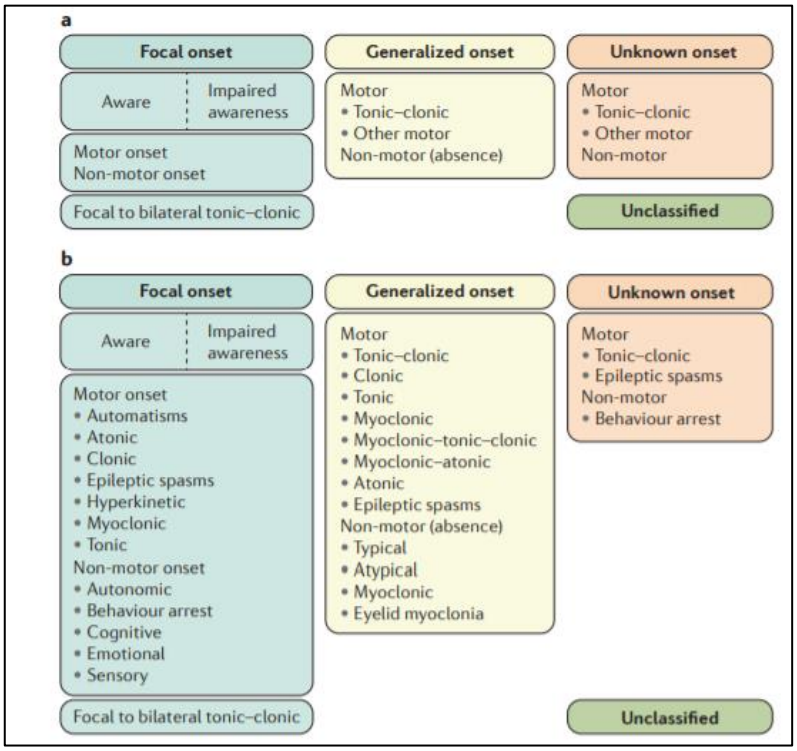

Table 1. Seizure classification. (A) Basic seizure classification, according to the International League Against Epilepsy 2017, for practitioners not specializing in epilepsy, and (B) the expanded classification for clinicians (Adapted from Devinsky et al. 2018).

2. Dravet Syndrome

Dravet syndrome (DS), also known as severe myoclonic epilepsy of infancy (SMEI), has been firstly described by Charlotte Dravet in 1978 (Dravet 1978) and recognized by the International League Against Epilepsy as a syndrome in 1989. It is a rare, early-onset epilepsy syndrome characterized by refractory

epilepsy and neurodevelopmental problems beginning in infancy. With an incidence between 1 in 16,000 to 1 in 40,000 live births, DS can affect males and females in equal proportions.

2.1 Clinical features

It is possible to distinguish three different stages in the course of epilepsy, starting with the “febrile stage” (Dravet and Oguni 2013). Clinical manifestations appear in the first year of life, when apparently normal babies face up to one convulsive seizure with variable duration (often longer than 15 minutes), related or not to fever, which starts as clonic seizure becoming later hemiclonic (affecting one entire side) or generalized. This seizure can be a focal, motor seizure, or a burst of myoclonic jerks, often hard to recognize as epileptic, considering that even EEG is usually normal, though subsequently, the seizure can evolve in status epilepticus. Later, other repeated seizures occur, febrile or not, most often of a hemiclonic nature. Despite the usage of Rectal diazepam affected babies are frequently hospitalized.

The second stage of DS epilepsy is the “worsening stage”, and it appears in the period between 1 and 4 years (Dravet and Oguni 2013). It is characterized by brief myoclonic seizures, atypical absences, and focal seizures. From this stage, patients start to develop crises more easily and frequently as a response to external and internal stimuli, as fever, emotional stress, excitement, and contrasting lights. Furthermore, other symptoms start to appear affecting psychomotor development, language,

fine and gross motor skills, together with attention disturbances, hyperactivity, and sometimes autistic features. Generally, in scholar age, the “stabilization stage” begins. In the following period convulsive seizures decrease, occurring mainly in sleep, myoclonias and absences can disappear, and focal seizures persist or decrease. Even if there can be an improvement in the behaviour and psychomotor development, cognitive impairment persists.

2.2 *SCN1A* mutations

In the past, given the low incidence of epileptic encephalopathies in the population, it wasn’t easy to study the genetic component of these pathologies, but with the introduction of next-generation sequencing (NGS), lots of genes involved in epilepsy have been identified (Helbig and Abou Tayoun 2016). *SCN1A* represents an exception: the connection between this gene and epileptic syndromes was reported before NGS introduction, in early 2001 (Claes et al. 2001). Mutations on *SCN1A* gene were first discovered by screening patients with inherited epilepsy, presenting mild phenotypes of genetic epilepsy with febrile

seizure plus (GEFS+), but later they were also associated with severe infant-onset epilepsy syndromes, as DS.

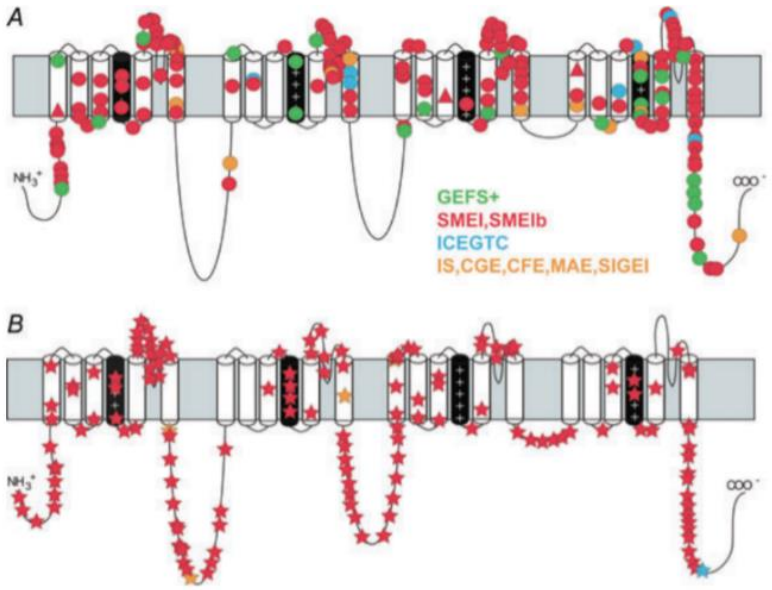

Figure 6. $Na_V1.1$ channel mutations in patients with epilepsy. A) missense mutations (circles) and in-frame deletions (triangles). B) truncation mutations (stars). (adapted from Catterall et al. 2010)

Over 80% of DS patients present causing epilepsy mutations on *SCN1A* gene in heterozygous condition, and through patients *SCN1A* gene analysis, more than 1000 variants of $Na_V1.1$ protein have been identified (https://www.scn1a.net/). Most mutations are de novo, although familial missense mutations occur in 5–10% of cases.

They can be located along all the gene, and they can be classified into three groups:

- truncating mutations (40%), which led to the generation of premature stop codons or deletions;

- missense mutations (40%), localized especially in the transmembrane segments, which severely impair channel function;

- splicing-site changes (20%) (Marini et al. 2011).

Furthermore, even if a high percentage of DS *SCN1A* mutations are placed in coding exons, a recent study demonstrates that non-coding regions, near *SCN1A*, may also contribute to disease in some patients. A recent study found that intron 20 region was very enriched for rare, deleterious variations causing developmental epileptic encephalopathies (Carvill et al. 2018). By studying the mechanism by which these variants might cause epilepsy, the authors of this work found that the insertion of this "poison" exon, also defined 20N (N = nonsense), in *SCN1A* transcript, can cause epilepsy by reducing the total amount of $Na_v1.1$ channel protein, as a result of the activation of nonsense-meditated decay (NMD) mechanism, which eliminate all "poisoned" transcripts.

Summing up, even if in some cases gain-of-function effects have been reported (Lossin et al. 2003; Ohmori et al. 2006; Volkers et al. 2011), loss of function is the main effect of *SCN1A* mutations, demonstrating that haploinsufficiency of *SCN1A* is pathogenic,

and most of them cause a reduction in the amount of Na^+ current (Ragsdale 2008). Considering that Na^+ channels are known to be essential for AP generation in neurons, as mentioned above, a reduction in the Na^+ current is expected to lead to an hypoexcitable condition rather than hyperexcitable one, as happens in epilepsy. The generation and the characterization of the first animal models of DS helped to clarify the mechanisms underlying hyperexcitability and co-morbidities occurring in SMEI, (F. H. Yu et al. 2006; Ogiwara et al. 2007).

2.3 Mouse models of DS

The first DS mouse model was created by Dr. Catterall group in 2006 (F. H. Yu et al. 2006). Ablation of *Scn1a* gene was obtained by inserting a deletion in exon 26, the last coding exon. The authors of this work reported that the null mutation of *Scn1a* leads to death within the second week of life, while in heterozygotes, which genetically mimic human SMEI, they described an epileptic phenotype. In 2007, Yamakawa group generated another DS mouse model carrying a truncating mutation on *Scn1a* gene exon 21, identical to the human SMEI mutation (R1407X) (Ogiwara et al. 2007). By using this model, they stated that $Na_v1.1$ is mainly expressed in the AIS of PV+ inhibitory interneurons, which regulate the firing of pyramidal neurons and are essential for inhibitory function in the brain. Later, other publications reported the involvement of other subpopulations of GINs in DS, like SST and vasoactive intestinal

peptide(VIP)+ interneurons (Tai et al. 2014; Goff and Goldberg 2019). All these works reported a reduction in Na^+ current density of this class of neurons, together with a reduction of APs number, frequency, and amplitude (F. H. Yu et al. 2006; Ogiwara et al. 2007). However, the threshold for the generation of the single AP was never affected, suggesting $Na_v1.1$ channel is important just to sustain trains of APs and not for the setting of the threshold (F. H. Yu et al. 2006; Ogiwara et al. 2007).

Other studies also suggested that dysfunction of excitatory neurons is also involved in Dravet pathogenesis. Specifically, a first work came out reporting hyperexcitability of pyramidal neurons in DS mice (Mistry et al. 2014), and more recently Almog and colleagues, focusing on the evoked synaptic activity of the CA1 hippocampal microcircuit, observed alteration of both inhibitory and pyramidal neurons (Almog et al. 2021). They revealed disfunctions of GINs in all different stages of DS, with the greatest dysfunction observed during the severe stage of epilepsy, and hyperexcitability in pyramidal neurons at the pre-epileptic stage, followed by a reduction in their activity at the onset of seizures.

However, specific deletion of *Scn1a* in GINs generated a more severe epileptic phenotype compared to deletion in both excitatory and inhibitory cells, suggesting that loss of *Scn1a* in pyramidal cells could be partially protective (Ogiwara et al. 2013).

Altogether these data suggest the presence of complex and reciprocal alterations in neuronal function of both inhibitory and

excitatory neurons, but the failure of excitability of GINs seems to determine a lack of inhibitory tone in the network, leading to an imbalance between excitation and inhibition in the brain, which can be considered as a possible cause for this intractable epilepsy syndrome.

DS mouse models also exhibit various behavioural manifestations including hyperactivity, anxiety, motor coordination, balance impairments, and moreover, impairment in spatial learning and memory consolidations (F. H. Yu et al. 2006; Ito et al. 2013; Griffin et al. 2018).

The whole phenotypical characterization of DS mouse models points out they are a valuable model of the disease, not only to dissect the pathological mechanisms, but also to test different therapeutical strategies. If therapies proved to effectively suppress seizures in *Scn1a* mutant mice, they would hold a strong value for clinical translation.

2.2 Current treatments and Gene therapy in DS

DS is one of the most pharmacoresistant epilepsy syndromes. Among all drugs used until now Valproate is the first to be mentioned, usually taken to prevent the recurrence of febrile seizures, while oral/nasal/rectal benzodiazepine is used for any long-lasting seizures, but these agents are most often insufficient (Chiron and Dulac 2011). Stiripentol is the only compound that proved its efficacy in DS, acting as a direct allosteric modulator

of the $GABA_A$ receptor, enhancing inhibitory neurotransmission (Chiron and Dulac 2011). However, even if in some cases stiripentol can relieve symptoms, it is not resolutive for all patients and indeed, about 41% of patients reported a symptomatic worsening with significative increase in the frequency of status epilepticus (Chiron and Dulac 2011; Myers et al. 2018).

For this reason, the research is recently focused on gene therapy as an approach to treat pathologies that remained resistant to pharmacological agents. In particular, in DS, considering the haploinsufficiency condition, two different approaches are being explored: supplying an extra healthy copy of *Scn1a* gene to the cells or boosting the expression of the healthy copy *Scn1a* gene.

In both cases, the first relevant problem to face is the gene delivery. Different types of viral vectors have been used in literature and each vector presents advantages and disadvantages. Among all viral vectors, the most characterized and used for targeting the CNS have been derived from retroviruses, adenoviruses, adeno-associated viruses (AAVs), and herpes simplex viruses (Ingusci et al. 2019). All these vectors present different capacities, cell tropism, and ability to integrate into the host genome. AAVs are small, non-enveloped, single-stranded DNA viruses; they are clinically safe and effective in transducing both dividing and quiescent cells, establishing a long-term transgene expression. For all these reasons many clinical trials for the treatment of genetic diseases

employ AAV vectors, obtaining a good safety profile and significant clinical benefit.

Systemic infusion of therapeutic AAVs has been already employed in spinal muscular atrophy (SMA) type 1 patients, to restore the normal level of SMN protein in motor neurons preventing neuronal death (Mendell et al. 2017). Nevertheless, *Scn1a* coding sequence is nearly 6 kb long, much more with respect to SMN1. It exceeds the strict cargo capacity for AAVs, and even if lentiviral vectors (LV), which present high capacity with respect to AAVs, can carry the entire sequence of *Scn1a*, they show limited spread in neural tissue, and for this reason, they are not ideal to treat pathologies affecting large brain area. Considering these focal points, the boosting strategy has been largely used for trying to treat DS.

The first approach has been developed by OPKO Health company. They identified a novel, evolutionarily conserved mechanism controlling the expression of *SCN1A* that is mediated by a long non-coding RNA (SCN1ANAT) (Hsiao et al. 2016). Using oligonucleotide-based compounds (AntagoNATs) targeting SCN1ANAT they induce specific upregulation of *SCN1A* both *in vitro* and *in vivo*, in DS mice and non-human primates. This upregulation led, *in vivo*, to significant improvements in seizure phenotype and excitability of hippocampal interneurons.

Stoke therapeutics developed another strategy to upregulate *SCN1A* expression, known as, targeted augmentation of nuclear

gene output, TANGO (Han et al. 2020). This approach targets transcripts which include the 20N poison exon. Targeting the splicing acceptor of the poison exon, by an antisense oligonucleotides (ASOs), they prevent its incorporation in the final mRNA thus enhancing the generation of a productive mRNA, at the expense of non-productive one. The final result is *SCN1A* gene upregulation, that given the conservation of this post transcriptional control (Carvill et al. 2018), can be achieved in both human cells and mouse brain, reducing the incidence of electrographic seizures and SUDEP.

3. Induced pluripotent stem cells (iPSCs): a new tool to model human pathologies

Conventional disease modeling studies, using animal model, have been consistently used to study disease pathology and therapeutic development but these systems always reported many limitations. Indeed, although different animal models exist, and have given a great contribution in understanding lots of aspects of neurodevelopment, they lack human-specific features essential in human corticogenesis (Florio et al. 2015; Pollen et al. 2015; Nowakowski et al. 2017). Humans present a higher brain to body ratio, higher number of neurons, and human brain develops during a longer gestational period, reaching a higher level of complexity. For this reason, a big step forward came when, years ago, in 2007, by introducing a cocktail of different trascriptional factors (Oct3/4, Sox2, c-Myc, Klf4) into somatic

cells, Dr Yamanaka and Dr Thomson, obtained mouse and then human iPSCs, which recapitulate features of embryonic stem cells (Takahashi et al. 2007; J. Yu et al. 2007), bypassing ethical concerns associated to the experimental use of human embryonic cells. iPSCs can be derived directly from patients with genetic or non-genetic diseases, and by differentiating them in specific cell types it is possible to model *in vitro* that disease, and have an access to the relationship between genotype and cellular phenotype (Gottesman and Gould 2003). This aspect is particularly relevant for diseases affecting the nervous system, given the impossibility to access primary human neurons from patients.

3.1 2D neuronal differentiation

Neuronal differentiation of iPSCs *in vitro* is always based on the use of specific factors that can promote or inhibit specific signaling pathways recapitulating embryonic development. Different methods have been published to guarantee high percentage of neurons, but what is more challenging is to obtain pure populations of specific subtypes of mature neurons. To date, by using different small molecules and/or different transcriptional factors, expressed by viral vectors, it is possible to generate a wide variety of neuronal cell types from iPSCs, including forebrain glutamatergic neurons (Zhang et al. 2013; Qi et al. 2017), GINs (Maroof et al. 2013; Nicholas et al. 2013; Colasante et al. 2015; Yang et al. 2017; Meganathan et al. 2017)

serotonergic neurons (Lu et al. 2016; Vadodaria et al. 2019) dopaminergic neurons (Kriks et al. 2012; Theka et al. 2013), motorneurons (Bianchi et al. 2018).

All the differentiation protocols developed in the last years are based on two major steps: the first promotes iPSCs induction into neuronal progenitors, and the second ensures final neuronal differentiation and maturation.

Two different approaches can be used to act the first step. Some protocols pass through formation of embryoid bodies (EBs) which are consequently plated to generate neural rosettes formed by NPCs (Nicholas et al. 2013; Meganathan et al. 2017; Bianchi et al. 2018; Vadodaria et al. 2019); in other cases, a direct differentiation from iPSCs to neuronal progenitors can be obtained bypassing that step (Kriks et al. 2012; Zhang et al. 2013; Maroof et al. 2013; Colasante et al. 2015; Lu et al. 2016; Qi et al. 2017; Yang et al. 2017). In both cases, this first process is based on the use of small molecules which inhibit SMAD signaling (Chambers et al. 2009), forcing neuralization at the expense of trophectoderm, mesendoderm and non-neural ectoderm generation. Then it is possible to subject NPCs to different concentrations of morphogens trying to recapitulate activation of different pathways occurring *in vivo* during development in the vertebrate CNS along the dorso/ventral or rostro/caudal axis (Figure 7). In this way it is possible to change the nature of neuronal progenitors, generating different neuronal populations (Figure 8). SHH or its analogues, are always used,

with different concentration, as ventrilizing molecules, which allow to obtain progenitors which can be found in the ventral region of the brain, like Nkx2.1+ GINs progenitors, located in the medial ganglionic eminences, or Nkx2.2+/Nkx6.1+ serotonergic neurons progenitors, located in the ventral hindbrain.

On the contrary, considering its role in the generation of glutamatergic neurons deriving from the dorsal region of the SVZ (Azim et al. 2014), the activation of Wnt pathway is fundamental to obtain dorsal Pax6+ NPCs, although different studies indicate this pathway is also essential to distinguish different NPCs along the antero/posterior axis in the brain during development. For this reason, small molecules that inhibit Wnt signaling are used to obtain progenitors located in the rostral region of the brain (Huang et al. 2009; Maroof et al. 2013; Qi et al. 2017; Meganathan et al. 2017), while to generate caudal NPCs is fundamental to use Wnt signaling activators, at different concentrations depending on the localization of the desired NPCs in the antero-posterior axis (Kriks et al. 2012; Lu et al. 2016; Vadodaria et al. 2019).

The second stage of all differentiation protocols foresees the use of media containing small molecules inducing neurons generation from NPCs and their maturation as ascorbic acid, the Brain-Derived Neurotrophic Factor (BDNF), the γ-secretase inhibitor DAPT and dibutyryl cyclic adenosine monophosphate (dbcAMP), which are essential to induce final neuronal differentiation, allowing the acquisition of neurons morphology

and neurons functionality (Shin et al. 2004; Traub et al. 2017; Chen et al. 2018; Zahir et al. 2009). Neuronal populations obtained are typically heterogeneous, presenting both mature and immature cells. All these differentiation processes require a significant amount of time, spanning from weeks to months (Srikanth and Young-Pearse 2014) and despite this maturation process, RNA expression analysis, generated from various differentiation stages, reports some transcriptomic changes which models the physiological gene expression pattern occurring *in vivo* during development, from early embryogenesis to late fetal period, (Ardhanareeswaran et al. 2018; Burke et al. 2020).

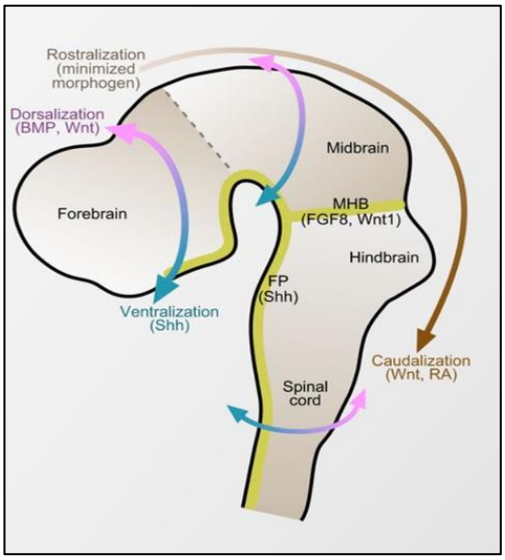

Figure 7. Regional patterning of CNS in embryos. The regional identities within the CNS are determined along the rostrocaudal and

dorsoventral axes through the action of morphogens derived from various organizing centers (yellow). FP, floor plate; MHB, midbrain-hindbrain boundary (adapted from (Suzuki and Vanderhaeghen 2015)

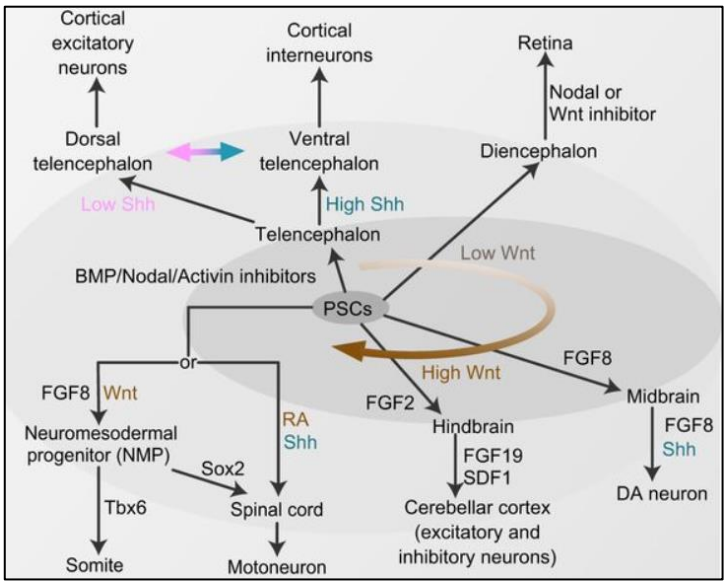

Figure 8. Regional specification in PSC neural differentiation. Processes mimicking *in vitro* the regional patterning occurring *in vivo* through the combinatorial use of the same morphogens in culture medium (adapted from (Suzuki and Vanderhaeghen 2015).

3.2 *In vitro* human modelling for neurodevelopmental disorders

Human iPSC (hiPSCs) derived neurons have been employed to model neurodevelopmental disorders. In many cases, they confirmed or expanded upon our previous understanding of the

pathology gained from post-mortem and rodent model studies. Thanks to hiPSC models different cellular and molecular mechanisms, that give rise to specific disorders, have been dissected and characterised, expanding at the same time the knowledge of human brain development. Furthermore, the usage of patient derived iPSCs provides the opportunity to study a phenotype strictly associated to a mutation in the context of the patient genetic background. Studying both Mendelian and multigenic/multifactorial disorders, genetic background and genetic modifiers can affect the phenotype (Burrows et al. 2016; Rouhani et al. 2014). For this reason, iPSCs derived from unaffected relatives have been used as control in those studies, even if some variability problems related to the different genetic background or different reprograming conditions were maintained. More recently, the development of gene-editing technology allowed to overcome this issue. Zinc Finger Nuclease (ZFNs) technology (Reinhardt et al. 2013), Transcription Activator-Like Effector Nuclease (TALENs) (Hockemeyer et al. 2012) or clustered regularly interspaced short palindromic repeats (CRISPR)-Cas9 system (Ding et al. 2013) can specifically modify the mutated gene allowing to generate iPSCs clones identical to the ones derived from patients except for the corrected gene locus. To reduce variability and obtain the best control for all the experiments using iPSCs, the gene-editing technologies have been largely employed to generate isogenic clones or to insert a specific mutation causing the disease phenotype into a WT iPSC line.

The generation of proper *in vitro* human models offers the unique opportunity for high-throughput drug screening, which can be directly conducted on patients derived cells to test the efficacy and the toxicity of a drug or the effect of a therapeutical approach. As a demonstration of the importance of human *in vitro* modeling, different papers have been published reporting relevant results in better understanding diseases or in finding therapeutical treatments. Among the first papers published in literature to model human pathologies *in vitro* with iPSCs, there is a work focused on Rett syndrome (RTT) in which the authors test the effect of IGF1 on glutamatergic iPSCs-derived neurons, trying to rescue RTT phenotype, characterized by a decreased level of synapses when compared with controls (Marchetto et al. 2010). They reported a positive effect derived from IGF1 neurons treatment, considering that the number of synapses formed was increased after IGF1 administration. The same molecule, IGF1, has been also used as treatment in the case of Phelan–McDermid syndrome (PMDS) (Shcheglovitov et al. 2013). In this case, glutamatergic neurons show impairment in synaptic transmission and a reduced number of synapses, both phenotypes restored with IGF1 administration.

SMA was another pathology, among the first ones, which presented very promising data derived from *in vitro* human experiments. iPSCs derived from SMA patients have been used to generate SMA motorneurons reporting degeneration associated to mitochondrial dysfunction, as occur *in vivo*, and they have been used to perform drug screening. These

experiments leading to the use of N-acetylcysteine as drug to improve mitochondrial functionality and rescue the neurodegeneration (Xu et al. 2016).

All these data highlight the importance of an *in vitro* human model to study neurodevelopmental disorders, even if, sometimes, when the pathology rise up later, postnatally, it could be harder to recreate *in vitro* the right condition to mimic a disease, and this is what happens in the case of DS.

3.3 Human DS modeling

Very few papers have been published in literature reporting *in vitro* human models of DS-related *SCN1A* mutations, and among them it is possible to distinguish different hypothesis regarding the mechanism at the basis of the pathology, and the population most affected.

In 2013, Jiao et al. (Jiao et al. 2013) derived iPSCs from two patients, presenting SMEI and mild febrile epilepsy. Patient iPSCs derived ExNs reported much more Na^+ current compared to an unaffected control. In particular, SMEI neurons showed more and larger evoked AP when compared to unaffected control. Though mild febrile seizures neurons showed the same alterations, a less severe phenotype has been reported.

Also, spontaneous APs showed higher frequency in SMEI and mild febrile seizure neurons compared to wild-type, denoting hyperexcitability. With these data, the authors demonstrated that

patient iPSC-derived neurons recapitulated abnormal sodium currents, APs and epileptiform firing. Furthermore, the authors demonstrated that this alteration was due to a lag in the inactivation timing of the Na^+ channel, and by using phenytoin, an antiepileptic drug, they showed a rescue of the epileptic phenotype. After treatment, patient iPSC-derived neurons showed reduced Na^+ currents, alleviated delayed inactivation of Na^+ channel, reduction of frequency and amplitude of evoked AP and, moreover, also the epileptic form of the spontaneous APs disappeared.

In the same year, Liu and colleagues (Y. Liu et al. 2013), reprogrammed iPSCs from two DS patients presenting mutations resulting in truncated unfunctional $Na_v1.1$ channel. They published data reporting the same alteration discovered by Jiao in glutamatergic neurons, in two distinct types of neurons distinguished between them only by using morphological criteria: bipolar and pyramidal-shaped neurons, expected to be respectively GINs and ExNs.

Nonetheless, various papers, in accordance with all data published using DS mouse models, report alterations specifically in GINs (Higurashi et al. 2013; Sun et al. 2016; Kim et al. 2018). By using different differentiation protocols, providing the generation of GABAergic (Sun et al. 2016) or $Na_v1.1$ reporters (Higurashi et al. 2013), or by using patch-seq (Kim et al. 2018), the authors of these papers showed impairments in AP

generation, and reduction of Na^+ current density specifically in GINs.

Altogether these data can result confusing, and not helpful in the understanding of DS in humans. Furthermore, supporting all these published data, there is an important difference to be mentioned about the localization of $Na_v1.1$ protein in human brain respect to mouse. While in mice $Na_v1.1$ is largely reported to be expressed in the AIS of GINs (Yu et al. 2006) and specifically in PV+ (Ogiwara et al. 2007), SST+ (Tai et al. 2014), and VIP+ neurons (Goff and Goldberg 2019), in the human brain its localization can vary. In fact, even if the colocalization of $Na_v1.1$ and PV is very high in postnatal ages, $Na_v1.1$ shows somatodendritic localization and expression also in pyramidal neurons, specifically in cortical layer V and in the hippocampus (Trimmer and Rhodes 2004; Wang et al. 2011), justifying the open question about the role of glutamatergic neurons in DS.

To complicate the situation, all the mentioned works reported data obtained by comparing DS patients-derived neurons to neurons generated from unaffected subjects. Considering the importance of the genetic background, together with the variability of different cell lines to differentiate into neurons and maturate, it is clear that the generation of isogenic controls is necessary to better understand the mechanisms of the disease *in vitro*. For this reason, in 2016, Liu and colleagues published the first paper in the field by using TALENs gene editing tool to generate an isogenic control iPSC line (J. Liu et al. 2016). They

revealed a decrease in sodium current density in patient iPSCs derived GINs compared to isogenic corrected control, but they also revealed phenotypical alterations in isogenic control samples when compared to other control samples derived from unaffected subjects. The voltage dependence of sodium current activation and AP threshold were different, suggesting a correlation between these alterations and patient genetic background.

Later, in 2020, Dr Xie and colleagues published a paper presenting data obtained from dual isogenic iPSC pairs (Xie et al. 2020). The authors of this work, generated iPSCs from two male siblings, one affected by GEFS+ and the other which had no known clinical diagnoses. From these two cell lines, by using CRISPR-Cas9 gene editing tool, they derived two isogenic clones, one, generated from the control sibling, reporting the disease-causing mutation in homozygous condition, and the other derived from the GEFS+ patient presenting the correction of the mutated nucleotide causing the disease. Then to characterize the alterations due to the presence of K1270T *SCN1A* mutation, located in S3 D3, they differentiated the iPSCs into neurons with a protocol allowing to obtain both glutamatergic and GABAergic populations. Then, by using two different reporters, labelling in a specific manner each population, they showed significant impairment in AP firing and reduced Na^+ current density in the homozygous mutated control interneurons compared to their counterpart. Furthermore, more unclear data emerged from ExNs analysis, considering that they found a

reduction in Na^+ current for the homozygous mutated neurons compared to their control, while an impairment in AP firing has been shown in patient derived neurons compared to the corrected control.

In the end, even this paper, which present very interesting data, failed in creating an *in vitro* human model that could show clear data with a unique interpretation. This lack, can be attributed to the difficulty of obtaining neuronal culture composed in high percentage of mature cells, resembling even early post-natal neurons, which are known to express $Na_v1.1$ channel. In accordance to this issue, Xie and colleagues (Xie et al. 2020), affirm to not obtain PV+ and SST+ interneurons in their culture, which are the two classes of inhibitory interneurons most affected by *SCN1A* loss, and could be very interesting to test.

Aim of the thesis

My PhD project aims to generate a human DS model based on patient derived iPSCs differentiated in neurons to test gene therapy-based approaches for the treatment of this neurological condition. In particular, we aim to generate iPSCs from two DS patients presenting different missense mutations and corresponding isogenic control derived by CRISPR/Cas9 gene editing of the mutations. We also aim to set a specific iPSC differentiation protocol to generate GINs including PV+ and SST+ subtypes, that are the neuronal populations most affected in DS and assess if the characteristic firing defect is resembled in this neuronal population. Finally, we aim to employ the activatory CRISPR-dCas9 tool to boost the expression of the wild-type allele of *SCN1A* gene to eventually rescue the observed defect.

In particular, in Chapter 2 will be presented all the work focused on human modeling, while Chapter 3 will show how the activatory CRISPR-dCas9 could efficiently work in a DS mouse model, reverting the pathological phenotype.

Chapter 4 will present a mini review I wrote with my co-tutor Dr Colasante about the importance of activatory and inhibitory CRISPR-dCas9 tools in the field of neurodevelopmental disorders.

References

Almog, Yael, Saja Fadila, Marina Brusel, Anat Mavashov, Karen Anderson, and Moran Rubinstein. 2021. “Developmental Alterations in Firing Properties of Hippocampal CA1 Inhibitory and Excitatory Neurons in a Mouse Model of Dravet Syndrome.” *Neurobiology of Disease* 148: 105209. https://doi.org/10.1016/j.nbd.2020.105209.

Ardhanareeswaran, Karthikeyan, Jessica Mariani, Gianfilippo Coppola, Alexej Abyzov, Flora M Vaccarino, New Haven, and New Haven. 2018. “Human Induced Pluripotent Stem Cells for Modeling Neurodevelopmental Disorders” 13 (5): 265–78. https://doi.org/10.1038/nrneurol.2017.45.Human.

Atallah, Bassam V., and Massimo Scanziani. 2009. “Instantaneous Modulation of Gamma Oscillation Frequency by Balancing Excitation with Inhibition.” *Neuron* 62 (4): 566–77. https://doi.org/10.1016/j.neuron.2009.04.027.

Azim, Kasum, Bruno Fischer, Anahi Hurtado-Chong, Kalina Draganova, Claudio Cantù, Martina Zemke, Lukas Sommer, Arthur Butt, and Olivier Raineteau. 2014. “Persistent Wnt / b - Catenin Signaling Determines Dorsalization of the Postnatal Subventricular Zone and Neural Stem Cell Specification into Oligodendrocytes and Glutamatergic Neurons.” *Stem Cells* 32: 1301–12.

Bezanilla, Francisco. 2008a. “How Membrane Proteins Sense Voltage.” *Nature Reviews Molecular Cell Biology* 9 (4): 323–32. https://doi.org/10.1038/nrm2376.

———. 2008b. “Ion Channels: From Conductance to Structure.”

Neuron 60 (3): 456–68. https://doi.org/10.1016/j.neuron.2008.10.035.

Bianchi, Fabio, Majid Malboubi, Yichen Li, Julian H. George, Antoine Jerusalem, Francis Szele, Mark S. Thompson, and Hua Ye. 2018. "Rapid and Efficient Differentiation of Functional Motor Neurons from Human IPSC for Neural Injury Modelling." *Stem Cell Research* 32 (September): 126–34. https://doi.org/10.1016/j.scr.2018.09.006.

Brew, Helen M., Joshua X. Gittelman, Robert S. Silverstein, Timothy D. Hanks, Vas P. Demas, Linda C. Robinson, Carol A. Robbins, et al. 2007. "Seizures and Reduced Life Span in Mice Lacking the Potassium Channel Subunit Kv1.2, but Hypoexcitability and Enlarged Kv1 Currents in Auditory Neurons." *Journal of Neurophysiology* 98 (3): 1501–25. https://doi.org/10.1152/jn.00640.2006.

Burke, Emily E., Joshua G. Chenoweth, Joo Heon Shin, Leonardo Collado-Torres, Suel Kee Kim, Nicola Micali, Yanhong Wang, et al. 2020. "Dissecting Transcriptomic Signatures of Neuronal Differentiation and Maturation Using IPSCs." *Nature Communications* 11 (1): 1–14. https://doi.org/10.1038/s41467-019-14266-z.

Burrows, Courtney K., Nicholas E. Banovich, Bryan J. Pavlovic, Kristen Patterson, Irene Gallego Romero, Jonathan K. Pritchard, and Yoav Gilad. 2016. "Genetic Variation, Not Cell Type of Origin, Underlies the Majority of Identifiable Regulatory Differences in IPSCs." *PLoS Genetics* 12 (1): 1–18. https://doi.org/10.1371/journal.pgen.1005793.

Carvill, Gemma L., Krysta L. Engel, Aishwarya Ramamurthy, J.

Nicholas Cochran, Jolien Roovers, Hannah Stamberger, Nicholas Lim, et al. 2018. “Aberrant Inclusion of a Poison Exon Causes Dravet Syndrome and Related SCN1A-Associated Genetic Epilepsies.” *American Journal of Human Genetics* 103 (6): 1022–29. https://doi.org/10.1016/j.ajhg.2018.10.023.

Catterall, W. A. 1986. “Molecular Properties of Voltage-Sensitive Sodium Channels.” *Annual Review of Biochemistry* VOL. 55: 953–85. https://doi.org/10.1146/annurev.bi.55.070186.004513.

Catterall, William A., Franck Kalume, and John C. Oakley. 2010. “NaV1.1 Channels and Epilepsy.” *Journal of Physiology* 588 (11): 1849–59. https://doi.org/10.1113/jphysiol.2010.187484.

Chambers, Stuart M., Christopher A. Fasano, Eirini P. Papapetrou, Mark Tomishima, Michel Sadelain, and Lorenz Studer. 2009. “Highly Efficient Neural Conversion of Human ES and IPS Cells by Dual Inhibition of SMAD Signaling.” *Nature Biotechnology* 27 (3): 275–80. https://doi.org/10.1038/nbt.1529.

Chen, Shuang-Qing, Fan Zhang, Chen-Lu Liu, Ming-Min Tong, and Zhong Zhao. 2018. “A Promotional Role of BDNF in Pluripotent Stem Cells Neural Differentiation via Wnt / β -Catenin and ERK /.” *Annals of Stem Cell Research & Therapy* 2 (4): 1–4.

Chiron, Catherine, and Olivier Dulac. 2011. “The Pharmacologic Treatment of Dravet Syndrome.” *Epilepsia* 52 (SUPPL. 2): 72–75. https://doi.org/10.1111/j.1528-1167.2011.03007.x.

Claes, Lieve, Jurgen Del-Favero, Berten Ceulemans, Lieven Lagae, Christine Van Broeckhoven, and Peter De Jonghe. 2001. “De Novo Mutations in the Sodium-Channel Gene SCN1A Cause Severe Myoclonic Epilepsy of Infancy.” *American Journal of*

Human Genetics 68 (6): 1327–32. https://doi.org/10.1086/320609.

Colasante, Gaia, Gabriele Lignani, Alicia Rubio, Lucian Medrihan, Latefa Yekhlef, Alessandro Sessa, Luca Massimino, et al. 2015. "Rapid Conversion of Fibroblasts into Functional Forebrain GABAergic Interneurons by Direct Genetic Reprogramming." *Cell Stem Cell* 17 (6): 719–34. https://doi.org/10.1016/j.stem.2015.09.002.

Costa, M. R.C., and W. A. Catterall. 1984. "Cyclic AMP-Dependent Phosphorylation of the α Subunit of the Sodium Channel in Synaptic Nerve Ending Particles." *Journal of Biological Chemistry* 259 (13): 8210–18. https://doi.org/10.1016/s0021-9258(17)39715-6.

Devinsky, Orrin, Annamaria Vezzani, Terence J. O'Brien, Nathalie Jette, Ingrid E. Scheffer, Marco De Curtis, and Piero Perucca. 2018. "Epilepsy." *Nature Reviews Disease Primers* 4 (May). https://doi.org/10.1038/nrdp.2018.24.

Ding, Qiurong, Stephanie N Regan, Yulei Xia, Leonie A Oostrom, Chad A Cowan, and Kiran Musunuru. 2013. "Enhanced Efficiency of Human Pluripotent Stem Cell Genome Editing through Replacing TALENs with CRISPRs." *Cell Stem Cell* 12 (4): 393–94. https://doi.org/10.1016/j.stem.2013.03.006.

Dravet, Charlotte, and Hirokazu Oguni. 2013. *Dravet Syndrome (Severe Myoclonic Epilepsy in Infancy)*. *Handbook of Clinical Neurology*. 1st ed. Vol. 111. Elsevier B.V. https://doi.org/10.1016/B978-0-444-52891-9.00065-8.

Dudek, F. Edward, and Thomas P. Sutula. 2007. "Epileptogenesis in

the Dentate Gyrus: A Critical Perspective." *Progress in Brain Research* 163 (801): 755–73. https://doi.org/10.1016/S0079-6123(07)63041-6.

Eaholtz, Galen, Todd Scheuer, and William A. Catterall. 1994. "Restoration of Inactivation and Block of Open Sodium Channels by an Inactivation Gate Peptide." *Neuron* 12 (5): 1041–48. https://doi.org/10.1016/0896-6273(94)90312-3.

Fisher, Robert S., Walter Van Emde Boas, Warren Blume, Christian Elger, Pierre Genton, Phillip Lee, and Jerome Engel. 2005. "Response: Definitions Proposed by the International League Against Epilepsy (ILAE) and the International Bureau for Epilepsy (IBE) [4]." *Epilepsia* 46 (10): 1701–2. https://doi.org/10.1111/j.1528-1167.2005.00273_4.x.

Florio, Marta, Mareike Albert, Elena Taverna, Takashi Namba, Holger Brandl, Eric Lewitus, Christiane Haffner, et al. 2015. "Human-Specific Gene ARHGAP11B Promotes Basal Progenitor Amplification and Neocortex Expansion." *Science* 27 (February): 6.

Goff, Kevin M., and Ethan M. Goldberg. 2019. "Vasoactive Intestinal Peptide-Expressing Interneurons Are Impaired in a Mouse Model of Dravet Syndrome." *ELife* 8: 1–28. https://doi.org/10.7554/eLife.46846.

Goldin, A. L., T. Snutch, H. Lubbert, A. Dowsett, J. Marshall, V. Auld, W. Downey, L. C. Fritz, H. A. Lester, and R. Dunn. 1986. "Messenger RNA Coding for Only the α Subunit of the Rat Brain Na Channel Is Sufficient for Expression of Functional Channels in Xenopus Oocytes." *Proceedings of the National Academy of Sciences of the United States of America* 83 (19): 7503–7.

https://doi.org/10.1073/pnas.83.19.7503.

Gottesman, Irving I, and Todd D Gould. 2003. “The Endophenotype Concept in Psychiatry: Etymology and Strategic Intentions.” *Am J Psychiatry* 160: 636–45.

Griffin, Aliesha, Kyla R. Hamling, Soon Gweon Hong, Mana Anvar, Luke P. Lee, and Scott C. Baraban. 2018. “Preclinical Animal Models for Dravet Syndrome: Seizure Phenotypes, Comorbidities and Drug Screening.” *Frontiers in Pharmacology* 9 (JUN): 1–15. https://doi.org/10.3389/fphar.2018.00573.

Guy, H. R., and P. Seetharamulu. 1986. “Molecular Model of the Action Potential Sodium Channel.” *Proceedings of the National Academy of Sciences of the United States of America* 83 (2): 508–12. https://doi.org/10.1073/pnas.83.2.508.

Haider, Bilal, Alvaro Duque, Andrea R. Hasenstaub, and David A. McCormick. 2006. “Neocortical Network Activity in Vivo Is Generated through a Dynamic Balance of Excitation and Inhibition.” *Journal of Neuroscience* 26 (17): 4535–45. https://doi.org/10.1523/JNEUROSCI.5297-05.2006.

Halassa, Michael M., Tommaso Fellin, and Philip G. Haydon. 2007. “The Tripartite Synapse: Roles for Gliotransmission in Health and Disease.” *Trends in Molecular Medicine* 13 (2): 54–63. https://doi.org/10.1016/j.molmed.2006.12.005.

Han, Zhou, Chunling Chen, Anne Christiansen, Sophina Ji, Qian Lin, Charles Anumonwo, Chante Liu, et al. 2020. “Antisense Oligonucleotides Increase Scn1a Expression and Reduce Seizures and SUDEP Incidence in a Mouse Model of Dravet Syndrome.” *Science Translational Medicine* 12 (558).

https://doi.org/10.1126/SCITRANSLMED.AAZ6100.

Helbig, Ingo, and Ahmad N. Abou Tayoun. 2016. “Understanding Genotypes and Phenotypes in Epileptic Encephalopathies.” *Molecular Syndromology* 7 (4): 172–81. https://doi.org/10.1159/000448530.

Higurashi, Norimichi, Taku Uchida, Christoph Lossin, Yoshio Misumi, Yohei Okada, Wado Akamatsu, Yoichi Imaizumi, et al. 2013. “A Human Dravet Syndrome Model from Patient Induced Pluripotent Stem Cells.” *Molecular Brain* 6.

Hockemeyer, Dirk, Haoyi Wang, Samira Kiani, Christine S Lai, Qing Gao, P John, Gregory J Cost, et al. 2012. “Genetic Engineering of Human ES and IPS Cells Using TALE Nucleases.” *Nat Biotechnol* 29 (8): 731–34. https://doi.org/10.1038/nbt.1927.Genetic.

Hodgkin, AL, and AF Huxley. 1952. “A QUANTITATIVE DESCRIPTION OF MEMBRANE CURRENT AND ITS APPLICATION TO CONDUCTION AND EXCITATION IN NERVE.” *Journal Physiology*, 500–544. https://doi.org/10.1113/jphysiol.1952.sp004764.

Hsiao, J., T. Y. Yuan, M. S. Tsai, C. Y. Lu, Y. C. Lin, M. L. Lee, S. W. Lin, et al. 2016. “Upregulation of Haploinsufficient Gene Expression in the Brain by Targeting a Long Non-Coding RNA Improves Seizure Phenotype in a Model of Dravet Syndrome.” *EBioMedicine* 9: 257–77. https://doi.org/10.1016/j.ebiom.2016.05.011.

Hu, Wenqin, Cuiping Tian, Tun Li, Mingpo Yang, Han Hou, and Yousheng Shu. 2009. “Distinct Contributions of Nav1.6 and Nav1.2 in Action Potential Initiation and Backpropagation.” *Nature*

Neuroscience 12 (8): 996–1002. https://doi.org/10.1038/nn.2359.

Huang, Shih Min A., Yuji M. Mishina, Shanming Liu, Atwood Cheung, Frank Stegmeier, Gregory A. Michaud, Olga Charlat, et al. 2009. "Tankyrase Inhibition Stabilizes Axin and Antagonizes Wnt Signalling." *Nature* 461 (7264): 614–20. https://doi.org/10.1038/nature08356.

Ingusci, Selene, Gianluca Verlengia, Marie Soukupova, Silvia Zucchini, and Michele Simonato. 2019. "Gene Therapy Tools for Brain Diseases." *Frontiers in Pharmacology* 10 (July): 1–19. https://doi.org/10.3389/fphar.2019.00724.

Isaacson, Jeffry S., and Massimo Scanziani. 2011. "How Inhibition Shapes Cortical Activity." *Neuron* 72 (2): 231–43. https://doi.org/10.1016/j.neuron.2011.09.027.

Isom, Author L L, K S De Jongh, D E Patton, B F X Reber, J Offord, K Walsh, A L Goldin, et al. 1992. "Primary Structure and Functional Expression of the Beta1 Subunit of the Rat Brain Sodium Channel" 256 (5058): 839–42.

Isom, L. L., D. S. Ragsdale, K. S. De Jongh, R. E. Westenbroek, B. F.X. Reber, T. Scheuer, and W. A. Catterall. 1995. "Structure and Function of the B2 Subunit of Brain Sodium Channels, a Transmembrane Glycoprotein with a CAM Motif." *Cell* 83 (3): 433–42. https://doi.org/10.1016/0092-8674(95)90121-3.

Ito, Susumu, Ikuo Ogiwara, Kazuyuki Yamada, Hiroyuki Miyamoto, Takao K. Hensch, Makiko Osawa, and Kazuhiro Yamakawa. 2013. "Mouse with Nav1.1 Haploinsufficiency, a Model for Dravet Syndrome, Exhibits Lowered Sociability and Learning Impairment." *Neurobiology of Disease* 49 (1): 29–40.

https://doi.org/10.1016/j.nbd.2012.08.003.

Jiao, Jiao, Yuanyuan Yang, Yiwu Shi, Jiayu Chen, Rui Gao, Yong Fan, Hui Yao, Weiping Liao, Xiao Fang Sun, and Shaorong Gao. 2013. "Modeling Dravet Syndrome Using Induced Pluripotent Stem Cells (IPSCs) and Directly Converted Neurons." *Human Molecular Genetics* 22 (21): 4241–52. https://doi.org/10.1093/hmg/ddt275.

Kim, Hyun Woo, Zhejiu Quan, Young Beom Kim, Eunji Cheong, Heung Dong Kim, Minjung Cho, Jiho Jang, et al. 2018. "Differential Effects on Sodium Current Impairments by Distinct SCN1A Mutations in GABAergic Neurons Derived from Dravet Syndrome Patients." *Brain and Development* 40 (4): 287–98. https://doi.org/10.1016/j.braindev.2017.12.002.

Kostović, I., and M. Judaš. 2015. "Embryonic and Fetal Development of the Human Cerebral Cortex." *Brain Mapping: An Encyclopedic Reference* 2: 167–75. https://doi.org/10.1016/B978-0-12-397025-1.00193-7.

Kriks, Sonja, Jae-Won Shim, Jinghua Piao, Yosif M. Ganat, Dustin R. Wakeman, Zhong Xie, Luis Carrillo-Reid, et al. 2012. "Floor Plate-Derived Dopamine Neurons from HESCs Efficiently Engraft in Animal Models of PD." *Nature* 480 (7378): 547–51. https://doi.org/10.1038/nature10648.Floor.

Leterrier, Christophe. 2018. "The Axon Initial Segment: An Updated Viewpoint." *Journal of Neuroscience* 38 (9): 2135–45. https://doi.org/10.1523/JNEUROSCI.1922-17.2018.

Liu, J., C. Gao, W. Chen, W. Ma, X. Li, Y. Shi, H. Zhang, et al. 2016. "CRISPR/Cas9 Facilitates Investigation of Neural Circuit Disease

Using Human IPSCs: Mechanism of Epilepsy Caused by an SCN1A Loss-of-Function Mutation." *Translational Psychiatry* 6 (November 2015). https://doi.org/10.1038/tp.2015.203.

Liu, Yu, Luis F Lopez-Santiago, Yukun Yuan, Julie M Jones, Helen Zhang, Heather A O'Malley, Gustavo A Patino, et al. 2013. "DRAVET SYNDROME PATIENT-DERIVED NEURONS SUGGEST A NOVEL EPILEPSY MECHANISM Yu." *Ann Neurol* 74 (1): 128–39. https://doi.org/10.1002/ana.23897.

Lossin, Christoph, Thomas H. Rhodes, Reshma R. Desai, Carlos G. Vanoye, Dao Wang, Sanda Carniciu, Orrin Devinsky, and Alfred L. George. 2003. "Epilepsy-Associated Dysfunction in the Voltage-Gated Neuronal Sodium Channel SCN1A." *Journal of Neuroscience* 23 (36): 11289–95. https://doi.org/10.1523/jneurosci.23-36-11289.2003.

Lu, Jianfeng, Xuefei Zhong, Huisheng Liu, Ling Hao, Cindy Tzu Ling Huang, Mohammad Amin Sherafat, Jeffrey Jones, Melvin Ayala, Lingjun Li, and Su Chun Zhang. 2016. "Generation of Serotonin Neurons from Human Pluripotent Stem Cells." *Nature Biotechnology* 34 (1): 89–94. https://doi.org/10.1038/nbt.3435.

Marchetto, Maria C, Cassiano Carromeu, Allan Acab, Diana Yu, Gene Yeo, Yangling Mu, Gong Chen, Fred H Gage, and Alysson R. Muotri. 2010. "A Model for Neural Development and Treatment of Rett Syndrome Using Human Induced Pluripotent Stem Cells." *Cell* 143 (4): 527–39. https://doi.org/10.1016/j.cell.2010.10.016.

Marín, Oscar, and John L.R. Rubenstein. 2003. "Cell Migration in the Forebrain." *Annual Review of Neuroscience* 26 (Figure 1): 441–83. https://doi.org/10.1146/annurev.neuro.26.041002.131058.

Marini, Carla, Ingrid E. Scheffer, Rima Nabbout, Arvid Suls, Peter De Jonghe, Federico Zara, and Renzo Guerrini. 2011. “The Genetics of Dravet Syndrome.” *Epilepsia* 52 (SUPPL. 2): 24–29. https://doi.org/10.1111/j.1528-1167.2011.02997.x.

Maroof, Asif M, Sotirios Keros, Jennifer A Tyson, Shui-Wang Ying, Yosif M Ganat, Florian T Merkle, Becky Liu, et al. 2013. “Directed Differentiation and Functional Maturation of Cortical Interneurons from Human Embryonic Stem Cells.” *Cell Stem Cell* 12 (5): 1-559–72. https://doi.org/10.1016/j.stem.2013.04.008.

Martynoga, Ben, Daniela Drechsel, and François Guillemot. 2012. “Molecular Control of Neurogenesis: A View from the Mammalian Cerebral Cortex.” *Cold Spring Harbor Perspectives in Biology* 4 (10). https://doi.org/10.1101/cshperspect.a008359.

Meganathan, Kesavan, Emily M.A. Lewis, Paul Gontarz, Shaopeng Liu, Edouard G. Stanley, Andrew G. Elefanty, James E. Huettner, Bo Zhang, and Kristen L. Kroll. 2017. “Regulatory Networks Specifying Cortical Interneurons from Human Embryonic Stem Cells Reveal Roles for CHD2 in Interneuron Development.” *Proceedings of the National Academy of Sciences of the United States of America* 114 (52): E11180–89. https://doi.org/10.1073/pnas.1712365115.

Mendell, Jerry R., Samiah Al-Zaidy, Richard Shell, W. Dave Arnold, Louise R. Rodino-Klapac, Thomas W. Prior, Linda Lowes, et al. 2017. “Single-Dose Gene-Replacement Therapy for Spinal Muscular Atrophy.” *New England Journal of Medicine* 377 (18): 1713–22. https://doi.org/10.1056/nejmoa1706198.

Mistry, Akshitkumar M, Christopher H Thompson, Alison R Miller, Carlos G Vanoye1, Alfred L George Jr, and Jennifer A Kearney.

2014. “Strain- and Age-Dependent Hippocampal Neuron Sodium Currents Correlate with Epilepsy Severity in Dravet Syndrome Mice.” *Neurobiology of Disease* 65: 1–11. https://doi.org/10.1016/j.nbd.2014.01.006.

Myers, Kenneth A., Paul Lightfoot, Shekhar G. Patil, J. Helen Cross, and Ingrid E. Scheffer. 2018. “Stiripentol Efficacy and Safety in Dravet Syndrome: A 12-Year Observational Study.” *Developmental Medicine and Child Neurology* 60 (6): 574–78. https://doi.org/10.1111/dmcn.13704.

Nicholas, Cory R, Jiadong Chen, Yunshuo Tang, Derek G Southwell, Daniel Vogt, Christine M Arnold, Ying-jiun J Chen, et al. 2013. “Functional Maturation of HPSC-Derived Forebrain Interneurons Requires an Extended Timeline and Mimics Human Neural Development.” *Cell Stem Cell* 12 (5): 573–86. https://doi.org/10.1016/j.stem.2013.04.005.

Noda, Masaharu, Takayuki Ikeda, Harukazu Suzuki, Hiroshi Takeshima, Tomoyuki Takahashi, Motoy Kuno, and Shosaku Numa. 1986. “Expression of Functional Sodium Channels from Cloned CDNA.” *Nature* 322 (6082): 826–28. https://doi.org/10.1038/322826a0.

Noda, Masaharu, Shin Shimizu, Tsutomu Tanabe, Toshiyuki Takai, Toshiaki Kayano, Takayuki Ikeda, Hideo Takahashi, et al. 1984. “Primary Structure of Electrophorus Electricus Sodium Channel Deduced from CDNA Sequence.” *Nature* 312 (5990): 121–27. https://doi.org/10.1038/312121a0.

Nowakowski, Tomasz J., Aparna Bhaduri, Alex A. Pollen, Beatriz Alvarado, Mohammed A. Mostajo-Radji, Elizabeth Di Lullo, Maximilian Haeussler, et al. 2017. “Spatiotemporal Gene

Expression Trajectories Reveal Developmental Hierarchies of the Human Cortex." *Science* 358 (6368): 1318–23. https://doi.org/10.1126/science.aap8809.

Ogiwara, Ikuo, Takuji Iwasato, Hiroyuki Miyamoto, Ryohei Iwata, Tetsushi Yamagata, Emi Mazaki, Yuchio Yanagawa, et al. 2013. "Nav1.1 Haploinsufficiency in Excitatory Neurons Ameliorates Seizure-Associated Sudden Death in a Mouse Model of Dravet Syndrome." *Human Molecular Genetics* 22 (23): 4784–4804. https://doi.org/10.1093/hmg/ddt331.

Ogiwara, Ikuo, Hiroyuki Miyamoto, Noriyuki Morita, Nafiseh Atapour, Emi Mazaki, Ikuyo Inoue, Tamaki Takeuchi, et al. 2007. "Nav1.1 Localizes to Axons of Parvalbumin-Positive Inhibitory Interneurons: A Circuit Basis for Epileptic Seizures in Mice Carrying an Scn1a Gene Mutation." *Journal of Neuroscience* 27 (22): 5903–14. https://doi.org/10.1523/JNEUROSCI.5270-06.2007.

Ohmori, Iori, Kristopher M. Kahlig, Thomas H. Rhodes, Dao W. Wang, and Alfred L. George. 2006. "Nonfunctional SCN1A Is Common in Severe Myoclonic Epilepsy of Infancy." *Epilepsia* 47 (10): 1636–42. https://doi.org/10.1111/j.1528-1167.2006.00643.x.

Okun, Michael, and Ilan Lampl. 2008. "Instantaneous Correlation of Excitation and Inhibition during Ongoing and Sensory-Evoked Activities." *Nature Neuroscience* 11 (5): 535–37. https://doi.org/10.1038/nn.2105.

Pollen, Alex A, Tomasz J Nowakowski, Jiadong Chen, Hanna Retallack, Carmen Sandoval-espinosa, Cory R Nicholas, Joe Shuga, et al. 2015. "Molecular Identity of Human Outer Radial Glia During Cortical Development." *Cell* 163 (1): 55–67.

https://doi.org/10.1016/j.cell.2015.09.004.Molecular.

Qi, Yuchen, Xin-jun Zhang, Nicolas Renier, Zhuhao Wu, Talia Atkin, Ziyi Sun, Zeeshan Ozair, et al. 2017. “Accelerated Cortical Neuron Differentiation Protocol” 35 (2): 154–63. https://doi.org/10.1038/nbt.3777.Combined.

Ragsdale, David S. 2008. “How Do Mutant Nav1.1 Sodium Channels Cause Epilepsy?” *Brain Research Reviews* 58 (1): 149–59. https://doi.org/10.1016/j.brainresrev.2008.01.003.

Rakic, Pasko. 2009. “Evolution of the Neocortex: A Perspective from Developmental Biology.” *Nature Reviews Neuroscience* 10 (10): 724–35. https://doi.org/10.1038/nrn2719.

Reinhardt, Peter, Benjamin Schmid, Lena F. Burbulla, David C. Schöndorf, Lydia Wagner, Michael Glatza, Susanne Höing, et al. 2013. “Genetic Correction of a Lrrk2 Mutation in Human IPSCs Links Parkinsonian Neurodegeneration to ERK-Dependent Changes in Gene Expression.” *Cell Stem Cell* 12 (3): 354–67. https://doi.org/10.1016/j.stem.2013.01.008.

Rouhani, Foad, Natsuhiko Kumasaka, Miguel Cardoso de Brito, Allan Bradley, Ludovic Vallier, and Daniel Gaffney. 2014. “Genetic Background Drives Transcriptional Variation in Human Induced Pluripotent Stem Cells.” *PLoS Genetics* 10 (6). https://doi.org/10.1371/journal.pgen.1004432.

Shcheglovitov, Aleksander, Olesya Shcheglovitova, Masayuki Yazawa, Thomas Portmann, Rui Shu, Vittorio Sebastiano, Anna Krawisz, et al. 2013. “Shank3 and IGF1 Restore Synaptic Deficits in Neurons from 22q13 Deletion Syndrome Patients.” *Nature* 503 (7475): 267–71. https://doi.org/10.1038/nature12618.

Shin, Dong Mi, Joon Ik Ahn, Ki Hwan Lee, Yong Sung Lee, and Yeon Sook Lee. 2004. “Ascorbic Acid Responsive Genes during Neuronal Differentiation of Embryonic Stem Cells.” *NeuroReport* 15 (12): 1959–63. https://doi.org/10.1097/00001756-200408260-00025.

Smart, Sharon L., Valeri Lopantsev, C. L. Zhang, Carol A. Robbins, Hao Wang, S. Y. Chiu, Philip A. Schwartzkroin, Albee Messing, and Bruce L. Tempel. 1998. “Deletion of the K(v)1.1 Potassium Channel Causes Epilepsy in Mice.” *Neuron* 20 (4): 809–19. https://doi.org/10.1016/S0896-6273(00)81018-1.

Speca, DJ, G Ogata, D Mandikian, HI Bishop, SW Wiler, K Eum, HJ Wenzel, et al. 2008. “Deletion of the Kv2.1 Delayed Rectifier Potassium Channel Leads to Neuronal and Behavioral Hyperexcitability.” *PLoS ONE* 32 (7): 736–40. https://doi.org/10.1111/gbb.12120.Deletion.

Srikanth, Priya, and Tracy L Young-Pearse. 2014. “Stem Cells on the Brain: Modeling Neurodevelopmental and Neurodegenerative Diseases Using Human IPSCs.” *J Neurogenet* 28: 5–29. https://doi.org/10.3109/01677063.2014.881358.

Stafstrom, Carl E, and Lionel Carmant. 2016. “Seizures and Epilepsy: An Overview for Neuroscientists.” *Epilepsy: The Intersection of Neurosciences, Biology, Mathematics, Engineering, and Physics*, 65–77. https://doi.org/10.1201/b10866-10.

Stühmer, Walter, Franco Conti, Harukazu Suzuki, Xiaodong Wang, Masaharu Noda, Naoki Yahagi, Hideo Kubo, and Shosaku Numa. 1989. “Structural Parts Involved in Activation and Inactivation of the Sodium Channel.” *Nature* 339 (6226): 597–603. https://doi.org/10.1038/339597a0.

Sun, Yishan, Sergiu P. Paşca, Thomas Portmann, Carleton Goold, Kathleen A. Worringer, Wendy Guan, Karen C. Chan, et al. 2016. "A Deleterious Nav1.1 Mutation Selectively Impairs Telencephalic Inhibitory Neurons Derived from Dravet Syndrome Patients." *ELife* 5 (2016JULY): 1–26. https://doi.org/10.7554/eLife.13073.

Suzuki, Ikuo K., and Pierre Vanderhaeghen. 2015. "Is This a Brain Which i See before Me? Modeling Human Neural Development with Pluripotent Stem Cells." *Development (Cambridge)* 142 (18): 3138–50. https://doi.org/10.1242/dev.120568.

Swartz, Kenton J. 2004. "Towards a Structural View of Gating in Potassium Channels." *Nature Reviews Neuroscience* 5 (12): 905–16. https://doi.org/10.1038/nrn1559.

Tai, Chao, Yasuyuki Abe, Ruth E. Westenbroek, Todd Scheuer, and William A. Catterall. 2014. "Impaired Excitability of Somatostatin- and Parvalbumin-Expressing Cortical Interneurons in a Mouse Model of Dravet Syndrome." *Proceedings of the National Academy of Sciences of the United States of America* 111 (30): 3139–48. https://doi.org/10.1073/pnas.1411131111.

Takahashi, Kazutoshi, Koji Tanabe, Mari Ohnuki, Megumi Narita, Tomoko Ichisaka, Kiichiro Tomoda, and Shinya Yamanaka. 2007. "Induction of Pluripotent Stem Cells from Adult Human Fibroblasts by Defined Factors." *Cell* 131 (5): 861–72. https://doi.org/10.1016/j.cell.2007.11.019.

Theka, Ilda, Massimiliano Caiazzo, Elena Dvoretskova, Damiana Leo, Federica Ungaro, Sebastiano Curreli, Francesca Managò, et al. 2013. "Rapid Generation of Functional Dopaminergic Neurons From Human Induced Pluripotent Stem Cells Through a Single-Step Procedure Using Cell Lineage Transcription Factors." *STEM*

CELLS Translational Medicine 2 (6): 473–79. https://doi.org/10.5966/sctm.2012-0133.

Traub, Stefanie, Heiko Stahl, Holger Rosenbrock, Eric Simon, and Ralf Heilker. 2017. “Upscaling of HiPS Cell-Derived Neurons for High-Throughput Screening.” *SLAS Discovery* 22 (3): 274–86. https://doi.org/10.1177/1087057116678161.

Trimmer, James S., and Kenneth J. Rhodes. 2004. “Localization of Voltage-Gated Ion Channels in Mammalian Brain.” *Annual Review of Physiology* 66 (1): 477–519. https://doi.org/10.1146/annurev.physiol.66.032102.113328.

Turrigiano, Gina. 2011. “Too Many Cooks? Intrinsic and Synaptic Homeostatic Mechanisms in Cortical Circuit Refinement.” *Annual Review of Neuroscience* 34: 89–103. https://doi.org/10.1146/annurev-neuro-060909-153238.

Vadodaria, Krishna C., Yuan Ji, Michelle Skime, Apua C. Paquola, Timothy Nelson, Daniel Hall-Flavin, Kelly J. Heard, et al. 2019. “Altered Serotonergic Circuitry in SSRI-Resistant Major Depressive Disorder Patient-Derived Neurons.” *Molecular Psychiatry* 24 (6): 808–18. https://doi.org/10.1038/s41380-019-0377-5.

Volkers, Linda, Kristopher M. Kahlig, Nienke E. Verbeek, Joost H.G. Das, Marjan J.A. van Kempen, Hans Stroink, Paul Augustijn, et al. 2011. “Na v1.1 Dysfunction in Genetic Epilepsy with Febrile Seizures-plus or Dravet Syndrome.” *European Journal of Neuroscience* 34 (8): 1268–75. https://doi.org/10.1111/j.1460-9568.2011.07826.x.

Wang, Wenze, Sachio Takashima, Yoshie Segawa, Masayuki Itoh,

Xiuyu Shi, Su Kyeong Hwang, Kazuki Nabeshima, Morishige Takeshita, and Shinichi Hirose. 2011. “The Developmental Changes of Nav1.1 and Nav1.2 Expression in the Human Hippocampus and Temporal Lobe.” *Brain Research* 1389: 61–70. https://doi.org/10.1016/j.brainres.2011.02.083.

William A. Catterall. 1980. “NEUROTOXINS THAT ACT ON VOLTAGE-SENSITIVE SODIUM CHANNELS IN EXCITABLE MEMBRANES,” 15–43.

———. 2000. “From Ionic Currents to Molecular Review Mechanisms: The Structure and Function of Voltage-Gated Sodium Channels.” *Neuron* 26: 13–25. https://www.cell.com/neuron/pdf/S0896-6273(00)81133-2.pdf.

Wilson, Stephen W., and John L.R. Rubenstein. 2000. “Induction and Dorsoventral Patterning of the Telencephalon.” *Neuron* 28 (3): 641–51. https://doi.org/10.1016/S0896-6273(00)00171-9.

Wulff, Heike, Neil A. Castle, and Luis A. Pardo. 2009. “Voltage-Gated Potassium Channels as Therapeutic Targets.” *Nature Reviews Drug Discovery* 8 (12): 982–1001. https://doi.org/10.1038/nrd2983.

Xie, Yunyao, Nathan N. Ng, Olga S. Safrina, Carmen M. Ramos, Kevin C. Ess, Philip H. Schwartz, Martin A. Smith, and Diane K. O’Dowd. 2020. “Comparisons of Dual Isogenic Human IPSC Pairs Identify Functional Alterations Directly Caused by an Epilepsy Associated SCN1A Mutation.” *Neurobiology of Disease* 134 (July 2019): 104627. https://doi.org/10.1016/j.nbd.2019.104627.

Xu, Chong Chong, Kyle R. Denton, Zhi Bo Wang, Xiaoqing Zhang, and Xue Jun Li. 2016. “Abnormal Mitochondrial Transport and

Morphology as Early Pathological Changes in Human Models of Spinal Muscular Atrophy." *DMM Disease Models and Mechanisms* 9 (1): 39–49. https://doi.org/10.1242/dmm.021766.

Yang, Nan, Soham Chanda, Samuele Marro, Yi-Han Ng, Justyna A Janas, Daniel Haag, Cheen Euong Ang, et al. 2017. "Generation of Pure GABAergic Neurons by Transcription Factor Programming" 14 (6): 621–28. https://doi.org/10.1038/nmeth.4291.

Yu, Frank H., Massimo Mantegazza, Ruth E. Westenbroek, Carol A. Robbins, Franck Kalume, Kimberly A. Burton, William J. Spain, G. Stanley McKnight, Todd Scheuer, and William A. Catterall. 2006. "Reduced Sodium Current in GABAergic Interneurons in a Mouse Model of Severe Myoclonic Epilepsy in Infancy." *Nature Neuroscience* 9 (9): 1142–49. https://doi.org/10.1038/nn1754.

Yu, Junying, Maxim A. Vodyanik, Kim Smuga-Otto, Jessica Antosiewicz-Bourget, Jennifer L. Frane, Shulan Tian, Jeff Nie, et al. 2007. "Induced Pluripotent Stem Cell Lines Derived from Human Somatic Cells." *Science* 318 (5858): 1917–20. https://doi.org/10.1126/science.1151526.

Zahir, Tasneem, Ying Fang Chen, John F. MacDonald, Nic Leipzig, Charles H. Tator, and Molly S. Shoichet. 2009. "Neural Stem/Progenitor Cells Differentiate in Vitro to Neurons by the Combined Action of Dibutyryl CAMP and Interferon-γ." *Stem Cells and Development* 18 (10): 1423–32. https://doi.org/10.1089/scd.2008.0412.

Zhang, Yingsha, Changhui Pak, Yan Han, Henrik Ahlenius, Zhenjie Zhang, Soham Chanda, Samuele Marro, et al. 2013. "Rapid Single-Step Induction of Functional Neurons from Human

Pluripotent Stem Cells" 78 (5): 785–98. https://doi.org/10.1016/j.neuron.2013.05.029.

Zuberi, S. M., L. H. Eunson, A. Spauschus, R. De Silva, J. Tolmie, N. W. Wood, R. C. McWilliam, J. P.B. Stephenson, D. M. Kullmann, and M. G. Hanna. 1999. "A Novel Mutation in the Human Voltage-Gated Potassium Channel Gene (Kv1.1) Associates with Episodic Ataxia Type 1 and Sometimes with Partial Epilepsy." *Brain* 122 (5): 817–25. https://doi.org/10.1093/brain/122.5.817.

CHAPTER 2

Human induced pluripotent stem cells differentiation in neuronal subtypes to model Dravet Syndrome

Ricci Raffaele[1,2], Rubio Alicia[2,3], Brusco Simone[2,3], Massimino Luca[2], Di Resta Chiara[4], Lignani Gabriele[5], Guerrini Renzo[6], Broccoli Vania[2,3] and Colasante Gaia[2]

1 University of Milano-Bicocca, DIMET PhD program, Milan, Italy; 2 Stem cell and Neurogenesis Unit, Division of Neuroscience, San Raffaele Scientific Institute, Milan, Italy; 3 CNR Institute of Neuroscience, Milan, Italy; 4 Vita-Salute San Raffaele University, Milan, Italy 5 Department of Clinical and Experimental Epilepsy, UCL Institute of Neurology, University College London, United Kingdom; 6 Pediatric Neurology, Neurogenetics and Neurobiology Unit and Laboratories, A. Meyer Children's Hospital, University of Florence, Florence, Italy

Unpublished work

Acronyms and abbreviations

AAV: adeno-associated virus

AP: action potential

CRISPR: clustered regularly interspaced short palindromic repeats

dNPCs: dorsal neural progenitor cells

CB: calbindin

CR: calretinin

dbcAMP: dibutyryl cyclic adenosine monophosphate

DS: Dravet Syndrome

EBs: embryoid bodies

EXX: embryonic day XX

ExNs: excitatory neurons

GEFS+: genetic epilepsy with febrile seizure plus

GINs: GABAergic interneurons

hCS: human cortical spheroids

HDR: homology directed repair

hESC: human embryonic stem cell

hSS: human subpallium spheroids

HuNu: human nuclei

IF: immunofluorescence

I_{Na}: sodium current

iNS: induced neurons

iPSCs: induced pluripotent stem cells

ISCN: international system for human cytogenetic nomenclature

LV: lentivirus

MGE: medial ganglionic eminences

NGS: NOD scid gamma mouse

NMD: nonsense-mediated decay

NPCs: neural progenitor cells

PBS: phosphate-buffered saline

PFA: paraformaldehyde

PV: parvalbumin

PXX: postnatal day XX

sgRNA: small guide RNA

SHH: Sonic Hedgehog

SMEI: severe myoclonic epilepsy in infancy

SST: somatostatin

SUDEP: sudden unexpected death in epilepsy

TALEN: transcription activator-like effector nucleases

TSS: transcription start site

VIP: vasoactive intestinal peptide

vNPCs: ventral neural progenitor cells

VPR: VP64-p65-Rta

Introduction

Dravet syndrome (DS) is a catastrophic developmental and epileptic encephalopathy characterized by severe, pharmaco-resistant seizures and high risk of Sudden Unexpected Death in Epilepsy (SUDEP). To date, no cure is effective in controlling seizures. About 80% of the patients show heterozygous mutations in *SCN1A* gene. Most mutations are *de novo*, although familial missense mutations occur in 5–10% of cases (Marini et al. 2011). Mutations can affect different regions of the gene and they can be classified into three groups: truncating mutations (40%), missense mutations (40%) and splicing-site changes (20%) (Marini et al. 2011). Considering all mutations reported, over than 1000 variants of $Na_v1.1$ protein have been identified (http://www.scn1a.net/).

Although some gain-of-function mutations have been reported (Lossin et al. 2003; Ohmori et al. 2006; Volkers et al. 2011), most of *SCN1A* mutations are loss-of-function, suggesting that the haploinsufficiency of *SCN1A* is pathogenic (Ragsdale 2008; Catterall, Kalume, and Oakley 2010; Escayg and Goldin 2010).

SCN1A gene encodes for the alpha-subunit of the voltage-gated sodium channel $Na_v1.1$.

The development and analysis of the first DS animal model highlighted that $Na_v1.1$ is essential for excitability of GABAergic interneurons (GINs) (Yu et al. 2006; Ogiwara et al. 2007; Martin et al. 2010; Cheah et al. 2012; Rubinstein, Westenbroek, et al. 2015). In particular, the haploinsufficiency of the channel impairs

action potential (AP) generation in parvalbumin (PV)+, somatostatin (SST)+, and vasoactive intestinal peptide (VIP)+ interneurons subtypes (Ogiwara et al. 2007; Dutton et al. 2013; Tai et al. 2014; Rubinstein, Han, et al. 2015; De Stasi et al. 2016; Goff and Goldberg 2019), and this probably underlies seizure development.

However, reduced function of GINs has been shown to be transient in mice, limited only to the severe stage (Favero et al. 2018; Tran et al. 2020), suggesting that complex mechanisms govern the pre-epileptic and stabilization stages of DS. Moreover, another study showed hyperexcitable excitatory neurons (ExNs) in DS mice, suggesting an involvement of this neuronal subtype in Dravet pathogenesis (Mistry et al. 2014). More recently, Almog and colleagues, focusing on evoked synaptic activity within the hippocampal CA1 microcircuit, revealed impairments in GINs functionality at all different stages of Dravet, with the greatest worsening at the severe stage (Almog et al. 2021). Then, by analysing pyramidal neurons, they found an hyperexcitability at the pre-epileptic stage, followed by a reduction in their activity at the onset of seizures. With these data they highlighted the presence of complex and reciprocal alterations in neuronal function, regarding both GINs and ExNs.

In the last years, also human models of the disease have been generated either by direct conversion of DS patient fibroblasts to induced neurons (iNs) (Jiao et al. 2013), or by differentiation of DS patient-derived induced pluripotent stem cells (iPSCs) to iNs

(Higurashi et al. 2013; Y. Liu et al. 2013; J. Liu et al. 2016; Sun et al. 2016; Kim et al. 2018; Xie et al. 2020).

The first works have shown different data reporting in some cases alterations in patient iPSC-derived GINs, as impairment of AP firing and reduction of sodium current density, while in others the ExNs were the subtypes most affected, displaying hyperexcitability with an increase in sodium current amplitudes (Higurashi et al. 2013; Jiao et al. 2013; Sun et al. 2016). Furthermore, an additional work came out in 2013 reporting an hyperexcitability state in both neuronal subtypes, GINs and ExNs (Y. Liu et al. 2013). Later, some papers were published by introducing the importance of isogenic controls in the setting of a DS human model (J. Liu et al. 2016; Xie et al. 2020). However, also in these cases, it was not possible to determine a clear DS phenotype, considering that these works reported different data, from one side ascribing to GINs the most important role in the etiology of the pathology, and from the other, reporting a mild hyperexcitable phenotype only in ExNs. All these studies lead to different conclusions about DS human modeling. The precise reason for all this variety is unclear but, considering that $Na_v1.1$ is expressed in a postnatal stage during development (Trimmer and Rhodes 2004; W. Wang et al. 2011), the problem could be related to the neuronal maturation state. Neurons derived from iPSCs *in vitro* always generate cultures composed of neurons presenting different states of maturation, and data derived from these heterogeneous cultures can lead to more complicated and altered analysis. Furthermore, in all published works the authors

generated GINs without detecting PV+ and SST+ neurons in their neuronal cultures, which are the most affected neuronal subtypes.

For these reasons, the generation of a more reliable human model of DS is necessary. Therefore, we focused the first part of our work on setting up a proper 2D neuronal differentiation protocol that can include PV+ and SST+ interneurons.

Then, considering the limitation of 2D models, which cannot reproduce the anatomy or physiology of a tissue for informative studies, we also tried to set a 3D DS human model, by using a protocol recently published (Birey et al. 2017), which allows to generate different spheroids resembling cortical and subpallium region of forebrain including different neuronal subtypes. By fusing these spheroids together, it is possible to study the 3D interactions between human GABAergic and glutamatergic neurons and to verify if alterations in these contacts could emerge in DS.

In the meantime, we also derived iPSCs from two patients with different missense mutations, C959S and Y1781H. We used CRISPR-Cas9 technology to produce isogenic control iPSC lines and differentiate these cells into GINs and ExNs, choosing the best differentiation protocol. Hereafter, we analized the electrophysiological properties of DS neurons compared to isogenic controls. Considering the maximal AP firing, patients' GINs revealed a trend of hypoexcitability compared to isogenic control even if not statistically significant. ExNs analysis

displayed a hyperexcitable state in patient 1 neurons compared to its control, while patient 2 didn't report any alteration in AP firing. The amount of sodium current in GINs and ExNs didn't change in any case between pairs.

Then, considering the importance of the neurons' maturation state to generate a proper DS human model, we established the setting to explore the functionality of neurons presenting two different conditions of maturation. First, we treated our neurons *in vitro* with a medium able to promote neuronal activity (BrainPhys medium). Secondly, we injected neural progenitor cells (NPCs) into immunodeficient mice brain, in order to set the basis for future experiments to evaluate the maturation state of human neurons transplanted and integrated into mouse circuits.

At last, given the interesting data obtained in our laboratory by using the activatory CRISPR-dCas9 system to revert DS phenotype, both *in vitro* and *in vivo,* in a DS mouse model (Colasante et al. 2019), we explored and demonstrated the efficacy of this system in inducing human *SCN1A* gene upregulation, in both cell line and hiPSC-derived neurons.

Results

Generation of iPSCs-derived neuronal culture including GINs

$Na_v1.1$ is mostly expressed in GINs (Yu et al. 2006; Sun et al. 2016), which indeed are the most affected neurons in DS (Yu et al. 2006; Martin et al. 2010; Cheah et al. 2012). For this reason, to generate a human model of the disease, we first worked to optimize an existing differentiation protocol that allows the generation of medial ganglionic eminences (MGE)-derived neuronal progenitors and neurons (Meganathan et al. 2017). This protocol consists of a multi-stage small molecules approach (Figure 1A), including the intermediate generation of embryoid bodies (EBs), neural rosettes and NPCs. The dual inhibition of SMAD signaling, important to efficiently induce neural conversion (Chambers et al. 2009), has been performed by using LDN-193189 (Stemgent) and SB431542 (Sigma-Aldrich) molecules. The tankyrase inhibitor, XAV939, inhibitor of WNT signaling (Huang et al. 2009), was added to enhance forebrain neurons generation (Maroof et al. 2013). By adding the continuous exposure to purmorphamine, a Sonic Hedgehog (SHH) agonist, it was possible to ventralize the cell culture towards inhibitory neurons' progenitor fate.

However, by testing Meganathan's conditions we had some problems. First of all, as a consequence of prolonged treatment with purmorphamine, we often reported the synthesis of purmorphamine crystals in our cell culture from around day 20-

30 of differentiation, which were toxic for neurons, inducing neuronal clumps and early cell death. Secondly, to obtain similar percentage of neuronal populations as published, we had to wait longer period, and however, by performing immunofluorescence (IF) analysis on our cultures after 50 days of differentiation (Figure 1B), we found around 40% of glutamatergic neurons, expressing vGLUT1, and 60% of GINs, including SST+ (20%), Calretinin(CR)+ (60%) and Calbindin(CB)+ (50%) with the lack of PV+ interneurons (Figure 1C). Considering the importance of PV+ neurons for our work, and also taking into account that PV+ neurons generation occurs later during neurodevelopment (Uylings et al. 2002), we wanted to try to extend the period of differentiation, but the synthesis of toxic crystals mentioned above hampered us. For this reason, a part of our work aimed towards reducing cells exposure time to purmorphamine, to obtain comparable results in terms of GINs percentage including SST+ and PV+ interneurons. By using a control iPSC line, previously characterized in our laboratory, we decided to test reduced time windows of exposure, taking the inspiration from another paper already published (Maroof et al. 2013) in which the treatment with purmorphamine and SHH was tested with different concentrations and time windows. For our experiments, we selected two different time windows to administer purmorphamine in acute condition, either from day 10 to day 18, or from day 10 to day 25, covering neural rosettes step partially or completely (Figure 2A). Additionally, the long exposure condition, reported by Meganathan and colleagues, was used as

positive control of the ventralization, and the condition “no purmorphamine” was used as negative control for this process. In order to test the protocol efficiency in inducing MGE fate, we started to verify by IF the expression of NKX2.1, a marker of ventral NPCs (vNPCs) (Sussel et al. 1999; Xu et al. 2004; Butt et al. 2008) (Figure 2B). We observed that on day 25 all the conditions except “no purmorphamine” showed around 80% NKX2.1+ cells counted on nuclei (Figure 2C). To complete this data, we also studied PAX6 expression, a marker of dorsal NPCs (dNPCs) (Molyneaux et al. 2007) (Figure 2B). The observed percentage of PAX6+ cells on nuclei was higher in cultures not treated with purmorphamine (~80%), but it strongly decreased in the presence of the ventralizing molecule (~20%) (Figure 2D). The acquired ventralization of the culture was also demonstrated by qRT-PCR data (Figure 3A-B). Ventral neural progenitor’s marker genes, as *NKX2.1*, *DLX5*, *LHX6* (Panganiban and Rubenstein 2002; Liodis et al. 2007; Fogarty et al. 2007; Butt et al. 2008), were overexpressed in all conditions with purmorphamine treatment (Figure 3A), on the contrary, some dorsal neural progenitor’s marker genes, such as *PAX6*, *TBR2*, *VGLUT1* (Molyneaux et al. 2007), expressed in the “No purmorphamine” condition, were downregulated in all ventralized samples (Figure 3B).

Then, we completed the differentiation by plating the NPCs in the neural differentiation medium containing components important to induce final neuronal differentiation as ascorbic acid, BDNF and the γ-secretase inhibitor DAPT (Shin et al. 2004; Traub et al.

2017; Chen et al. 2018). For the final medium, DAPT was substituted with dibutyryl cyclic adenosine monophosphate (dbcAMP), important to induce neuronal functionality (Zahir et al. 2009). By IF analysis we studied the percentage of obtained GINs after 50 (Figure 4A-B) and 90 days of differentiation (Figure 5A-B). We quantified around 60% of GINs in all samples treated with purmorphamine, compared to 30-40% revealed in the no purmorphamine condition. This percentage remained stable between these two time points. We also quantified the presence of SST+ and PV+ subtypes. Some SST+ interneurons appeared after 50 days of differentiation (Figure 6A). We confirmed the 20% already obtained by using Meganathan's protocol in the condition with long exposure to purmorphamine, while we revealed a very low percentage (<5%) in all other conditions (Figure 6B). On day 90, SST+ cells reached ~12% in the conditions providing short treatment with purmorphamine, ~7% in the not treated condition, and slightly decreased in the long exposure condition, reaching ~17% (Figure 7A-B). In this last condition we often reported a lot of neuronal clumps, as sign of cell culture suffering, and neuronal death. Few PV+ interneurons appeared in all conditions only after 90 days of differentiation (Figure 8). Given the very low number we obtained per coverslip, we didn't quantify this data.

To complete the characterization of our neuronal cultures, we also analized by qRT-PCR the expression of some voltage-gated Na^+ channels important for neuronal activity and associated with epilepsy (J. Wang, Ou, and Wang 2017; Gu et al. 2018) after 50

and 90 days of differentiation, in all conditions (Figure 9A-B). Among all channels, only *SCN1A* gene expression showed significant changes between these two timepoints, displaying a 3-fold increase on day 90 compared to day 50, for no purmorphamine and purmorphamine day 10-18 protocols, and 2-fold increase in purmorphamine day 10-25 condition (Figure 9C).

We also studied by qRT-PCR the expression of some voltage-gated K^+ channels, essential for the repolarization phase after the AP (Gu et al. 2018; Rudy and McBain 2001), at the same time points, but their expression didn't change significantly leaving neurons in culture for a longer period (Figure 9D-E).

Then, considering our interest in obtaining functional GINs including SST+ and PV+ subtypes, which also express high level of *SCN1A* gene, we decided to perform all electrophysiological experiment by using the protocol with the shortest ventralization treatment (from day 10 to day 18) and to perform the analysis after 90 days of differentiation.

3D modeling to study the interaction between GINs and cortical neurons

In recent years, the potential of organoids to complement existing model systems and extend basic biological research, is becoming more and more widely appreciated. However, the development of this tool is still at the beginning in comparison to established cell lines or animal models, with different challenges

still to overcome. Anyway, different groups have obtained interesting results by using organoids to model genetic and infectious diseases or different types of cancer (Gao et al. 2014; Dang et al. 2016; Jacob et al. 2020; Banfi et al. 2021). Furthermore, long-term culture of human brain organoids could allow to obtain enhanced neuronal maturation, characterized by the presence of dendritic spine-like structures, which have been difficult to generate with an *in vitro* directed differentiation (Quadrato et al. 2017).

For our work, we decided to explore 3D modelling to test long-term culture-derived neuronal maturation with functional analysis and to verify if any alteration in the 3D interaction between GINs and cortical neurons can occur in DS. For this reason, by using a protocol recently published (Birey et al. 2017), we tried to generate human cortical (hCS) and subpallium spheroids (hSS), to be fused after specification.

Birey's protocol is similar to protocols used to generate 2D neuronal cultures which present the intermediate state of EBs (Figure 10A). Also, the small molecules used are largely the same. Two inhibitors of SMAD signaling are used to induce neuralization (Chambers et al. 2009), Dorsomorphin (Sigma-Aldrich) and SB431542 (Sigma-Aldrich). Then, a period of cell proliferation is induced by treating spheroids with the growth factors FGF2 (R&D Systems) and EGF (R&D Systems). To specify spheroids resembling the ventral forebrain or the

subpallium, they are exposed to IWP-2 (Sellekkem), that inhibit WNT pathway, and SAG (Selleckchem), a SHH agonist.

From day 40 we confirmed by IF the different specification of hCS, characterized by large expression of dNPCs markers SATB2 and TBR1 (Molyneaux et al. 2007)(Figure 10B), and hSS, distinguished for the expression of NKX2.1 vNPCs marker (Sussel et al. 1999; Xu et al. 2004; Butt et al. 2008)(Figure 10C). From day 90 we also observed an enrichment of GINs in hSSs, including SST+ and PV+ subtypes (Figure 11). At this point, once confirmed in our hand the efficiency of Birey's protocol (Birey et al. 2017) to generate distinct spheroids including excitatory and inhibitory neurons, we proceeded by fusing them to obtain full brain spheroids to firstly perform functional experiments.

Generation of DS patient iPSCs and isogenic controls with CRISPR/Cas9 technology

To generate a human model of DS, primary fibroblasts were derived from skin biopsies obtained from two DS affected kids and were reprogrammed into iPSC lines using the non-integrating Sendai virus (Figure 12A). Patients showed two different point mutations in heterozygous condition on *SCN1A* gene: the first patient had a cysteine (C) to serine (S) substitution in domain 2, position 959 (C959S), while the second presented a tyrosine (Y) to histidine (H) substitution in domain 4, position 1781 (Y1781H) (Figure 12A). To verify the presence of the mutations mentioned above, a 500 bp region including each

mutation was amplified by PCR by using DNA extracted from fibroblasts (data not shown) and iPSC lines and sequenced (Sanger sequencing) (Figure 12A). To minimize uncontrolled genetic or epigenetic variability due to interindividual differences we used CRISPR/Cas9 gene editing tool to perform gene correction on patients' derived iPSCs. Two different strategies have been employed (Figure 12B): spCas9 with NGG PAM site, and spCas9 VQR with NGA PAM site, for patient 1 and patient 2 respectively. In order to specifically target the mutated allele, the selected small guide RNA (sgRNA) included the patients' point mutation. In both cases a single-stranded oligodeoxynucleotide donor template has been used to induce homology directed repair (HDR) after the double strand break induced by the Cas9 protein. To recognize recombinant isogenic clones, a silent point mutation close to the cutting site was inserted in the single stranded oligodeoxynucleotide, without altering the amino acid sequence. One isogenic clone per patient was selected and its genotype was confirmed by sanger sequencing (Figure 12B).

Subsequently, the four obtained iPSC lines underwent equivalent quality control procedures, including checking of maintenance of a normal euploid karyotype over several passages *in vitro* (Figure S1) and assessment of crucial pluripotency markers expression, such as TRA1-60, OCT-4 and SOX2, that they showed in a homogeneous and comparable manner (Figure 13). To demonstrate the multilineage differentiation capacity of all cell lines, a spontaneous differentiation in 10% FBS medium was performed. The expression of markers belonging to endoderm,

mesoderm and ectoderm, respectively FOXA2, SMA and TUJ1, were verified by IF (Figure 14).

Potential off-target sites with 1 or 2 mismatch respects to sgRNAs sequences, were evaluated by amplifying these regions by PCR, and sequencing the products (Figure S2A-B). There were no off-target mutations in candidate genes in the corrected patient lines.

Electrophysiological characterization of DS patient iPSC-derived GINs

In order to identify GINs during live recording, we transduced control neurons with a lentivirus (LV) containing TdTomato fluorescence protein under the control of a mouse Dlx5/6 enhancer region (Figure 15A), which has been shown to reliably deliver reporter genes in GINs (Dimidschstein et al. 2016). The efficiency of this reporter was confirmed in our hands by performing IF analysis to reveal neurons stained positive for GABA signal and counting GABA and TdTomato double positive cells over the TdTomato+ cells, obtaining ~70% of colocalization (Figure 15B-C).

Next, in 3D condition, we transduced control hSSs with our LV GABAergic reporter and proceeded to the fusion of hCSs and transduced hSSs from day 70 (Figure 15D). To verify if after the fusion fluorescent migrated GINs could be found into the hCS, we analized the site of interaction between spheroids by IF at

different timepoints (Figure 15E). In this way, we could confirm the capacity of GINs to migrate from hSS to hCS and, considering that from day 120 of differentiation we found scattered TdTomato+ cells in hCSs (Figure 15E), we proceeded from this time point to test their functionality by patch clamp to verify their level of maturation before focusing on further experiments. However, patched cells resulted very immature, also after 6 months in culture (data not shown), and not adapted to perform experiments aiming to reveal a DS phenotype. For this reason, all other functional experiments aiming to generate a human DS model were performed by using neurons growth in 2D condition.

Then, to examine the electrophysiological properties of patient-derived neurons and isogenic controls in 2D condition, we differentiated all iPSC lines by using the protocol mentioned above with purmorphamine exposure from day 10 to day 18 and we demonstrated that all cell lines were able to generate GINs with comparable efficiency (~70%) (Figure 16A-B). Also we introduced the transduction of all NPCs with our LV GABAergic reporter.

Next, cultures were visualized with fluorescent lamps to identify and record DLX5/6-positive GINs. As previously established, we conducted current-clamp experiments on cells differentiated for 90 days, considering also that neurons analized at earlier time points produced unreliable responses, suggesting a not complete maturation. For our electrophysiological analysis we

selected neurons presenting the following conditions: (1) clear DLX5/6-TdTomato fluorescence; (2) mature neuronal morphology with a large cell body and prolonged neurites; (3) resting membrane potential at −30 mV or more negative.

Following these criteria, we examined neurons of all groups and we found no difference in both active and passive cell properties (Figure S3). We then determined the input–output relationship using sustained 500-ms injections of depolarizing current steps to induce AP (Figure 17B,E). No differences were highlighted between Dravet conditions and isogenic controls (n=13 Isogenic Pat 1, n=11 Patient 1, ns p = 0,5989; n=5 Isogenic Pat 2, n=6 Patient 2, ns p = 0,1303, Two-way ANOVA,), even if we revealed a trend of reduction in the mean of maximal number of evoked APs in patients' neurons compared with controls' (Figure 17C,F) (n=13 Isogenic Pat 1, n=11 Patient 1, ns p = 0,1816; n=5 Isogenic Pat 1, n=6 Patient 1, ns p = 0,3371 t-test).

Then, we analyzed the voltage-dependent Na^+ currents (I_{Na}) and we detected no difference in peak sodium current density between patients and isogenic controls (Figure 17H,J).

Functional properties of DS patients iPSCs-derived ExNs

Previous studies in mouse models and iPSCs showed that *SCN1A* mutations induce alterations in GINs functionality (Yu et al. 2006; Martin et al. 2010; Hedrich et al. 2014; Sun et al. 2016). Nevertheless, other works reported different mutations affecting

both GINs and ExNs (Jiao et al. 2013; Y. Liu et al. 2013; Mistry et al. 2014; Almog et al. 2021). To verify if a phenotypic alteration emerged between our DS patients and controls derived ExNs, we generated them by using a protocol, already published, based on a combined small molecules treatment (Qi et al. 2017), with the addition of a LV transduction with one inducible transcriptional factor, Ngn2, capable alone to induce cortical neurons differentiation in iPSCs (Zhang et al. 2013) (Figure 18A). After 5 weeks of differentiation, once obtained cortical neuronal cultures, we proceeded with electrophysiological characterization.

First of all, we assessed excitability of Dravet and isogenic control neurons in response to increasing amplitude 500ms current step injection (Figure 18C,F). The input-output curve showed an increase in the ability of patient 1 derived cortical neurons to sustain repetitive firing (n=12 Isogenic Pat 1, n=17 Patient 1, * p = 0,0414 Two-way ANOVA). This hyperexcitable phenotype was also confirmed by analysing the maximal AP frequency (Figure 18D), revealing higher values in patient's ExNs compared to isogenic control (n=12 Isogenic Pat 1, n=17 Patient 1, * p = 0,0360, t-test). A different condition was shown for the second pair; indeed, patient 2 and isogenic control cortical neurons revealed the same capacity to sustain repetitive firing (Figure 18F) and comparable values for maximal AP frequency (Figure 18G). No differences were detected in AP threshold or amplitude between both pairs (Figure S4).

When we analized I_{Na}, we detected no difference in peak sodium current density between the two experimental conditions (Figure 18I,K).

How to improve neuronal maturation?

iPSC-derived neuronal cultures are always composed by a heterogeneous population of neurons with different maturation stages. Unfortunately, within the mixed population, the majority of neurons present cell properties resembling fetal neurons. For this reason, we decided to test in parallel two different conditions of maturation, aiming to obtain cells that could likely present a higher expression of $Na_v1.1$ protein channel with the potential to generate a human model of DS.

From one side, we decided to introduce in our differentiation protocol a specific neuronal commercially available medium, BrainPhys medium (Stem Cell Technologies). It is reported that it promotes neuronal activity by helping neuronal maturation. As a pilot study, we differentiated one pair of iPSC lines into GINs by using the protocol with purmorphamine exposure from day 10 to day 18 and we introduced the treatment to our cells with BrainPhys medium from day 31 on instead of the usual neuronal differentiation medium (Figure 19A). After two months of differentiation in BrainPhys medium, we analized the functionality of our neurons by using the same criteria mentioned above. This study led to different results. The ability of patient 1 derived neurons to sustain repetitive firing wasn't statistically different

compared to isogenic control (Figure 19C) (n=10 Isogenic Pat 1, n=9 Patient 1, ns p = 0,3393, Two-way ANOVA), but by considering the maximal AP frequency (Figure 19D), a significant decrease in patient values compared to isogenic control was highlighted (n=10 Isogenic Pat 1, n=9 Patient 1, ** p = 0,0087, t-test). Essentially, the trend towards reduction, observed in this case in patient GINs only at high intensity stimulation, aligns with the significant decrease in the maximal AP firing frequency revealing a mild DS phenotype.

Next, we analized the I_{Na} in Dravet and control cells (Figure 19F). No difference in peak Na^+ current density was detected between the two experimental groups.

In parallel, we also harvested some cells for RNA extraction, and we analized by qRT-PCR the expression of *SCN1A* gene, together with some activity-dependent genes reported to be important markers of neuronal maturation: *NPAS4*, *FOS*, *EGR1* and *DHCR7* (Boulting et al. 2021). By comparing DCT values of these genes obtained from neurons treated with the usual medium and BrainPhys medium, we revealed no changes in *SCN1A* gene expression, but a trend of overexpression was reported for all other genes (Figure 19G) in BrainPhys medium treated neurons, suggesting an increase in the maturation state.

On the other side, we wanted to explore the possibility to perform functional assays on human neurons transplanted into mouse brain and integrated, to characterize their maturation state. Indeed, several works reported that human neurons can

integrate efficiently into mouse circuits (Zhang et al. 2013; Qi et al. 2017; Meganathan et al. 2017). Also, a recent work reported that human transplanted GINs could help to ameliorate symptoms related to seizures in a mouse model of temporal lobe epilepsy (Cunningham et al. 2014). Moreover, for our aim, assuming to select for functional studies only migrated and integrated cells among all injected, we could select only the ones displaying an active response to transplantation, which could possibly display the best maturation condition compared to the others.

To achieve this aim, we performed pilot experiments to derive vNPCs, from a control iPSC line, to inject into immunodeficient mice brain. More specifically, during neuronal differentiation, after the usual detachment performed on day 25, we transduced in suspension our vNPCs with the LV GABAergic reporter and injected them in postnatal day(P)30 mice. Then, we verified the presence of human cells in the mouse brain one month after the injection by performing IF for human nuclei (HuNu) (Figure 20A). All cells positive for TdTomato signal stained also positive for the HuNu, indicating that no lentiviral contamination occurred in the mouse brain. According to Cunningham's work, we waited 5 months after the injection to perform further experiments. At this point, we verified that our protocol could induce GINs generation even after vNPCs transplantation by IF analysis to reveal GABA signal (Figure 20B). Then, we observed that ~80% of HuNu+ cells stained double positive for HuNu and NeuN (Figure 20C,D), as a demonstration that human cells neither have lost their

neuronal faith nor formed teratocarcinoma. The majority of the human cells remained in the locus of injection, but we also reported some of them, ~25% that were out of this locus, independently from the distance, trying to integrate into the mouse cortex (Figure 20E,F).

Future experiments will aim to perform patch clamp recording of these migrated human GINs, in order to understand if the environment and the stimuli provided by the mouse brain could ameliorate their maturation, compared to the *in vitro* condition.

Activatory CRISPR-dCas9 to upregulate *SCN1A* gene expression

Besides exploring different strategies to optimize DS modelling, we explored the efficiency of activatory CRISPR-dCas9 in upregulating the expression of *SCN1A* gene. Considering that several works highlighted that dCas9 activation system works better in upregulating the gene of interest if the sgRNAs sequences are localized within 500 bp from the gene transcription start site (TSS) (Cheng et al. 2013; Maeder et al. 2013; Konermann et al. 2015), we firstly looked for *SCN1A* TSS regions. Three different TSSs were previously identified (Martin et al. 2007) (Figure S6A). To confirm that observation, we performed epigenetic analysis to verify if regions upstream these TSSs could present epigenetic characteristics related to transcription (Figure S6B). The first region, distal from the ATG, displayed two CHIP-seq peaks, one indicating the acetylation of

lysine 27 on histone 3 (H3K27ac) and the other indicating the mono-methylation of lysine 4 on the same histone (H3K4me1), suggesting that this region could work as enhancer region. The second region analized, the intermedial, displayed H3K4me1, tri-methylation on lysine 4 (H3K4me3) and DNase peaks, suggesting a promoter region. At last, the proximal region to ATG didn't report any epigenetic modification important for *SCN1A* gene transcription. However, for our sgRNA screening, we tested all three regions (Figure 21A). These sequences have been submitted to CRISPOR web tool (http://crispor.tefor.net) for sgRNA design. We selected 6 sgRNAs for sequence A and 8 sgRNAs respectively for sequence B and C (Figure 21A). Then we determined whether dCas9 fused to VP160 (dCas9-VP160), a transcriptional activator that carries 10 tandem copies of VP16 (a herpes simplex virus type 1 transcription factor), in association with the selected sgRNAs, was able to upregulate *SCN1A* gene expression in SH-SY5Y neuroblastoma cell line (Figure 21B). All sgRNAs and one control guide, targeting the β-galactosidase bacterial sequence (sgLacZ), were cloned into the pU6 vector containing also the blasticidine resistance gene and individually located in a LV. SH-SY5Y cells were transduced with two LVs, one containing the sgRNA, and the other containing the construct Ef1a-dCas9-VP160-T2A-Puromycine resistance gene. Then, cells were selected by antibiotics treatment and harvested for RNA extraction and qRT-PCR. Two sgRNAs located in the region A, sg2A and sg4A, significantly stimulate *SCN1A* transcription inducing 8-fold increase, and only one sgRNA located in the

region B, sg2B, induces a 28-fold increase compared to sgLacZ (Figure 21C).

Subsequently we proceeded to test our selected sgRNAs on iPSCs-derived human neurons. In order to verify the efficiency of the activatory dCas9 system on GINs, avoiding both the limitations associated to the co-transduction and the toxicity due to high levels of LVs in the culture, we produced single LVs containing the construct sg-dCas9-VP160-T2A-eGFP for each sgRNA we decided to test (sg2A, sg4A, sg2B, sgLacZ). We differentiated iPSCs by using the first protocol we tested on our iPSCs (Meganathan et al. 2017), obtaining neuronal culture enriched in GINs and we transduced neurons at day 26 (Figure 22A). After 50 days of differentiation, we harvested cells for RNA extraction and qRT-PCR analysis. The efficiency of these sgRNAs was confirmed even if with different results. A 4-fold increase was detected by using sg2A and sg4A, and a 10-fold increase was detected by using sg2B (Figure 22B). To verify if the increasing levels of *SCN1A* transcription could also generate a functional effect in our neurons in terms of Na^+ current density, we patched eGFP+ neurons (Figure 22C) transduced with sg2B, comparing them with sgLacZ controls. We detected a significant increase in I_{Na} (Figure 22D), indicating that this approach can be used to upregulate $Na_v1.1$ expression, and possibly to rescue a pathological phenotype in neurons presenting low I_{Na} compared to controls.

Discussion

In this study we established a differentiation protocol which enabled us to generate human neurons, with a high percentage of GINs from iPSCs starting from an already published work (Meganathan et al. 2017). This protocol, which allows to generate GINs through EB, neural rosette and NPC stages, is based on the long exposure of chemical compound purmorphamine, a SHH agonist, in the cell culture. SHH is essential to generate GINs, considering that its pathway is highly activated in their progenitor cells, vNPCs, which arise during neurodevelopment from MGE, in the ventral region of the brain (Wilson and Rubenstein 2000).

We confirmed that purmorphamine is fundamental to induce the expression of genes as *NKX2.1*, *DLX5* or *LHX6,* encoding for transcriptional factors important for GINs fate (Panganiban and Rubenstein 2002; Liodis et al. 2007; Fogarty et al. 2007; Butt et al. 2008). However, long periods of treatment with this molecule could lead to cell toxicity and early cell death. Neuronal functionality is a fundamental variable for our work, and therefore we tried to reduce the purmorphamine exposure to time windows covering parts or the full period of neural rosettes, taking inspiration from other differentiation protocols that indeed identified a strict ventralization time window (Maroof et al. 2013; Nicholas et al. 2013). Thanks to these experiments, we managed to target the proper period to induce NPCs ventralization. Therefore, we were able to obtain a high percentage of NKX2.1+

vNPCs, which also express other ventral neural progenitor marker genes, and are able to generate GINs including some SST+ and PV+ interneurons.

Moreover, we tried to generate cortical and subpallium spheroids by using an already published protocol (Birey et al. 2017), with the intention to create a 3D DS model, which could allow us to perform functional studies on neurons cultured for longer periods compared to the ones derived in 2D condition, and to focus on the 3D interaction between GINs and ExNs in a structure more similar to the brain. However, considering the immature state of GINs migrated in hCSs we revealed by patch clamp after 6 months in culture, we subsequently decide to perform all functional experiments only in 2D cultures.

In parallel, we generated iPSCs from skin fibroblasts of two DS patients carrying C959S and H1781Y missense mutations. With CRISPR-Cas9 gene editing tool we derived isogenic controls for both cell lines. Once characterized all iPSC lines, we performed experiments to set up a 2D DS human model. To achieve it, we differentiated patient-derived iPSCs and isogenic controls into GINs by using our well-established protocol, with the shortest ventralization treatment. To study the specific functionality of GINs we transduced our cells with the LV reporter mDlx5/6-TdTomato, which specifically marks GINs (Dimidschstein et al. 2016). By comparing Dravet and control neurons, we revealed only a trend of hypoexcitability considering the number of maximal APs in response to sustained current injection.

However, considering the amount of Na^+ currents, we didn't detect any alteration in the patient-derived neurons.

An opposite situation appeared when ExNs, derived from the same iPSC lines, were analized by using a protocol matching the best approaches published in literature to generate cortical ExNs (Zhang et al. 2013; Qi et al. 2017). In this case, patient 1-derived neurons appeared more excitable or prone to elicit action potential compared to isogenic control, but even in this case, no differences in the Na^+ current were reported.

Furthermore, not relevant differences were found when we analized the functionality of ExNs derived from the second pair, patient 2 and its isogenic control.

The variability of these results may be associated with $Na_v1.1$ protein expression levels. Indeed, even if we reported good levels of *SCN1A* mRNA, comparable to human cortex mRNA, we didn't detect appreciable level of $Na_v1.1$ protein by western blot analysis, suggesting the existence of post-transcriptional mechanisms controlling protein synthesis and post-transcriptional modification important for cell membrane translocation of the protein. One of them, already known, works physiologically during neurodevelopment to control $Na_v1.1$ and $Na_v1.6$ protein synthesis, avoiding it before birth (Carvill et al. 2018). This mechanism is based on an alternative splicing associated with the insertion of a "poison exon", designated as 20N (N = nonsense) in *Scn1a* and 18N in *Scn8a* mRNA, which lead the transcript to degradation by nonsense-mediated decay

(NMD), preventing the synthesis of these proteins in cells or tissues where they would be toxic.

More recently Voskobiynyk and colleagues analized an already existent RNA-seq dataset of mouse cortex at multiple developmental time points (Yan et al. 2015) and evaluated the expression of *Scn1a* mRNA including or not 20N poison exon (Voskobiynyk et al. 2021). They revealed that ~70% of *Scn1a* transcripts include 20N at embryonic day(E)14.5, but this percentage gradually decreases until values under 10% in P30 mice, remaining minimal for all lifelong. This pattern is inversely correlated with the level of total *Scn1a* mRNA detected, which displays very low levels at E14.5 to reach the maximum levels at P30. They also confirm a similar pattern by analysing the usage of poison exon 18N in *Scn8a*.

These discoveries suggest that poison exons inclusion can represent a normal and precisely regulated mechanism, to ensure that different voltage-gated sodium channels are expressed at the correct time and place in the developing nervous system. This also provides a mechanistic explanation for the time at which clinical features due to deficiency for *SCN1A* or *SCN8A* first become apparent in patients. Indeed, in DS patients the seizure onset can occur as early as 4–6 months of age (Ragona et al. 2010; Wirrell et al. 2017; Cetica et al. 2017), and it is in this period that the percentage of *SCN1A* mRNA displaying the exon 20N inclusion start to decline from 60–80%,

accumulated during embryonic development, to 5–10% (Cardoso-Moreira et al. 2019; Helbig et al. 2021).

Future experiments could be performed by using NMD inhibitors in culture on GINS to verify if these events controlling $Na_v1.1$ synthesis also occur in iPSC-derived human neurons.

Furthermore, $Na_v1.1$ has been reported to be expressed in postnatal stage neurons (Trimmer and Rhodes 2004; W. Wang et al. 2011; Cheah et al. 2013), while iPSC-derived neurons often resemble late fetal neurons (Ardhanareeswaran et al. 2018; Burke et al. 2020). For this reason, it is possible that the I_{Na} we detected in our iNs was not completely controlled by the $Na_v1.1$ channel, but also by other Na^+ channels.

$Na_v1.1$ and $Na_v1.3$ display complementary time course expressions in rats, mice, and humans during neurodevelopment. More in detail, immunoblotting of membrane proteins isolated from wild-type C57Bl/6 mouse cerebral cortex at several time points showed that $Na_v1.3$ channel, which is highly expressed during fetal period, reaches its lowest levels at P21. Conversely, $Na_v1.1$ channel starts to be expressed in the postnatal period, around P20, until P30 (Cheah et al. 2013). In correlation with this data, the susceptibility to thermally induced seizures starts to appear in mouse model of Severe Myoclonic Epilepsy in infancy (SMEI) at P20, with an increase in the frequency of spontaneous seizures and death between P20 to P25 (Oakley et al. 2009). Similar data derived from non-epileptic human post-mortem cerebral cortex (Cheah et al.

2013). $Na_v1.3$ channel displayed the highest levels of expression at birth, decreasing to the lowest levels at 6 months of age. On the contrary, $Na_v1.1$ expression begins at birth, reaching the highest levels at 20 months of age. Between 5 and 6 months of age there is the exact time at which the decrease of $Na_v1.3$ expression crosses the increasing of $Na_v1.1$, and this time point correlates with the time of seizure onset in patients with DS. These data clearly explained why DS onset can appear only in postnatal periods.

Furthermore, considering the complementarity of expression and the similar localization in neuronal cell bodies (Trimmer and Rhodes 2004), $Na_v1.1$ and $Na_v1.3$ channels are thought to perform similar functions. For this reason, considering that our GINs presented high expression levels of *SCN3A* (Figure 9A,B), we reasoned that possibly the majority of the activity we observed could be imputed to $Na_v1.3$, which may be protective against $Na_v1.1$ missense mutations. These considerations point towards interesting future experiments aiming to improve neuronal maturation to obtain iNs possibly resembling postnatal neurons.

Following this idea, we performed pilot experiments to set new maturation conditions to test. Firstly, we introduced BrainPhys medium (Stemcell) in our differentiation protocol. We derived GINs from patient 1 and its isogenic control and we found that BrainPhys treated neurons showed a significant overexpression of some activity-dependent genes (Boulting et al. 2021)

compared to neurons treated with the usual medium, suggesting an advanced state of maturation, even if they didn't change significantly *SCN1A* expression levels. In accordance with this data, by performing functional assays, we could reveal a mild hypoexcitability phenotype in our DS neurons compared to controls analysing the mean of the maximal APs. Future studies could be performed to implement the number of patched cells to verify if this setting of experiments could help us in the generation of a DS human model.

At the same time, we also set the condition to explore the functionality of human neurons transplanted and integrated into immunodeficient mice brain. Indeed, several works reported that human neurons, generated with different protocols, can engraft into mouse cortex, creating synapses and joining to the host circuits (Zhang et al. 2013; Qi et al. 2017; Meganathan et al. 2017). Furthermore, Cunningham and colleagues transplanted human GINs into the brain of a mouse model of temporal lobe epilepsy, showing not only that they can integrate in the mouse cortex, but also that they can positively modulate mouse circuits, inducing an amelioration of the symptoms (Cunningham et al. 2014).

More recently, Linaro and colleagues (Linaro et al. 2019) demonstrated that human embryonic stem cell (hESC)-derived cortical neurons transplanted into mouse brain can reach an advanced stage of spine maturation compared to the one reported in human models of corticogenesis *in vitro,* based on

adherent cultures or organoids (Lancaster and Knoblich, 2014; Di Lullo and Kriegstein, 2017; Astick and Vanderhaeghen, 2018). This data suggests that the host brain could be an advantageous environment for spine morphogenesis and synaptogenesis, denoting by extension that human neurons can reach an advanced state of maturation inside the cytoarchitecture of a mouse brain, which could potentially be associated with a good level of $Na_v1.1$ protein expression, which is the most important maturation parameter for our aims. For this reason, we performed our first injections of control vNPCs, marked with our LV GABAergic reporter, in the hippocampus of P30 NOD scid gamma (NGS) mice. We verified the presence of human cells in mouse brains one month after the injection, by performing IF for HuNu and then, in accordance with Cunningham work (Cunningham et al. 2014), we waited for the right time to verify if neuronal migration and possibly integration occurred. After 5 months from the injection, we confirmed the presence of human cells, which were also positively stained for GABA signal, suggesting that our protocol could generate GINs also *in vivo*. We verified that most of the cells, ~80%, stained also for NEUN, avoiding the possibility that our vNPCs could have generated teratocarcinoma, losing neuronal fate. Most importantly, even if we found the majority of the cells still placed in the site of injection, ~25% of cells moved out of this locus. In the future, we aim to verify the functionality of these migrated neurons, assuming that by selecting these cells among all injected, we could select the ones responding to mouse brain stimuli and

reaching a good maturation state, possibly correlated with higher expression of $Na_v1.1$ compared to neurons cultured *in vitro* in 2D condition.

However, more experiments are required following these two alternative strategies, to try to establish a more reliable DS human model.

In parallel to the generation of the human model of DS, we set an activatory CRISPR-dCas9 approach to up-regulate the human *SCN1A* gene. We previously exploited this strategy in a mouse model of DS (Colasante et al. 2019). We identified an sgRNA, sg1p, which aligns in the proximal promoter of *Scn1a*, that, in association with dCas9 fused to the transcriptional activator VP160, was able to significantly stimulate *Scn1a* expression in cell line and primary neuronal cultures. Then, by using DS primary neuronal cultures as model for our experiment, we found that the dCas9 system was able to increase the total amount of $Na_v1.1$ protein, leading to expression levels comparable to WT mice, and rescue the excitability of mutated GINs. Also, we demonstrated that this system could be efficiently delivered *in vivo* by dual Adeno-associated virus(AAV)-mediated gene transfer in *Scn1a*$^{+/-}$ mice to ameliorate temperature-induced seizures. In the same years, another group explored the activatory CRISPR-dCas9 system in DS by using a different approach (Yamagata et al. 2020). The authors of this work employed a different transcriptional activator fused to the dCas9, VP65-p65-Rta (VPR), and they reported different results,

defining efficacious sgRNAs targeting the distal promoter of the gene. They also used a different way to deliver this system *in vivo*, considering that they crossed DS mice with dCas9VPR mice, while sgRNAs were delivered by systemic AAV injection. Furthermore, they perform preliminary experiments to verify the efficiency of the activatory dCas9 system in a human cell line, indicating some sgRNAs working efficiently in upregulating *SCN1A* gene.

For our work, encouraged by the results we obtained in mouse, to definitely test the efficiency of activatory CRISPR-dCas9 in humans, we isolated three different regions important for *SCN1A* transcription (distal, intermedial and proximal). We screened different sgRNAs to test their efficiency together with dCas9-VP160 in order to upregulate *SCN1A* gene expression in SH-SY5Y neuroblastoma cell line. We found that three different guides, sg2A, sg4A and sg2B, efficiently upregulated *SCN1A* gene expression. The efficiency of these sgRNAs was also confirmed from experiments performed on human GINs. Furthermore, comparing I_{Na} of neurons transduced with sg2B-dCas9-GFP lentiviral construct to neurons transduced with the control, sgLacZ-dCas9-GFP, we reported an increase in the amount of Na^+ current. These results attest that also the human *SCN1A* gene promoter is responsive to transcriptional boost mediated by the activatory CRISPR-dCas9. Furthermore, this data becomes advantageous when a solid DS human model will be established, as it could verify the efficiency of this tool in reverting the pathological phenotype. Overall, these studies may

eventually open the way towards the application of different therapeutic approaches pointing to upregulate the wild type allele of patients as a potential cure.

Material and methods

Fibroblasts reprogramming and maintenance of hiPSCs

Human skin fibroblasts were reprogrammed to pluripotency using CytoTune®-iPS Reprogramming Kit (Invitrogen) following the manufacturer's instructions. iPSC cell lines were maintained in feeder-free conditions in mTeSR1 (Stem Cell Technologies) supplemented with 1% Pen/Strep (Sigma-Aldrich) and seeded on hESC-qualified Matrigel (Corning)-coated six-well plates; cells were fed daily and passaged in cell clumps weekly using Accutase solution (Sigma-Aldrich). iPSCs were used at passages between 25 and 50 for all the subsequent experiments.

CRISPR/Cas9 gene editing on DS iPSCs

sgRNAs were designed using optimized CRISPOR (http://crispor.tefor.net/) to screen for highly selective sgRNAs in the region of interest surrounding patients' mutations. Then, selected sgRNAs (listed in Table 4) were cloned using BsmBI restriction enzyme in the U6-filler-sgRNA scaffold cassette derived from LentiCRISPR v2 (Addgene 52961). This cassette was previously subcloned, as described by Giannelli et al.

(Giannelli et al. 2018), in a lentiviral backbone carrying blasticidin antibiotic resistance under the control of Ef1a core promoter.

iPSCs were co-transfected using Lipofectamine Stem Transfection Reagent (ThermoFisher Scientific) with plasmids carrying mutant version patient-specific sgRNAs and pCAG-Cas9-P2A-PuroR or EF1a-Cas9 VQR-T2A-PuroR together with a 120 bps single stranded oligodeoxynucleotide as a homologous repair template. After a double-antibiotic selection, surviving cells underwent a limiting dilution step to obtain the subsequent formation of single-cell clones, which were then picked and amplified till they reached a sufficient quantity to obtain genomic DNA to perform a PCR. To verify mutations' correction, purified (Wizard SV gel and PCR Clean-Up System, Promega) PCR products, obtained by using primers listed in Table 2, were subjected to Sanger sequencing (GATC Biotech) after the usage of Zero Blunt Topo PCR cloning kit (ThermoFisher Scientific), to clone PCR product of single allele from each iPSCs clone. Genotyping of parental original iPSC lines was performed with the same procedure.

Off-target analysis

The potential off-target sites of both sgRNAs were selected according to online tool: http://crispor.tefor.net. In brief, we chose off-target hits, falling in gene-coding regions, displaying 1 or 2 mismatches considering sgRNA sequence. These sites were amplified by genomic PCR (primers are listed in Table 2) and

obtained amplicons underwent Sanger sequencing in order to assess the absence of alterations.

Karyotype analysis

iPSCs cytogenetic analysis was performed in collaboration with Genomics for the diagnosis of human pathologies Unit at San Raffaele University by using standard procedures. Briefly, active cell division was blocked at metaphase by 50 µg/ml of colcemid (Irvine Scientific) for 2–3 h at 37 °C. Thereafter, cells were detached using trypsin–EDTA, subsequently incubated in 1% hypotonic solution (sodium citrate tribasic dihydrate) and then fixed with Carnoy's fixative (3:1 methanol to acetic acid) onto glass slides. Q-banded metaphases were analized and interpreted according to the International System for Human Cytogenetic Nomenclature (ISCN 2013). A minimum of 16 metaphase spreads per sample were analized with an Olympus BX51 microscope coupled to a charge-coupled device camera COHU 4912 (Olympus, Milan, Italy). Captured images were analized using Ikaros (v 5.8.12) (MetaSystems).

Multi-germ layer differentiation

iPSCs at 70–80% confluence were detached by Accutase solution incubation at 37 °C for 10 min to obtain a single-cell suspension. Cells were centrifuged, counted, and seeded onto hESC-qualified Matrigel-coated glass coverslips at a density of

$2,5x10^4/cm^2$ in mTeSR1 medium supplemented with 10 µM ROCK inhibitor Y27632 (Selleckchem) and 1% Pen/Strep. Twenty-four hours after seeding, medium was replaced with DMEM/F12 containing 1% Pen/Strep, 2 mM glutamine (Sigma-Aldrich), 1% nonessential amino acids (MEM NEAA, ThermoFisher Scientific), 10% fetal bovine serum (FBS, Sigma-Aldrich). Cells were cultured for 4 weeks with medium replacement every other day and then analized by IF.

iPSCs differentiation into GINs

For neural differentiation, hPSCs were detached by incubation with Accutase solution for 8 min to obtain a single-cell suspension. To form EBs 50.000 cells/well were plated in v-bottom 96-well plates and cultured in Neurobasal A (ThermoFisher Scientific) containing 1% B-27 supplement without Vitamin A, 1% Pen/Strep (Sigma-Aldrich), 2 mM glutamine, 10 µM SB431542 (Sigma-Aldrich), 10 µM Y27632 (Selleckchem), 2 µM XAV939 (Sigma-Aldrich), 100 nM LDN-193189 (Stemgent) (vNPC medium). Medium change was done on days 4 and 7. After 10 days, 24 EBs/well were attached on matrigel coated 6-well plates by using the same medium without Y-27632. Rosette structures can be observed around days 10–16. Medium change was done on days 15, 18, and 21. From day 15 the medium used was essentially composed only by Neurobasal A, 1% B-27 supplement without vitamin A, 1% P/S, 2 mM glutamine. On day 25, neural rosette colonies were

detached by using accutase solution incubation for 20 min at 37°C obtaining single cell suspension. vNPCs were plated $1,5x10^5/cm^2$ in 24-wells plates on poly-L-lysine/laminin/fibronectin pre-coated coverslips for further neuronal differentiation in the same vNPC medium. On day 27 the medium was implemented with 0.2 mM ascorbic acid (Sigma-Aldrich), 20 ng/ml BDNF (Peprotech), 10 µM DAPT (Sigma-Aldrich). In the same day mouse astrocytes were added to the culture, $4x10^4/cm^2$, to help neurons maturation and functionality. At day 31, the medium was deprived of DAPT and implemented with 0.2 mM dbcAMP (Selleckchem). This final medium was used until the end of the culture. In case of LV infection, LVs were added to the culture at day 26 and removed at day 27 before adding mAstrocytes.

Purmorphamine 1.5 µM was used to ventralize the neuronal culture with the timing depending on the protocol used: throughout the whole culture period, from day 10 to day 18, and from day 10 to day 25.

Spheroids generation

The generation of hCS and hSS from hiPSCs cells was performed as published (Birey et al. 2017) with few modifications. Essentially, to initiate the generation of hCS or hSS, hiPS cells colonies were treated with Accutase with 8 minutes at 37°C to obtain a single cell suspension and plated 30.000 cells/well in v-bottom 96well plate in DMEM-KSR supplemented with the two

SMAD inhibitors 5 µM dorsomorphin (Sigma-Aldrich) and 10 µM SB-431542 (Sigma-Aldrich), and 10 µM ROCK inhibitor Y-27632 (Selleckchem). For the first five days, the medium was changed every day and supplemented with dorsomorphin and SB-431542. On the sixth day in suspension, neural spheroids were transferred to neural medium containing neurobasal-A (Life Technologies), B-27 supplement without vitamin A (Life Technologies), 1% Glutamine (Life Technologies), 1% Pen/Strep (Life Technologies) and supplemented with 20 ng/ml EGF (R&D Systems) and 20 ng/ml FGF2 (R&D Systems) until day 24. For the generation of hSS, the medium was supplemented with additional small molecules during the first 23 days in culture: 5 µM IWP-2 (Selleckchem) from day 4 until day 24, and 100 nM SAG (Selleckchem) from day 12 to day 24. From day 25 to 42, the neural medium for both the hCS and hSS conditions, was supplemented with 20 ng/ml BDNF (Peprotech) and 20 ng/ml NT3 (Peprotech) with medium changes every other day. From day 43 onwards, hCS and hSS were maintained in an unsupplemented neural medium with medium changes every four to six days.

For the LV transduction, spheroids were transferred to a 1,5 ml microcentrifuge Eppendorf tube containing 300 µl neural medium with virus and incubated overnight at 37°C in the incubator. The next day, neural spheroids were transferred again into fresh neural medium in ultralow attachment plates.

ExNs generation

On day −1 of differentiation, 90% confluent iPSC cultures were infected with the lentiviral vector TetO-Ngn2-T2A-Puro in mTeSR1 medium supplemented with doxycycline (2 µg/ml), overnight; doxycycline was maintained for all the experiments. On day 0, medium was replaced with differentiation medium "mTeSR1 + LSBX". Differentiation medium was replaced daily according to the following scheme:

Day 0,1: mTeSR1 + LSBX

Days 2,3: mTeSR1 + LSBX + PSD

Days 4,5: 2/3 mTeSR1 + 1/3 N2 / B-27 medium +LSX + PSD

Days 6,7: 1/3 mTeSR1 + 2/3 N2 / B-27 medium + PSD

On day 8, cells were detached by Accutase solution incubation at 37 °C for 20 min in order to obtain a single-cell suspension. Cells were centrifuged, counted, and seeded in 24-well plates at a density of $7{,}5x10^4$ cells/cm^2 onto poly-L-lysine/laminin/fibronectin-coated coverslip in neuronal maturation medium supplemented with ROCK inhibitor Y27632 (10 µM) for the first 24 h. The neuronal maturation medium was composed by Neurobasal A (ThermoFisher Scientific) supplemented with 1% B-27 supplement without vitamin A, 2 mM glutamine, 1% Pen/Strep, BDNF (Peprotech, 20 ng/ml), ascorbic acid (Sigma-Aldrich, 100 nM), Laminin (1 µg/µl), DAPT (10 µM), dbcAMP (Selleckchem, 250 µM). The culture medium was replaced the next day to remove the ROCK inhibitor, and then

half of the medium was replaced with a fresh neuronal maturation medium twice a week. Mouse astrocytes were added $7{,}5x10^4/cm^2$ from day 9.

LSBX: LDN193189 (Stemgent, 250 nm), SB-431542 (Sigma-Aldrich, 10 µM) XAV939 (Sigma-Aldrich, 5 µM). PSD: PD0325901 (8 µM), SU5402 (10 µM), DAPT (10 µM). N-2 / B-27 medium: DMEM/F12 with B-27 supplement (0.5×) and N-2 supplement (0.5×).

Immunostaining and imaging

Cells were seeded on coated glass coverslips, and they were fixed for 20 min on ice in 4% paraformaldehyde (PFA, Sigma), solution in phosphate-buffered saline (PBS, Euroclone). Then they were washed twice with PBS and were permeabilized for 30' in blocking solution, containing 0.1% Triton X-100 (Sigma-Aldrich) and 10% donkey serum (Euroclone), and incubated overnight at 4 °C with the primary antibodies diluted in blocking solution according to information in the antibody datasheet (see Table 1 for the complete list of primary antibodies used and their working dilution). The next day, cells were washed three times with PBS for 5 min and incubated for 1 hour at room temperature with Hoechst 33342 (ThermoFischer Scientific) and with secondary antibodies (ThermoFisher Scientific) in blocking solution. Images were acquired with epifluorescence microscope Nikon DS-Qi2 and analized with Fiji software.

RNA isolation and qRT-PCR

RNA was extracted using the TRI Reagent isolation system (Sigma-Aldrich) according to the manufacturer's instructions. For quantitative RT-PCR (qRT-PCR), 0,5 µg of RNA was reverse transcribed using the ImProm-II Reverse Transcription System (Promega), thereafter qRT-PCR was performed in duplicate with custom-designed oligos (see Table 1) using the CFX96 Real-Time PCR Detection System (Bio-Rad, USA) and the Titan HotTaq EvaGreen qPCR Mix (BIOATLAS). Obtained cDNA was amplified in a 20 µl reaction mixture containing 1 µl of diluted cDNA, 1× Titan HotTaq EvaGreen qPCR Mix (Bioatlas, Estonia), and 0.4 mM of each primer. Analysis of relative expression was performed using the ∆Ct method, using β-ACTIN mRNA as housekeeping gene and CFX Manager software (Bio-Rad, USA).

Whole-cell recording

Current-clamp recordings were performed using a MultiClamp 700B amplifier (Molecular Devices) with pCLAMP 10 software. Signals were low-pass-filtered at 10 kHz and sampled at 50–100 kHz; the signal was digitized using a Digidata 1550 D/A converter (Molecular Devices). Cells were held at room temperature. The extracellular solution contained 140 mM NaCl, 2 mM CaCl2, 4 mM KCl, 10mM HEPES, 1 mM MgCl2 and 10 mM D-glucose (pH 7.4 with KOH). For current-clamp recordings, the internal solution contained the patch pipette contained 124 mM KH2PO4, 5 mM KCl, 2 mM MgCl2, 10 mM NaCl, 10 mM HEPES, 0.5 mM EGTA,

2 mM Na-ATP, and 0.2 mM Na-GTP (pH 7.25, adjusted with KOH). Bridge balance compensation was applied. Passive properties were calculated from the hyperpolarizing steps of the current-clamp step protocol. Capacitance was calculated in the current-clamp hyperpolarizing step as as the ratio between voltage derivative (dV)/dI (voltage/current) and then the cell time constant (tau) which is obtained fitting the voltage changing between baseline and hyperpolarizing plateau. Capacitance was calculated as tau/resistance. Capacitance has been defined as the time constant of the voltage between the baseline and the plateau during an hyperpolarizing step.

Sodium currents were recorded from isolated single neurons in voltage clamp configuration. Patch pipette (1.5-2.1 MOhm resistance) were filled with an internal solution containing: 125 mM CH3O3SCs, 10 mM NaCl, 2 mM MgCl2, 10 mM HEPES, 2 mM Mg-ATP, and 0.2 mM Na-GTP (pH 7.25, adjusted with CsOH). After reaching whole-cell configuration series resistances between 5 and 10 MΩ and they were compensated up to 70–85% using the amplifier circuitry to minimize the voltage error; linear leak currents and capacitance artefacts were removed using P/N leak subtraction. Mixed sodium/calcium currents were evoked by 100ms depolarizing voltage steps (from -60 to + 60 mV, 10mV delta) preceded from a 100ms hyperpolarizing step to -120mV in order to remove any inactivation. I_{Na} was then defined as the component sensitive to 500nM TTX. Peak I_{Na} was then normalized to cell capacitance.

Signals were low-pass-filtered at 20 kHz and sampled at 50–100 kHz.

Bioinformatic analysis

Transcriptomics and epigenomics coverage bigwig files from GM23338-derived bipolar neurons were downloaded from ENCODE (https://www.encodeproject.org/) and displayed with Gviz (https://link.springer.com/protocol/10.1007%2F978-1-4939-3578-9_16).

Molecular cloning

Selected sgRNAs to generate isogenic clones or to induce upregulation of *SCN1A* gene expression (all listed in Table 4) were cloned using BsmBI restriction enzyme in the U6-filler-sgRNA lentiviral vector, also containing the blasticidin resistance gene. Then, respect to all sgRNAs used for CRISPRa, only few of them, sg2A, sg4A, sg2B, sg2C, and sgLacZ were removed from U6 vector using HpaI restriction enzyme and cloned in Ef1alpha-dCas9VP160-T2A-eGFP construct, already present in the lab. Replication-incompetent, VSVg-coated lentiviral particles were packaged in 293T cells.

GINs injections in P30 mouse brain

vNPCs were transplanted into NGS immunodeficient mice at the following coordinates: AP -3; ML ±2.8; V -3.8 and -2.8.

A total of 1.5×10^5 vNPCs in a 3 µl volume of PBS were delivered at each of the target coordinates.

Immunohistochemistry

Transplanted mice were terminally anesthetized with CO_2 and perfused transcardially with NaCl saline solution followed by 4% PFA 1 month or 5 months post grafting. Brains were removed, postfixed in 4% PFA for 12 hours, equilibrated in 20% sucrose/PBS solution, and then sectioned coronally at 30µm using a freezing cryostat. Brain sections were blocked in 10% donkey serum and 0.3% Triton X-100 for 1 hour at room temperature. Incubation with primary antibodies was performed at 4°C O/N (see Table 1 for primary antibodies used). Secondary antibodies were applied to sections for 1 hour at room temperature in a blocking solution containing Hoechst 33342. Finally, slices were washed and mounted in Fluorescent Mounting Medium (Dako Cytomation). Images were acquired with epifluorescence microscope Nikon DS-Qi2 and analized with Fiji software.

A similar procedure was used to perform IF on spheroids. Spheroids were fixed in 4% paraformaldehyde (PFA) for 30 min to 2 h and equilibrated in 8% sucrose. They were then washed in

PBS, transferred to 15% sucrose solution overnight at 4 °C and then to 30% sucrose for 48–72h. Subsequently, they were transferred into embedding medium (Tissue-Tek OCT Compound 4583, Sakura Finetek), snap-frozen on dry ice and stored at −80 °C. For immunohistochemistry, 10- to 30-µm-thick sections were cut using a cryostat (Leica). Sections were directly attached on the slides and treated with blocking solution as mentioned for mouse brain slices.

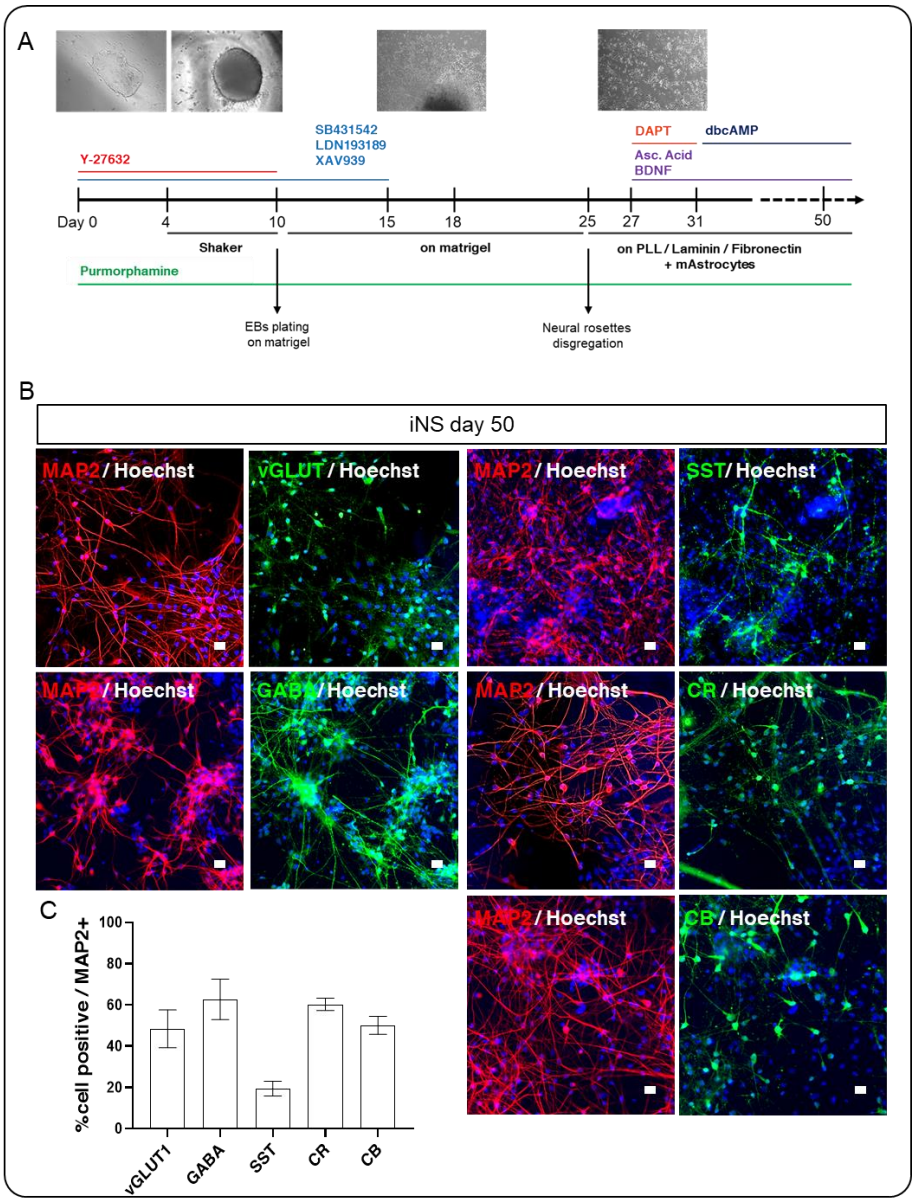

Figure 1. Neuronal differentiation protocol to obtain GINs. (A) Schematic representation of human GINs generation protocol with representative light microscopic images and days of treatment. (B) IF to characterize neuronal populations and GINs subpopulations obtained at day 50 with (C) quantifications (data

are means ± SEM; n = 3 independent batches of cell cultures). Images have been taken at the same magnification. Scale bar: 10 µM.

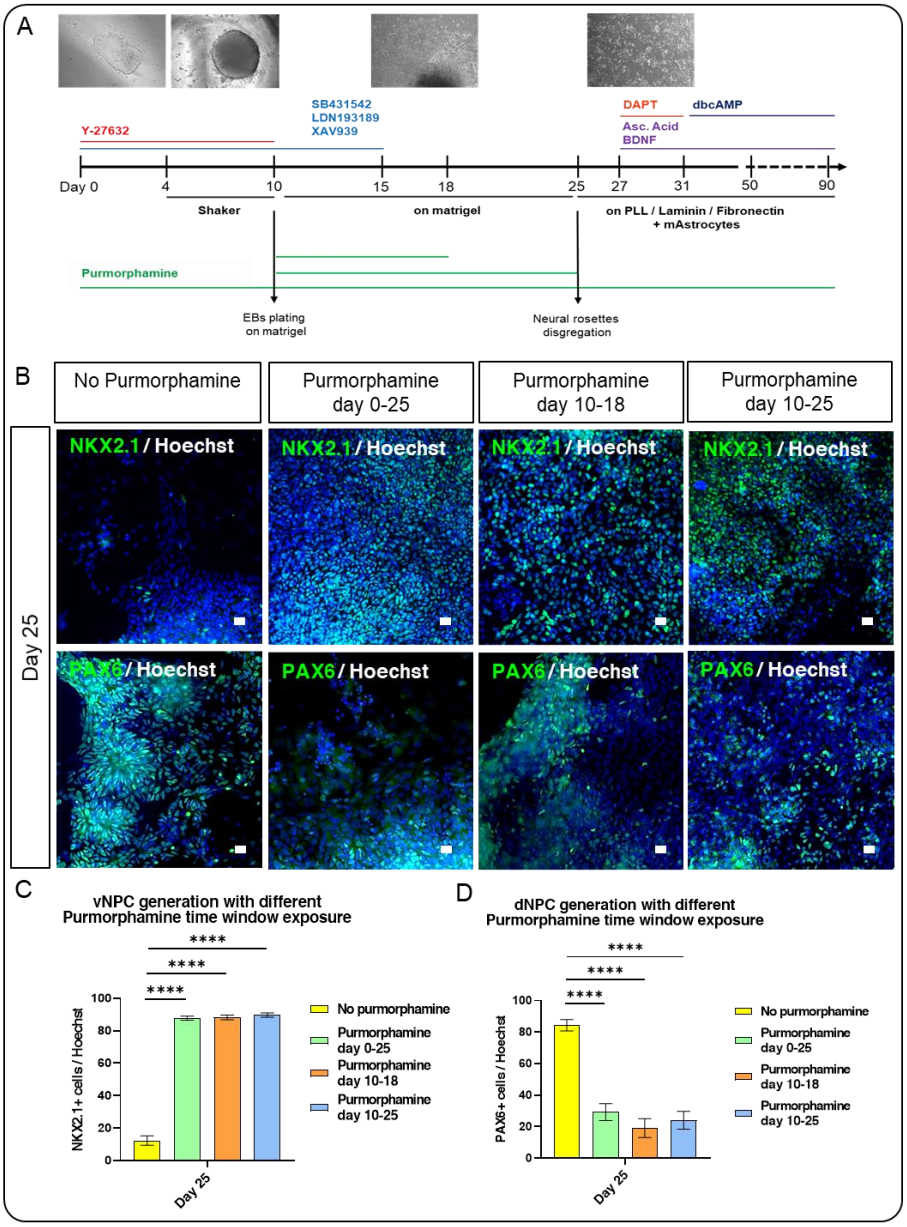

Figure 2. Ventralization of NPCs. (A) Schematic representation of human GINs generation protocol with the alternative purmorphamine time windows used for our experiments. (B) IF for NKX2.1 and PAX6 on day 25 of differentiation. Treatment with

purmorphamine for long period (day 0-25) or for time windows (day 10-18 or day 10-25) significantly enhanced the derivation of (C) NKX2.1+ vNPCs, inducing also a decrease in the generation of (D) PAX6+ dNPCs (data are means ± SEM; n = 3 independent batches of cell cultures; **** p<0,0001 one-way ANOVA with Bonferroni multiple comparisons). Images have been taken at the same magnification. Scale bar: 10 µM.

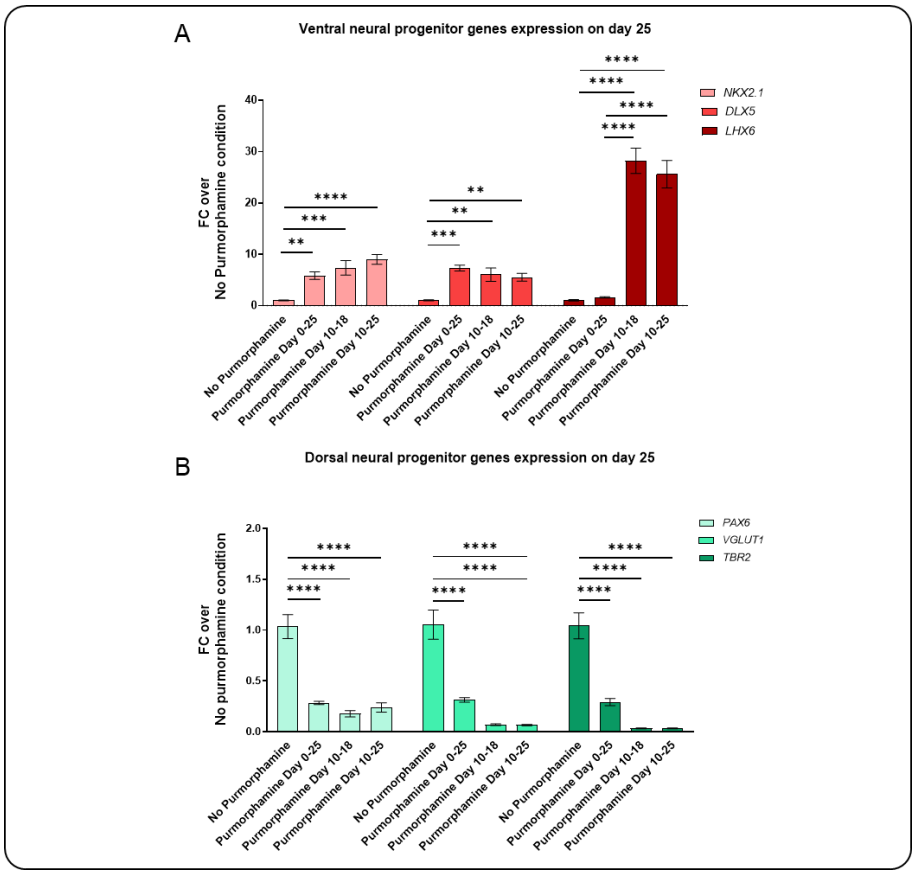

Figure 3. NPCs characterization. qRT-PCR analysis on day 25 of differentiation shows (A) overexpression of ventral telencephalic markers *NKX2.1*, *DLX5*, *LHX6* and (B) downregulation of dorsal telencephalic markers *PAX6*, *VGLUT1, TBR2* in all samples treated with purmorphamine in comparison with no treated condition. Data are normalized on *β-ACTIN* and shown as fold change (FC) over no purmorphamine condition (data are means ± SEM; n=3 independent batches of cell cultures; ** p< 0,01 *** p<0,001 **** p<0001, one-way ANOVA with Bonferroni multiple comparisons).

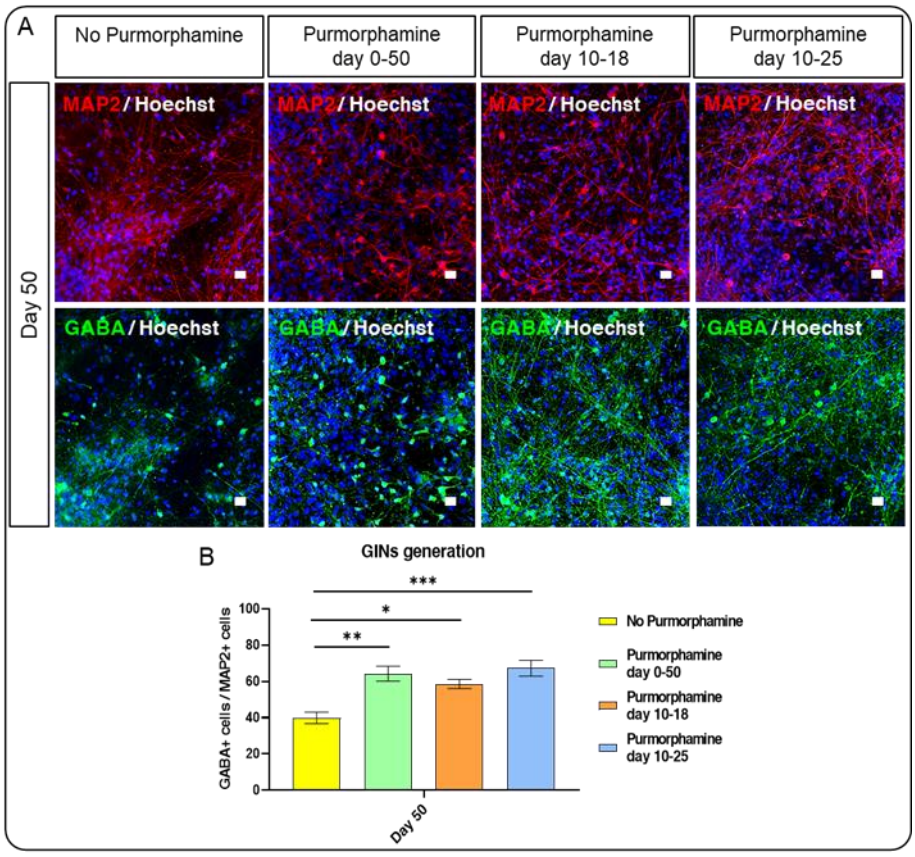

Figure 4. GINs generation on day 50. (A) IF to reveal GINs on day 50 of differentiation. Treatment with purmorphamine in any condition significantly increased the derivation of GABA+ interneurons, as quantified in (B); (data are means ± SEM; n = 3 independent batches of cell cultures; * p< 0,01 ** p< 0,01 *** p<0,001 one-way ANOVA with Bonferroni multiple comparisons). Images have been taken at the same magnification. Scale bar: 10 µM.

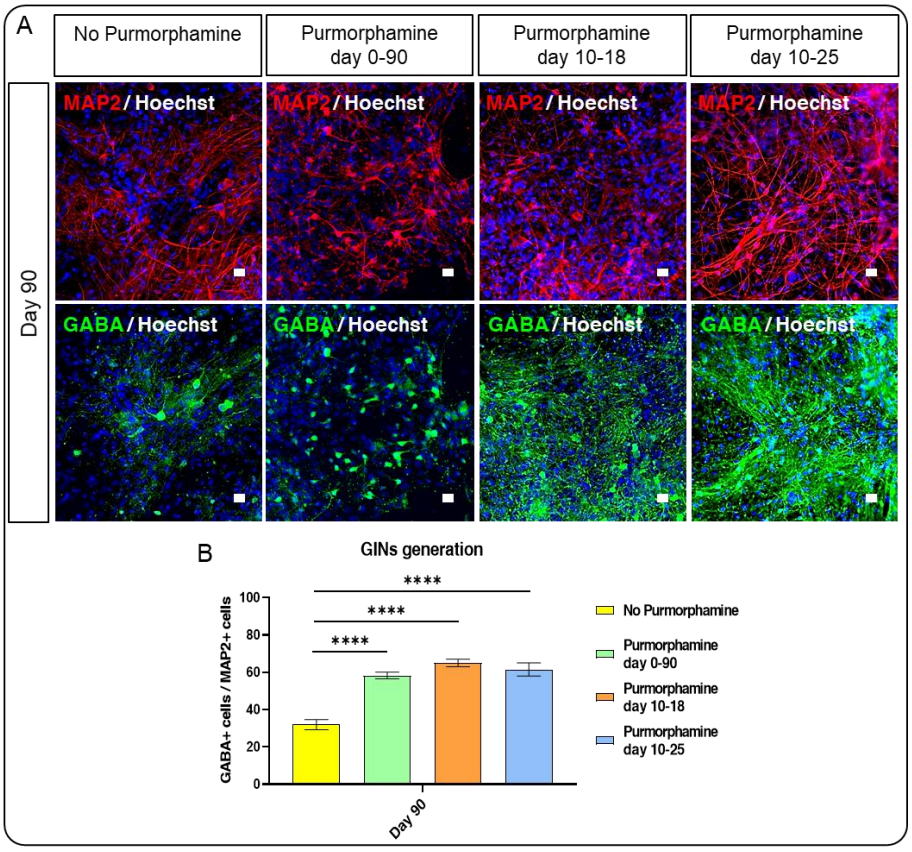

Figure 5. GINs generation on day 90. (A) IF to reveal GINs on day 90 of differentiation. Treatment with purmorphamine in any condition significantly increased the derivation of GABA+ interneurons also after 3 months of differentiation, as quantified in (B) (data are means ± SEM; n = 3 independent batches of cell cultures; **** p<0,0001 one-way ANOVA with Bonferroni multiple comparisons). Images have been taken at the same magnification. Scale bar: 10 µM.

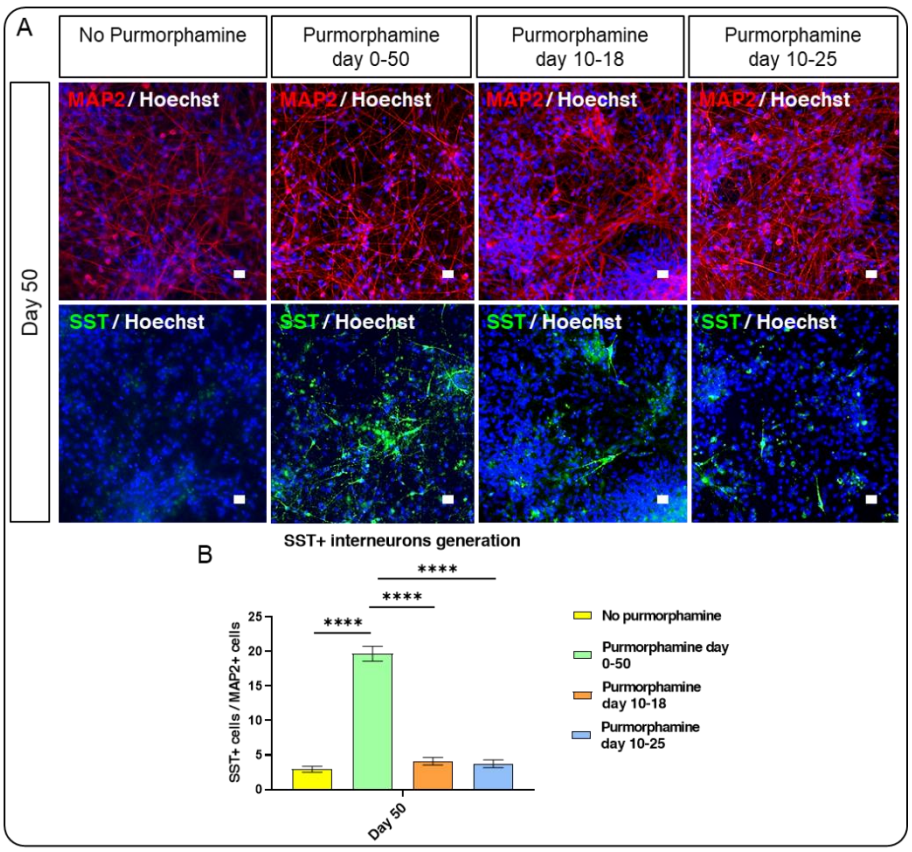

Figure 6. SST+ interneurons generation on day 50. (A) IF to reveal SST+ interneurons at day 50 of differentiation. Treatment with purmorphamine for long period (day 0-50) significantly enhanced the derivation of SST+ interneurons compared to all other conditions, as quantified in (B) (data are means ± SEM; n = 3 independent batches of cell cultures; **** p<0,0001 one-way ANOVA with Bonferroni multiple comparisons). Images have been taken at the same magnification. Scale bar: 10 µM.

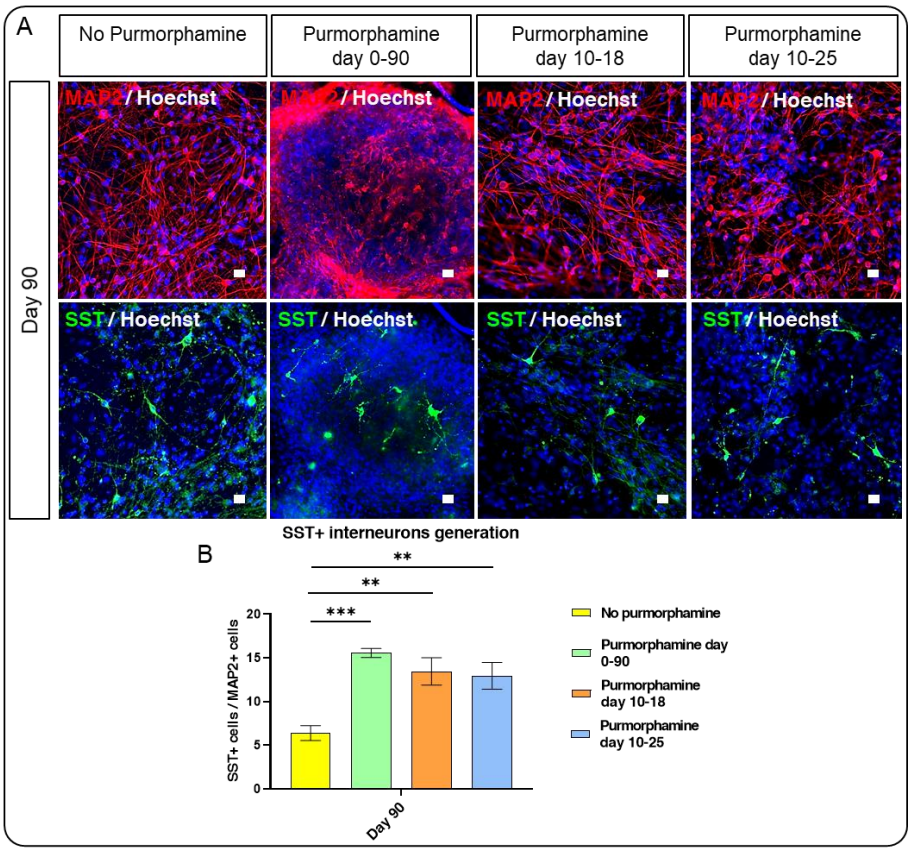

Figure 7. SST+ interneurons generation on day 90. (A-B) IF to reveal SST+ interneurons on day 90 of differentiation. Purmorphamine treatment, in any condition, significantly enhanced the derivation of SST+ interneurons, as quantified in (B) (data are means ± SEM; n = 3 independent batches of cell cultures; ** p<0,01 *** p<0,001 one-way ANOVA with Bonferroni multiple comparisons). Images have been taken at the same magnification. Scale bar: 10 µM.

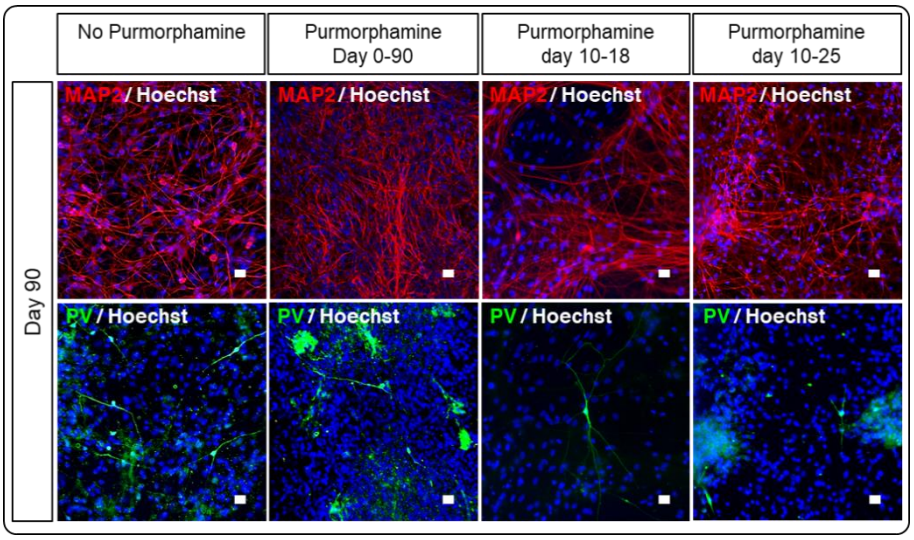

Figure 8. PV+ interneurons derivation. Representative images of IF displaying few PV+ interneurons which appeared in every condition only after 90 days of differentiation. Images have been taken at the same magnification. Scale bar: 10 µM.

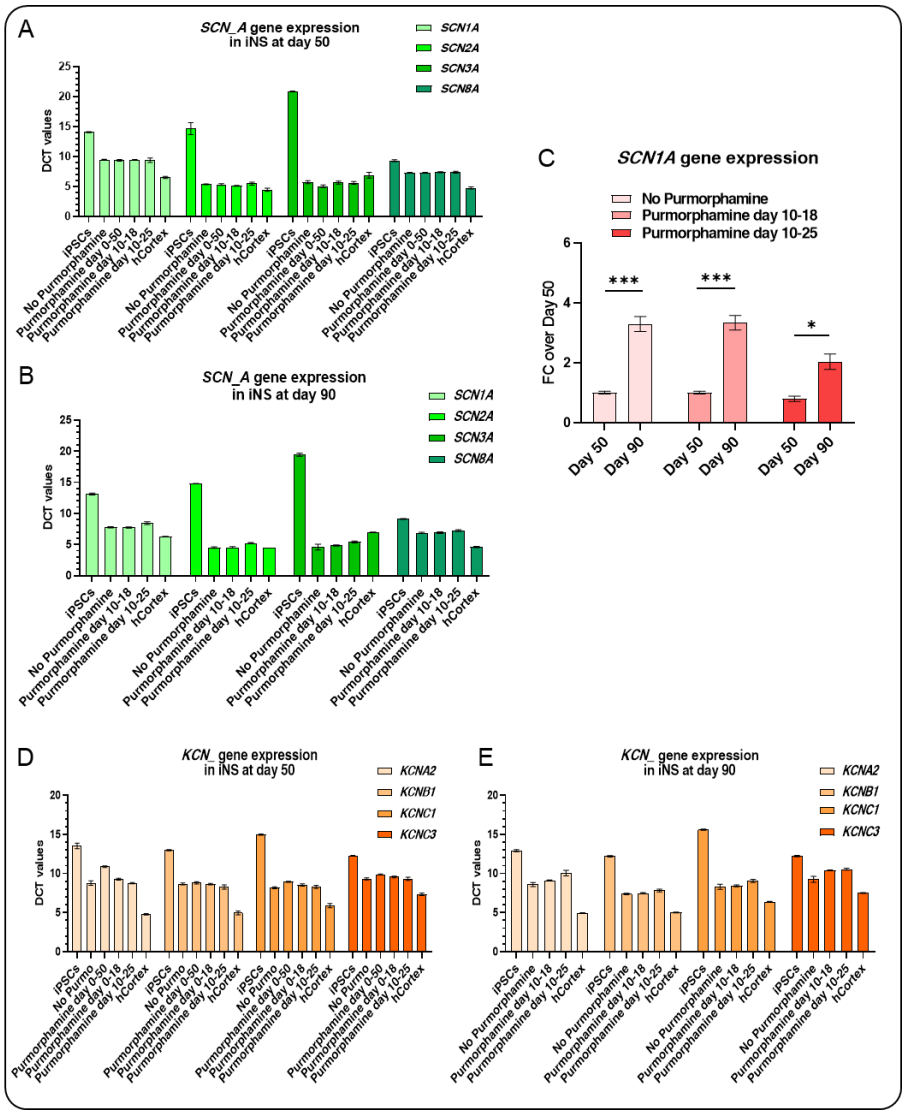

Figure 9. Na^+ and K^+ channels genes expression in GINs. (A,D) On day 50 and (B,E) 90 of differentiation, neurons were used for RNA isolation and subsequently qRT-PCR analysis of the (A,B) Na^+ (*SCN1A*, *SCN2A*, *SCN3A*, *SCN8A*) and (D,E) K^+ (*KCNA2*, *KCNB1*, *KCNC1*, *KCNC3*) channels genes. Data are presented as DCT and normalized on the *β-ACTIN* mRNA. iPSCs and human cortex (hCortex) samples are reported as

respectively negative and positive controls for the reactions (data are means ± SEM; n = 3 independent batches of cell cultures by using a control iPSC line, with each experiment presenting all the conditions). Considering that Purmorphamine treatment was always toxic for cells when extended beyond two months, this condition was excluded from the analysis on day 90. (C) The analysis of *SCN1A* gene expression between 50 and 90 days of differentiation in all conditions, except for purmorphamine day 0-90, that was excluded from the analysis, shows how *SCN1A* expression increases when cells are left in culture for longer period. Data are shown as FC over day 50 (data are means ± SEM; n = 3 independent batches of cell cultures; * $p<0,05$ *** $p<0,001$, t-test).

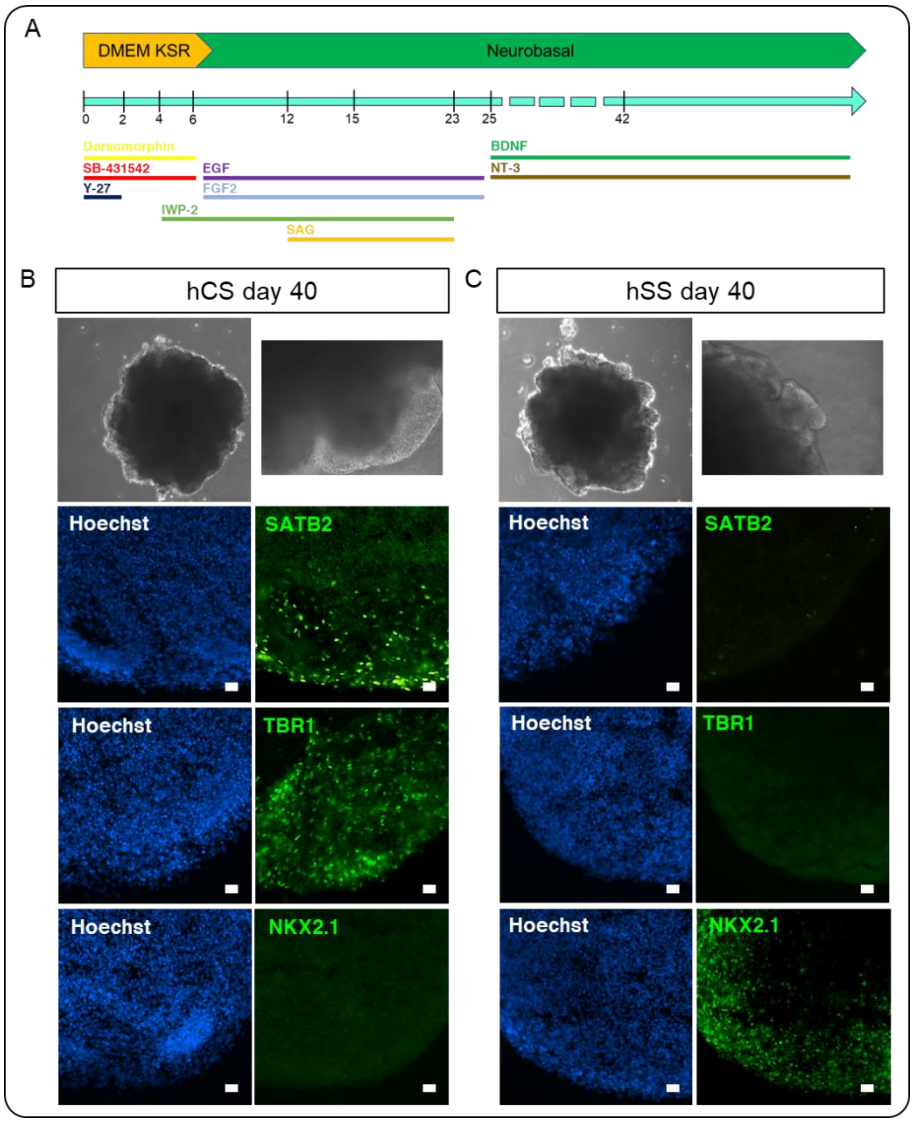

Figure 10. Spheroids characterization. (A) Schematic representation of hCS and hSS generation protocol with days of treatment derived from Birey et al. 2017. IWP-2 and SAG molecules were added to the medium only to generate hSS. (B,C) Representative bright field pictures of a hCS and a hSS also showing in magnification the presence of neuroepithelium,

organized in large convolutions, and IF images to confirm the presence of ventral (NKX2.1) and dorsal (SATB2 and TBR1) neural progenitor markers on day 40, as reported in Birey et al. 2017. Images have been taken at the same magnification. Scale bar: 10 µM.

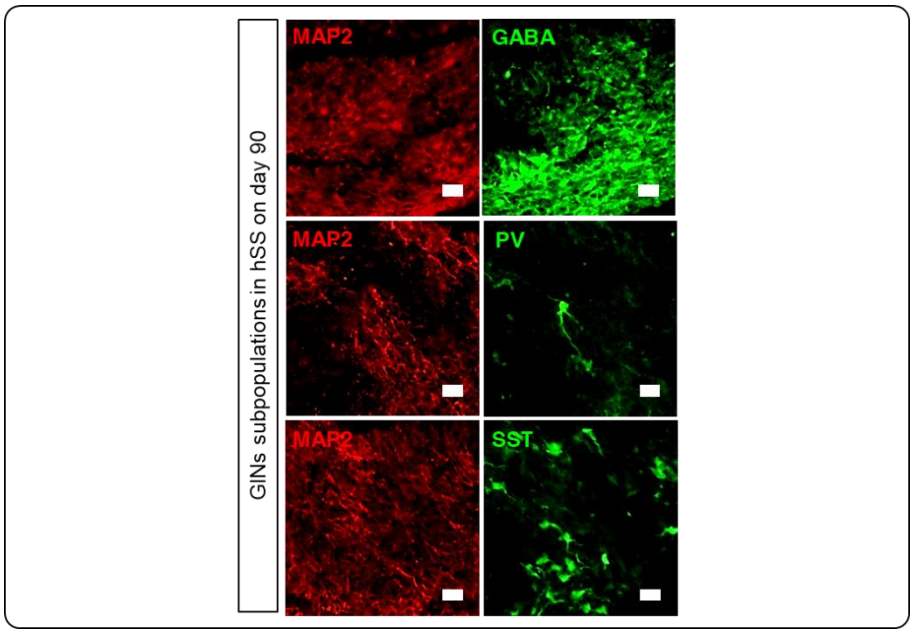

Figure 11. hSS characterization. Representative IF pictures displaying the presence of different GINs subpopulations at day 90 in hSSs. Images have been taken at the same magnification. Scale bar: 10 µM.

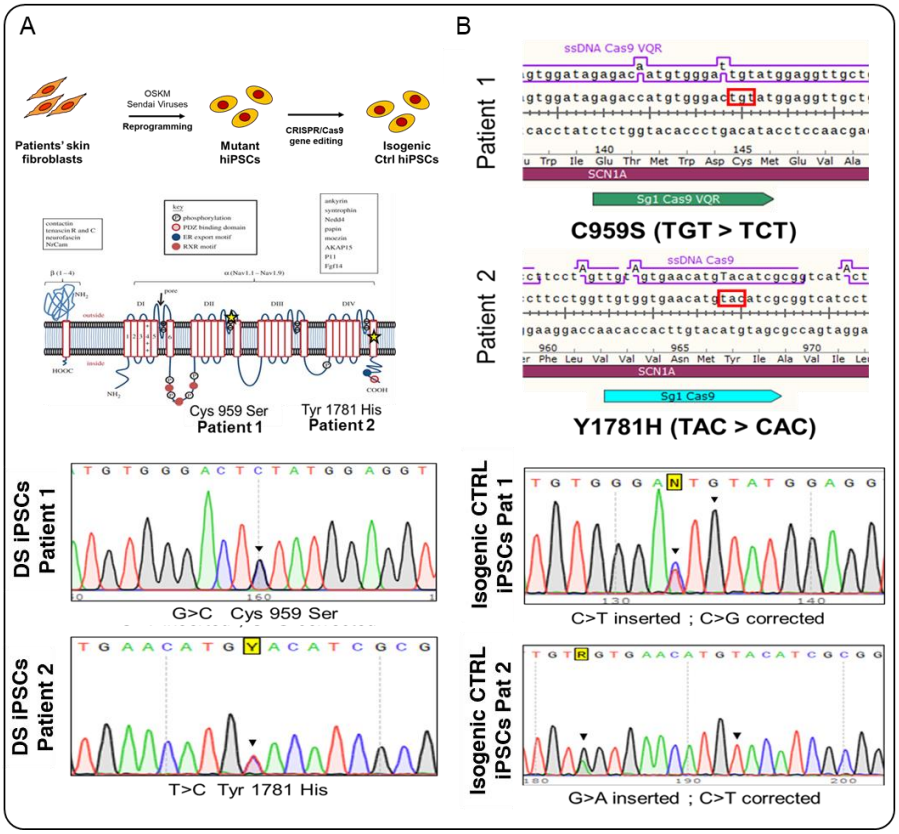

Figure 12. DS patients' iPSCs and isogenic controls generation. (A) DS patients' skin fibroblasts have been reprogrammed to hiPSCs using Sendai viruses. Different clones have been amplified, in feeder-free condition, and isogenic controls have been generated by CRISPR/Cas9 technology (upper panel). Specific mutations of patients 1 and 2 are reported as stars on $Na_V1.1$ protein image (middle panel). Sanger sequencing confirms the presence of patient-specific mutations (C959S in patient 1 and Y1781H in patient 2) (lower panel). (B) Strategies used to generate isogenic clones. Single stranded oligodeoxinucleotides WT donors used for gene correction reported mutations to distinguish isogenic recombinant clones.

spCas9 has been used for patient 1 strategy (NGG PAM site) and spCas9 VQR for patient 2 strategy (NGA PAM site) (upper panel). Isogenic clones were verified by sanger sequencing (lower panel) (correction efficiency: 3/24 and 3/12 screened clones for patient 1 and 2 respectively).

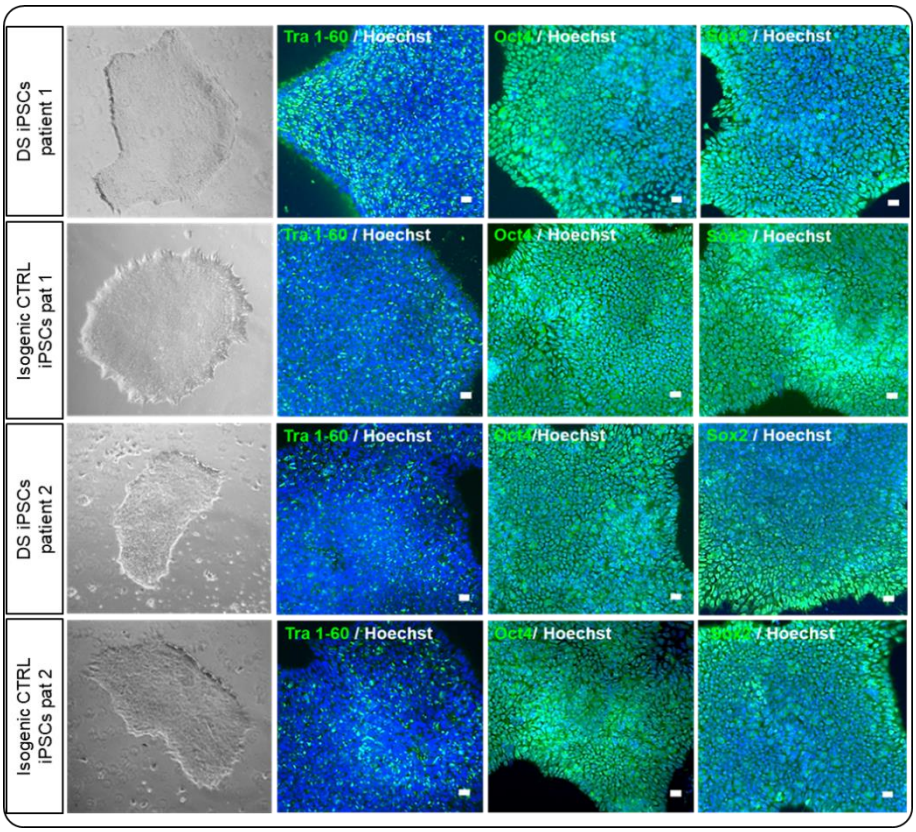

Figure 13. iPSCs characterization. iPSCs of two isogenic pairs were stained with nuclei marker Hoechst and pluripotency markers TRA1-60, OCT-3/4 and SOX2 individually. Representative brightfield images and IF analysis show normal hiPSCs colonies morphology, and their positivity for all

pluripotency markers. Images have been taken at the same magnification. Scale bar: 10 µM.

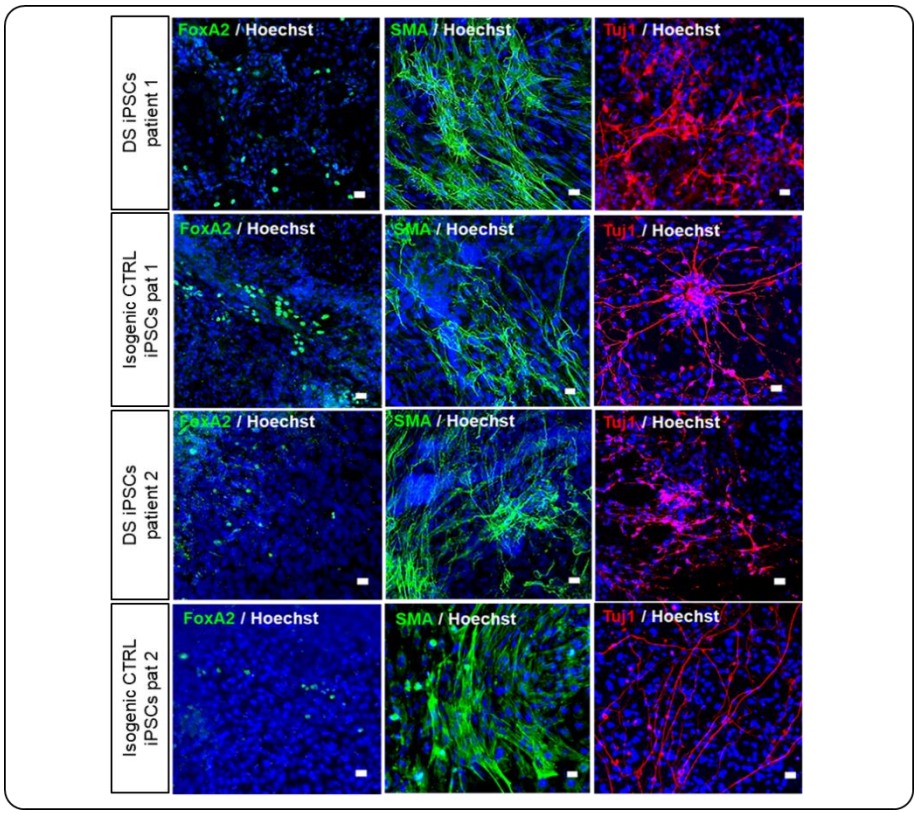

Figure 14. Three germ layers spontaneous differentiation of iPSC lines. hiPSCs multilineage spontaneous differentiation has been demonstrated by IF verifying the expression of markers used to distinguish the three different germ layers (FOXA2 for endoderm, SMA for mesoderm and TUJ1 for ectoderm). Images have been taken at the same magnification. Scale bar: 10 µM.

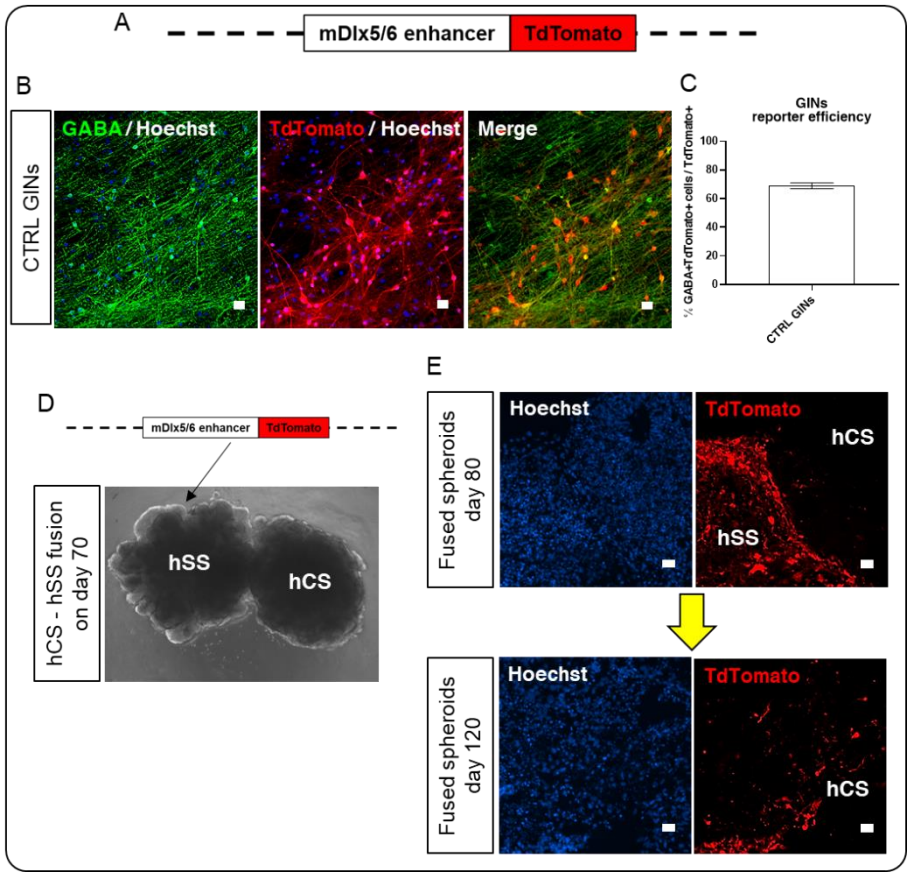

Figure 15. GINs LV reporter efficiency. (A) LV mDlx5/6-TdTomato reporter construct (from Dimidschstein et al. 2016) and (B) IF to confirm its efficiency to reveal GINs on day 90 of differentiation by using the protocol with purmorphamine exposure from day 10 to 18. (B) GABA co-localization with TdTomato protein has been quantified as double positive GABA+/TdTomato+ cells on the total amount of TdTomato+ cells (data are means ± SEM; n = 3 independent batches of cell cultures). (D) Brightfield image of the assembly of hSS, previously transduced with LV mDlx5-TdTomato, and hCS at day 70. (E) Fluorescence pictures show how TdTomato+ cells migrated from the hSS to the hCS from day 80 to day 120. Images have been taken at the same magnification. Scale bar: 10 µM.

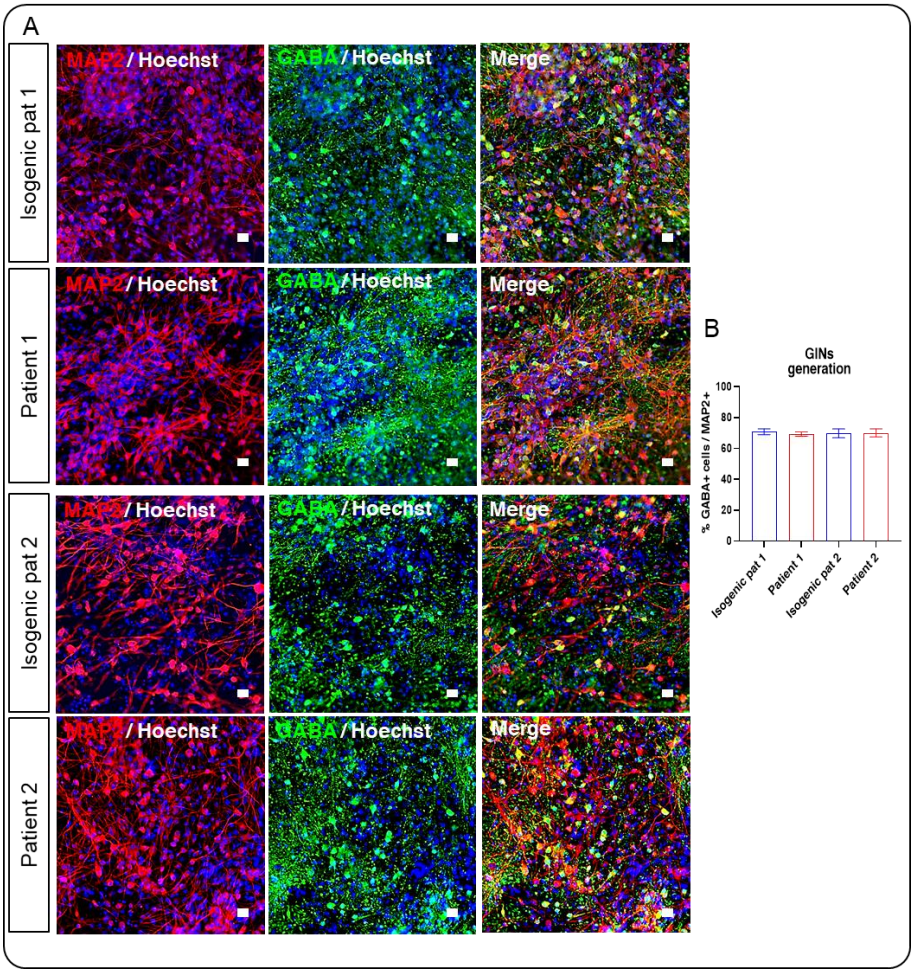

Figure 16. GINs derivation. (A) Representative images from cultures of our two pairs of iPSC-derived GINs stained with neuronal subtype marker GABA on day 90, and (B) quantification. No significant difference between cell lines was reported (data are means ±SEM; n = 3 independent batches of cell cultures; ns p>0,05 one-way ANOVA). Images have been taken at the same magnification. Scale bar: 10 µM.

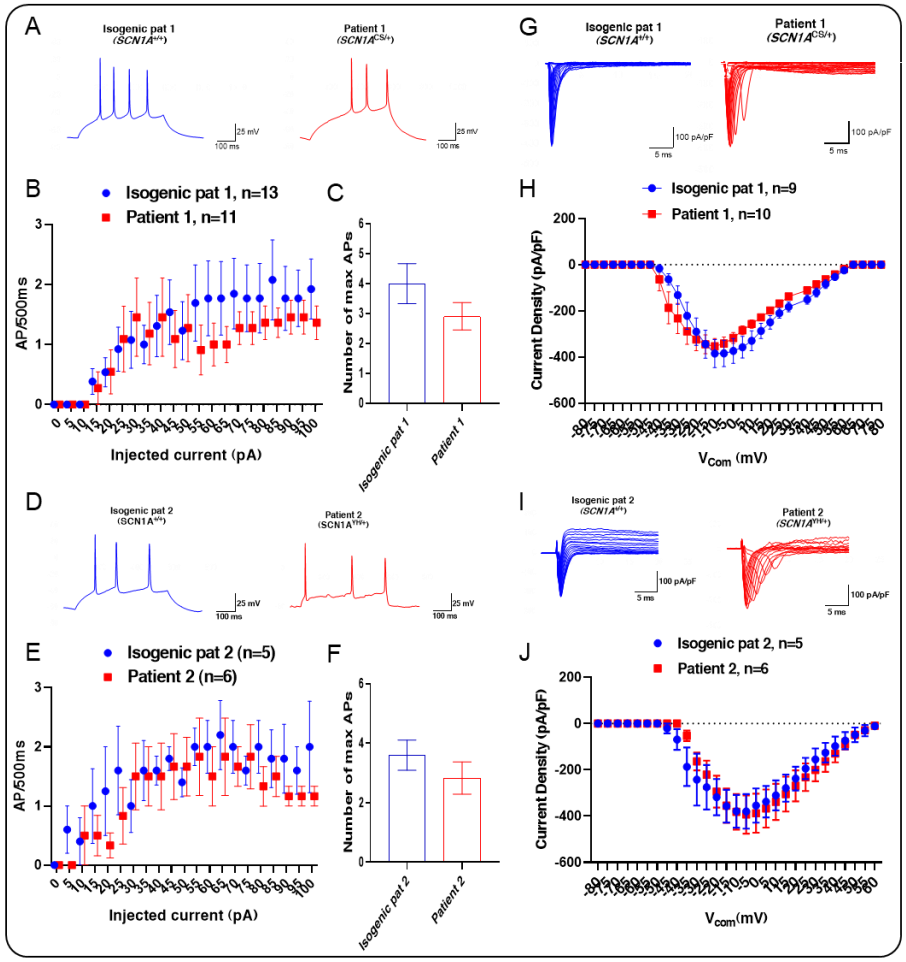

Figure 17. GINs electrophysiological characterization. (A,D) Current clamp showing firing profile of GINs derived from all our iPSC lines. (B,E) Input-output curve shows no difference between the two experimental groups (data are means ± SEM; n=13 isogenic pat 1 and n=11 patient 1, ns p = 0,5989; n=5 isogenic pat 2 and n=6 patient 2, ns p = 0,1303 Two-way ANOVA). (C,F) The maximal mean AP frequency induced by 500-ms current steps of GINs shows a trend of decrease in patients' values compared to isogenic controls' (data are means ± SEM; n=13 isogenic pat 1 and n=11 patient 1, ns p = 0,1816; n=5 isogenic pat 2 and n=6 patient 2, ns p = 0,3371 , t-test). (G,I)

Representative voltage clamp traces from GINs derived from both pairs of iPSC lines. Current has been normalized to cell capacitance. (H,J) Peak Na^+ current recorded in voltage clamp from the previously cited experimental group do not differ at any tested voltage as shown from I/V plot (data are means ± SEM; n=9 isogenic pat 1 and n=10 patient 1, ns p = 0,7707; n=5 isogenic pat 2 and n=6 patient 2, ns p = 0,9708, Two-way ANOVA).

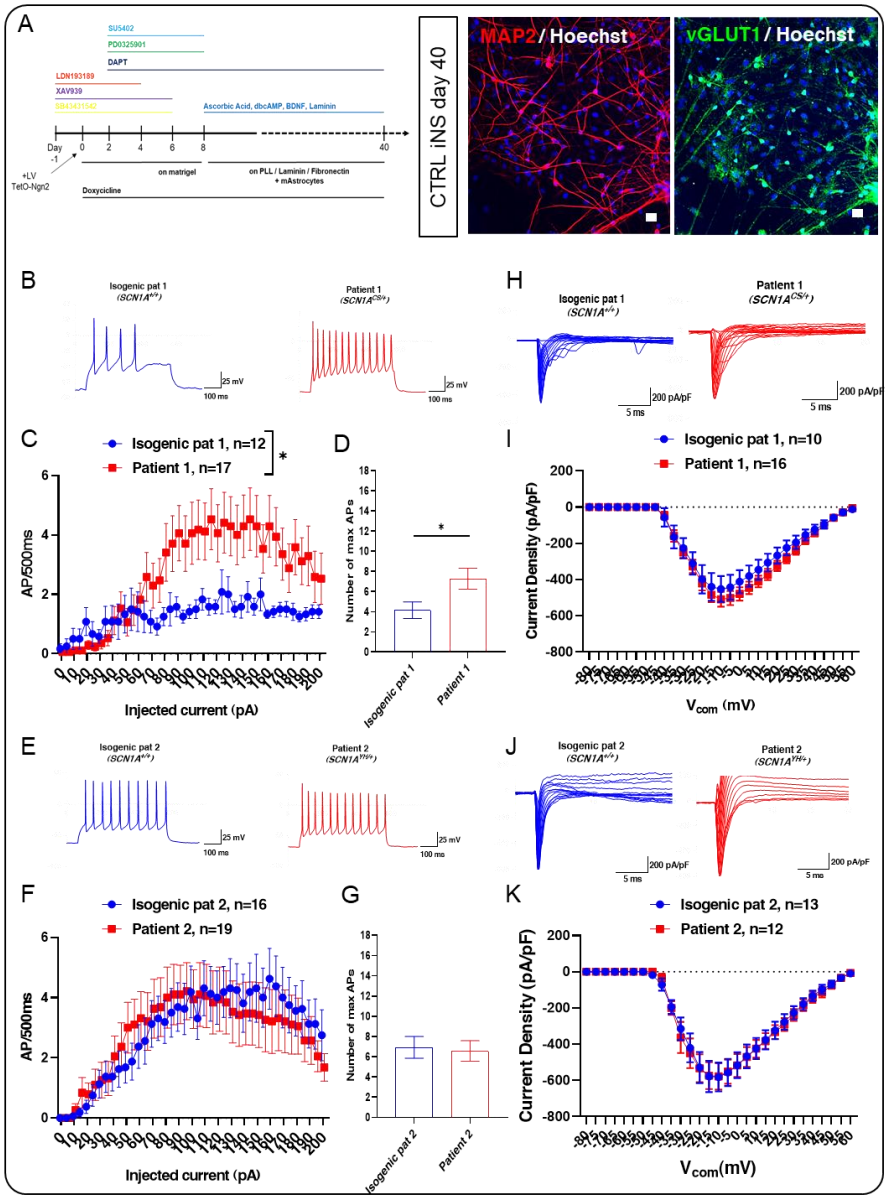

Figure 18. ExNs electrophysiology. (A) Schematic representation of human cortical excitatory neurons generation process with days of treatment and representative IF image representing neurons expression of excitatory neuronal marker vGLUT1 on day 40 of differentiation. Images have been taken at the same magnification.

Scale bar: 10 µM. (B-E) Current clamp showing patients and isogenic controls derived ExNs firing profile. (C-F) Input-output curves showing an increase in APs generated in patient 1 ExNs compared to their isogenic controls and no difference between the two experimental groups in the case of patient 2 and control (data are means ± SEM; n=12 isogenic pat 1 and n=17 patient 1 * p=0,0414, n=16 isogenic pat 2 and n=19 patient 2, ns p = 0,9309, Two-way ANOVA). (D-G) The maximal AP frequency of ExNs induced by 500-ms current steps highlighted a significant increase only in patient 1 values compared to its control; no difference between patient 2 and its control has been reported (data are means ± SEM; n=12 isogenic pat 1 and n=17 patient 1, * p=0,0360; n=16 isogenic pat 2 and n=19 patient 2, ns p=0,8094, t-test). (H-J) Representative voltage clamp traces from isogenic pat 1 / patient 1 and isogenic pat 2 / patient 2 derived excitatory neurons. Current has been normalized to cell capacitance. (I-K) Peak Na^+ current recorded in voltage clamp from the previously cited experimental group do not differ at any tested voltage as shown from I/V plot (data are means ± SEM; n=10 isogenic pat 1, n=16 patient 1, ns p =0,4078 and n=13 isogenic pat 2, n=12 patient 2, ns p= 0,9309, Two-way ANOVA).

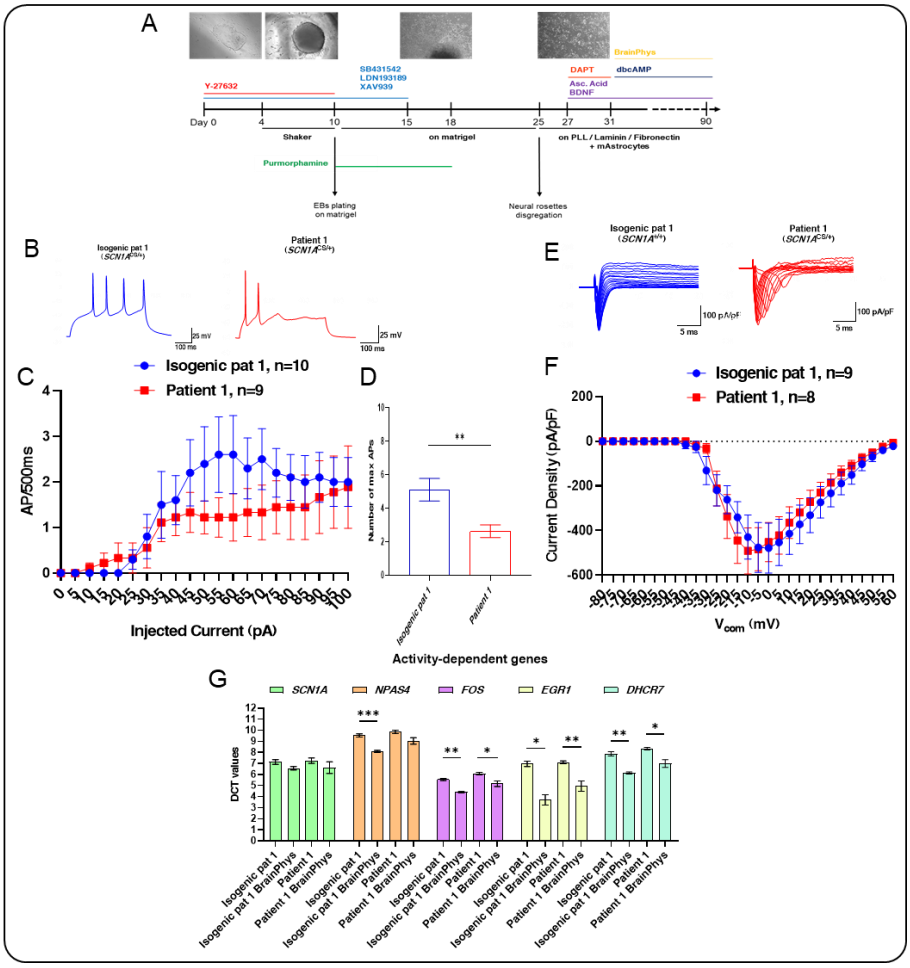

Figure 19. GINs functionality after treatment with BrainPhys medium. (A) BrainPhys medium was used instead of usual neuronal differentiation medium from day 31 on. (B) Current clamp showing firing profile of isogenic pat 1 and patient 1 derived GINs treated with BrainPhys medium for 60 days. (C) Input-output curve shows no difference between the two experimental groups (data are means ± SEM; n=10 isogenic pat 1 and n=9 patient 1, ns p = 0,3393, Two-way ANOVA). (D) The maximal mean AP frequency induced by 500-ms current steps of GINs shows significant decrease in patient 1 values compared to isogenic control (data are means ± SEM; n=10 isogenic

pat 1 and n=9 patient 1, ** p = 0,0087, t-test). (E) Representative voltage clamp traces from isogenic pat 1 and patient 1 derived GINs. Current has been normalized to cell capacitance. (F) Peak Na^+ current recorded in voltage clamp from the previously cited experimental group do not differ at any tested voltage as shown from I/V plot (data are means ± SEM; n=9 isogenic pat 1 and n=8 patient 1, ns p = 0,8067, Two-way ANOVA). (G) qRT-PCR analysis of *SCN1A* gene together with some activity-dependent genes as markers of neuronal maturation on neurons treated with BrainPhys medium compared to the usual neural differentiation medium on day 90 of differentiation. Data are normalized on *β-ACTIN* and shown as DCT (data are means ± SEM; n = 3 independent batches of cell cultures * p<0,05 ** p< 0,01 *** p<0,001 t-test).

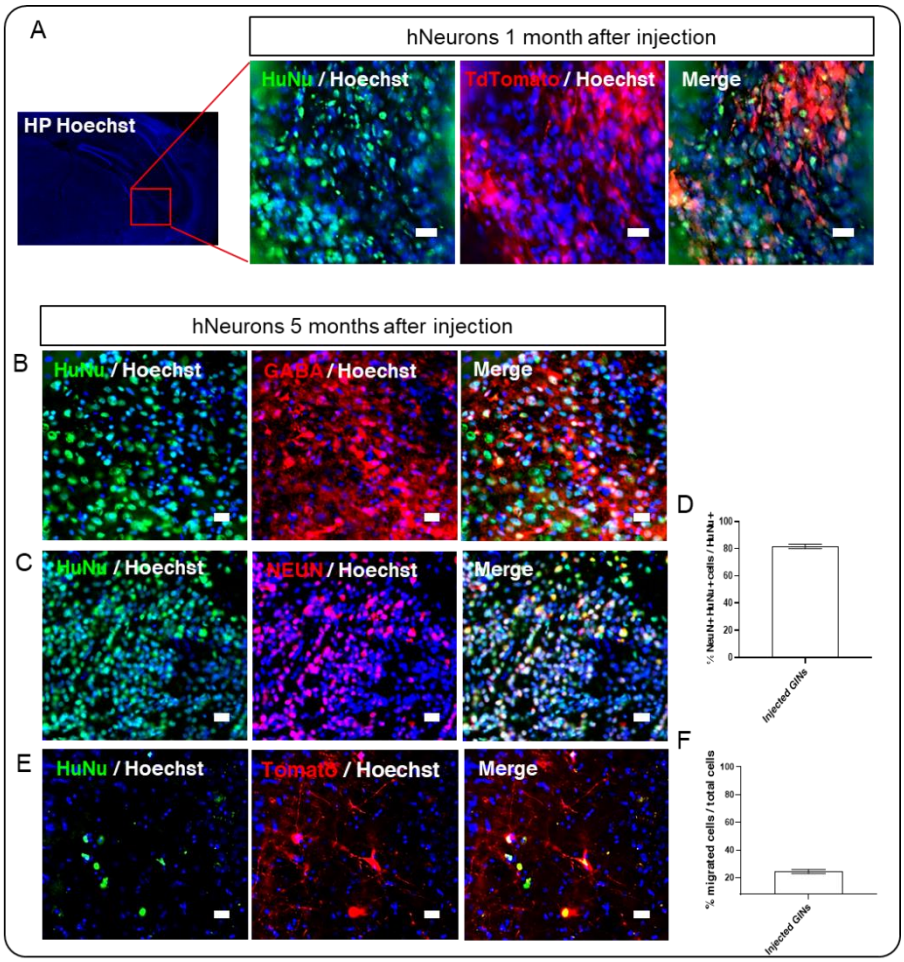

Figure 20. GINs transplantation into immunodeficient mouse brain. (A) IF images showing human neurons, obtained by using the protocol with purmorphamine exposure from day 10-18, transduced with LV mDlx5-TdTomato reporter, injected in P30 hippocampal region of immunosuppressed mouse brain. HuNu staining has been used to demonstrate the human nature of TdTomato+ cells one month after the injection. (B) Representative image showing that transplanted human vNPCs were able to differentiate into GINs also *in vivo*. (C) IF analysis to reveal NEUN expression in human cells, with (D) quantification (data are means ± SEM; n=3 brains). (E) IF images showing cells migrated

to the mouse cortex from the locus of injection, with (F) quantification. This data derived from the counting of all cells outside the locus of injection, independently from the distance, and expressed as percentage on the total amount of transplanted cells counted in each brain (data are means ± SEM; n=3 brains).

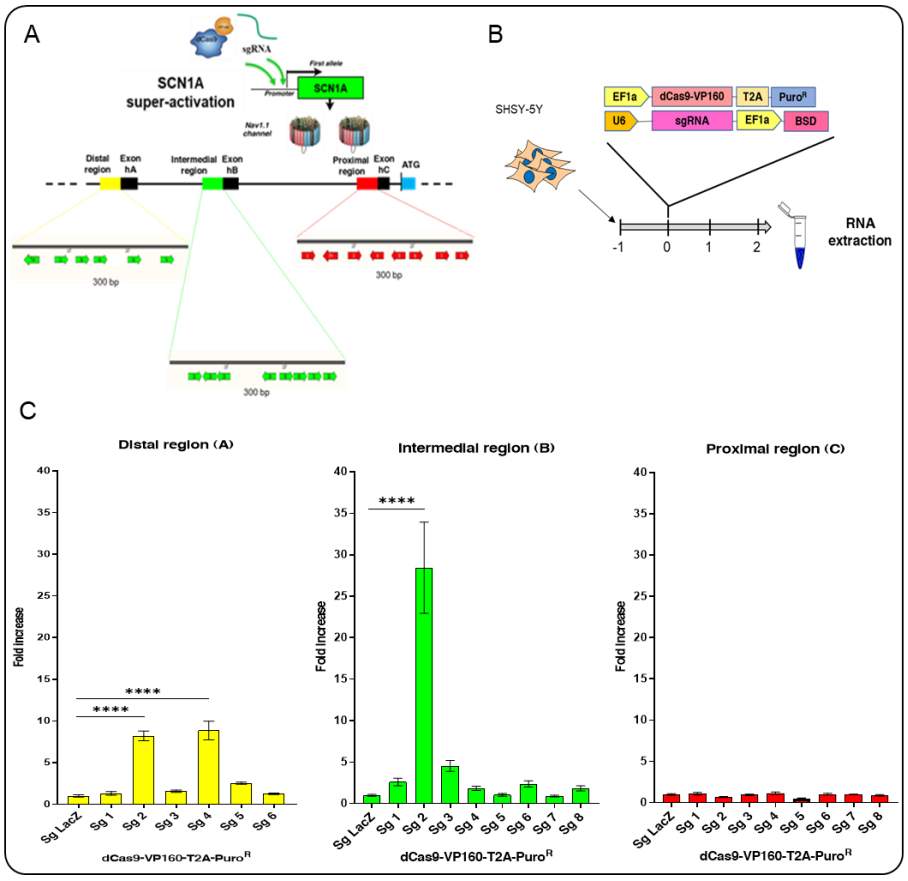

Figure 21. *SCN1A*-activatory CRISPR/dCas9. (A) Strategy to upregulate *SCN1A* by using dCas9-VP160. Schematic representation of the *SCN1A* gene with distal, intermedial and proximal promoter regions; the positions of the sgRNAs selected for this screening are highlighted. (B) Experimental setting for the sgRNA screening in SH-SY5Y cells and schematic representation of the constructs employed

for cell transduction. One day after plating, SH-SY5Y cells were transduced with LVs containing our constructs, and the subsequent day antibiotics were added to the culture medium to select transduced cells. At day 2, the cells were processed for RNA extraction. (C) qRT-PCRs for *SCN1A* mRNA levels performed on RNA extracted from SH-SY5Y cells transduced with dCas9VP160-T2A-Puro^{R} together with sgRNAs targeting the distal, intermedial or proximal promoter. Data are normalized on the *β-ACTIN* mRNA and relative to sgLacZ-transduced cells. Sg2A-4A and Sg2B induce significant up-regulation of *SCN1A* compared to SgLacZ (data are means ±SEM; n=6, **** $p < 0.0001$, one-way ANOVA with Bonferroni multiple comparisons).

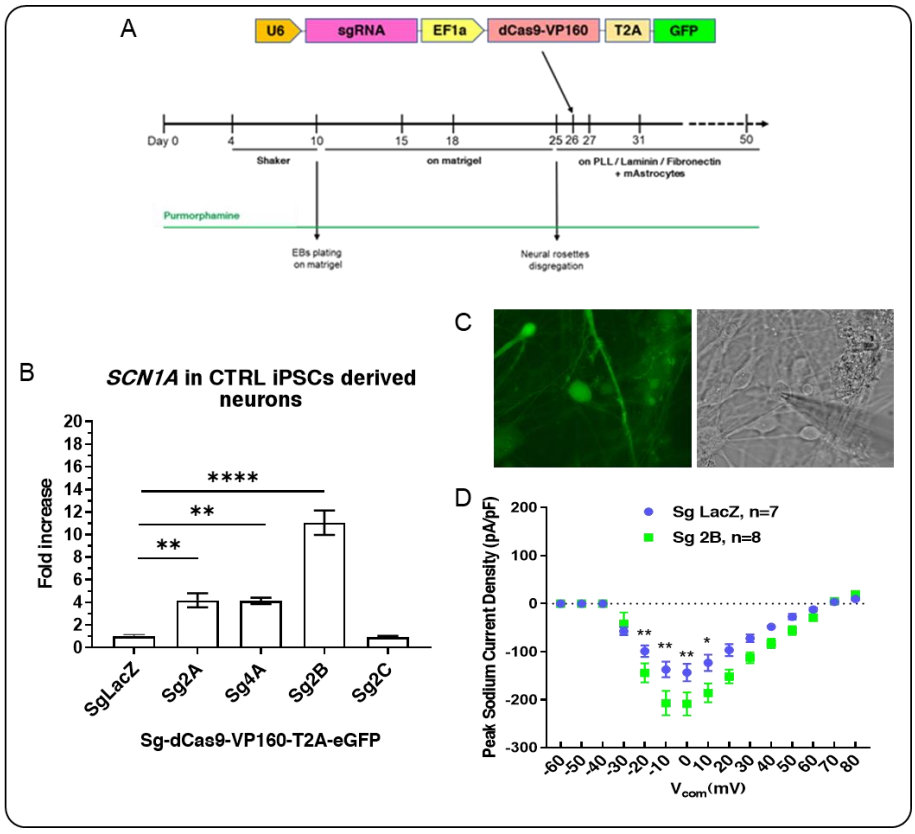

Figure 22. *SCN1A*-activatory CRISPR/dCas9 on GINs. (A) Schematic drawing depicting the experimental setting to deliver the Ctrl- and *SCN1A*-activatory CRISPR/dCas9 system in iPSC-derived neurons. To upregulate *SCN1A* expression in human GINS, three sgRNAs were selected from the screening in SH-SY5Y: two localised in the distal region (Sg 2A-4A) and one in the intermedial region (Sg 2B). Ctrl neurons were derived by using the protocol with long exposure with purmorphamine and were co-transduced with a LV carrying U6-sgRNA-Ef1a-dCas9-VP160-T2AGFP on day 26. mAstrocytes were added on day 27. (B) Their efficiency in increasing basal *SCN1A* gene expression was determined by qRTPCR. Data are normalized on the *β-ACTIN* mRNA and relative to control sg LacZ-transduced cells. Sg 2A-4A and Sg 2B induce significant upregulation of *SCN1A* compared

to SgLacZ in human neurons (data are means ±SEM; n=6, ** p<0,01 **** p< 0,0001, one-way ANOVA with Bonferroni multiple comparisons). (C) GFP+ neurons were analized by patch clamp and (D) recording from Sg2B-transduced neurons showed an increase in Na^+ current density compared to Sg LacZ-transduced neurons (data are means ±SEM; n=7 Sg LacZ and n=8 Sg 2B, * p<0,05 ** p<0,01 Two-way ANOVA with Bonferroni multiple comparisons).

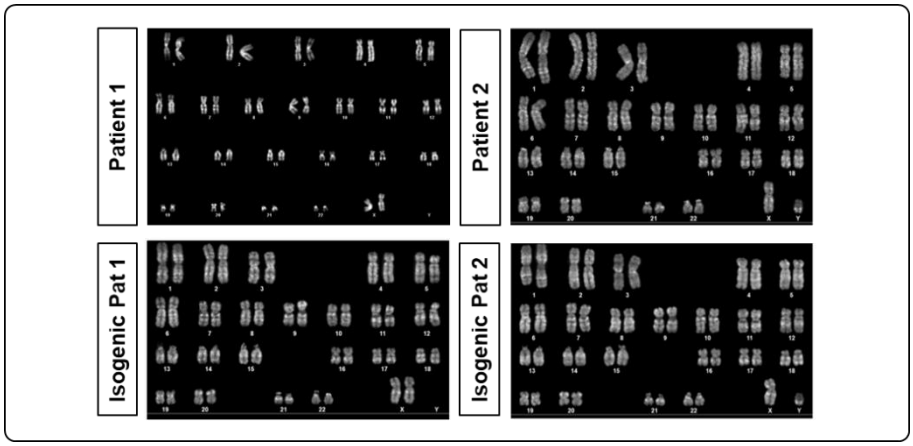

Supplemental figure 1. Karyotypes. Normal karyotype has been reported for all lines used: Patient 1 / Isogenic Pat 1 (46, XX) and Patient 2 / Isogenic Pat 2 (46, XY).

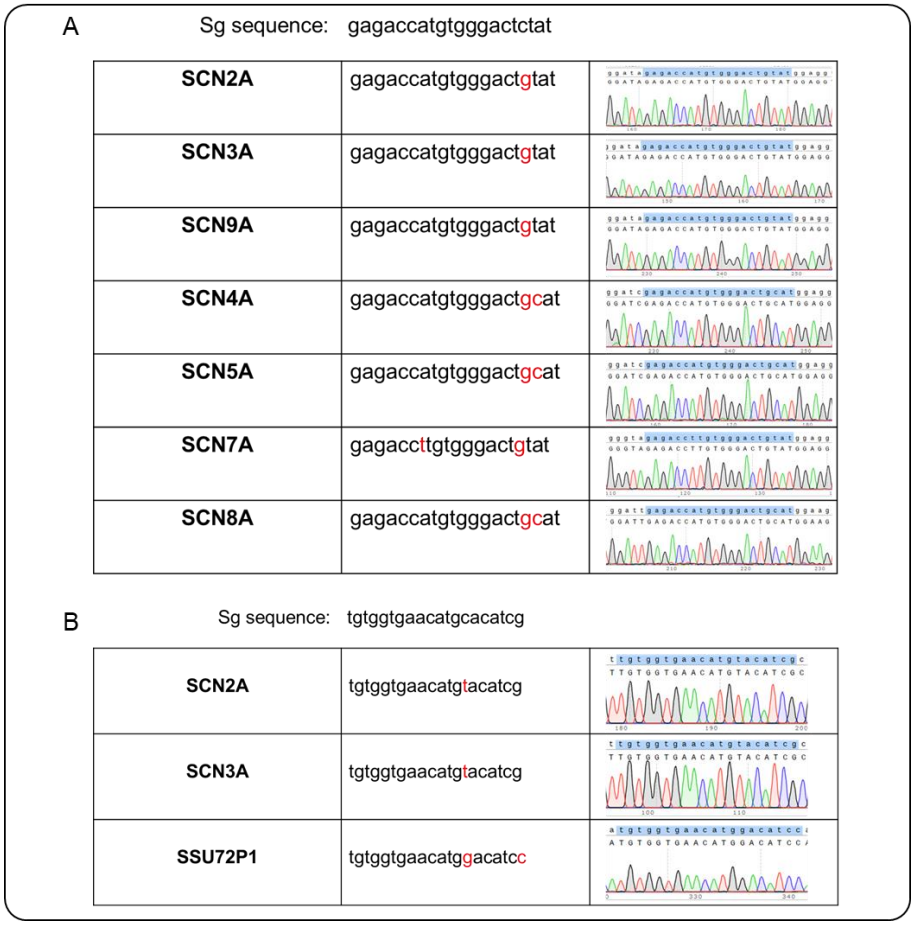

Supplemental figure 2. Off target genes for isogenic iPSCs generation. The top potential off-target sites from CRISPR/Cas9 editing, presenting one or two mismatches with both sg sequences used distinctly for patient 1 and 2, were found by using CRISPOR design tool (http://crispor.tefor.net/). All these regions have been amplified by PCR and sequenced to verify their integrity.

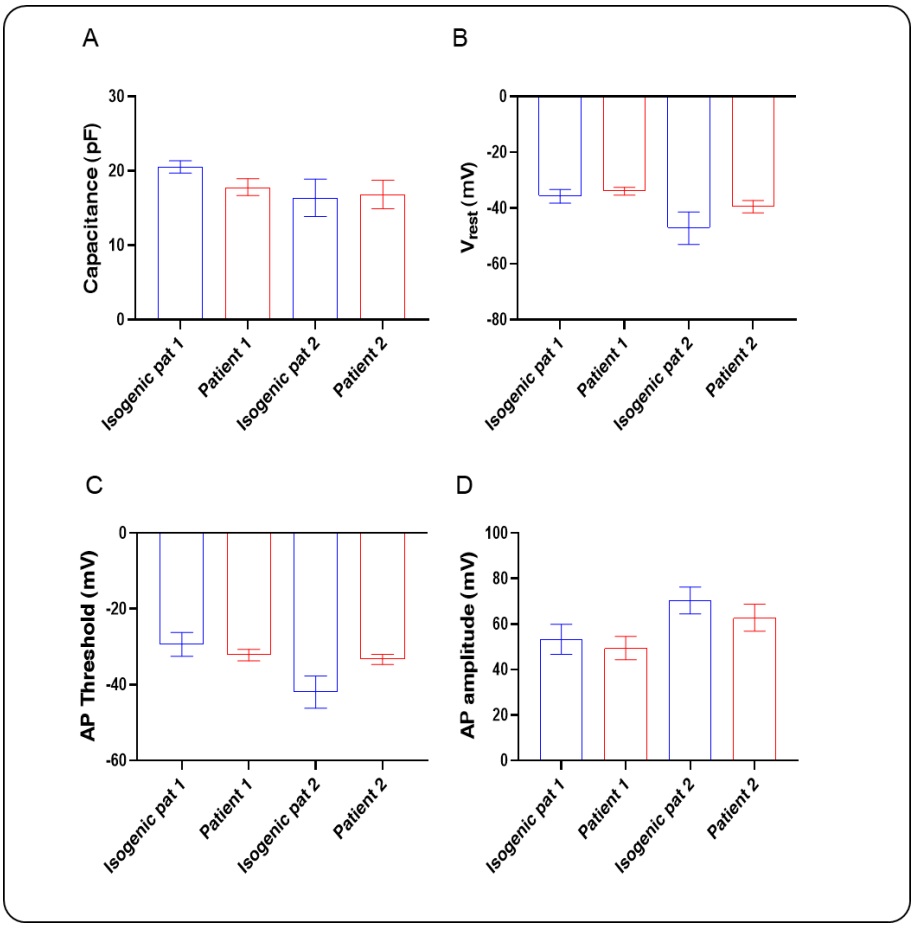

Supplemental figure 4. Active and passive cell properties of all iPSCs-derived GINs. (A) Capacitance, (B) resting membrane potential, (C) action potential firing threshold and (D) amplitude. No statistical differences were found in all parameters (data are means ±SEM; ns $p>0.05$, t-test).

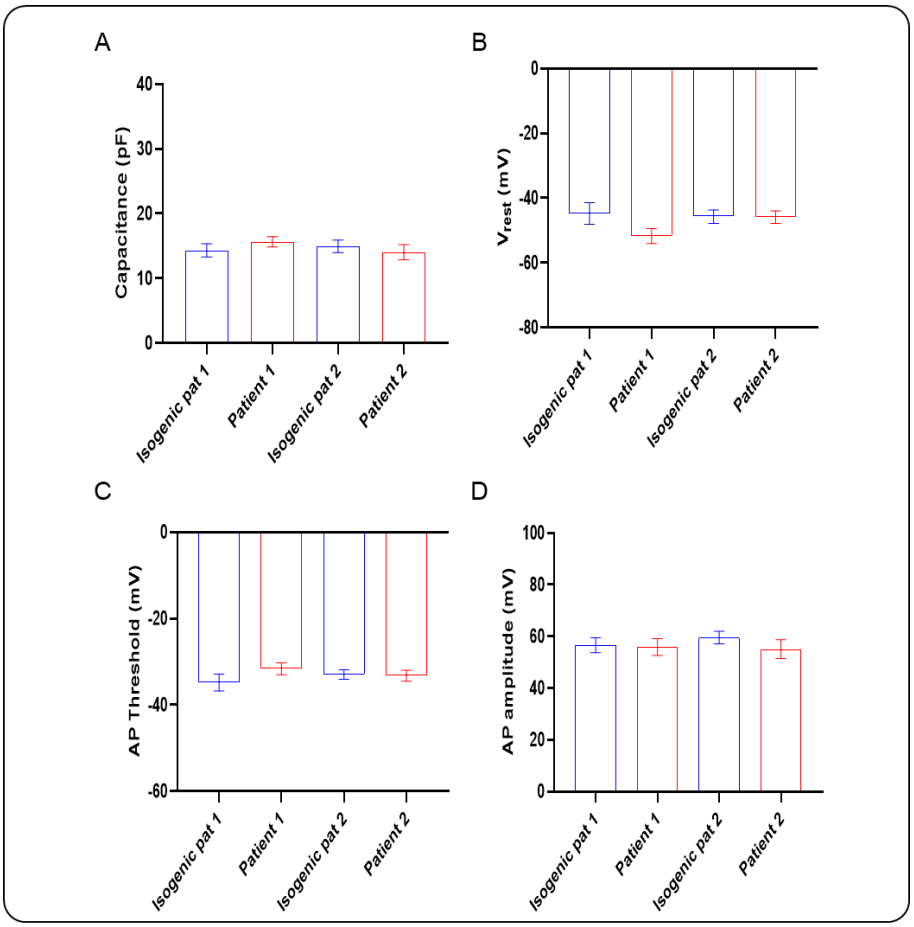

Supplementary figure 5. Active and passive cell properties of all iPSCs-derived cortical ExNs. (A) Capacitance, (B) resting membrane potential, (C) action potential firing threshold and (D) amplitude. No statistical differences were found in all parameters (data are means ±SEM; ns $p>0.05$, t-test).

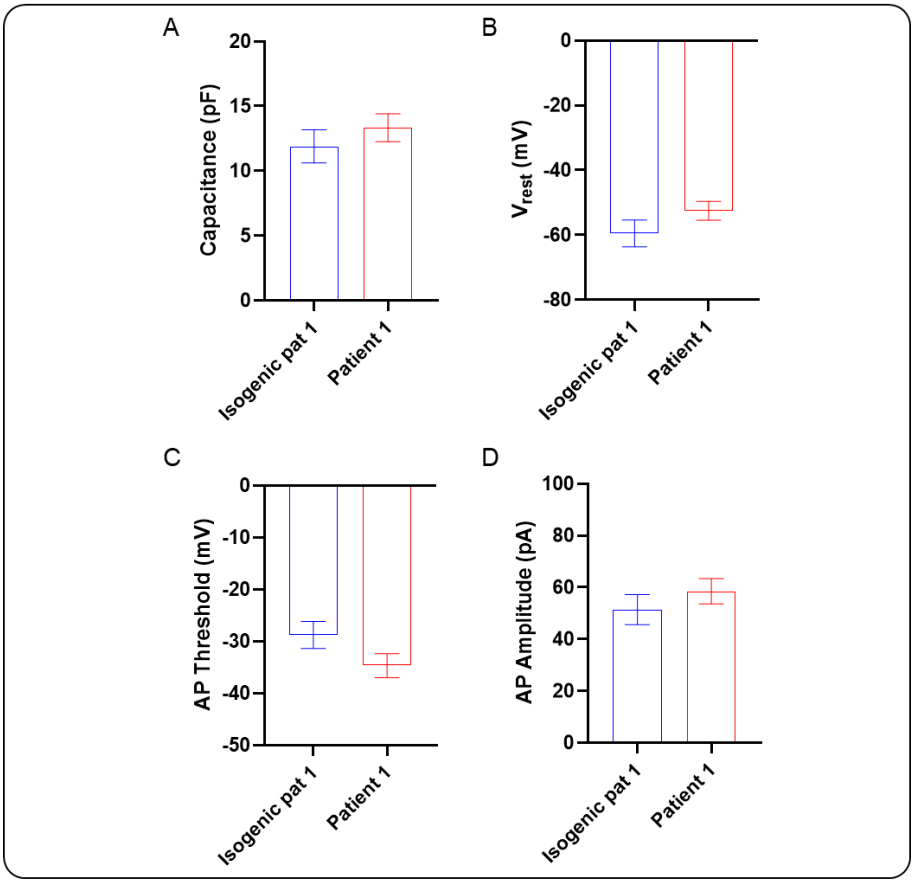

Supplemental figure 6. Active and passive cell properties of all iPSCs-derived GINs treated with BrainPhys medium. (A) Capacitance, (B) resting membrane potential, (C) action potential firing threshold and (D) amplitude. No statistical differences were found in all parameters (data are means ±SEM; ns $p>0.05$, t-test).

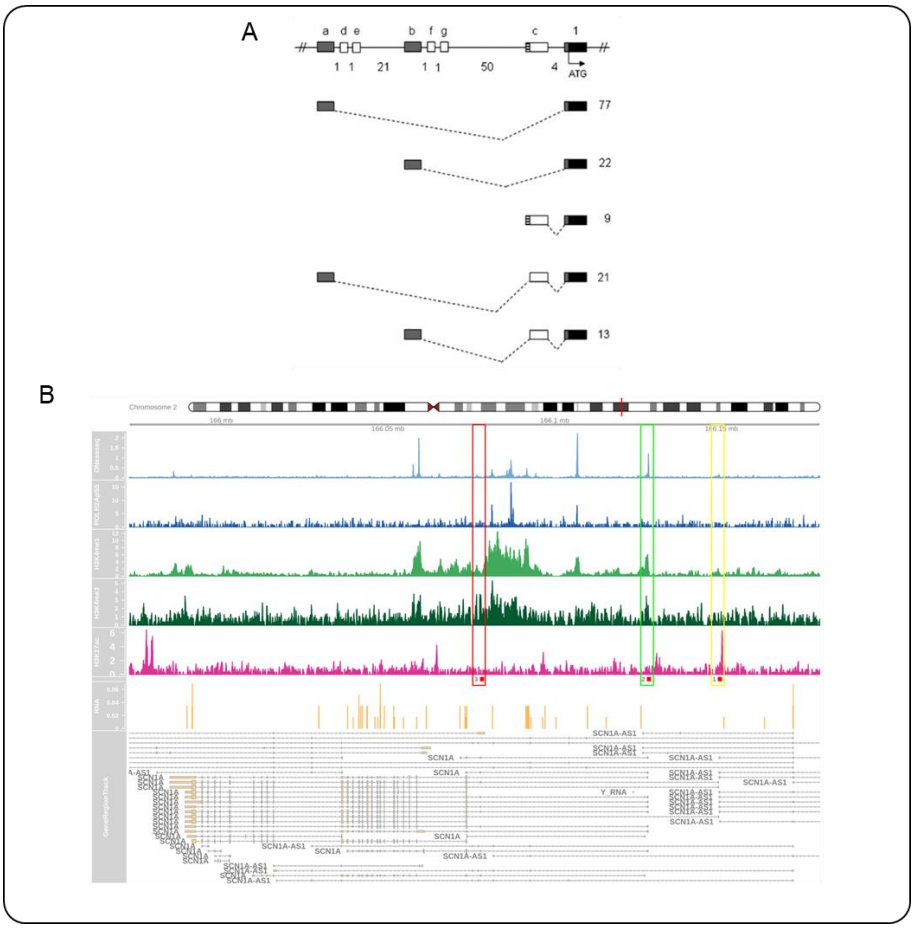

Supplemental figure 7. Analysis of the *SCN1A* gene locus for promoter regulatory region prediction. (A) Published data reported three TSSs for *SCN1A* gene (Martin et al. 2007). (B) IGV tracks showing epigenetic markers defining *SCN1A* TSS. The distal region (yellow) present K27ac and K4me1 CHIP-seq peaks defining an enhancer region. The intermedial region (green) present K4me1, K4me3 and DNase peaks defining a promoter region.

Name	Species	Catalog	Dilution
NKX2.1	Rabbit	Biopat Immunotechnologies PA0100	1:1000
PAX6	Rabbit	Covanxe PRB-278P	1:200
GABA	Rabbit	Sigma-Aldrich A2052	1:1000
MAP2	Chicken	Abcam ab92434	1:500
SST	Rat	R&D MAB2358	1:200
PV	Rabbit	Swant PV27	1:1000
TRA1-60	Mouse	Millipore MAB4360	1:200
OCT4	Rabbit	Abcam ab18976	1:300
SOX2	Rabbit	Abcam AB59776	1:200
FOXA2	Rabbit	Abcam AB40874	1:200
SMA	Mouse	Sigma-Aldrich A5228	1:500
TUJ1	Rabbit	Covance PRB-435P	1:500
VGLUT1	Guinea pig	Synaptic System 135 304	1:300
Human Nuclei	Mouse	Millipore MAB1281	1:100
NEUN	Mouse	Millipore MAB377	1:300
SATB2	Mouse	Invitrogen PA5-83092	1:200
TBR1	Rabbit	Abcam ab31940	1:300

Table 1. List of Abs used in IF

Gene		Sequence 5' -> 3'
NKX2.1	FW	caccatgaggaacagcgcctct
	RV	gctcatgttcatgccgctcgcc
DLX5	FW	ctcgctgggattgacacaaa
	RV	gggcatctccccgttttt
LHX6	FW	tggtcgaggagaaggtgctctg
	RV	agggcactgccccctccaacgt
PAX6	FW	aagcggaagctgcaaagaaa
	RV	cgggcaaacacatctggata
VGLUT1	FW	ccatcgtctccatggtcaat
	RV	gaggccgacagtctctggat
TBR2	FW	ctgtggcaaagccgacaata
	RV	tttcccgaatgaaatctcctg
NPAS4	FW	gccctctgccctggacac
	RV	cacgagtttgttgcctgcact
FOS	FW	caggaggggcaaggtggaac
	RV	cctccggttgcggcatttg
EGR1	FW	agcagcaccttcaaccctca
	RV	ctccaccagcaccttctcgt
DHCR7	FW	tggtcctggtcaacgtcctg
	RV	ccgaagtggtcatggcagatg
SCN1A	FW	gacggttttattgtgacgcttag
	RV	ttaacgttggccaagattttgc
SCN2A	FW	tgatggtcatggtgattggaa
	RV	cagtggcagcaagattgtcag
SCN3A	FW	catgttggtcatggtcattgg
	RV	tcatcagtagcagcaaggttgtc
SCN8A	FW	ggcggaaggacagaatcaac
	RV	catggcgggcactttctc
KCNA2	FW	agcttcacgtctctggtcag
	RV	ccaggaagcacaggagcatt
KCNB1	FW	ggagaagcccaattcctctg
	RV	cagcgtgttgagggacagg
KCNC1	FW	gaggacgagctggagatgac
	RV	cgatctccgtcttgttcacg
KCNC3	FW	ggctcaggaggaggtgattg
	RV	ggtcaatggctgggcagtcctc
ACTIN	FW	accccagccatgtacgtt
	RV	ggtgaggatcttcatgaggtag

Table 2. List of qRT-PCR Primers

Gene		Sequence 5' -> 3'
SCN1A Pat 1 mut	FW	tcaagttggcaaaatcttggccaac
	RV	tttaagttttagggtacatgtgcacaatg
SCN1A Pat 2 mut	FW	agttgggatcgatgacatgttcaact
	RV	ggcagattgagaggcggttcaag
SCN2A	FW	tcattggcaattctgtgggg
	RV	ggtagtttaagggtttgtgtgga
SCN3A	FW	tcattggcaattctgtgggg
	RV	aaaccagagcccaggagaag
SCN9A	FW	ctccgagtcttcaagttggcaaaat
	RV	gggttatttggctaggaaaactaat
SCN4A	FW	ctgcgggtcttcaagctggccaagt
	RV	cctaagtgattcttacacaggttaa
SCN5A	FW	atcatcgggaactcagtggg
	RV	ggtgggtagctgggtagatg
SCN7A	FW	tggtcctgttgttgttcaca
	RV	tgtaagacttcaaatctggtgca
SCN8A	FW	ctccgagtcttcaaattggccaaat
	RV	ccttagggtttctgggccaa
SCN2A	FW	agttgggatcgatgacatgttcaact
	RV	ctctcacccaaaacacgctt
SCN3A	FW	ttacaacctctgctggctgg
	RV	ctttggaggggtttgatgcc
SSU72P1	FW	cggtggtgtgctggaataac
	RV	cctggcctctcttcttctcc

Table 3. List of PCR primers

sgRNA	Sequence
sg patient 1	gagaccatgtgggactctat
sg patient 2	tgtggtgaacatgcacatcg
sg1A	ctcttttgaaatattttgga agg
sg2A	atgcaaactcccagcctgcc tgg
sg3A	ccaatacttcttgctcttgc tgg
sg4A	ttcagagagctccccagcac tgg
sg5A	ggagacacactgctggcctg tgg
sg6A	tcaggggttatggaagctgg agg
sg1B	gctatttgctgatttgtatt agg
sg2B	ttcatcctcgcctcactcta tgg
sg3B	agacctctgcagtatcctct cgg
sg4B	caagggctgcagtctcactg ggg
sg5B	ctttgacacctttgcaaga agg
sg6B	atctgaacaattgcaactga agg
sg7B	cattgttatcatctcgtctt tgg
sg8B	atgctgttcctcactgcaga tgg
sg1C	tttccataatgtcatatagt tgg
sg2C	ttgaaagaagcaatctaaaa tgg
sg3C	agtttctccatgtcttttca tgg
sg4C	ggaatattactcagcattaa agg
sg5C	gtgaatggataaataacctg tgg
sg6C	aggacatcttggttgcttcc agg
sg7C	tgctgtatacatccgtgtgc agg
sg8C	acataagttttcaactcctt tgg

Table 4. List of sgRNAs used to generate isogenic clones from patient iPSCs by using CRISPR/Cas9 gene editing and sgRNAs used to test activatory CRISPR/dCas9 on *SCN1A* gene

References

Almog, Yael, Saja Fadila, Marina Brusel, Anat Mavashov, Karen Anderson, and Moran Rubinstein. 2021. “Developmental Alterations in Firing Properties of Hippocampal CA1 Inhibitory and Excitatory Neurons in a Mouse Model of Dravet Syndrome.” *Neurobiology of Disease* 148: 105209. https://doi.org/10.1016/j.nbd.2020.105209.

Ardhanareeswaran, Karthikeyan, Jessica Mariani, Gianfilippo Coppola, Alexej Abyzov, Flora M Vaccarino, New Haven, and New Haven. 2018. “Human Induced Pluripotent Stem Cells for Modeling Neurodevelopmental Disorders” 13 (5): 265–78. https://doi.org/10.1038/nrneurol.2017.45.Human.

Astick, M., and Vanderhaeghen, P. (2018). From Human Pluripotent Stem Cells to Cortical Circuits. Curr. Top. Dev. Biol. 129, 67–98.

Banfi, Federica, Alicia Rubio, Mattia Zaghi, Luca Massimino, Giulia Fagnocchi, Edoardo Bellini, Mirko Luoni, et al. 2021. “SETBP1 Accumulation Induces P53 Inhibition and Genotoxic Stress in Neural Progenitors Underlying Neurodegeneration in Schinzel-Giedion Syndrome.” *Nature Communications* 12 (1): 1–21. https://doi.org/10.1038/s41467-021-24391-3.

Birey, Fikri, Jimena Andersen, Christopher D. Makinson, Saiful Islam, Wu Wei, Nina Huber, H. Christina Fan, et al. 2017. “Assembly of Functionally Integrated Human Forebrain Spheroids.” *Nature* 545 (7652): 54–59. https://doi.org/10.1038/nature22330.

Boulting, Gabriella L., Ershela Durresi, Bulent Ataman, Maxwell A. Sherman, Kevin Mei, David A. Harmin, Ava C. Carter, et al. 2021. “Activity-Dependent Regulome of Human GABAergic Neurons

Reveals New Patterns of Gene Regulation and Neurological Disease Heritability." *Nature Neuroscience* 24 (3): 437–48. https://doi.org/10.1038/s41593-020-00786-1.

Burke, Emily E., Joshua G. Chenoweth, Joo Heon Shin, Leonardo Collado-Torres, Suel Kee Kim, Nicola Micali, Yanhong Wang, et al. 2020. "Dissecting Transcriptomic Signatures of Neuronal Differentiation and Maturation Using IPSCs." *Nature Communications* 11 (1): 1–14. https://doi.org/10.1038/s41467-019-14266-z.

Butt, Simon JB, Vitor H Sousa, Marc V Fuccillo, Jens Hjerling-Leffler, Goichi Miyoshi, Shioko Kimura, and Gordon Fishell. 2008. "The Requirement of Nkx2-1 in the Temporal Specification of Cortical Interneuron Subtypes." *Neuron* 59 (5): 722–32. https://doi.org/10.1016/j.neuron.2008.07.031.The.

Cardoso-Moreira M, Halbert J, Valloton D, Velten B, Chen C, Shao Y, et al. Gene expression across mammalian organ development. Nature. 2019;571(7766):505–9. Epub 2019/06/28. pmid:31243369; PubMed Central PMCID: PMC6658352.

Carvill, Gemma L., Krysta L. Engel, Aishwarya Ramamurthy, J. Nicholas Cochran, Jolien Roovers, Hannah Stamberger, Nicholas Lim, et al. 2018. "Aberrant Inclusion of a Poison Exon Causes Dravet Syndrome and Related SCN1A-Associated Genetic Epilepsies." *American Journal of Human Genetics* 103 (6): 1022–29. https://doi.org/10.1016/j.ajhg.2018.10.023.

Catterall, William A., Franck Kalume, and John C. Oakley. 2010. "NaV1.1 Channels and Epilepsy." *Journal of Physiology* 588 (11): 1849–59. https://doi.org/10.1113/jphysiol.2010.187484.

Cetica V, Chiari S, Mei D, Parrini E, Grisotto L, Marini C, et al. Clinical and genetic factors predicting Dravet syndrome in infants with SCN1A mutations. Neurology. 2017;88(11):1037–44. Epub 2017/02/17. pmid:28202706; PubMed Central PMCID: PMC5384833.

Chambers, Stuart M., Christopher A. Fasano, Eirini P. Papapetrou, Mark Tomishima, Michel Sadelain, and Lorenz Studer. 2009. “Highly Efficient Neural Conversion of Human ES and IPS Cells by Dual Inhibition of SMAD Signaling.” *Nature Biotechnology* 27 (3): 275–80. https://doi.org/10.1038/nbt.1529.

Cheah, Christine S., Ruth E. Westenbroek, William H. Roden, Franck Kalume, John C. Oakley, Laura A. Jansen, and William A. Catterall. 2013. “Correlations in Timing of Sodium Channel Expression, Epilepsy, and Sudden Death in Dravet Syndrome.” *Channels* 7 (6): 468–72. https://doi.org/10.4161/chan.26023.

Cheah, Christine S., Frank H. Yu, Ruth E. Westenbroek, Franck K. Kalume, John C. Oakley, Gregory B. Potter, John L. Rubenstein, and William A. Catterall. 2012. “Specific Deletion of NaV1.1 Sodium Channels in Inhibitory Interneurons Causes Seizures and Premature Death in a Mouse Model of Dravet Syndrome.” *Proceedings of the National Academy of Sciences of the United States of America* 109 (36): 14646–51. https://doi.org/10.1073/pnas.1211591109.

Chen, Shuang-Qing, Fan Zhang, Chen-Lu Liu, Ming-Min Tong, and Zhong Zhao. 2018. “A Promotional Role of BDNF in Pluripotent Stem Cells Neural Differentiation via Wnt / β -Catenin and ERK /.” *Annals of Stem Cell Research & Therapy* 2 (4): 1–4.

Cheng, Albert W., Haoyi Wang, Hui Yang, Linyu Shi, Yarden Katz,

Thorold W. Theunissen, Sudharshan Rangarajan, Chikdu S. Shivalila, Daniel B. Dadon, and Rudolf Jaenisch. 2013. “Multiplexed Activation of Endogenous Genes by CRISPR-on, an RNA-Guided Transcriptional Activator System.” *Cell Research* 23 (10): 1163–71. https://doi.org/10.1038/cr.2013.122.

Colasante, Gaia, Gabriele Lignani, Simone Brusco, Claudia Di Berardino, Jenna Carpenter, Serena Giannelli, Nicholas Valassina, et al. 2019. “DCas9-Based Scn1a Gene Activation Restores Inhibitory Interneuron Excitability and Attenuates Seizures in Dravet Syndrome Mice.” *Molecular Therapy* 28 (1): 235–53. https://doi.org/10.1016/j.ymthe.2019.08.018.

Cunningham, Miles, Jun-Hyeongf Chod, Amanda Leunga, George Savvidisa, Sandra Ahna, Minho Moona, Paula KJ Leea, et al. 2014. “Human PSC-Derived Maturing GABAergic Interneurons Ameliorate Seizures and Abnormal Behavior in Epileptic Mice.” *Cell Stem Cell* 15 (5): 559–73. https://doi.org/10.1016/j.stem.2014.10.006.

Dang, J, SK Tiwari, G Lichinchi, Y Qin, VS Patil, AM Eroshkin, and Rana TM. 2016. “Zika Virus Depletes Neural Progenitors in Human Cerebral Organoids through Activation of the Innate Immune Receptor TLR3.” *Cell Stem Cell* 19 (2): 258–65. https://doi.org/10.1016/j.stem.2016.04.014.Zika.

Di Lullo, E., and Kriegstein, A.R. (2017). The use of brain organoids to investigate neural development and disease. Nat. Rev. Neurosci. 18, 573–584.

Dimidschstein, Jordane, Qian Chen, Robin Tremblay, Stephanie L. Rogers, Giuseppe Antonio Saldi, Lihua Guo, Qing Xu, et al. 2016. “A Viral Strategy for Targeting and Manipulating Interneurons

across Vertebrate Species." *Nature Neuroscience* 19 (12): 1743–49. https://doi.org/10.1038/nn.4430.

Dutton, Stacey B, Christopher D Makinson, Ligia A Papale, Anupama Shankar, Bindu Balakrishnan, Kazu Nakazawa, and Andrew Escayg. 2013. "Preferential Inactivation of Scn1a in Parvalbumin Interneurons Increases Seizure Susceptibility Stacey." *Neurobiology of Disease* 0: 211–20. https://doi.org/10.1016/j.nbd.2012.08.012.Preferential.

Escayg, Andrew, and Alan L Goldin. 2010. "Sodium Channel SCN1A and Epilepsy: Mutations and Mechanisms." *Epilepsia* 51 (9): 16. https://doi.org/10.1111/j.1528-1167.2010.02640.x.Sodium.

Favero, Morgana, Nathaniel P. Sotuyo, Emily Lopez, Jennifer A. Kearney, and Ethan M. Goldberg. 2018. "A Transient Developmental Window of Fast-Spiking Interneuron Dysfunction in a Mouse Model of Dravet Syndrome." *Journal of Neuroscience* 38 (36): 7912–27. https://doi.org/10.1523/JNEUROSCI.0193-18.2018.

Fogarty, Matthew, Matthew Grist, Diego Gelman, Oscar Marín, Vassilis Pachnis, and Nicoletta Kessaris. 2007. "Spatial Genetic Patterning of the Embryonic Neuroepithelium Generates GABAergic Interneuron Diversity in the Adult Cortex." *Journal of Neuroscience* 27 (41): 10935–46. https://doi.org/10.1523/JNEUROSCI.1629-07.2007.

Gao, Dong, Ian Vela, Andrea Sboner, Phillip J. Iaquinta, Wouter R. Karthaus, Anuradha Gopalan, Catherine Dowling, et al. 2014. "Organoid Cultures Derived from Patients with Advanced Prostate Cancer." *Cell* 159 (1): 176–87. https://doi.org/10.1016/j.cell.2014.08.016.

Giannelli, Serena G., Mirko Luoni, Valerio Castoldi, Luca Massimino, Tommaso Cabassi, Debora Angeloni, Gian Carlo Demontis, Letizia Leocani, Massimiliano Andreazzoli, and Vania Broccoli. 2018. “Cas9/SgRNA Selective Targeting of the P23H Rhodopsin Mutant Allele for Treating Retinitis Pigmentosa by Intravitreal AAV9.PHP.B-Based Delivery.” *Human Molecular Genetics* 27 (5): 761–79. https://doi.org/10.1093/hmg/ddx438.

Goff, Kevin M., and Ethan M. Goldberg. 2019. “Vasoactive Intestinal Peptide-Expressing Interneurons Are Impaired in a Mouse Model of Dravet Syndrome.” *ELife* 8: 1–28. https://doi.org/10.7554/eLife.46846.

Gu, Yuanzheng, Dustin Servello, Zhi Han, Rupa R. Lalchandani, Jun B. Ding, Kun Huang, and Chen Gu. 2018. “Balanced Activity between Kv3 and Nav Channels Determines Fast-Spiking in Mammalian Central Neurons.” *IScience* 9: 120–37. https://doi.org/10.1016/j.isci.2018.10.014.

Hedrich, Ulrike B.S., Camille Liautard, Daniel Kirschenbaum, Martin Pofahl, Jennifer Lavigne, Yuanyuan Liu, Stephan Theiss, et al. 2014. “Impaired Action Potential Initiation in GABAergic Interneurons Causes Hyperexcitable Networks in an Epileptic Mouse Model Carrying a Human Nav1.1 Mutation.” *Journal of Neuroscience* 34 (45): 14874–89. https://doi.org/10.1523/JNEUROSCI.0721-14.2014.

Higurashi, Norimichi, Taku Uchida, Christoph Lossin, Yoshio Misumi, Yohei Okada, Wado Akamatsu, Yoichi Imaizumi, et al. 2013. “A Human Dravet Syndrome Model from Patient Induced Pluripotent Stem Cells.” *Molecular Brain* 6.

Huang, Shih Min A., Yuji M. Mishina, Shanming Liu, Atwood Cheung,

Frank Stegmeier, Gregory A. Michaud, Olga Charlat, et al. 2009. “Tankyrase Inhibition Stabilizes Axin and Antagonizes Wnt Signalling.” *Nature* 461 (7264): 614–20. https://doi.org/10.1038/nature08356.

Jacob, Fadi, Ryan D. Salinas, Daniel Y. Zhang, Phuong T.T. Nguyen, Jordan G. Schnoll, Samuel Zheng Hao Wong, Radhika Thokala, et al. 2020. “A Patient-Derived Glioblastoma Organoid Model and Biobank Recapitulates Inter- and Intra-Tumoral Heterogeneity.” *Cell* 180 (1): 188-204.e22. https://doi.org/10.1016/j.cell.2019.11.036.

Jiao, Jiao, Yuanyuan Yang, Yiwu Shi, Jiayu Chen, Rui Gao, Yong Fan, Hui Yao, Weiping Liao, Xiao Fang Sun, and Shaorong Gao. 2013. “Modeling Dravet Syndrome Using Induced Pluripotent Stem Cells (IPSCs) and Directly Converted Neurons.” *Human Molecular Genetics* 22 (21): 4241–52. https://doi.org/10.1093/hmg/ddt275.

Kim, Hyun Woo, Zhejiu Quan, Young Beom Kim, Eunji Cheong, Heung Dong Kim, Minjung Cho, Jiho Jang, et al. 2018. “Differential Effects on Sodium Current Impairments by Distinct SCN1A Mutations in GABAergic Neurons Derived from Dravet Syndrome Patients.” *Brain and Development* 40 (4): 287–98. https://doi.org/10.1016/j.braindev.2017.12.002.

Konermann, Silvana, Mark D. Brigham, Alexandro E. Trevino, Julia Joung, Omar O. Abudayyeh, Clea Barcena, Patrick D. Hsu, et al. 2015. “Genome-Scale Transcriptional Activation by an Engineered CRISPR-Cas9 Complex.” *Nature* 517 (7536): 583–88. https://doi.org/10.1038/nature14136.

Lancaster, M.A., and Knoblich, J.A. (2014). Organogenesis in a dish:

modeling development and disease using organoid technologies. Science 345, 1247125.

Linaro, Daniele, Vermaercke, Ben, Iwata, Ryohei, Ramaswamy, Arjun, Libé-Philippot, Baptiste, Boubakar, Leila et al. 2019. Xenotransplanted Human Cortical Neurons Reveal Species-Specific Development and Functional Integration into Mouse Visual Circuits. Neuron 104 (5); 972-986.

Liodis, Petros, Myrto Denaxa, Marirena Grigoriou, Cynthia Akufo-Addo, Yuchio Yanagawa, and Vassilis Pachnis. 2007. “Lhx6 Activity Is Required for the Normal Migration and Specification of Cortical Interneuron Subtypes.” *Journal of Neuroscience* 27 (12): 3078–89. https://doi.org/10.1523/JNEUROSCI.3055-06.2007.

Liu, J., C. Gao, W. Chen, W. Ma, X. Li, Y. Shi, H. Zhang, et al. 2016. “CRISPR/Cas9 Facilitates Investigation of Neural Circuit Disease Using Human IPSCs: Mechanism of Epilepsy Caused by an SCN1A Loss-of-Function Mutation.” *Translational Psychiatry* 6 (November 2015). https://doi.org/10.1038/tp.2015.203.

Liu, Yu, Luis F Lopez-Santiago, Yukun Yuan, Julie M Jones, Helen Zhang, Heather A O’Malley, Gustavo A Patino, et al. 2013. “DRAVET SYNDROME PATIENT-DERIVED NEURONS SUGGEST A NOVEL EPILEPSY MECHANISM Yu.” *Ann Neurol* 74 (1): 128–39. https://doi.org/10.1002/ana.23897.

Lossin, Christoph, Thomas H. Rhodes, Reshma R. Desai, Carlos G. Vanoye, Dao Wang, Sanda Carniciu, Orrin Devinsky, and Alfred L. George. 2003. “Epilepsy-Associated Dysfunction in the Voltage-Gated Neuronal Sodium Channel SCN1A.” *Journal of Neuroscience* 23 (36): 11289–95. https://doi.org/10.1523/jneurosci.23-36-11289.2003.

Maeder, Morgan L., Samantha J. Linder, Vincent M. Cascio, Yanfang Fu, Quan H. Ho, and J. Keith Joung. 2013. “CRISPR RNA-Guided Activation of Endogenous Human Genes.” *Nature Methods* 10 (10): 977–79. https://doi.org/10.1038/nmeth.2598.

Marini, Carla, Ingrid E. Scheffer, Rima Nabbout, Arvid Suls, Peter De Jonghe, Federico Zara, and Renzo Guerrini. 2011. “The Genetics of Dravet Syndrome.” *Epilepsia* 52 (SUPPL. 2): 24–29. https://doi.org/10.1111/j.1528-1167.2011.02997.x.

Maroof, Asif M, Sotirios Keros, Jennifer A Tyson, Shui-Wang Ying, Yosif M Ganat, Florian T Merkle, Becky Liu, et al. 2013. “Directed Differentiation and Functional Maturation of Cortical Interneurons from Human Embryonic Stem Cells.” *Cell Stem Cell* 12 (5): 1-559–72. https://doi.org/10.1016/j.stem.2013.04.008.

Martin, Melinda S., Karoni Dutt, Ligia A. Papale, Céline M. Dubé, Stacey B. Dutton, Georgius De Haan, Anupama Shankar, et al. 2010. “Altered Function of the SCN1A Voltage-Gated Sodium Channel Leads to γ-Aminobutyric Acid-Ergic (GABAergic) Interneuron Abnormalities.” *Journal of Biological Chemistry* 285 (13): 9823–34. https://doi.org/10.1074/jbc.M109.078568.

Martin, Melinda S., Bin Tang, Nga Ta, and Andrew Escayg. 2007. “Characterization of 5′ Untranslated Regions of the Voltage-Gated Sodium Channels SCN1A, SCN2A, and SCN3A and Identification of Cis-Conserved Noncoding Sequences.” *Genomics* 90 (2): 225–35. https://doi.org/10.1016/j.ygeno.2007.04.006.

Meganathan, Kesavan, Emily M.A. Lewis, Paul Gontarz, Shaopeng Liu, Edouard G. Stanley, Andrew G. Elefanty, James E. Huettner, Bo Zhang, and Kristen L. Kroll. 2017. “Regulatory Networks Specifying Cortical Interneurons from Human Embryonic Stem

Cells Reveal Roles for CHD2 in Interneuron Development." *Proceedings of the National Academy of Sciences of the United States of America* 114 (52): E11180–89. https://doi.org/10.1073/pnas.1712365115.

Mistry, Akshitkumar M, Christopher H Thompson, Alison R Miller, Carlos G Vanoye1, Alfred L George Jr, and Jennifer A Kearney. 2014. "Strain- and Age-Dependent Hippocampal Neuron Sodium Currents Correlate with Epilepsy Severity in Dravet Syndrome Mice." *Neurobiology of Disease* 65: 1–11. https://doi.org/10.1016/j.nbd.2014.01.006.

Molyneaux, Bradley J., Paola Arlotta, Joao R.L. Menezes, and Jeffrey D. Macklis. 2007. "Neuronal Subtype Specification in the Cerebral Cortex." *Nature Reviews Neuroscience* 8 (6): 427–37. https://doi.org/10.1038/nrn2151.

Nicholas, Cory R, Jiadong Chen, Yunshuo Tang, Derek G Southwell, Daniel Vogt, Christine M Arnold, Ying-jiun J Chen, et al. 2013. "Functional Maturation of HPSC-Derived Forebrain Interneurons Requires an Extended Timeline and Mimics Human Neural Development." *Cell Stem Cell* 12 (5): 573–86. https://doi.org/10.1016/j.stem.2013.04.005.

Ogiwara, Ikuo, Hiroyuki Miyamoto, Noriyuki Morita, Nafiseh Atapour, Emi Mazaki, Ikuyo Inoue, Tamaki Takeuchi, et al. 2007. "Nav1.1 Localizes to Axons of Parvalbumin-Positive Inhibitory Interneurons: A Circuit Basis for Epileptic Seizures in Mice Carrying an Scn1a Gene Mutation." *Journal of Neuroscience* 27 (22): 5903–14. https://doi.org/10.1523/JNEUROSCI.5270-06.2007.

Ohmori, Iori, Kristopher M. Kahlig, Thomas H. Rhodes, Dao W. Wang,

and Alfred L. George. 2006. “Nonfunctional SCN1A Is Common in Severe Myoclonic Epilepsy of Infancy.” *Epilepsia* 47 (10): 1636–42. https://doi.org/10.1111/j.1528-1167.2006.00643.x.

Panganiban, Grace, and John L R Rubenstein. 2002. “Developmental Functions of the Distal-Less/Dlx Homeobox Genes.” *Development (Cambridge, England)* 129 (19): 4371–86.

Qi, Yuchen, Xin-jun Zhang, Nicolas Renier, Zhuhao Wu, Talia Atkin, Ziyi Sun, Zeeshan Ozair, et al. 2017. “Accelerated Cortical Neuron Differentiation Protocol” 35 (2): 154–63. https://doi.org/10.1038/nbt.3777.Combined.

Quadrato, Giorgia, Tuan Nguyen, Evan Z. Macosko, John L. Sherwood, Sung Min Yang, Daniel R. Berger, Natalie Maria, et al. 2017. “Cell Diversity and Network Dynamics in Photosensitive Human Brain Organoids.” *Nature* 545 (7652): 48–53. https://doi.org/10.1038/nature22047.

Ragona F, Brazzo D, De Giorgi I, Morbi M, Freri E, Teutonico F, et al. Dravet syndrome: early clinical manifestations and cognitive outcome in 37 Italian patients. Brain & development. 2010;32(1):71–7. Epub 2009/10/27. pmid:19854600.

Ragsdale, David S. 2008. “How Do Mutant Nav1.1 Sodium Channels Cause Epilepsy?” *Brain Research Reviews* 58 (1): 149–59. https://doi.org/10.1016/j.brainresrev.2008.01.003.

Rubinstein, Moran, Sung Han, Chao Tai, Ruth E. Westenbroek, Avery Hunker, Todd Scheuer, and William A. Catterall. 2015. “Dissecting the Phenotypes of Dravet Syndrome by Gene Deletion.” *Brain* 138 (8): 2219–33. https://doi.org/10.1093/brain/awv142.

Rubinstein, Moran, Ruth E. Westenbroek, Frank H. Yu, Christina J.

Jones, Todd Scheuer, and William A. Catterall. 2015. “Genetic Background Modulates Impaired Excitability of Inhibitory Neurons in a Mouse Model of Dravet Syndrome.” *Neurobiology of Disease* 73: 106–17. https://doi.org/10.1016/j.nbd.2014.09.017.

Rudy, Bernardo, and Chris J. McBain. 2001. “Kv3 Channels: Voltage-Gated K+ Channels Designed for High-Frequency Repetitive Firing.” *Trends in Neurosciences* 24 (9): 517–26. https://doi.org/10.1016/S0166-2236(00)01892-0.

Shin, Dong Mi, Joon Ik Ahn, Ki Hwan Lee, Yong Sung Lee, and Yeon Sook Lee. 2004. “Ascorbic Acid Responsive Genes during Neuronal Differentiation of Embryonic Stem Cells.” *NeuroReport* 15 (12): 1959–63. https://doi.org/10.1097/00001756-200408260-00025.

Stasi, Angela Michela De, Pasqualina Farisello, Iacopo Marcon, Stefano Cavallari, Angelo Forli, Dania Vecchia, Gabriele Losi, et al. 2016. “Unaltered Network Activity and Interneuronal Firing during Spontaneous Cortical Dynamics in Vivo in a Mouse Model of Severe Myoclonic Epilepsy of Infancy.” *Cerebral Cortex* 26 (4): 1778–94. https://doi.org/10.1093/cercor/bhw002.

Sun, Yishan, Sergiu P. Paşca, Thomas Portmann, Carleton Goold, Kathleen A. Worringer, Wendy Guan, Karen C. Chan, et al. 2016. “A Deleterious Nav1.1 Mutation Selectively Impairs Telencephalic Inhibitory Neurons Derived from Dravet Syndrome Patients.” *ELife* 5 (2016JULY): 1–26. https://doi.org/10.7554/eLife.13073.

Sussel, Lori, Oscar Marin, Shioko Kimura, and John L.R. Rubenstein. 1999. “Loss of Nkx2.1 Homeobox Gene Function Results in a Ventral to Dorsal Molecular Respecification within the Basal Telencephalon: Evidence for a Transformation of the Pallidum into

the Striatum." *Development* 126 (15): 3359–70. https://doi.org/10.1242/dev.126.15.3359.

Tai, Chao, Yasuyuki Abe, Ruth E. Westenbroek, Todd Scheuer, and William A. Catterall. 2014. "Impaired Excitability of Somatostatin- and Parvalbumin-Expressing Cortical Interneurons in a Mouse Model of Dravet Syndrome." *Proceedings of the National Academy of Sciences of the United States of America* 111 (30): 3139–48. https://doi.org/10.1073/pnas.1411131111.

Tran, Conny H., Michael Vaiana, Johan Nakuci, Ala Somarowthu, Kevin M. Goff, Nitsan Goldstein, Priya Murthy, Sarah F. Muldoon, and Ethan M. Goldberg. 2020. "Interneuron Desynchronization Precedes Seizures in a Mouse Model of Dravet Syndrome." *Journal of Neuroscience* 40 (13): 2764–75. https://doi.org/10.1523/JNEUROSCI.2370-19.2020.

Traub, Stefanie, Heiko Stahl, Holger Rosenbrock, Eric Simon, and Ralf Heilker. 2017. "Upscaling of HiPS Cell-Derived Neurons for High-Throughput Screening." *SLAS Discovery* 22 (3): 274–86. https://doi.org/10.1177/1087057116678161.

Trimmer, James S., and Kenneth J. Rhodes. 2004. "Localization of Voltage-Gated Ion Channels in Mammalian Brain." *Annual Review of Physiology* 66 (1): 477–519. https://doi.org/10.1146/annurev.physiol.66.032102.113328.

Uylings, H. B.M., I. Delalle, Z. Petanjek, and M. J.T. Koenderink. 2002. "Structural and Immunocytochemical Differentiation of Neurons in Prenatal and Postnatal Human Prefrontal Cortex." *Neuroembryology* 1 (4): 176–86. https://doi.org/10.1159/000066268.

Volkers, Linda, Kristopher M. Kahlig, Nienke E. Verbeek, Joost H.G. Das, Marjan J.A. van Kempen, Hans Stroink, Paul Augustijn, et al. 2011. “Na v1.1 Dysfunction in Genetic Epilepsy with Febrile Seizures-plus or Dravet Syndrome.” *European Journal of Neuroscience* 34 (8): 1268–75. https://doi.org/10.1111/j.1460-9568.2011.07826.x.

Wang, Jun, Shao Wu Ou, and Yun Jie Wang. 2017. “Distribution and Function of Voltage-Gated Sodium Channels in the Nervous System.” *Channels* 11 (6): 534–54. https://doi.org/10.1080/19336950.2017.1380758.

Wang, Wenze, Sachio Takashima, Yoshie Segawa, Masayuki Itoh, Xiuyu Shi, Su Kyeong Hwang, Kazuki Nabeshima, Morishige Takeshita, and Shinichi Hirose. 2011. “The Developmental Changes of Nav1.1 and Nav1.2 Expression in the Human Hippocampus and Temporal Lobe.” *Brain Research* 1389: 61–70. https://doi.org/10.1016/j.brainres.2011.02.083.

Wirrell EC, Laux L, Donner E, Jette N, Knupp K, Meskis MA, et al. Optimizing the Diagnosis and Management of Dravet Syndrome: Recommendations From a North American Consensus Panel. Pediatric Neurology. 2017;68:18–34.e3. pmid:28284397

Wilson, Stephen W., and John L.R. Rubenstein. 2000. “Induction and Dorsoventral Patterning of the Telencephalon.” *Neuron* 28 (3): 641–51. https://doi.org/10.1016/S0896-6273(00)00171-9.

Xie, Yunyao, Nathan N. Ng, Olga S. Safrina, Carmen M. Ramos, Kevin C. Ess, Philip H. Schwartz, Martin A. Smith, and Diane K. O’Dowd. 2020. “Comparisons of Dual Isogenic Human IPSC Pairs Identify Functional Alterations Directly Caused by an Epilepsy Associated SCN1A Mutation.” *Neurobiology of Disease* 134 (July 2019):

104627. https://doi.org/10.1016/j.nbd.2019.104627.

Xu, Qing, Inma Cobos, Estanislao D. De La Cruz, John L. Rubenstein, and Stewart A. Anderson. 2004. “Origins of Cortical Interneuron Subtypes.” *Journal of Neuroscience* 24 (11): 2612–22. https://doi.org/10.1523/JNEUROSCI.5667-03.2004.

Yamagata, Tetsushi, Matthieu Raveau, Kenta Kobayashi, Hiroyuki Miyamoto, Tetsuya Tatsukawa, Ikuo Ogiwara, Shigeyoshi Itohara, Takao K. Hensch, and Kazuhiro Yamakawa. 2020. “CRISPR/DCas9-Based Scn1a Gene Activation in Inhibitory Neurons Ameliorates Epileptic and Behavioral Phenotypes of Dravet Syndrome Model Mice.” *Neurobiology of Disease* 141 (May): 104954. https://doi.org/10.1016/j.nbd.2020.104954.

Yan, Qinghong, Sebastien M. Weyn-Vanhentenryck, Jie Wu, Steven A. Sloan, Ye Zhang, Kenian Chen, Jia Qian Wu, Ben A. Barres, and Chaolin Zhang. 2015. “Systematic Discovery of Regulated and Conserved Alternative Exons in the Mammalian Brain Reveals NMD Modulating Chromatin Regulators.” *Proceedings of the National Academy of Sciences of the United States of America* 112 (11): 3445–50. https://doi.org/10.1073/pnas.1502849112.

Yu, Frank H., Massimo Mantegazza, Ruth E. Westenbroek, Carol A. Robbins, Franck Kalume, Kimberly A. Burton, William J. Spain, G. Stanley McKnight, Todd Scheuer, and William A. Catterall. 2006. “Reduced Sodium Current in GABAergic Interneurons in a Mouse Model of Severe Myoclonic Epilepsy in Infancy.” *Nature Neuroscience* 9 (9): 1142–49. https://doi.org/10.1038/nn1754.

Zahir, Tasneem, Ying Fang Chen, John F. MacDonald, Nic Leipzig, Charles H. Tator, and Molly S. Shoichet. 2009. “Neural Stem/Progenitor Cells Differentiate in Vitro to Neurons by the

Combined Action of Dibutyryl CAMP and Interferon-γ." *Stem Cells and Development* 18 (10): 1423–32. https://doi.org/10.1089/scd.2008.0412.

Zhang, Yingsha, Changhui Pak, Yan Han, Henrik Ahlenius, Zhenjie Zhang, Soham Chanda, Samuele Marro, et al. 2013. "Rapid Single-Step Induction of Functional Neurons from Human Pluripotent Stem Cells" 78 (5): 785–98. https://doi.org/10.1016/j.neuron.2013.05.029.

CHAPTER 3

dCas9-based *Scn1a* gene activation restores inhibitory interneuron excitability and attenuates seizures in Dravet Syndrome mice

Gaia Colasante[1], Gabriele Lignani[2], Simone Brusco[1], Claudia Di Berardino[1], Jenna Carpenter[2], Serena Giannelli[1], Nicholas Valassina[1], Simone Bido[1], Raffaele Ricci[1], Valerio Castoldi[3], Silvia Marenna[3], Timothy Church[2], Luca Massimino[1], Giuseppe Morabito[1], Fabio Benfenati[4,5], Stephanie Schorge[2], Letizia Leocani[3], Dimitri M. Kullmann[2] and Vania Broccoli[1,6]

[1]Stem Cell and Neurogenesis Unit, Division of Neuroscience, San Raffaele Scientific Institute, 20132 Milan, Italy; [2]Department of Clinical and Experimental Epilepsy, UCL Institute of Neurology, University College London, Queen Square, London WC1N 3BG, UK; [3]Experimental Neurophysiology Unit, Institute of Experimental Neurology (INSPE), San Raffaele Scientific Institute, 20132 Milan, Italy; [4]Center for Synaptic Neuroscience and Technology, Istituto Italiano di Tecnologia, 16132 Genova, Italy; [5]IRCCS Ospedale Policlinico San Martino, University of Genova, 16132 Genova, Italy; [6]CNR Institute of Neuroscience, 20129 Milan, Italy

Published on Molecular Therapy 28 (1), 235-253.

Summary

Dravet syndrome (DS) is a severe epileptic encephalopathy caused mainly by heterozygous loss-of-function mutations of the *SCN1A* gene, indicating haploinsufficiency as the pathogenic mechanism. Here we tested whether catalytically deadCas9 (dCas9)-mediated *Scn1a* gene activation can rescue *Scn1a* haploinsufficiency in a mouse DS model and restore physiological levels of its gene product, the $Na_v1.1$ voltage-gated sodium channel. We screened single guide RNAs (sgRNAs) for their ability to stimulate *Scn1a* transcription in association with the dCas9 activation system. We identified a specific sgRNA that increases *Scn1a* gene expression levels in cell lines and primary neurons with high specificity. $Na_v1.1$ protein levels were augmented, as was the ability of wild-type immature GABAergic interneurons to fire action potentials. A similar enhancement of *Scn1a* transcription was achieved in mature DS interneurons, rescuing their ability to fire. To test the therapeutic potential of this approach, we delivered the *Scn1a*-dCas9 activation system to DS pups using adeno-associated viruses. Parvalbumin interneurons recovered their firing ability, and febrile seizures were significantly attenuated. Our results pave the way for exploiting dCas9-based gene activation as an effective and targeted approach to DS and other disorders resulting from altered gene dosage.

Introduction

Dravet syndrome (DS) is a severe epileptic encephalopathy beginning in the first year of life with seizures often associated with fever that evolve into frequent, prolonged, and clustered epileptic crises.1–3 In subsequent years, patients often develop psychomotor delay, behavioral disturbances, and cognitive impairment.4 DS is a genetic condition mainly caused by mutations in the *SCN1A* gene encoding for the $Na_v1.1$ voltage-gated sodium channel α subunit.5,6 Over 650 missense and nonsense *SCN1A* mutations have been described in DS patients. Although most are de novo, some mutations have been found to be inherited in familial cases.7 *SCN1A* mutations affect only one copy of the gene, typically leading to loss of function and indicating that a haploinsufficient genetic mechanism is responsible for DS. These data suggest that a reduced amount of $Na_v1.1$ channel impairs neuronal activity and function. *Scn1a* heterozygous mutant mice display similar neurological symptoms, including severe epilepsy, behavioral alterations, and premature death.8–11 Functional studies revealed that cortical fast-spiking GABAergic inhibitory interneurons exhibit reduced intrinsic excitability and defects in action potential firing.8,10,12 In contrast, both excitability and firing of cortical excitatory neurons from *Scn1a* heterozygous mutant mice appear to be substantially unaltered.8,13 These findings potentially resolve the paradox that epilepsy arises from loss-of-function mutations in $Na_v1.1$, which contributes to the fast depolarization of neuronal membranes during an action potential. Of note, $Na_v1.1$ has been

found to be mainly expressed in inhibitory interneurons by immuno-histochemistry analysis, suggesting that this sodium channel isoform has a preponderant function in that neuronal population.10 Accordingly, selective inactivation of *Scn1a* in cortical interneurons is sufficient to elicit neurological deficits comparable with those described in constitutive mutant mice,14,15 and, conversely, *Scn1a* loss restricted to the dorsal-telencephalic (e.g., neocortical, hippocampal) excitatoryneurons has ameliorating effects on epileptic seizures and sudden death.13 *Scn1a* heterozygous mutant mice develop spontaneous and recurrent seizures starting from 3 weeks after birth, often leading to premature and sudden death.8–10 Remarkably, body temperature elevation triggers myoclonic and generalized seizures in these mice,recapitulating febrile seizures in DS patients.16 Thus, DS mice represent a valuable model of the disease, not only to dissect the pathological mechanisms but also to evaluate the efficacy of innovative therapies. Drug treatment of DS patients, including stiripentol in combination with clobazam and valproate, has limited efficacy and poorly controls convulsive seizures.17,18 Cannabidiol or serotonin up-take inhibitors have been reported to reduce seizure frequency in some patients, but larger studies are needed to appreciate the exact therapeutic indications for these treatments.19–21 Nonetheless, complete seizure cessation is rarely obtained with any of these pharmacological anticonvulsants. Gene therapy approaches for neurodevelopmental disorders are in rapid development because of the introduction of novel serotypes of

recombinant adeno-associatedviruses (AAVs), allowing efficient transduction of neurons.22 However, the *SCN1A* coding sequence is 6 kb long, exceeding the strict cargo limit for AAVs. Although lentiviruses (LVs) can carry the *SCN1A* gene sequence, they show limited spread in neural tissue and are therefore inadequate to treat diseases affecting large brain areas.23 These obstacles have prevented substantial advances in gene-based therapies for DS. Given that one copy of the *SCN1A* gene is still functional in DS, stimulating its endogenous expression over physiological levels might lead to increased availability of the$Na_v1.1$ channel protein, potentially leading to symptomatic improvement. Thus, a system able to induce *SCN1A* gene expression in neurons in a regulated manner, without significant off-target effects, would be a strong therapeutic candidate tool for DS. CRISPR-Cas9 technology has become a powerful tool for genome editing, allowing DNA to be targeted with high efficiency and specificity. As demonstrated by pioneering works in several cell types and organisms, the Cas9/single guide RNA (sgRNA) complex can efficiently generate double-strand breaks, which then trigger non-homologous end joining-mediated gene knockout or homology-directed repair-mediated recombination.24–26 A modified version of the CRISPR-Cas9 system has been developed by generating a nuclease-deadCas9 (dCas9) fused to effector domains for transcriptional gene regulation. Hence, the dCas9/sgRNA complex has provided a crucial platform for programming diverse types of transcriptional or epigenetic

manipulation of the genome without cleaving the target DNA.27–29 Seminal studies have shown that dCas9-based gene activation is highly specific in DNA binding and gene regulation and promotes chromatin remodeling of the regulatory elements of the gene of interest.30–32 This system has been successfully implemented to investigate hierarchies in gene regulatory networks, screening for cellular phenotypes and directing somatic cell fate.33–36 In the activatory CRISPR system, dCas9 is fused to multiple VP16 transcriptional activator domains that robustly boost gene transcription when combined with one or more sgRNAs targeting sequences in the proximal promoters or close to transcription start sites (TSSs).26,36,37 As proof of concept, this technology has also been employed to activate endogenous genes in mouse models of disease to ameliorate biomarkers of diabetes, muscular dystrophy, and acute kidney disease.30 More recently, it has been applied to enhance expression of the Sim1 gene in the hypothalamus and to rescue the associated obesity phenotype.38 Here we describe a dCas9-based system that significantly upregulates *Scn1a* expression and restores $Na_v1.1$ protein levels in both cellular and animal models of DS. This targeted gene activation rescues membrane excitability and action potential firing in DS cortical interneurons and significantly attenuates hyperthermia-induced seizures in DS mice.

Results

A single sgRNA enhances *Scn1a* gene expression by targeting its proximal promoter

To achieve upregulation of *Scn1a* gene transcription, we sought to define the necessary dCas9/sgRNA elements by a candidate approach *in vitro*. Through an extensive bioinformatics analysis, we determined the *Scn1a* gene promoter regions to focus the sgRNA design. Several studies have pointed out that sgRNAs can transactivate genes of interest more efficiently when localized within 500 bp from the gene TSS.34 We interrogated the Encyclo-pedia of DNA Elements (ENCODE) and Fantom5 databases for the expression profiling and epigenetic marks of actively transcribed genes in the adult mouse brain. In addition, CAGE-seq and DNase-seq datasets were queried to determine the exact TSSs for *Scn1a* (Figure S1). We identified two regions in the *Scn1a* locus where RNA polymerase II (Pol II), mono- and tri-methylation of lys4, and acetylation of lys27 of H3 histone were strongly enriched and revealed DNase I-hypersensitive sites. CAGE-seq peaks were aligned to the same sequences, confirming the existence of two active TSSs (TSS1 and TSS2) located upstream of two non-coding exons (exon A and exon B) (Figure S1) and producing two different mRNA isoforms, both expressed in the adult mouse brain.39 200 bp upstream of the exon A (distal promoter) and 250 bp upstream of exon B (proximal promoter) (Figure 1A) were submitted to the CRISPOR web tool (http://crispor.tefor.net) for sgRNA design. We selected

five guides in the distal promoter and six in the proximal one with specificity scores higher than 50% (Figures 1B and 1C; Table S1). Then we determined whether dCas9 fused to VP160 (dCas9-VP160), a transcriptional activator that carries 10 tandem copies of VP16 (a herpes simplex virus type 1 transcription factor), in association with the selected sgRNAs was able to upregulate *Scn1a* gene expression in the P19 murine teratocarcinoma cell line. sgRNAs specific for *Scn1a* promoters and one control guide (sgCtrl), targeting the β-galactosidase bacterial sequence, were cloned into the pU6 vector and individually lipofected into P19 cells together with the Ef1a-dCas9-VP160-T2A-GFP (Figure 1D), and 3 days later, after ascertaining GFP expression, cells were harvested for RNA extraction and qRT-PCR (Figure 1D). Interestingly, none of the sgRNAs targeting the distal promoter were able to significantly alter the basal expression of *Scn1a* (Figure 1E). Conversely, among the guides targeting the proximal promoter, only sg1P was found to significantly increase *Scn1a* mRNA levels with respect to sgCtrl (Figure 1F). Comparable results were obtained when sgRNAs were lipofected with dCas9 linked to a puromycin resistance cassette (Ef1a-dCas9-VP160-T2A-PuroR) and puromycin was added to the culture medium the day after transfection (Figures S2A–S2C), indicating that antibiotic selection and consequent enrichment of lipofected cells were not strictly necessary to detect sg1P-mediated *Scn1a* induction. sg1P upregulated *Scn1a* gene expression to a similar extent in primary mouse embryonic fibroblasts (MEFs) (Figure S2D). In

conclusion, we identified sg1P as an sgRNA that is sufficient, when associated with the dCas9 activation system, to stimulate basal transcription of *Scn1a* consistently indifferent cell types.

sg1P/dCas9-VP160 lentiviral transduction upregulates *Scn1a* expression in primary neurons

We asked whether the sg1P/dCas9-VP160 system could stimulate *Scn1a* expression in primary hippocampal neurons. Neurons were co-transduced with Ef1a-dCas9VP160-T2A-GFP and pU6-sg1P or pU6-sgCtrl LVs the day after plating to maximize transduction effi ciency (Figure 2A). Immunofluorescence analysis performed at 10 days *in vitro* (DIV) showed that almost 50% of the plated neurons were transduced (Figure 2B). With this intermediate efficiency, we decided to purify the infected cells to obtain reliable information regarding the regulation of *Scn1a* expression. Thus, 10 DIV transduced GFP+ neurons from sgCtrl- and sg1P-treated samples were isolated by fluorescence-activated cell sorting (FACS) (Figure 2C), and the RNA was extracted for gene expression analysis. *Scn1a* expression levels were robustly increased when transduced with sg1P with respect to sgCtrl (Figure 2D). However, FACS is detrimental to neurons and prevents their func-tional analysis. For this reason, we generated a single lentiviral vector carrying both sg1P and dCas9-VP160 (Fig-ure 2E), which improved transduction efficiency up to75% (Fig-ure 2F). In this setting, a 4-fold increase in *Scn1a* expression was

detected in sg1P with respect to sgCtrl-treated neurons. Moreover, no alteration in the transcriptional levels of the second *Scn1a* mRNA isoform carrying exon A was detectable (Figure 2G), indicating that the sg1P/dCas9-VP160 activation system does not affect the transcriptional status of the distal promoter. To evaluate whether increased transcription of *Scn1a* led to higher $Na_v1.1$ protein levels, we performed western blot analysis of membrane lysates isolated from transduced 10 DIV primary neuronal cultures, which showed a 2-fold increase in membrane-associated $Na_v1.1$ protein (Figure 2H). Taken together, these results indicate that sg1P associated with thedCas9 activation system can modulate *Scn1a* gene activity in primary neurons and, accordingly, increase the levels of the $Na_v1.1$ channel protein.

dCas9-based gene activation is highly specific for *Scn1a* in primary neurons

We examined the specificity of the dCas9 activation system by assessing global gene expression in primary neurons transduced with dCas9-VP160 together with either sg1P or sgCtrl. RNA sequencing (RNA-seq) was performed on 3 DIV neurons 2 days after lentiviral transduction with either sg1P or the sgCtrl (Figure 3A). Notably, the only gene with significantly increased expression relative to the control was *Scn1a* (log2 fold change > 1.5, $p < 0.005$), indicating the high specificity of the dCas9 activation system in primary neuronal cells (Figures 3B, red

dots). CRISPOR provided a list of 195 putative off-target genes associated with sg1P. Because dCas9A is nuclease defective, we reasoned that aspecific transcription activation could occur only when off-target sequences were in close proximity to TSSs of genes. Therefore, we filtered the list using the web tool Galaxy to investigate which of those putative off-targets were located within 500 bp of TSSs of any annotated gene. Only 4 of 195 putative off-target genes were identified in the putative promoter regions upstream of the *Prp4*, *BC02*, *Olfr919*, and *Plrg1* genes. However, as shown by both sequencing and qRT-PCR analizes, the expression of these genes was not altered after delivery of the dCas9 activation system (Figures 3B and 3C, left panel, yellow dots). Absolute and relative levels of the various Na_v α subunits are strictly regulated, allowing a fine balance of neuronal membrane excitability.40 Therefore, we examined the expression of other Na_v α subunit-encoding genes. The global transcriptional analysis revealed no significant changes in their expression levels (Figure 3B, right panel, yellow dots). These results were confirmed by qRT-PCR assays of independent cellular replicates (Figure 3C, right panel). In conclusion, the global and targeted gene expression analizes of primary neurons transduced with the sg1P-dCas9 activation system (here after called *Scn1a*-dCas9A) confirmed the high specificity for *Scn1a* gene transactivation at a genome-wide level.

dCas9-based *Scn1a* gene activation enhances neuronal activity in immature wild-type (WT) cortical interneurons

To evaluate whether the increased levels of $Na_v1.1$ protein in primary neurons were sufficient to alter neuronal excitability, whole-cell patch-clamp experiments were carried out in dCas9A-transduced neurons. We conceived a dual LV-inducible system designed with a first lentivector carrying dCas9-VP160 with the tdTomato reporter regulated by the reverse tetracycline-controlled transactivator(rtTA)-responsive element (TRE) and a second lentivector carrying the transactivator rtTA and sgRNAs (sg1P or sgCtrl) to explore a setting that would be relevant in *in vivo* experiments (Figure 4A; Figure S3A). Indeed, the split of *Scn1a*-dCas9A in two vectors is required for *in vivo* delivery mediated by AAVs, characterized by a limited cargo capacity. In this setting, upon doxycycline (dox) administration, about 60% of neurons were transduced (Figure S3B). A 2-foldincrease in the basal level of *Scn1a* gene expression (*Scn1a*-dCas9A versus Ctrl-dCas9A) in WT neurons at 7 DIV was observed upon dox administration (Figure S3C, +dox), but not under dox-absent conditions (-dox), although some leaky expression of dCas9A couldbe detected (Figure S3D). Because $Na_v1.1$ channel loss mainly affects GABAergic interneurons, we established primary neuronal cultures from GAD67-GFP mouse embryos that were transduced with either the Ctrl-dCas9A or *Scn1a*-dCas9A system and analyzed when double-positive for GFP and tdTomato (Figures 4A and 4B). First recordings were performed on 9–11 DIV primary neurons before their achievement of full functional

maturation. Current step injections showed a significant increase in firing rate in interneurons transduced with the *Scn1a*-compared with the Ctrl-dCas9 activation system (Ctrl-dCas9A, n = 11; *Scn1a*-dCas9A, n = 15; p = 0.03, Mann-Whitney non-parametric t test) (Figures 4C–4E; Figure S4). No alteration of neuronal firing rate was mediated by *Scn1a*-dCas9A in the absence of dox (Figure S3E). These results underline the potential efficiency of *Scn1a*-dCas9A to increase interneuron excitability upon alteration of *Scn1a* gene dosage, at least in an immature network. Recently, we developed a new electrophysiological approach ("activity clamp") to analyze how a neuron in a given epileptic network responds to antiepileptic drugs.41 Here we modified this method toadapt it for primary neuronal cultures to compare interneurons trans-duced with either the Ctrl-dCas9A or *Scn1a*-dCas9A system. First, we recorded in interneurons the barrage of α-amino-3-hydroxy-5-methyl-4-isoxazolepropionic acid (AMPA) receptor-mediated excitatory synaptic currents that occurs in the presence of the chemoconvulsant potassium channel blocker 4-aminopyridine (4-AP). Then we converted the recorded currents into a conductance wave form, and, by applying dynamic current clamp, we fed them back to interneurons pharmacologically isolated from the network. We then compared neurons transduced with either the *Scn1a*- or Ctrl-dCas9A system (Figures 4F–4I). Activity clamp showed that GABAergic interneurons transduced with *Scn1a*-dCas9A exhibited an increase in the number of action potentials (APs) evoked by the

same epileptic inputs as well as higher firing frequencies reached during the protocol (Ctrl-dCas9A, n = 10; *Scn1a*-dCas9A, n = 12; p = 0.0009, parametric Student's t test) (Figure 4I). Altogether, these results indicate that increased expression of *Scn1a* obtained by the dCas9A system is sufficient to increase interneuron excitability in response to epileptiform barrages of synaptic excitation.

dCas9-based *Scn1a* activation increases $Na_v1.1$ protein levels and rescues excitability in *Scn1a*$^{+/-}$ mutant cortical interneurons

The experiments described above show that the *Scn1a*-dCas9A system upregulates *Scn1a* expression in WT interneurons, increasing $Na_v1.1$ protein levels and enhancing their excitability. We asked whether this system could also boost transcription of the single WT *Scn1a* allele in DS mice to reach sufficient $Na_v1.1$ protein levels to compensate for haploinsufficiency and attenuate the pathology. We tested the efficacy of the *Scn1a*-dCas9A system in *Scn1a*$^{+/-}$ neurons derived from a DS mouse model (Figure 5A).10 Considering that the *Scn1a* gene starts to be expressed around postnatal day 10 (P10),10,42 the analysis was done at DIV 22–25 to ensure display of the characteristic DS phenotype. Interestingly, at this time point, WT neurons seemed to be unresponsive to *Scn1a*-dCas9A treatment (Figure 5B), whereas we observed a 3.5-fold increase in levels of *Scn1a* expression in *Scn1a*-dCas9A- compared with Ctrl-dCas9A-

treated DS neurons (Figure 5C). To assess the nature of *Scn1a*-dCas9A-induced mRNA, we performed deep sequencing of PCR amplicons spanning the mutation region and found out that, in Ctrl-dCas9A-transduced neurons corresponding to basal conditions, WT and mutant transcripts were approximately equally abundant (almost 50% each) (Figure 5D). The same relative proportion was maintained in *Scn1a*-dCas9A-treated neurons (Figure 5D). These data indicate that mutant mRNA is stable in DS neurons and, consequently, that *Scn1a*-dCas9A treatment induces upregulation of both transcripts. However, at the protein level, untreated *Scn1a*$^{+/-}$ postnatal brains showed an ~50% reduction in $Na_v1.1$ protein levels with respect to the control counterparts (Figures 5E and 5F). In accordance with mRNA data, the levels of $Na_v1.1$ protein did not change upon *Scn1a*-dCas9A treatment in *Scn1a*$^{+/+}$ neurons, whereas, remarkably, *Scn1a*-dCas9A-treated *Scn1a*$^{+/-}$ neurons exhibited almost doubled $Na_v1.1$ protein levels compared with Ctrl-dCas9A-treated *Scn1a*$^{+/-}$ neurons at 25 DIV (Figures 5E and 5F). An immunoblot signal lower than 170 kDa and corresponding to truncated $Na_v1.1$ protein was not observed, neither in *Scn1a*$^{+/-}$ adult brains nor in *Scn1a*$^{+/-}$ neurons under basal conditions (Ctrl-dCas9A) or treated with *Scn1a*-dCas9A (Figure 5E). These results imply that the mutant protein is likely degraded and not targeted to the plasma membrane. To assess whether rescue of $Na_v1.1$ protein levels has a functional effect on DS neurons, electrophysiological experiments were repeated in *Scn1a*$^{+/-}$;GAD67-GFP GABAergic interneurons transduced either with the

Ctrl-dCas9A or *Scn1a*-dCas9A system (Figures 6A and6B). Recordings were performed on 18–20 DIV neuronal cultures to treat fully mature and functional interneurons. Current step injections showed a decreased frequency-current relationship and maximum AP frequency in *Scn1a*$^{+/-}$ interneurons compared with the WT when both were transduced with the Ctrl-dCas9A system (Figures 6C–6E). Accordingly, an increased current threshold to trigger a single AP was observed (Figure 6G). These defects in *Scn1a*$^{+/-}$ interneurons were completely rescued by transducing the *Scn1a*-dCas9A system (Ctrl WT, n = 12; Ctrl *Scn1a*$^{+/-}$, n = 10; *Scn1a*-dCas9A WT, n = 10; *Scn1a*-dCas9A *Scn1a*$^{+/-}$, n = 11; p =0.02, p = 0.04, 2-way ANOVA followed by Bonferroni's multiple comparisons test) (Figures 6D–6H). Activity clamp confirmed rescue of DS mutant interneuron firing in the face of epileptiform activity following *Scn1a*-dCas9A treatment compared with Ctrl-dCas9A treatment (Ctrl-dCas9A WT, n = 12; Ctrl-dCas9A *Scn1a*$^{+/-}$, n = 10; *Scn1a*-dCas9A WT, n = 10; *Scn1a*-dCas9A *Scn1a*$^{+/-}$, n = 11; p = 0.03, 2-way ANOVA followed by Bonferroni's multiple comparisons test) (Figure 6I). As expected from the molecular data, the increase in excitability in *Scn1a*-dCas9A-treated WT interneurons observed at 9–10 DIV was no longer observed at 18–20 DIV (Figures6C–6J).

AAV-mediated *Scn1a*-dCas9A transduction of cortical interneurons rescues parvalbumin (PV)+ interneuron deficiency and protects *Scn1a*$^{+/-}$ mutant mice from hyperthermia-induced seizures

Given the encouraging results with *Scn1a*-dCas9A treatment obtained on neuronal cultures, we sought to test its efficacy in rescuing the epileptic phenotype in a DS mouse model. To exploit the *Scn1a*-dCas9A system *in vivo*, we sought to stimulate *Scn1a* expression selectively in forebrain GABAergic interneurons. We used a dual AAV9-based system because these viral particles diffuse efficiently in the brain parenchyma after intracerebroventricular (i.c.v.) injections in neonatal mouse pups.43 The VP64 activator domain, carrying four tandem copies of VP16, was chosen for *in vivo* delivery because its smaller size allows this dCas9A together with the TRE promoter to fit in an AAV vector. Similar to the aforementioned dual lentiviral system, a second AAV9 was packaged with the sg1P cassette, followed by the mDlx5/6 promoter driving selective expression of the rtTA-T2A-Tomato cassette in forebrain GABAergic interneurons (Figure 7A). 44,45 When the mDlx5/6-promoter driven dCas9A elements were virally transduced in GAD67-GFP transgenic pups, we estimated that about 85% of the viral reporter tdTomato+ cells in the cerebral cortex also expressed the GFP transgene (Figures S7A–S7C and S7F). Furthermore, different interneuron subtypes could be targeted specifically by our system, as shown by co-labeling of tdTomato with parvalbumin, somatostatin, neuropeptide Y (NPY), or vasoactive intestinal

peptide (VIP) (Figures S6B–S6F). Histological characterization of WT litters injected with the dCas9A elements revealed discrete transduction efficiency along the antero-posterior axis, with about 20% of total GABAergic interneurons transduced in cortical areas close to injection sites (Cx1_L, left, and Cx1_R, right; Figure S6G). Neatly, in these same areas, a significant increase in *Scn1a* gene expression was detected in 2-week-old mice treated with the *Scn1a*-dCas9A system compared with the Ctrl-dCas9A system (Figures 7B and 7C). To assess whether *Scn1a*-dCas9A has a functional effect on PV interneurons *in vivo*, we performed patch-clamp analysis on treated *Scn1a*$^{+/+}$ and *Scn1a*$^{+/-}$ mice crossed with PV-Cre;Ai9-tdTomato mice at P21–P28 (Figure S7A). Current step injections highlighted a decreased frequency-current relationship (Figure S7C) and maximum AP frequency (Figure S7D)in *Scn1a*$^{+/-}$ PV interneurons compared with *Scn1a*$^{+/+}$ when injected with Ctrl-dCas9A. These defects in *Scn1a*$^{+/-}$ PV interneurons were rescued by transducing the *Scn1a*-dCas9A system (*Scn1a*+/+;Ctrl-dCas9A, n = 9; *Scn1a*$^{+/-}$;Ctrl-dCas9A, n = 12; *Scn1a*$^{+/-}$;*Scn1a*-dCas9A, n = 11; input/output (I/O), p = 0.003; two-way ANOVA (Figures S7C and S7D). At 1 month, *Scn1a*$^{+/-}$ mice were implanted with electrodes, and an electroencephalogram (EEG) was recorded after subjecting the mice to hyperthermia-induced seizures. When *Scn1a*$^{+/-}$ mice were exposed to hyperthermia, we observed that the seizure threshold temperature was increased in *Scn1a*-dCas9A-compared with Ctrl-dCas9A-treated mice (Ctrl-dCas9A: 41.93±0.1687, n = 6; *Scn1a*-dCas9A: 42.343±0.1453, n = 6; p =

0.0048, Student's t test) (Figure 7F). Furthermore, *Scn1a*-dCas9A-treated *Scn1a*$^{+/-}$ mice displayed seizures with a generally lower average clinical severity score than Ctrl-dCas9A-treated mice (Ctrl-dCas9A: 5.83±0.17, n = 6; *Scn1a*-dCas9A: 4.83±0.31, n = 6; p = 0.02, chi-square test) (Fig-ure 7G). The average seizure duration defined by EEG recordings was also shorter (Ctrl-dCas9A: 33.5±2.7 s, n = 5; *Scn1a*-dCas9A:23.9±2.6 s, n = 6; p = 0.029, Student's t test) (Figure 7H). Finally, we observed a non-significant trend for the spike frequency to belower in *Scn1a*-dCas9A-treated mice compared with Ctrl-dCas9A-treated mice (Figures 7I and 7J). The upregulation of $Na_v1.1$ during development *in vivo* may be protective against epileptic insults because loss of $Na_v1.1$, in the inverse scenario, is epileptogenic. To test this hypothesis, we performed intraventricular injections of P0 pups with either Ctrl-dCas9A or *Scn1a*-dCas9A viruses using a pan-neuronal promoter. At P14–P17, pups were injected with lipopolysaccharide (LPS) to elicit fever by infection, 46,47 followed by repeated low-dose kainic acid (KA) injections every 30 min 2 h later. Epileptic seizures were scored according to the Racine scale, and pups were observed every 10 min until they reached grade 5, marked by tonic-clonic convulsive seizures (Fig-ure S8A). The time taken to reach grade 5 was used to define susceptibility to epileptic insults. Pups injected with *Scn1a*-dCas9A had a higher seizure threshold compared with sham and Ctrl-dCas9A injected animals, confirming the hypothesis that upregulation of $Na_v1.1$ during development is protective against seizures (Figure S8B).

In conclusion, these results show that the *Scn1a*-dCas9A system can be efficiently delivered *in vivo* by AAV-mediated gene transfer in *Scn1a*$^{+/-}$ mice to ameliorate temperature-induced seizures characteristic of this DS mouse strain.

Discussion

DS poses severe challenges for developing an effective therapeutic strategy to control epileptic seizures and associated neurodevelopmental dysfunctions. Currently available antiepileptic drugs are inadequate to suppress recurrent seizures. Furthermore, novel gene therapy approaches for *Scn1a* gene replacement are hampered by the relatively large size of the *Scn1a* gene, which exceeds the packaging cargo size of AAV particles. Finally, *Scn1a* transcriptional levels need to be carefully gauged to maintain an $Na_v1.1$ protein level compatible with physiological membrane excitability in mature neurons. In light of these significant hurdles, we propose that the dCas9A-guided approach for *Scn1a* gene regulation has invaluable advantages for developing an effective and safe gene therapy strategy for this disease. We identified the sg1P guide, targeting a sequence close to the *Scn1a* proximal promoter, capable of significantly stimulating *Scn1a* expression. A preliminary genomic analysis confirmed that this promoter region is transcriptionally active in the adult mouse and human neurons, showing the exact transcriptional starting site (TSS) by CAGE-seq and the crucial epigenetic modifications associated with its

functional state. Rapid advances regarding our knowledge of the transcriptional and epigenetic state of the regulatory elements across the genome of neurons will improve the design of effective guides. Importantly, our data provide evidence that this dCas9-based activation system can further stimulate *Scn1a*, increasing its basal expression in young post-mitotic neurons. Surprisingly, we could not detect a significant increase in *Scn1a* expression in mature WT neurons, whereas it was evident in *Scn1a*$^{+/-}$ neurons at both the mRNA and protein levels upon *Scn1a*-dCas9A treatment. Considering that approximately 70% of the newly synthesized $Na_v1.1$ constitutes a metabolically stable intracellular pool of protein and only 30% is trafficked to the plasma membrane and axon initiation segment (AIS), 48 we can speculate that excessive accu-mulation of $Na_v1.1$ induces negative regulation of the *Scn1a* transcript that cannot be overcome even by *Scn1a*-dCas9A treatment in a WT situation. Conversely under *Scn1a*$^{+/-}$ conditions, only half of the protein is produced, and this “saturation” is not achieved. In light of this, we propose that the total amount of $Na_v1.1$ channel available in the cell can exert control by repressing transcription or destabilizing *Scn1a* mRNA. Further studies are required to determine the details of this regulation and to assess whether stimulation of *Scn1a* gene expression alters the chromatin marks within the promoter region with specific histone modifications associated with this particular transcriptional state. These results have valuable implications for manipulation of gene expression in the adult brain, providing a tool for targeted and tunable

transcriptional regulation of potentially any genetic element. We achieved good gene transcriptional activa-tion using dCas9 fused with the effector domain VP64 or VP160. However, recent studies have identified novel transactivators that can elicit higher levels of gene activation. 29,34,49 Establishment of different Cas9 activator systems, each with its own advantages, can provide an invaluable toolbox for obtaining the rightfine-tuning of transcriptional levels adequate for each specific application. Using global RNA-seq, we showed that targeted *Scn1a* gene activation was exquisitely specific, with no detectable off-target gene activation in primary neurons. These data reveal the high specificity of this approach, which will contribute to the high safety level for its future therapeutic applications. In fact, both the new models for accurate prediction of sgRNA off-targets and the strict requirement for targeting promoter regions close to the TSS contribute to elevating the level of specificity of this approach. Additionally, use of dCas9 eliminates the risks of DNA cleavage and its consequences in post-mitotic neurons that have lost the ability to activate homology-directed repair mechanisms to resolve DNA damage. 50,51 Importantly, dCas9-based stimulation of *Scn1a* expression led to a significant increase in membrane-associated $Na_v1.1$ protein levels that restored correct functioning of DS mutant inhibitory interneurons *in vitro*. Our approach did not distinguish between the two *Scn1a* alleles and also stimulated expression of the mutant *Scn1a* allele (R1407X). Multiple studies have confirmed that the great majority of *SCN1A* mutations are loss-of-function ones and have a negligible effect

because they do not produce any stable protein capable of functioning at the neuronal membrane. 10 However, few mutations in *SCN1A* have been hypothesized from *in vitro* studies to cause the disease through a gain-of-function mechanism. 52 We anticipate that, in these particular cases, our approach would not be of any advantage. Neuropathological studies have shown that, even in advanced stages of the disease, there is no evident sign of neuronal cell loss in patients. 53 These observations strongly imply that dysfunctional interneurons can potentially recover their activity whenever a sufficient amount of $Na_v1.1$ channel is available and indicate that at least some DS pathological defects are reversible. Altogether, these results raise the prospect of a cure for this disease even when pathological manifestations are already evident. In this study, the different elements of the dCas9 activation system were packaged in two different AAVs but designed to provide interdependent expression of the different genetic elements. Considering that DS globally affects forebrain interneurons, we carried out AAV i.c.v. injections in neonatal mouse pups to cover the entire forebrain structures with a single treatment. In patients, because symptomon set generally occurs within the first two years of life and some more time is required to as certain *Scn1a* gene mutation by exon sequencing, later delivery of gene therapy will be required. Nevertheless, the recent discovery of new AAV synthetic serotypes capable of crossing the blood-brain barrier from the bloodstream might open new opportunities for delivery of therapeutic AAVs for treating CNS disorders. In this respect,

peripheral injections of AAV9 in infants with spinal muscular atrophy (SMA), a devastating infantile neurological disorder affecting spinal motor neurons, have recently shown substantial and long-term clinical benefits. 54 In fact, a single intravenous infusion of the AAV9 expressing the corrected gene resulted in wide protection of motor skills for an extensive period of time and longer survival. 54 This unprecedented clinical success regarding SMA with a systemic AAV gene therapy approach might facilitate the introduction of a similar strategy to treat other incurable neurological infantile disorders and DS in particular. Our gene therapy strategy was targeted selectively to forebrain interneurons using the small *Dlx5/6* enhancer, which has been shown to reliably deliver reporter genes within these neuronal classes. 44,45 Similarly, we reported that this regulatory element also ensured restricted expression of the transgenes in the GAD67-GFP neuronal sub-population in DS adult mice. Even though *Scn1a* is also expressed in subpopulations of cortical excitatory neurons, our strategy almost completely avoided *Scn1a* gene activation in these cells. Nevertheless, *Scn1a* deletion in this neuronal population does not induce notice able abnormalities in mice, whereas it ameliorates the pathological phenotype of mice with *Scn1a* deletion in GABAergic neurons. 13 *Scn1a* expression levels are likely different in cortical excitatory and inhibitory neurons, and our approach does not allow us to deliver different levels of gene activation in different neuronal subtypes. Thus, we considered it safer to employ the *Dlx5/6* enhancer to exclusively target the neuronal population,

whose dysfunction leads to pathological manifestations. The possibility that transduction of extra-cortical interneurons may affect treatment efficacy needs to be considered. Alternatively, a more selective promoter driving expression of the *Scn1a*-dCas9A system only in cortical interneurons and not in other interneurons (i.e., striatal) could be exploited. The *Scn1a* gene activation system attenuated induced epileptic seizures in terms of threshold temperature, total duration, overall clinical severity, and recovery period. However, seizures were not completely suppressed. The results can be explained by the relatively low co-infection efficiency of the two separate AAVs in the interneuron population, reaching around 20% in the injected area. In fact, the considerable size of SpCas9 requires use of two independent AAVs to assemble all elements of the activation system. Thus, future work is necessary to improve this strategy to package all of the system in a unique AAV vector by using significantly smaller Cas9 orthologs, such as SaCas9, 55 GeoCas9, 56 CjCas9. 57 When the AAV vector for *Scn1a*-dCas9A treatment is optimized, it would be interesting to also test its effect on the survival rate and spontaneous seizure number and severity in Dravet mice. In conclusion, we showed that the dCas9 acti-vation system can be tailored to obtain a robust and highly specific activation of the *Scn1a* gene both in cultured neurons and in brain tissue. Moreover, the dCas9 activation system can be packaged into AAVs to establish a gene therapy approach for treating DS mice and obtaining protection from temperature-induced epileptic seizures. A similar approach can

then be considered for other haploinsufficient genetic disorders where stimulation of the WT allele can rescue molecular dysfunction and lead to a clinical benefit.

MATERIALS AND METHODS

Bioinformatics Analysis

Transcriptomics and epigenetics next-generation sequencing (NGS) data were downloaded from the ENCODE[58] and Functional Annotation of the Mammalian Genome (FANTOM)[59] databases. Tracks are visualized along the mm10 mouse reference genome with the Integrative Genome Viewer (IGV).[60]

Molecular Cloning

sgRNAs were cloned in a LV-U6 vector as described previously. Ef1alpha-dCas9VP160-T2A- PuroR was generated from pAC94-pmaxdCas9VP160-2A-puro, a gift from R. Jaenisch (Addgene plasmid 48226).[61] The dCas9VP160-2A-puro cassette was cut with AgeI and inserted into the TetO-FUW vector digested with AgeI. The dCas9VP160-2A-puro cassette was restriction digested with HpaI/ AfeI and blunt-cloned into the Ef1alpha-GFP promoter, where GFP was removed by SmaI/EcoRV digestion. Ef1alpha-dCas9VP160-T2A-GFP was obtained by restriction digestion of Ef1alphadCas9VP160-T2A-PuroR with AscI/XbaI; the VP160-T2A fragment was obtained by AscI/XhoI digestion from Ef1alpha-dCas9VP160-T2A-PuroR, whereas the GFP

fragment was PCR amplified with primers containing XhoI/XbaI restriction sites; the vector and the two fragments were ligated together. LV-TRE-dCas9VP160-T2A-tdTomato was obtained from TetOFUW dCas9VP160-2A-puro digested with AscI/XbaI; the VP160- T2A fragment was obtained by AscI/XhoI digestion from Ef1alphadCas9VP160-T2A-PuroR, whereas the tdTomato fragment was PCR amplified with primers containing XhoI/XbaI restriction sites; the vector and the two fragments were ligated together. The LVsgRNA-hPGK-rtTA vector was obtained by digesting LV-U6-sgRNA with BamHI and cloning rtTA fragment BamHI digested from LV-hPGK-rtTA. The intermediate LV-U6-rtTA was ClaI-XhoI digested, and the PGK promoter was PCR amplified with primers with ClaI/XhoI and then cloned. AAV-TRE-dCas9-VP64 was obtained by restriction digestion of AAV-SpCas9 (a kind gift from F. Zhang, Addgene PX551),[51] where the Mecp2 promoter was removed by XbaI/AgeI digestion and the TRE promoter was amplified with the following primers: FW XbaI (5'-GCTCTAGACCAGTTTGGTTAGATCTC-3') and RV AgeI (5'-GCACCGGTGCGATC TGACGGTTCACT-3'). SpCas9 was removed with AgeI/EcoRI and Cas9m4-VP64 (a kind gift from G. Church, Addgene 47319)[26] was digested with AgeI EcoRI. The VP64 fragment was PCR amplified with the following primers with EcoRI sites: FW: 5'-GATCATCGAGC AAATAAGCGAATTCTC-3' and RV: 5'-gctaaGAATTCTTATCTAGAGTTAATCAGCATG-3'.

Virus Production

LVs were produced as described previously.[62] For AAV production, replication- incompetent, recombinant viral particles were produced in 293T cells by polyethylenimine (PEI) (Polyscience) co-transfection of three different plasmids: a transgene-containing plasmid, a packaging plasmid for rep and cap genes, and pAdDeltaF6 for the three adenoviral helper genes. The cells and supernatant were harvested at 120 h. Cells were lysed in Tris buffer (50 mM Tris (pH 8.5), and 150 mM NaCl; Sigma-Aldrich) by repetitive freezing-thawing cycles (3 times), lysed in Tris buffer, and combined with correspondent cell lysates. To clarify the lysate, benzonase treatment was performed (250 U/mL, 37°C for 30 min; Sigma-Aldrich) in the presence of 1 mM MglCl2 (Sigma-Aldrich), and cellular debris was separated by centrifugation (2,000 g, 30 min). The viral phase was isolated by an iodixanol step gradient (15%, 25%, 40%, and 60% Optiprep; SigmaAldrich) in the 40% fraction and concentrated in PBS with a 100,000 molecular weight cutoff concentrator (Vivaspin 20, Sartorius Stedim). Virus titers were determined by measuring the number of DNase I-resistant viral particles, using qPCR with a linearized genome plasmid as a standard. TRE-dCas9-VP64 was produced by VectorBuilder (CA, USA).

Mice

Mice were maintained at the San Raffaele Scientific Institute institutional mouse facility (Milan, Italy). *Scn1a*$^{+/-}$[10] mice were backcrossed with 129Sv mice, whereas GAD67-GFP,[63] *Pvalb*$^{tm1(cre)Arbr}$ (JAX 017320, PV-Cre), and Rosa26$^{LSL\text{-}tdTomato}$ (JAX 007909, Ai9) mice were backcrossed with C57BL/6N mice. PV-Cre$^{+/+}$ mice were crossed to Ai9$^{+/+}$ mice to generate PV-Cre$^{+/+}$ Ai9$^{+/+}$ mice. Those mice were then crossed with 129Sv.Scn1a+/ mice to generate *Scn1a*$^{+/-}$;PVCre$^{+/-}$ Ai9$^{+/-}$ mice and Scn1a$^{+/-}$;PV-Cre$^{+/-}$ Ai9$^{+/-}$. All procedures were performed according to protocols approved by the internal institutional animal care and use committee (IACUC) and reported to the Italian Ministry of Health according to European Commission Council Directive 2010/63/EU and in accordance with the UK Animals (Scientific Procedures) Act of 1986.

Cell Cultures and Primary Neuron Derivation

P19 cells were cultured in alpha-MEM (Sigma-Aldrich) supplemented with 10% fetal bovine serum (Sigma- Aldrich), 1% non-essential amino acids (Gibco), 1% sodium pyruvate (Sigma-Aldrich), 1% glutamine (Sigma-Aldrich), and 1% penicillin/streptomycin (SigmaAldrich). Cells were split every 2–3 days using 0.25% trypsin (Sigma-Aldrich). For transfection, Lipofectamine 300 (Thermo Fisher Scientific) was used according to the manufacturer's protocol. Primary cultures of mouse embryonic hippocampal neurons were prepared from

embryonic day 17.5 (E17.5) embryos or P0 pups derived from GAD67-GFP knockin and *Scn1a*+/;GAD67-GFP pregnant females. In the latter case, each brain was processed separately, and a skin biopsy was used for genotyping. Briefly, after dissection, hippocampi were enzymatically digested with 0.025% trypsin (Gibco) in Hank's balanced salt solution (HBSS; Euroclone) for 20 min at 37°C. Then HBSS with trypsin was removed, and the hippocampi were washed with plating medium (neurobasal medium [Gibco] supplemented with 2% B27, 3.3 mM glucose, 1% glutamine, and penicillin/streptomycin) and mechanically dissociated with a P1000 pipette to obtain a homogeneous cell suspension. Cells were then plated on plates coated with poly-L-lysine (PLL; 0.1 mg/mL) and coverslips. LV infection was performed at DIV 1, and neurons were used at DIV 10 or 21 for electrophysiology, western blot analysis, and immunofluorescence. For recordings from interneurons, we patched cells that showed co-localization of both green (indicating interneurons) and red (indicating successful lentiviral transduction) fluorescent signals.

Western Blotting

Total cerebral cortices from *Scn1a*$^{+/-}$ mice, WT mice, and primary neurons were homogenized using the Mem-PER Plus Membrane Protein Extraction Kit (Thermo Fisher Scientific) according to the manufacturer's instructions to enrich for the membrane-bound proteins. Western blot analysis was performed

on Nupage 4%–12% gradient gels (Thermo Fisher Scientific) using primary antibodies against the following proteins: anti-$Na_v1.1$ (1:200, Millipore) and anti-Calnexin (1:5,000, Sigma).

RNA Isolation qRT-PCR

RNA was extracted using TRI reagent (Merck) according to the manufacturer's instructions. For qRT-PCR, cDNA synthesis was obtained using the ImProm-II Reverse Transcription System (Promega), and then qRT-PCR was performed in triplicate with custom-designed oligos (Table S2) using Titan HotTaq EvaGreen qPCR Mix (no ROX) (BIOATLAS). Analysis of relative expression was performed using the ΔΔCt method.

RNA-Seq

RNA libraries were generated starting from 1 mg of total RNA extracted from Ctrl-dCas9A and *Scn1a*-dCas9A neurons. RNA quality was assessed by using a Tape Station instrument (Agilent). To avoid over-representation of 3' ends, only high-quality RNA with a RNA integrity number (RIN) of 8 or higher was used. RNA was processed according to the QuantSeq 3' mRNA-Seq Library Prep Kit protocol. The libraries were sequenced on an Illumina HiSeq 2500 with 50-bp stranded reads using Illumina TruSeq technology. Image processing and basecall were performed using the Illumina real-time analysis software. Fastq files were aligned to the mouse genome (NCBI37/mm9) with

Bowtie2.64 Differential gene expression and functional enrichment analizes were performed with DESeq2.65. Statistical analysis was performed with the SPSS statistical package (IBM). Data were deposited in NCBI GEO: GSE111436.

Deep Sequencing Data Analysis

Indexed paired-end libraries were generated starting from 1 mg of PCR amplicon spanning the *Scn1a*^{RX} gene mutation[10] performed on cDNA obtained from RT RNA using Illumina TruSeq Nano DNA Library Prep Kits according to the manufacturer's instructions. Libraries were sequenced on an Illumina MiSeq. FASTQ reads were aligned to the hg38 human reference genome with Bowtie2. Alignments were visualized and quantified with the IGV genome browser.

In Vitro Electrophysiology

Current Steps

For current-clamp recordings, the internal solution contained 126 mM K-gluconate, 4 mM NaCl, 1 mM MgSO4, 0.02 mM $CaCl_2$, 0.1 mM 1,2-bis(2-aminophenoxy)ethane-N,N,N',N'-tetraacetic acid (BAPTA), 15 mM glucose, 5 mM 4-(2-hydroxyethyl)-1-piperazineethanesulfonic acid (HEPES), 3 mM ATP-Na_2, and 0.1 mM GTP-Na (pH 7.3). The extracellular (bath) solution contained 2 mM $CaCl_2$, 140 mM NaCl, 1 mM $MgCl_2$, 10 mM HEPES, 4 mM KCl, and 10 mM glucose (pH 7.3). D-()-2-amino-5-

phosphonopentanoic acid (D-AP5; 50 mM), 6-cyano-7-nitroquinoxaline-2,3-dione (CNQX; 10 mM), and picrotoxin (PTX; 30 mM) were added to block synaptic transmission. Experiments were performed at room temperature (22°C–24°C). Transduced cortical and hippocampal interneurons were identified because of GAD67-GFP and tdTomato (dCas9A system) expression. Neurons with unstable resting potential (or more than 50 mV), bridge balance of more than 15 MU, and/or holding current of more than 200 pA at 70 mV were discarded. Bridge balance compensation was applied, and the resting membrane potential was held at 70 mV. Current step protocols were used to evoke APs, injecting 250-ms-long depolarizing current steps of increasing amplitude (Δ 10 pA, max 280 pA). Recordings were acquired using a Multiclamp 700A amplifier (Axon Instruments, Molecular Devices) and a Power3 1401 (Cambridge Electron Design [CED]) interface combined with Signal software (CED), filtered at 10 kHz, and digitized at 50 kHz. Passive properties were calculated from the hyperpolarizing steps of the current-clamp step protocol. Input resistance is an average of three steps (2 negative and 1 positive) and is defined as the as ΔV/I. Capacitance was calculated in the current-clamp hyperpolarizing step as follows. First, the resistance was determined as voltage derivative (dV)/DI (voltage/current), and then the cell time constant (tau) was obtained, fitting the voltage changing between baseline and hyperpolarizing plateau. Capacitance was calculated as tau/resistance. Capacitance is the time constant of the voltage between the baseline and the plateau during a

hyperpolarizing step. Single AP parameters were calculated as described previously.[62] An event was detected as an AP when cross 0 mV and when the rising slope was more than 20 mV/ms in a range of injected current from 0 pA to 500 pA. All recordings and analizes were carried out blinded to the transduced vector.

Activity Clamp

For activity clamp experiments, current traces in voltage-clamp configuration in the presence of 4AP were recorded, holding GFPpositive interneurons (18 DIV) at 70 mV in the presence of GABAA and N-methyl-D-aspartate (NMDA) blockers. The resulting AMPA current traces were converted in conductance (G = I/V). Using Signal dynamic clamp software in conjunction with CED Power 1401-3 (CED), the conductance traces were used to inject currents into interneurons in current-clamp configuration. During recordings, the voltage of the patched neurons was read in real time and used to calculate the current to be injected from the 4AP conductance trace. To compare different cells, the conductance threshold was calculated in each neuron prior to each dynamic clamp experiment. For voltage-clamp spontaneous excitatory synaptic activity of the epileptic traces (4AP, 100 µM) and current-clamp recordings in dynamic clamp configuration, the internal and extracellular solutions were the same as described above for neuronal whole-cell patchclamp recordings. For voltage-clamp recordings in the extracellular solution, D-AP5 (50 µM) and PTX (30 µM) were added to block

GABAA and NMDA receptors, respectively. For current-clamp recordings, D-AP5 (50 µM), CNQX (10 µM), and PTX (30 µM) were added to block NMDA receptors, AMPA receptors, and GABAA receptors, respectively. Experiments were performed at room temperature (22°C–24°C). For voltage-clamp recordings, neurons with unstable resting potential and/or a leak current of more than 100 pA were discarded, and neurons were clamped at 70 mV. For current-clamp recordings, neurons with unstable resting potential and/or a bridge balance of more than 15 MΩ were discarded. Bridge balance compensation was applied, and the resting membrane potential was held at 70 mV. An AMPA conductance step protocol (Erev = 0 mV; τ = 1 ms; ΔG = 1 nS) was used to find the conductance threshold that elicited an AP, and then the epileptic conductance trace was scaled to the 15% of the conductance threshold. Neurons that were unable to generate at least one AP were therefore excluded. The sampling frequencies in voltage- and current-clamp configuration were set at 20 kHz to perfectly overlap the conductance traces with the software voltage reading. To analyze the dynamic clamp traces, an automatic MATLAB script was used[41] to detect events and calculate APs parameters. An event was selected as an AP when its peak crossed 0 mV and its dV/time derivative (dt) was more than 20. Voltage threshold was calculated as the first point with a derivative of more than 20 V/s. All recordings and analizes were carried out blinded to the transduced vector. Recordings were acquired using a Multiclamp 700A amplifier (Axon Instruments, Molecular Devices, Sunnyvale, CA, USA) and Signal dynamic

clamp software in conjunction with CED Power 1401-3 (CED, Cambridge Electronic Design), filtered at 10 kHz, and digitized at 50 kHz.

Ex Vivo Electrophysiology

Mice were sacrificed after deep isoflurane anesthesia, and brains were extracted. 350-µm-thick coronal sections were cut using a Leica VTS 1000 vibratome. After the cut, the slices were allowed to recover for 30 min at 32°C in modified artificial cerebrospinal fluid (ACSF) containing 92 mM sucrose, 87 mM NaCl, 2.5 mM KCl, 1.25 mM NaH_2PO_4, 25 mM $NaHCO_3$, 25 mM glucose, and 10 mM $MgSO_4$ aerated with 95% O2 and 5% CO2 (pH 7.4); slices were then allowed to recover at room temperature for at least 45 min before recording. Current-clamp recordings were performed using a MultiClamp 700B amplifier (Molecular Devices) with pCLAMP 10 software. Pipette capacitance and resistance were always compensated. Signals were low-pass-filtered at 10 kHz and sampled at 50–100 kHz; the signal was digitized using a Digidata 1550 D/A converter (Molecular Devices). Cells were held at 30°C–32°C. The extracellular solution contained 125 mM NaCl, 25 mM $NaHCO_3$, 2 mM $CaCl_2$, 2.5 mM KCl, 1.25 mM NaH_2PO_4, 1 mM $MgSO_4$, and 10 mM D-glucose aerated with 95% O2 and 5% CO2 (pH 7.4). The patch pipette contained 124 mM KH_2PO_4, 5 mM KCl, 2 mM $MgCl_2$, 10 mM NaCl, 10 mM HEPES, 0.5 mM EGTA, 2 mM Na-ATP, and 0.2 mM Na-GTP (pH 7.25, adjusted with KOH). Ctrl-and *Scn1a*-dCas9A PV+

interneurons were identified via tdTomato and GFP expression visualized with epifluorescence microscopy. The input/output relationship was determined by plotting AP frequency in response to progressive 500-ms, 50-pA current step injection. An AP was defined as spikes having a rising slope of more than 20 V/s and an amplitude exceeding 15 mV. Maximal steady-state firing frequency was defined as the maximal mean firing frequency in response to a current injection. Input resistance (Rm) was calculated from a 50 pA step from the resting membrane potential. AP amplitude was calculated from the AP threshold, defined as the voltage at which the first derivative (dV/dt) of the AP waveform reached 10 mV/ms, to the absolute value of the AP peak for the first spike obtained at the rheobase (defined as the minimal current injection able to elicit neuronal firing, determined through 10-pA current steps). Spike width was determined at half-amplitude (half-width) between the AP threshold and peak. Spike frequency adaptation (SFA) was calculated as the ratio of the first to the 10^{th} inter-spike interval (ISI1/ISI10). Maximal rise and decay slope were defined, respectively, as the maximal and minimal value of the first derivative of the AP waveform.

Intracerebroventricular Injections

Neonatal mice were anesthetized in ice for 3 min. 5 ml of viral suspension containing two AAVs (titer, 10^{13} viral genomes [vg]/mL) (TREdCas9-VP64 and pU6-sgCrtl/sg1P-mDlx5enh-

rtTa-T2A-Tomato/ GFP, 1:1), and 0.05% Fast Green FCF (Sigma Aldrich) was injected into lateral ventricles using a Hamilton syringe with a 33G needle. After injections, pups were placed on a warming pad until they regained normal color and movement. Subsequently, they were rubbed with bedding to prevent rejection before reintroducing the mother into the cage. Dox was administered immediately in drinking water or food. One week after the injections, mice were genotyped.

Immunostaining

Cells and neurons were fixed in ice-cold 4% paraformaldehyde (PFA) in phosphate buffer (PB) for 20 min. Mice were anesthetized with ketamine/xylazine and t perfused with 0.1 M PB at room temperature at pH 7.4 with freshly prepared PFA in PB. Tissues were post-fixed in 4% PFA overnight and then soaked in cryoprotective solution (30% sucrose in PBS). Tissues were sectioned using a cryostat after optimal cutting temperature (OCT) compound embedding in dry ice. For immunofluorescence, free-floating, 30-mm-thick coronal sections or plated cells were rinsed in PBS and incubated for 20 min with 2% Triton X-100, and 3% BSA for 1 h was used to saturate the nonspecific binding site before overnight incubation with the primary antibody (diluted in a solution containing 1% BSA and Triton X-100 at room temperature). Following incubation, sections were rinsed three times in PBS and incubated for 1 h with the secondary antibody. Primary antibodies for the following

epitopes were used: red fluorescent protein (RFP) (rabbit, 1:500, MBL International), GFP (chicken, 1:500, Molecular Probes), Calbindin (mouse, 1:200, Swant), PV (mouse, 1:500, Swant), somatostatin (SST) (rat, 1:200, Millipore), NPY (rabbit, 1:500, Immunostar), VIP (rabbit, 1:500, Immunostar), Map2 (mouse, 1:250, Immunological Science), GABA (rabbit, 1:1,000, Sigma-Aldrich). Slices and cell coverslips were mounted with fluorescent mounting medium (Dako). Images were captured with a Nikon Eclipse 600 fluorescence microscope.

Surgery for Electrode Implantation, Seizure Induction, and EEG

At least 5 days before recordings, epidural stainless steel screw electrodes (0.9 mm in diameter and 3 mm long) were surgically implanted under intraperitoneal anesthesia (100 mg/kg ketamine, 10 mg/kg xylazine) and secured using dental cement (Ketac Cem, ESPE Dental, Seefeld, Germany). Two active electrodes were placed on the right and left parietal areas (2 mm lateral to the midline, 1 mm posterior to the bregma) and one over the occipital area (1 mm posterior to lambda) as a common reference. For video EEG recording, the implanted electrodes were connected via flexible cables to an amplifier, and the EEG signal was sampled at 256 Hz, coded with 16 bits, and digitally saved using a System Plus device (Micromed, Mogliano Veneto, Italy). To obtain a good signal-to-noise ratio for seizure display, after acquisition, EEG traces were bandpass-filtered between 0.3

and 10 Hz. Video EEG recordings were inspected to detect seizures, defined as high-amplitude (at least twice the baseline) rhythmic discharges lasting at least 5 s. We defined the beginning of the seizure as the first EEG change; the end of the seizure was defined as the end of ictal EEG activity. To induce seizures, we adopted a protocol modified from Oakley et al.[16] Mice were placed in a glass beaker and heated with an infrared heat lamp (HL-1, Phisitemp, Clifton, New Jersey) controlled by a TCAT-2DF thermocontroller (Phisitemp, Clifton, New Jersey). Mouse rectal temperature was continuously monitored with a RET-4 probe (Phisitemp, Clifton, New Jersey). Seizures were identified by EEG recording and video analysis. First, mice were recorded at baseline for 15 min, and then seizures were evoked by progressively increasing the body temperature by 0.5°C every 30 s. The heating bulb was then promptly switched off to allow recovery; the mice were then monitored until the EEG and temperature returned to the baseline or until death occurred. For EEG analysis, Neuroscore (Data Sciences International, St. Paul, MN) was used. For spike detection, EEG traces were first bandpassfiltered between 5 and 70 Hz. Threshold temperature, seizure duration, number of spikes during the attack, and spike frequency were considered. Spikes were detected by threshold analysis and then visually inspected to reject artifacts. All recordings and analysis were carried out blinded to the transduced viruses. Seizure severity was scored using a modification of the Racine scale.[66]

KA-Induced Febrile Seizures in Pups

A rectal temperature probe was used in P14–P17 pups to measure the basal body temperature before each injection. A single LPS injection (2 µg/mouse, Sigma, L4516) was administrated intraperitoneally (i.p.) 2 h before the experiment to induce fever and increase the temperature of the pups. Low-dose i.p. KA injections (5 mg/kg, Tocris, 0222) were performed every hour, and seizures were scored using the Racine scale every 10 min. Mice were culled after grade 5 was reached, and the time taken to reach grade 5 was used as a readout of seizure susceptibility. Seizure scoring was performed blinded to the identity of the injected virus.

Statistical Analysis

The results were analyzed with GraphPad Prism. Mean comparisons among different groups were performed with Student's t test or twoway ANOVA followed by Bonferroni's multiple comparisons test. In the case of non-normally distributed data, median comparisons between two groups were performed with a Mann-Whitney U test. The normality in the data distribution was assessed using the D'Agostino and Pearson omnibus test. For seizure score comparison, the chi-square test was employed. Individual statistical analizes and details regarding experimental design are described in detail alongside each experiment in Results and in the figure legends.

ACKNOWLEDGMENTS

We are thankful to Dr. K. Yamakawa for Scn1a mutant mice; L. Muzio, S. Levi, and D. Zacchetti for providing valuable reagents; S. Comai and M. Simonato for sharing the *in vivo* EEG recording instrumentation; C. Butti and E. Fraviga for technical help; and D. Bonanomi and all members of the Broccoli lab for helpful discussions. We acknowledge the FRACTAL core facility for expert supervision of flow cytometry. This work was supported by the Associazione Gruppo Famiglie Dravet (to V.B.), European Union FP7 Integrating Project “Desire” (602531 to F.B. and V.B.), the Cariplo Foundation (2016-0532 to G.C.), the Italian Ministry of Health (GR-2016-02363972 to G.C.), the Telethon Foundation (GGP19249 to G.C.), a Marie Curie individual fellowship (Marie Skłodowska-Curie grant agreement no. 658418 to G.L.), and an MRC gene therapy grant (MR/L01095X/1 to D.M.K. and S.S.).

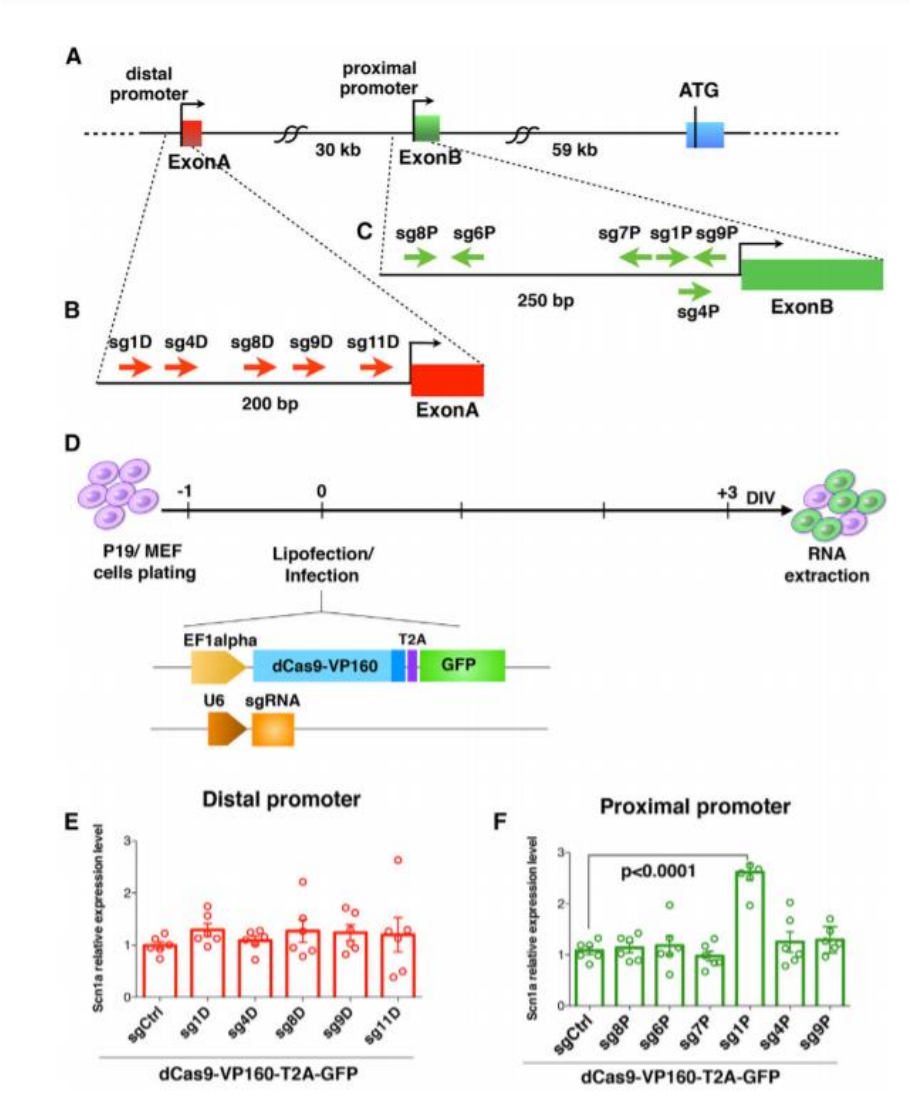

Figure 1. sgRNA Design and Screening for Stimulating *Scn1a* Gene Expression with the dCas9 Activation System in P19 Cells

(A–C) Schematic representation of the *Scn1a* gene (A) with distal (B) and proximal (C) promoter regions; the positions of the sgRNAs selected for this screening are highlighted. (D) Experimental setting for the sgRNA screening in P19 cells and schematic representation of the

constructs employed for cell lipofection. One day after plating, P19 cells were lipofected, and the subsequent day, GFP expression was ascertained. At 3 DIV, the cells were processed for RNA extraction. (E and F) qRT-PCRs for Scn1a mRNA levels performed on RNA extracted from P19 cells lipofected with dCas9VP160-T2A-GFP together with sgRNAs targeting the distal (E) or proximal (F) promoter. Data are normalized on the 18S rRNA and relative to sgCtrl-lipofected cells. sg1p induces significant upregulation of *Scn1a* compared with sgCtrl ($n = 6$, $p < 0.0001$, one-way ANOVA followed by Bonferroni multiple comparisons test). Data are shown as mean ± SEM, with dots representing individual samples.

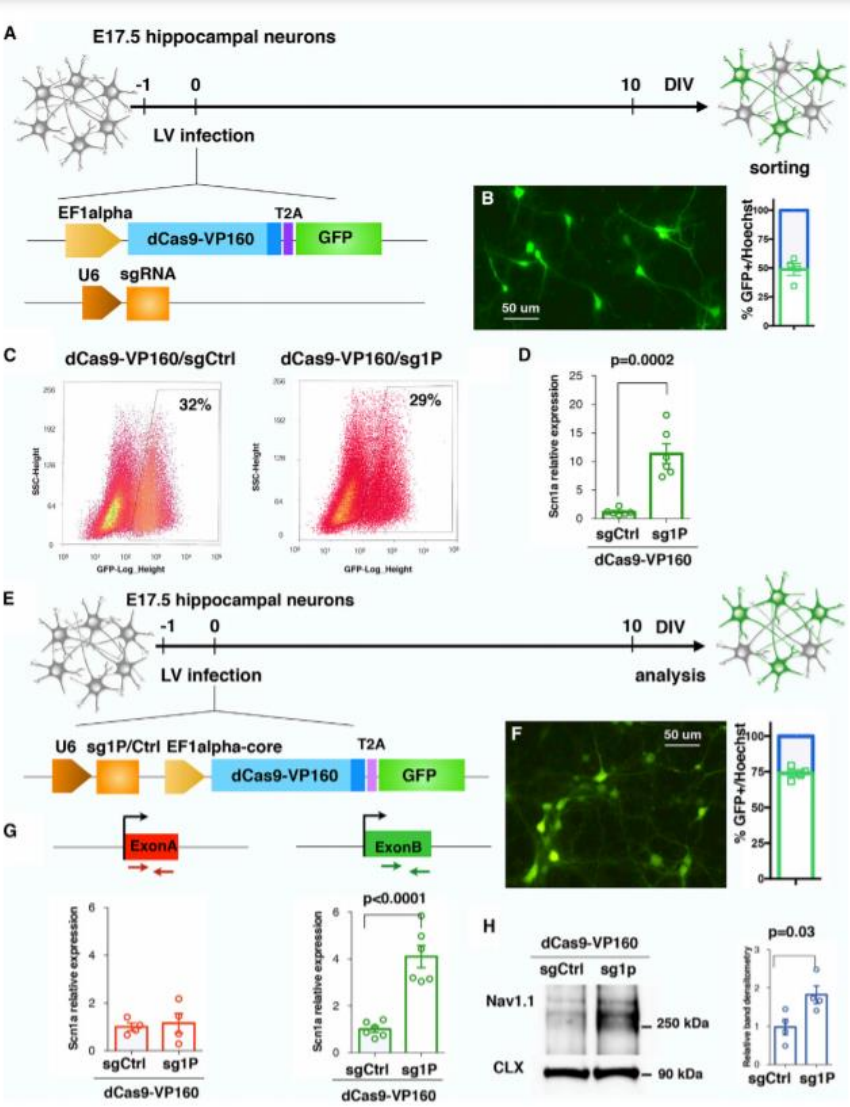

Figure 2. dCas9-VP160/sg1P Potentiates *Scn1a* Gene Transcription in Primary Hippocampal Neurons. (A) Schematic drawing depicting the experimental setting to deliver the Ctrl- and *Scn1a*-dCas9A system in primary neurons. Hippocampal neurons were derived from E17.5 embryos and, the day after plating, were co-transduced with two distinct lentiviruses (LVs) carrying Ef1a-dCas9-VP160- T2A-GFP and pU6-sg1P or pU6-sgCtrl guides, respectively.

(B) Representative image of anti-GFP immunofluorescence at 10 DIV and quantification of GFP+ transduced neurons over the total cell number. Scale bar, 50 mm. (C) Representative FACS images of GFP+ neurons transduced with either the sgCtrl- or sg1P-dCas9 activation system. (D) qRT-PCR reveals the increased *Scn1a* transcriptional levels in hippocampal neurons infected with sg1P with respect to sgCtrl conditions (n = 6, p = 0.0002, Student's t test). Data are shown as mean ± SEM, with dots representing individual samples. (E) Schematic setting of E17.5 neurons transduced with a LV carrying both the pU6-sgRNA cassette and dCas9-VP160-T2A-GFP sequence under control of the EF1alpha core promoter. (F) Anti-GFP immunofluorescence at 10 DIV and relative quantification of transduced GFP+ cells over total, showing that a single LV reaches a transduction efficiency of 75%. Scale bar, 50 mm. (G) qRT-PCR for *Scn1a* with primers amplifying the first (exon A) and second 50 UTR exon (exon B). Data are normalized on 18S rRNA and expressed as relative to sgCtrl. Exon A, sg1P versus sgCtrl: p = 0.7353; exon B, sg1P versus sgCtrl: p < 0.0001; Student's t test). (H) Left: western blot for $Na_v1.1$ and Calnexin on protein lysates from Ctrl-dCas9A- and *Scn1a*-dCas9A-treated neurons at 10 DIV. Right: quantification obtained through densitometry and normalized on Calnexin levels and expressed as *Scn1a*-dCas9A relative to Ctrl-dCas9A (data are shown as mean ± SEM, with dots representing individual samples); n = 4; sg1P versus sgCtrl: p = 0.03, Student's t test.

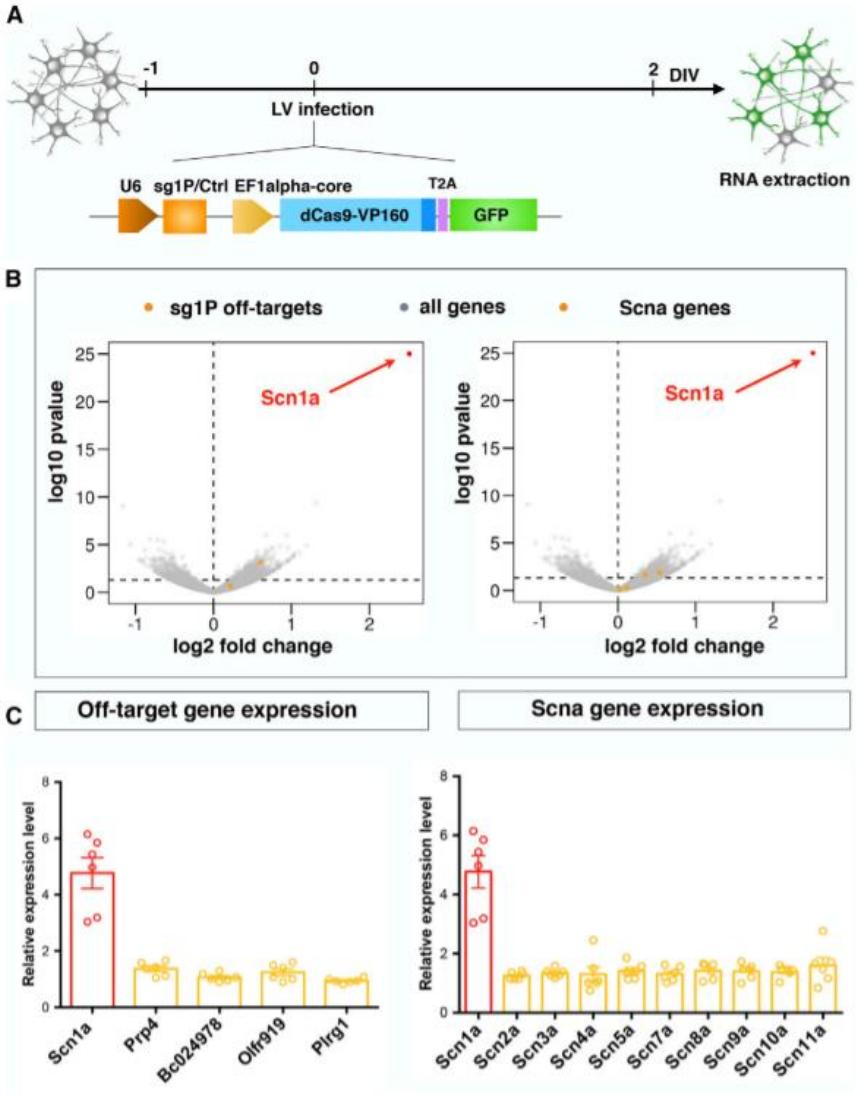

Figure 3. Global Gene Expression analysis of Transduced Neurons Confirms the High Specificity Profile of the *Scn1a*-dCas9A System. (A) Schematic view of the experimental setting to perform gene expression profiling of Ctrl-dCas9A- and *Scn1a*-dCas9A-treated primary neurons. E17.5 embryo-derived neurons were transduced with single LVs at DIV 1 expressing either the Ctrl-dCas9A or *Scn1a*-dCas9A elements and processed for RNA extraction 48 h

later (DIV 3). (B) Volcano plots showing the log10 p value as a function of log2 fold changes in gene expression in *Scn1a*-dCas9A-treated neurons with respect to Ctrl-dCas9A. Scn1a is shown as a red dot. Yellow dots represent off-target genes in the left panel and other *Scna* genes in the right panel. All other genes are shown as gray dots. (C) qRT-PCRs for profiling the expression of predicted off-targets (genes *Prp4*, *BC024978*, *Olfr919*, and *Plrg1*; left panel) or other *Scna* genes (*Scn2a*, *Scn3a*, *Scn4a*, *Scn5a*, *Scn7a*, *Scn8a*, *Scn9a*, and *Scn11a*; right panel). Plotted values are normalized on 18S rRNA and expressed as relative to sgCtrl-treated samples (value = 1, data not shown). n = 6; sg1p versus sgCtrl $p < 0.0004$, Student's t test. Data are shown as mean ± SEM, with dots representing individual samples.

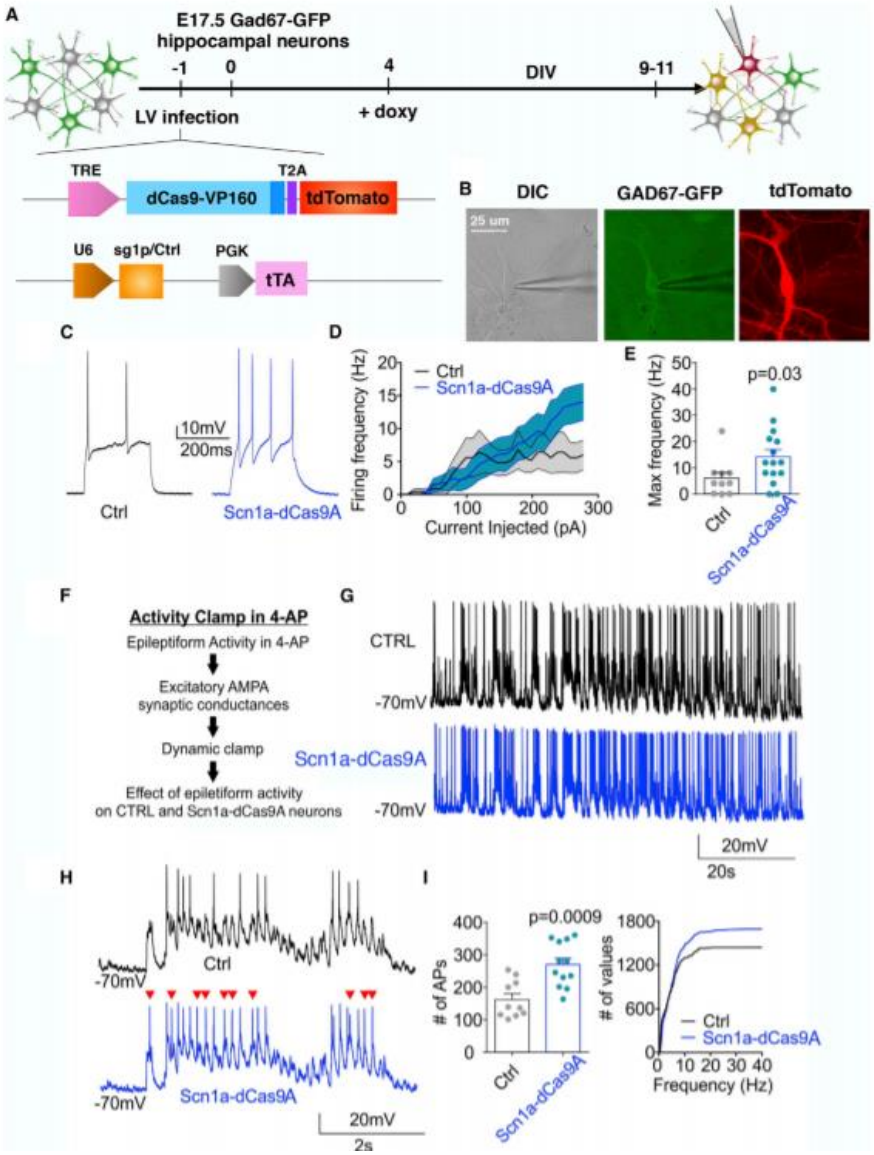

Figure 4. *Scn1a*-dCas9A Increases Neuronal Excitability in Cortical Immature Wild-Type Interneurons. (A) Schematic drawing showing the timeline of transduction with LVs expressing the dCas9A systems on primary wild-type GAD67-GFP neurons and their subsequent functional analysis. (B) Representative images of a patch-clamp-recorded interneuron expressing both GFP under the GAD67

promoter and tdTomato, reflecting the active Scn1a-dCas9A system. Scale bar, 25 mm. (C) Representative current-clamp traces of APs induced by a single current step in dCas9A (black trace, sgCtrl) or *Scn1a*-dCas9A interneurons (blue trace, sg1P). (D) Firing frequency versus injected current for Ctrl- and *Scn1a*-dCas9A-transduced interneurons (Ctrl-dCas9A, n = 11; *Scn1a*-dCas9A n = 15). (E) Histogram of the maximum frequency reached by interneurons during the current step protocol (p = 0.03, Mann-Whitney U test). (F) Experimental design of activity clamp in primary neuronal cultures in the presence of 4AP (Materials and Methods). (G and H) Representative full traces (G) and magnified traces (H) for the activity clamp protocol in Ctrl-dCas9A (black trace, sgCtrl) and *Scn1a*-dCas9A (blue trace, sg1P) interneurons. (I) Activity clamp analysis for the number of events during the full traces (left) and cumulative plot for AP frequency (right) (Ctrl, n = 10; *Scn1a*-dCas9A, n = 12; p = 0.0009, unpaired Student‘s t test).

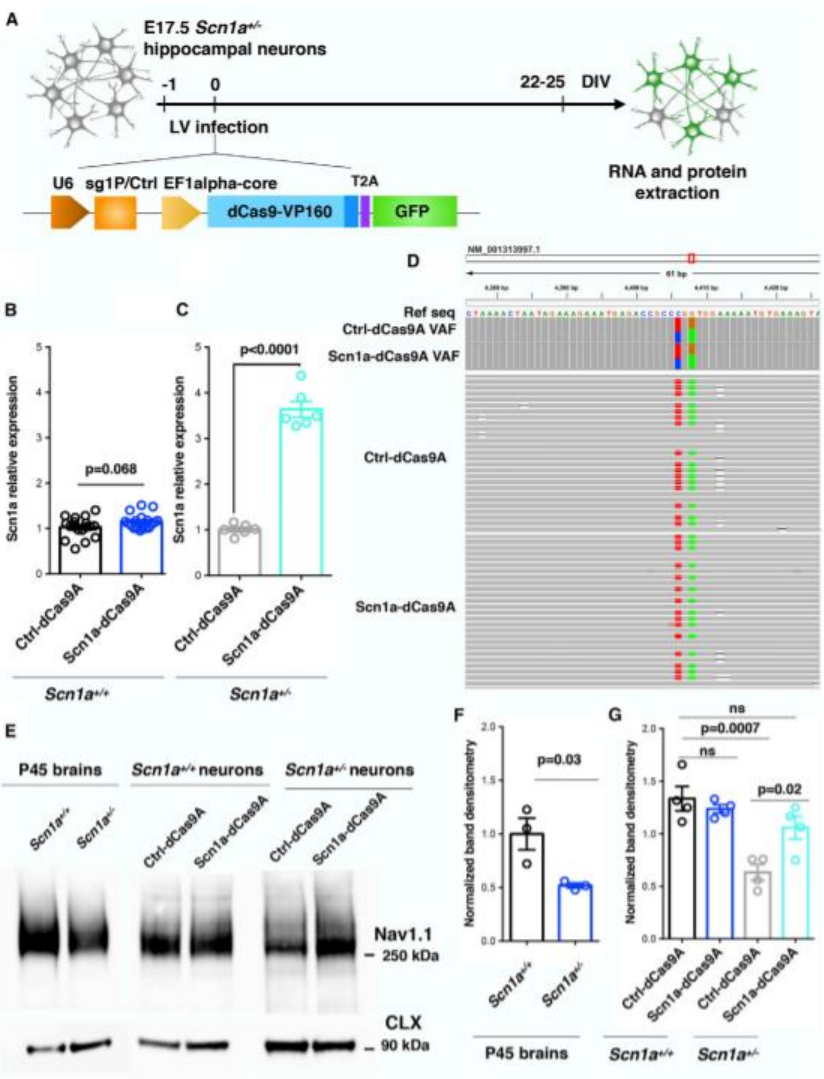

Figure 5. *Scn1a*-dCas9A Stimulates *Scn1a* Basal Expression and $Na_v1.1$ Protein Levels in *Scn1a*$^{+/-}$ Hippocampal Neurons. (A) Schematic drawing of the dCas9A treatments in E17.5 *Scn1a*$^{+/-}$ primary neurons. Neurons were transduced with either the Ctrl-dCas9A or *Scn1a*-dCas9A system 1 day after plating and processed for RNA and protein extraction at 22–25 DIV. (B and C) qRT-PCRs for *Scn1a* transcriptional levels performed on RNA extracted from CtrldCas9A- or *Scn1a*-dCasA-treated *Scn1a*$^{+/+}$(B) and *Scn1a*$^{+/-}$ (C) primary neurons.

Plotted data are expressed as relative to Ctrl-dCas9A. *Scn1a*$^{+/+}$: n = 18, p = 0.068; *Scn1a*$^{+/-}$: n = 4, p < 0.0001; Student's t test. (D) Binary alignment map (BAM) within the mouse *Scn1a* transcript (NM_001313997.1). The red box indicates the region amplified and sequenced with high coverage. Ctrl-dCas9A and *Scn1a*-dCas9A variant allele frequency (VAF) tracks show the observed VAF. Ctrl-dCas9A and *Scn1a*-dCas9A read tracks display a sample of about 30 different sequencing reads per sample; nucleotides diverging from the reference genome are highlighted. (E) Western blot for $Na_v1.1$ and Calnexin on protein lysates from adult (P45) *Scn1a*$^{+/+}$ and *Scn1a*$^{+/-}$ mice (left panel) and from Ctrl-dCas9A- and Scn1a-dCasA-treated *Scn1a*$^{+/+}$ and *Scn1a*$^{+/-}$ neurons at 22–25 DIV (center and right panels). (F) Densitometric quantification of immunoreactive bands in the western blots of adult mouse brains. Values corresponding to the $Na_v1.1$ band were normalized to Calnexin levels (n = 3, p = 0.03, Student's t test). (G) Densitometric quantification of immunoreactive bands in the western blots of *Scn1a*$^{+/+}$ and *Scn1a*$^{+/-}$ neurons transduced with Ctrl-and *Scn1a*-dCas9A.Values corresponding to the $Na_v1.1$ band were normalized to Calnexin levels (n = 4, one-way ANOVA followed by Turkey's multiple comparisons test). Data are shown as mean ± SEM, with dots representing individual samples.

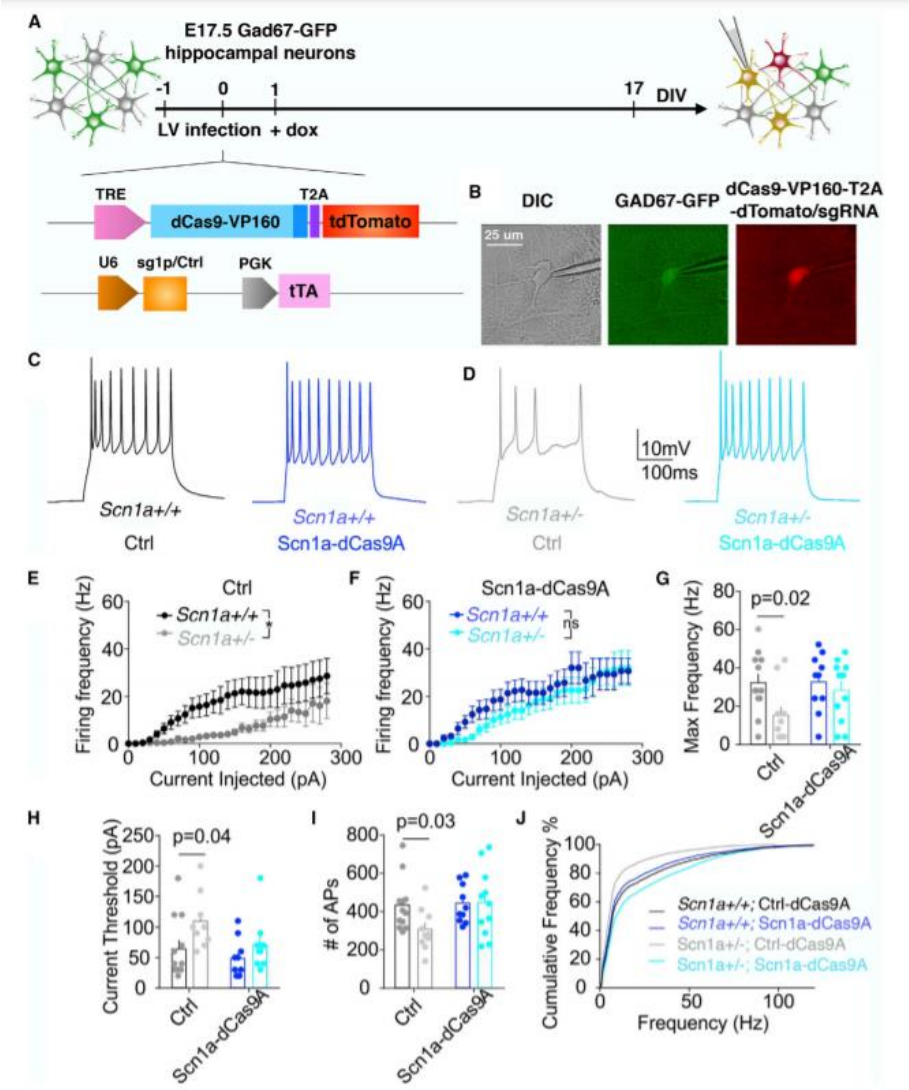

Figure 6. *Scn1a*-dCas9A Rescues Neuronal Excitability Defects in Cortical Mature *Scn1a*$^{+/-}$ Interneurons

(A) Schematic drawing showing the experimental time frame for lentiviral transductions and functional analysis of *Scn1a*$^{+/+}$;GAD67-GFP+ or *Scn1a*$^{+/-}$;GAD67-GFP+ primary hippocampal neurons transduced with the two depicted lentiviruses. (B) Representative images of a patch-clamp-recorded *Scn1a*$^{+/-}$ interneuron expressing

both GFP under the GAD67 promoter and tdTomato reflecting the active Scn1a-dCas9A system (Materials and Methods). (C and D) Representative current-clamp traces of APs induced by single current steps administered to Ctrl-dCas9A-transduced WT interneurons (black trace, C), Scn1a-dCas9A-transduced $Scn1a^{+/+}$ interneurons (blue trace, C), Ctrl-dCas9A-transduced $Scn1a^{+/-}$ interneurons (gray trace, D), and *Scn1a*-dCas9A-transduced Scn1a+/ interneurons (cyan trace, D). (E and F) Firing frequency versus injected current for Ctrl-dCas9A-transduced (E) and Scn1a-dCas9A-transduced (F) Scn1a+/+ and Scn1a+/ interneurons. Ctrl-dCas9A wild-type, n = 12; Ctrl-dCas9A Scn1a+/, n = 10; Scn1a-dCas9A wild-type, n = 10; Scn1a-dCas9A Scn1a+/, n = 1 ($p < 0.05$, 2-way ANOVA). (G and H), Histogram plots of the maximum frequency (G) and current threshold (H) reached by interneurons during the current step protocol ($p = 0.02$, $p = 0.04$, 2-way ANOVA/Bonferroni's multiple comparisons tests). (I and J) Activity clamp analysis for the number of events during the full traces (I) and cumulative plot for AP frequency (J) ($p = 0.03$, 2-way ANOVA/ Bonferroni's multiple comparisons tests).

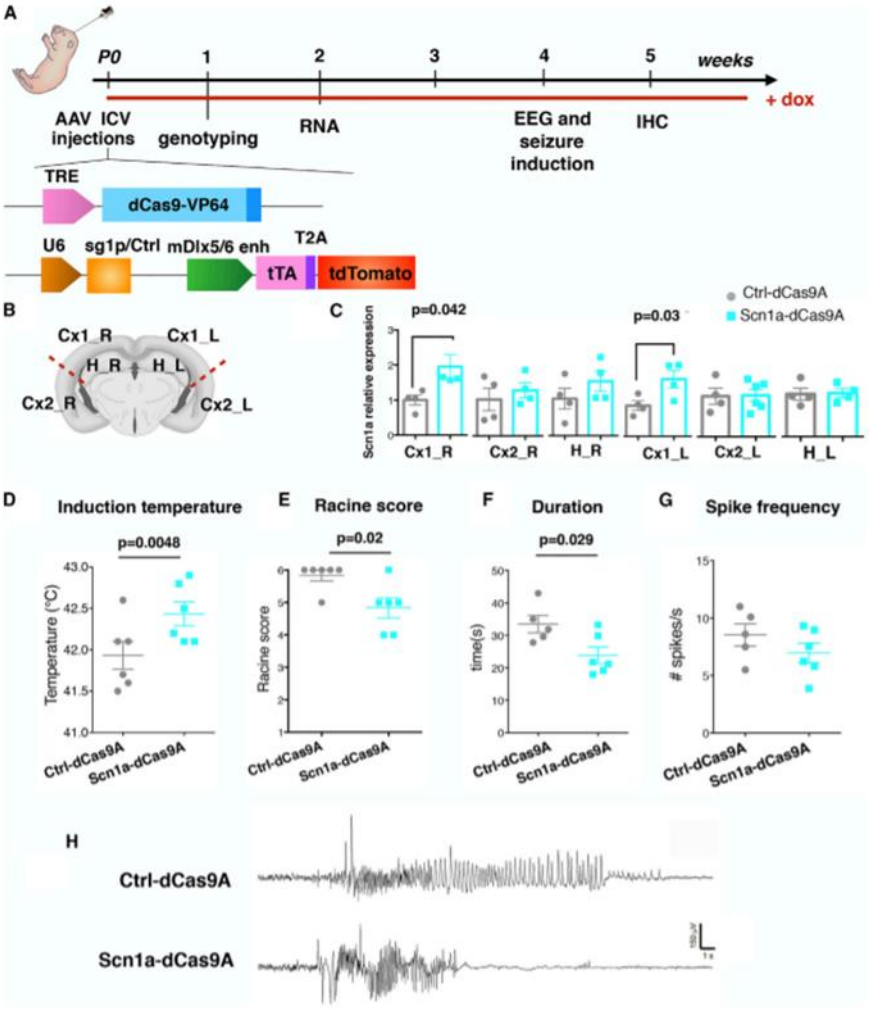

Figure 7. *In Vivo* Scn1a-dCas9A Delivery through Intracerebroventricular Brain Injections Attenuates Seizures in the *Scn1a*$^{+/-}$ Mice. (A) Schematic illustration showing the experimental setting for *in vivo* delivery of the Scn1a-dCas9A system through intracerebroventricular injections into P0 pups of AAVs (2.9) carrying the Ctrl-dCas9A and Scn1a-dCas9A system. After 1 week, treated mice were genotyped, and then *Scn1a*$^{+/-}$ animals then selected for

implantation of EEG electrodes and analysis of the epileptic phenotype. Wild-type (WT) litters were processed for molecular (2 weeks) and histological (5 weeks) characterization of *in vivo* AAV targeting. Doxycycline (dox) was administered in drinking water or food until final analysis. (B) Scheme of cerebral cortex dissection in treated mice for *Scn1a* expression at the mRNA level (Cx1, medial cortex; Cx2, lateral cortex; R, right; L, left). (C) qRT-PCRs performed on dissected areas of the brains in Ctrl-dCas9A- and Scn1a-dCas9A-treated wild-type mice (n = 6 for each group, p = 0.042 for Cx1_R, p = 0.03 for Cx1_L, Student's t test). (D and E) Mean (± SEM) threshold temperatures (D) for the occurrence of myoclonic seizures (n = 6 for each group, p = 0.048, Student's t test) and severity of the epileptic seizures, evaluated by a modified Racine score (E) in Ctrl-dCas9A-and Scn1a-dCas9A-treated Scn1a+/ mice (n = 6 for each group, p = 0.02, chi-square test). (F and G) Duration (F) and spike frequency (G) of temperature-induced seizures in Ctrl-dCas9A-or Scn1a-dCas9A-treated Scn1a+/ mice (n = 5 for Ctrl-dCas9A and n = 6 for Scn1a-dCas9A treated mice, p = 0.029 for duration and p = 0.2 for spike frequency, Student's t test). (H) Representative EEG traces of hyperthermia-induced seizures in Ctrl-dCas9A-and Scn1a-dCas9A-treated Scn1a+/ mice.

REFERENCES

1. Kullmann, D.M. (2010). Neurological channelopathies. Annu. Rev. Neurosci. 33, 151–172.
2. Dravet, C. (2011). Dravet syndrome history. Dev. Med. Child Neurol. 53, 1–6.
3. Meisler, M.H., and Kearney, J.A. (2005). Sodium channel mutations in epilepsy and other neurological disorders. J. Clin. Invest. 115, 2010-7.
4. Nickels, K.C., and Wirrell, E.C. (2017). Cognitive and Social Outcomes of Epileptic Encephalopathies. Semin. Pediatr. Neurol. 24, 264–275.
5. Kasperaviciute, D., Catarino, C.B., Matarin, M., Leu, C., Novy, J., Tostevin, A., Leal, B., Hessel, E.V., Hallmann, K., Hildebrand, M.S., et al.; UK Brain Expression Consortium (2013). Epilepsy, hippocampal sclerosis and febrile seizures linked by common genetic variation around SCN1A. Brain 136, 3140–3150.
6. Cetica, V., Chiari, S., Mei, D., Parrini, E., Grisotto, L., Marini, C., Pucatti, D., Ferrari, A., Sicca, F., Specchio, N., et al. (2017). Clinical and genetic factors predicting Dravet syndrome in infants with SCN1A mutations. Neurology 88, 1037–1044.
7. Marini, C., Scheffer, I.E., Nabbout, R., Suls, A., De Jonghe, P., Zara, F., and Guerrini, R. (2011). The genetics of Dravet syndrome. Epilepsia 52 (Suppl 2), 24–29.
8. Yu, F.H., Mantegazza, M., Westenbroek, R.E., Robbins, C.A., Kalume, F., Burton, K.A., Spain, W.J., McKnight,

G.S., Scheuer, T., and Catterall, W.A. (2006). Reduced sodium current in GABAergic interneurons in a mouse model of severe myoclonic epilepsy in infancy. Nat. Neurosci. 9, 1142–1149.

9. Han, S., Tai, C., Westenbroek, R.E., Yu, F.H., Cheah, C.S., Potter, G.B., Rubenstein, J.L., Scheuer, T., de la Iglesia, H.O., and Catterall, W.A. (2012). Autistic-like behaviour in Scn1a+/- mice and rescue by enhanced GABA-mediated neurotransmission. Nature 489, 385–390.
10. Ogiwara, I., Miyamoto, H., Morita, N., Atapour, N., Mazaki, E., Inoue, I., Takeuchi, T., Itohara, S., Yanagawa, Y., Obata, K., et al. (2007). Nav1.1 localizes to axons of parvalbumin-positive inhibitory interneurons: a circuit basis for epileptic seizures in mice carrying an Scn1a gene mutation. J. Neurosci. 27, 5903–5914.
11. Ito, S., Ogiwara, I., Yamada, K., Miyamoto, H., Hensch, T.K., Osawa, M., and Yamakawa, K. (2013). Mouse with Nav1.1 haploinsufficiency, a model for Dravet syndrome, exhibits lowered sociability and learning impairment. Neurobiol. Dis. 49, 29–40.
12. Hedrich, U.B.S., Liautard, C., Kirschenbaum, D., Pofahl, M., Lavigne, J., Liu, Y., Theiss, S., Slotta, J., Escayg, A., Dihné, M., et al. (2014). Impaired action potential initiation in GABAergic interneurons causes hyperexcitable networks in an epileptic mouse model carrying a human Na(V)1.1 mutation. J. Neurosci. 34, 14874–14889.

13. Ogiwara, I., Iwasato, T., Miyamoto, H., Iwata, R., Yamagata, T., Mazaki, E., Yanagawa, Y., Tamamaki, N., Hensch, T.K., Itohara, S., and Yamakawa, K. (2013). Nav1.1 haploinsufficiency in excitatory neurons ameliorates seizure-associated sudden death in a mouse model of Dravet syndrome. Hum. Mol. Genet. 22, 4784–4804.
14. Tai, C., Abe, Y., Westenbroek, R.E., Scheuer, T., and Catterall, W.A. (2014). Impaired excitability of somatostatin- and parvalbumin-expressing cortical interneurons in a mouse model of Dravet syndrome. Proc. Natl. Acad. Sci. USA 111, E3139–E3148.
15. Tatsukawa, T., Ogiwara, I., Mazaki, E., Shimohata, A., and Yamakawa, K. (2018). Impairments in social novelty recognition and spatial memory in mice with conditional deletion of Scn1a in parvalbumin-expressing cells. Neurobiol. Dis. 112, 24–34.
16. Oakley, J.C., Kalume, F., Yu, F.H., Scheuer, T., and Catterall, W.A. (2009). Temperature- and age-dependent seizures in a mouse model of severe myoclonic epilepsy in infancy. Proc. Natl. Acad. Sci. USA 106, 3994–3999.
17. Wirrell, E.C. (2016). Treatment of Dravet Syndrome. Can. J. Neurol. Sci. 43, S13–S18.
18. Chiron, C., and Dulac, O. (2011). The pharmacologic treatment of Dravet syndrome. Epilepsia 52 (Suppl 2), 72–75.

19. Griffin, A., Hamling, K.R., Knupp, K., Hong, S., Lee, L.P., and Baraban, S.C. (2017). Clemizole and modulators of serotonin signalling suppress seizures in Dravet syndrome. Brain 140, 669–683.
20. Sourbron, J., Schneider, H., Kecskés, A., Liu, Y., Buening, E.M., Lagae, L., Smolders, I., and de Witte, P. (2016). Serotonergic Modulation as Effective Treatment for Dravet Syndrome in a Zebrafish Mutant Model. ACS Chem. Neurosci. 7, 588–598.
21. Devinsky, O., Cross, J.H., and Wright, S. (2017). Trial of Cannabidiol for DrugResistant Seizures in the Dravet Syndrome. N. Engl. J. Med. 377, 699–700.
22. Murlidharan, G., Samulski, R.J., and Asokan, A. (2014). Biology of adeno-associated viral vectors in the central nervous system. Front. Mol. Neurosci. 7, 76.
23. Kay, M.A., Glorioso, J.C., and Naldini, L. (2001). Viral vectors for gene therapy: the art of turning infectious agents into vehicles of therapeutics. Nat. Med. 7, 33–40.
24. Wright, A.V., Nuñez, J.K., and Doudna, J.A. (2016). Biology and Applications of CRISPR Systems: Harnessing Nature's Toolbox for Genome Engineering. Cell 164, 29–44.
25. Hsu, P.D., Lander, E.S., and Zhang, F. (2014). Development and applications of CRISPR-Cas9 for genome engineering. Cell 157, 1262–1278.
26. Mali, P., Aach, J., Stranges, P.B., Esvelt, K.M., Moosburner, M., Kosuri, S., Yang, L., and Church, G.M.

(2013). CAS9 transcriptional activators for target specificity screening and paired nickases for cooperative genome engineering. Nat. Biotechnol. 31, 833–838.

27. Dominguez, A.A., Lim, W.A., and Qi, L.S. (2016). Beyond editing: repurposing CRISPR-Cas9 for precision genome regulation and interrogation. Nat. Rev. Mol. Cell Biol. 17, 5–15.
28. Sander, J.D., and Joung, J.K. (2014). CRISPR-Cas systems for editing, regulating and targeting genomes. Nat. Biotechnol. 32, 347–355.
29. Liu, J., Gao, C., Chen, W., Ma, W., Li, X., Shi, Y., Zhang, H., Zhang, L., Long, Y., Xu, H., et al. (2016). CRISPR/Cas9 facilitates investigation of neural circuit disease using human iPSCs: mechanism of epilepsy caused by an SCN1A loss-of-function mutation. Transl Psychiatry 6, e703.
30. Liao, H.-K., Hatanaka, F., Araoka, T., Reddy, P., Wu, M.Z., Sui, Y., Yamauchi, T., Sakurai, M., O'Keefe, D.D., Núñez-Delicado, E., et al. (2017). In Vivo Target Gene Activation via CRISPR/Cas9-Mediated Trans-epigenetic Modulation. Cell 171, 1495–1507.e15.
31. Hilton, I.B., D'Ippolito, A.M., Vockley, C.M., Thakore, P.I., Crawford, G.E., Reddy, T.E., and Gersbach, C.A. (2015). Epigenome editing by a CRISPR-Cas9-based acetyltransferase activates genes from promoters and enhancers. Nat. Biotechnol. 33, 510–517.

32. Liu, X.S., Wu, H., Ji, X., Stelzer, Y., Wu, X., Czauderna, S., Shu, J., Dadon, D., Young, R.A., and Jaenisch, R. (2016). Editing DNA Methylation in the Mammalian Genome. Cell 167, 233–247.e17.
33. Zhou, H., Liu, J., Zhou, C., Gao, N., Rao, Z., Li, H., Hu, X., Li, C., Yao, X., Shen, X., et al. (2018). In vivo simultaneous transcriptional activation of multiple genes in the brain using CRISPR-dCas9-activator transgenic mice. Nat. Neurosci. 21, 440–446.
34. Konermann, S., Brigham, M.D., Trevino, A.E., Joung, J., Abudayyeh, O.O., Barcena, C., Hsu, P.D., Habib, N., Gootenberg, J.S., Nishimasu, H., et al. (2015). Genome-scale transcriptional activation by an engineered CRISPR-Cas9 complex. Nature 517, 583–588.
35. Simeonov, D.R., Gowen, B.G., Boontanrart, M., Roth, T.L., Gagnon, J.D., Mumbach, M.R., Satpathy, A.T., Lee, Y., Bray, N.L., Chan, A.Y., et al. (2017). Discovery of stimulation-responsive immune enhancers with CRISPR activation. Nature 549, 111–115.
36. Gilbert, L.A., Larson, M.H., Morsut, L., Liu, Z., Brar, G.A., Torres, S.E., SternGinossar, N., Brandman, O., Whitehead, E.H., Doudna, J.A., et al. (2013). CRISPRmediated modular RNA-guided regulation of transcription in eukaryotes. Cell 154, 442–451.
37. Kearns, N.A., Genga, R.M., Enuameh, M.S., Garber, M., Wolfe, S.A., and Maehr, R. (2014). Cas9 effector-mediated regulation of transcription and differentiation in

human pluripotent stem cells. Development 141, 219–223.

38. Matharu, N., Rattanasopha, S., Tamura, S., Maliskova, L., Wang, Y., Bernard, A., Hardin, A., Eckalbar, W.L., Vaisse, C., and Ahituv, N. (2019). CRISPR-mediated activation of a promoter or enhancer rescues obesity caused by haploinsufficiency. Science 363, eaau0629.
39. Nakayama, T., Ogiwara, I., Ito, K., Kaneda, M., Mazaki, E., Osaka, H., Ohtani, H., Inoue, Y., Fujiwara, T., Uematsu, M., et al. (2010). Deletions of SCN1A 50 genomic region with promoter activity in Dravet syndrome. Hum. Mutat. 31, 820–829.
40. Grubb, M.S., and Burrone, J. (2010). Activity-dependent relocation of the axon initial segment fine-tunes neuronal excitability. Nature 465, 1070–1074.
41. Morris, G., Leite, M., Kullmann, D.M., Pavlov, I., Schorge, S., and Lignani, G. (2017). Activity Clamp Provides Insights into Paradoxical Effects of the Anti-Seizure Drug Carbamazepine. J. Neurosci. 37, 5484–5495.
42. Cheah, C.S., Westenbroek, R.E., Roden, W.H., Kalume, F., Oakley, J.C., Jansen, L.A., and Catterall, W.A. (2013). Correlations in timing of sodium channel expression, epilepsy, and sudden death in Dravet syndrome. Channels (Austin) 7, 468–472.
43. Hammond, S.L., Leek, A.N., Richman, E.H., and Tjalkens, R.B. (2017). Cellular selectivity of AAV serotypes for gene delivery in neurons and astrocytes by neonatal

intracerebroventricular injection. PLoS ONE 12, e0188830.

44. Dimidschstein, J., Chen, Q., Tremblay, R., Rogers, S.L., Saldi, G.A., Guo, L., Xu, Q., Liu, R., Lu, C., Chu, J., et al. (2016). A viral strategy for targeting and manipulating interneurons across vertebrate species. Nat. Neurosci. 19, 1743–1749.
45. Stühmer, T., Puelles, L., Ekker, M., and Rubenstein, J.L.R. (2002). Expression from a Dlx gene enhancer marks adult mouse cortical GABAergic neurons. Cereb. Cortex 12, 75–85.
46. Eun, B.-L., Abraham, J., Mlsna, L., Kim, M.J., and Koh, S. (2015). Lipopolysaccharide potentiates hyperthermia-induced seizures. Brain Behav. 5, e00348.
47. Heida, J.G., Teskey, G.C., and Pittman, Q.J. (2005). Febrile convulsions induced by the combination of lipopolysaccharide and low-dose kainic acid enhance seizure susceptibility, not epileptogenesis, in rats. Epilepsia 46, 1898–1905.
48. Schmidt, J.W., and Catterall, W.A. (1986). Biosynthesis and processing of the a subunit of the voltage-sensitive sodium channel in rat brain neurons. Cell 46, 437–444.
49. Chavez, A., Tuttle, M., Pruitt, B.W., Ewen-Campen, B., Chari, R., Ter-Ovanesyan, D., Haque, S.J., Cecchi, R.J., Kowal, E.J.K., Buchthal, J., et al. (2016). Comparison of Cas9 activators in multiple species. Nat. Methods 13, 563–567.

50. Staahl, B.T., Benekareddy, M., Coulon-Bainier, C., Banfal, A.A., Floor, S.N., Sabo, J.K., Urnes, C., Munares, G.A., Ghosh, A., and Doudna, J.A. (2017). Efficient genome editing in the mouse brain by local delivery of engineered Cas9 ribonucleoprotein complexes. Nat. Biotechnol. 35, 431–434.
51. Swiech, L., Heidenreich, M., Banerjee, A., Habib, N., Li, Y., Trombetta, J., Sur, M., and Zhang, F. (2015). In vivo interrogation of gene function in the mammalian brain using CRISPR-Cas9. Nat. Biotechnol. 33, 102–106.
52. Rhodes, T.H., Lossin, C., Vanoye, C.G., Wang, D.W., and George, A.L., Jr. (2004). Noninactivating voltage-gated sodium channels in severe myoclonic epilepsy of infancy. Proc. Natl. Acad. Sci. USA 101, 11147–11152.
53. Catarino, C.B., Liu, J.Y., Liagkouras, I., Gibbons, V.S., Labrum, R.W., Ellis, R., Woodward, C., Davis, M.B., Smith, S.J., Cross, J.H., et al. (2011). Dravet syndrome as epileptic encephalopathy: evidence from long-term course and neuropathology. Brain 134, 2982–3010.
54. Mendell, J.R., Al-Zaidy, S., Shell, R., Arnold, W.D., Rodino-Klapac, L.R., Prior, T.W., Lowes, L., Alfano, L., Berry, K., Church, K., et al. (2017). Single-Dose GeneReplacement Therapy for Spinal Muscular Atrophy. N. Engl. J. Med. 377, 1713–1722.
55. Chen, B., Hu, J., Almeida, R., Liu, H., Balakrishnan, S., Covill-Cooke, C., Lim, W.A., and Huang, B. (2016). Expanding the CRISPR imaging toolset with

Staphylococcus aureus Cas9 for simultaneous imaging of multiple genomic loci. Nucleic Acids Res. 44, e75.

56. Harrington, L.B., Paez-Espino, D., Staahl, B.T., Chen, J.S., Ma, E., Kyrpides, N.C., and Doudna, J.A. (2017). A thermostable Cas9 with increased lifetime in human plasma. Nat. Commun. 8, 1424.
57. Kim, E., Koo, T., Park, S.W., Kim, D., Kim, K., Cho, H.Y., Song, D.W., Lee, K.J., Jung, M.H., Kim, S., et al. (2017). In vivo genome editing with a small Cas9 orthologue derived from Campylobacter jejuni. Nat. Commun. 8, 14500.
58. Davis, C.A., Hitz, B.C., Sloan, C.A., Chan, E.T., Davidson, J.M., Gabdank, I., Hilton, J.A., Jain, K., Baymuradov, U.K., Narayanan, A.K., et al. (2018). The Encyclopedia of DNA elements (ENCODE): data portal update. Nucleic Acids Res. 46 (D1), D794– D801.
59. Carninci, P., Sandelin, A., Lenhard, B., Katayama, S., Shimokawa, K., Ponjavic, J., Semple, C.A., Taylor, M.S., Engström, P.G., Frith, M.C., et al. (2006). Genomewide analysis of mammalian promoter architecture and evolution. Nat. Genet. 38, 626–635.
60. Thorvaldsdóttir, H., Robinson, J.T., and Mesirov, J.P. (2013). Integrative Genomics Viewer (IGV): high-performance genomics data visualization and exploration. Brief. Bioinform. 14, 178–192.
61. Cheng, A.W., Wang, H., Yang, H., Shi, L., Katz, Y., Theunissen, T.W., Rangarajan, S., Shivalila, C.S., Dadon,

D.B., and Jaenisch, R. (2013). Multiplexed activation of endogenous genes by CRISPR-on, an RNA-guided transcriptional activator system. Cell Res. 23, 1163–1171.

62. Colasante, G., Lignani, G., Rubio, A., Medrihan, L., Yekhlef, L., Sessa, A., Massimino, L., Giannelli, S.G., Sacchetti, S., Caiazzo, M., et al. (2015). Rapid Conversion of Fibroblasts into Functional Forebrain GABAergic Interneurons by Direct Genetic Reprogramming. Cell Stem Cell 17, 719–734.
63. Tamamaki, N., Yanagawa, Y., Tomioka, R., Miyazaki, J., Obata, K., and Kaneko, T. (2003). Green fluorescent protein expression and colocalization with calretinin, parvalbumin, and somatostatin in the GAD67-GFP knock-in mouse. J. Comp. Neurol. 467, 60–79.
64. Langmead, B., Trapnell, C., Pop, M., and Salzberg, S.L. (2009). Ultrafast and memory-efficient alignment of short DNA sequences to the human genome. Genome Biol. 10, R25.
65. Love, M.I., Huber, W., and Anders, S. (2014). Moderated estimation of fold change and dispersion for RNA-seq data with DESeq2. Genome Biol. 15, 550.
66. Velísková, J., and Velísek, L. (2017). Behavioral characterization and scoring of seizures in rodents. In Models of Seizures and Epilepsy, A. Pitkänen, P.S. Buckmaster, A.S. Galanopoulou, and S.L. Moshé, eds. (Academic Press), pp. 111–123.

SUPPLEMENTAL INFORMATION

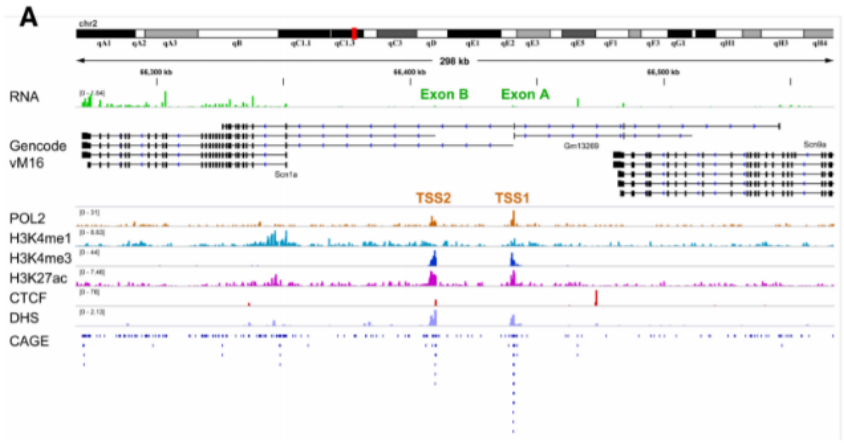

Figure S1 | Bioinformatics analysis of the *Scn1a* gene locus for promoter regulatory region prediction. Alignment to the *Scn1a* gene reference sequence of RNA-seq, ChIP-seqs, DNase-seq and CAGE-seq profiles related to adult mouse brains. The enrichment of markers associated with transcriptional activation in the regions upstream of the first two untranslated exons (Exon A and Exon B) of the gene highlights the presence of two TSS (TSS1 and TSS2) and allows to localize a distal promoter in the 200 bp upstream of exon-A and a proximal promoter upstream of the exon-B. POL2, RNA polymerase II ChIP-seq; H3K4me3, tri-methylation of lysine 4 on the histone H3 ChIP-seq; H3K4me1, mono- methylation of lysine 4 on histone H3 ChIP-seq; H3K27ac, acetylation of lysine 27 on histone H3 ChIP-seq; CTCF, factor that binds the CCCTC; DHS, DNase I Hyper Sensitivity mapping; CAGE-seq, Cap Analysis of Gene Expression-sequencing

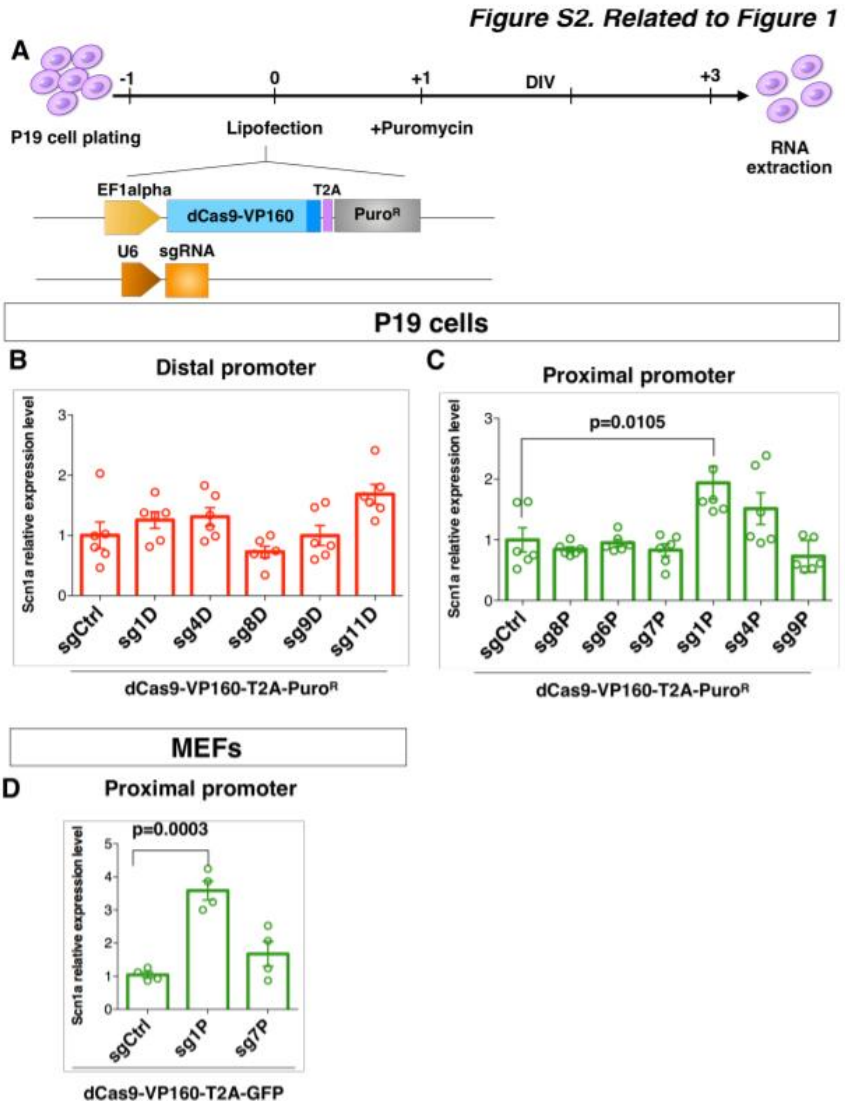

Figure S2 | Screening of sgRNAs for *Scn1a* gene activation by targeting its distal or proximal promoter in association with the dCas9-VP160-T2A-GFP in different cell types. a, Screening of the guides lipofected in P19 cells in association with dCas9VP160-T2A-PuroR. Quantitative RT-PCRs performed on RNA extracted from P19 cells 3 days after lipofection with dCas9VP160-T2A-PuroR and sgRNAs targeting distal (b) or proximal (c) promoters to evaluate levels

of *Scn1a* gene transcript. Data are normalized on 18S rRNA and relative to sgCtrl lipofected cells; n = 6, p = 0.0001, one-way ANOVA followed by Bonferroni multi comparison tests. d, RTqPCR on RNA extracted from MEFs infected with sg1P and sg7P in association with dCas9VP160- T2A-PuroR; n = 4, p = 0.0003, One-way ANOVA followed by Bonferroni's multiple comparison tests. Data are shown as mean ± s.e.m. with dots representing individual samples**.**

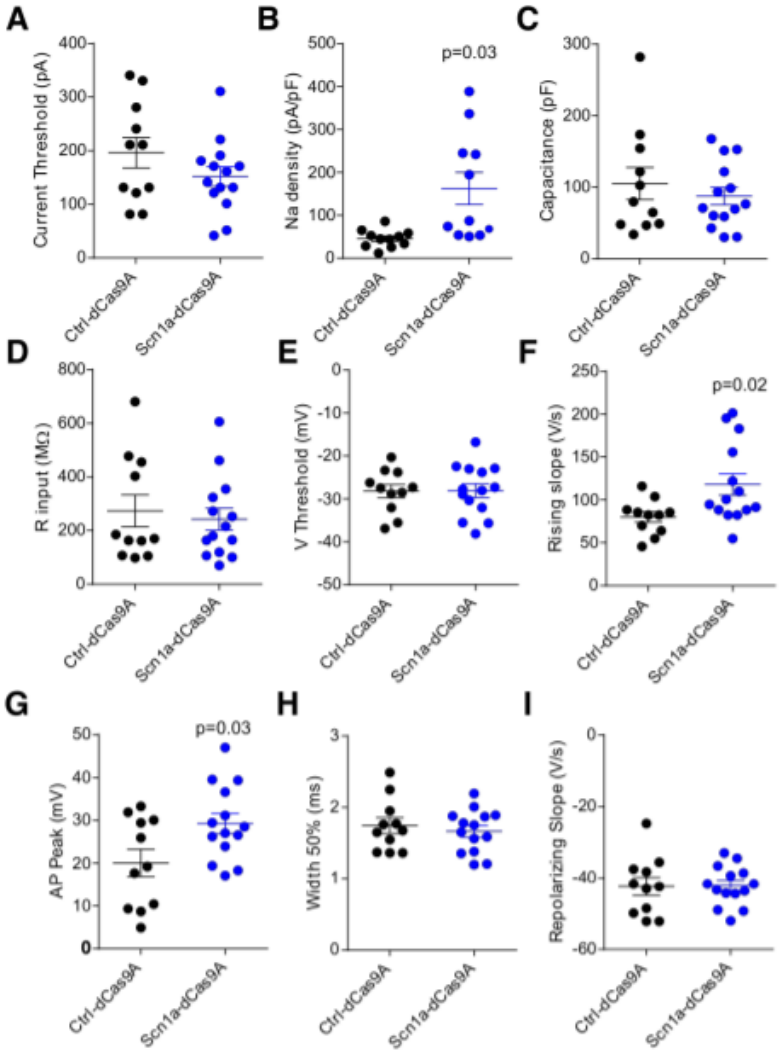

Figure S3 | The Scn1a-dCas9A system accelerates functional maturation of primary wild-type hippocampal neurons at 9-11 DIV. Analysis of passive properties, voltage steps and current threshold (a-d), and single AP shape (e-i) in 9-11 DIV wild-type primary neurons transduced with either the Ctrl-dCas9A or Scn1a-dCas9A system. Student's t test was used for statistical analysis.

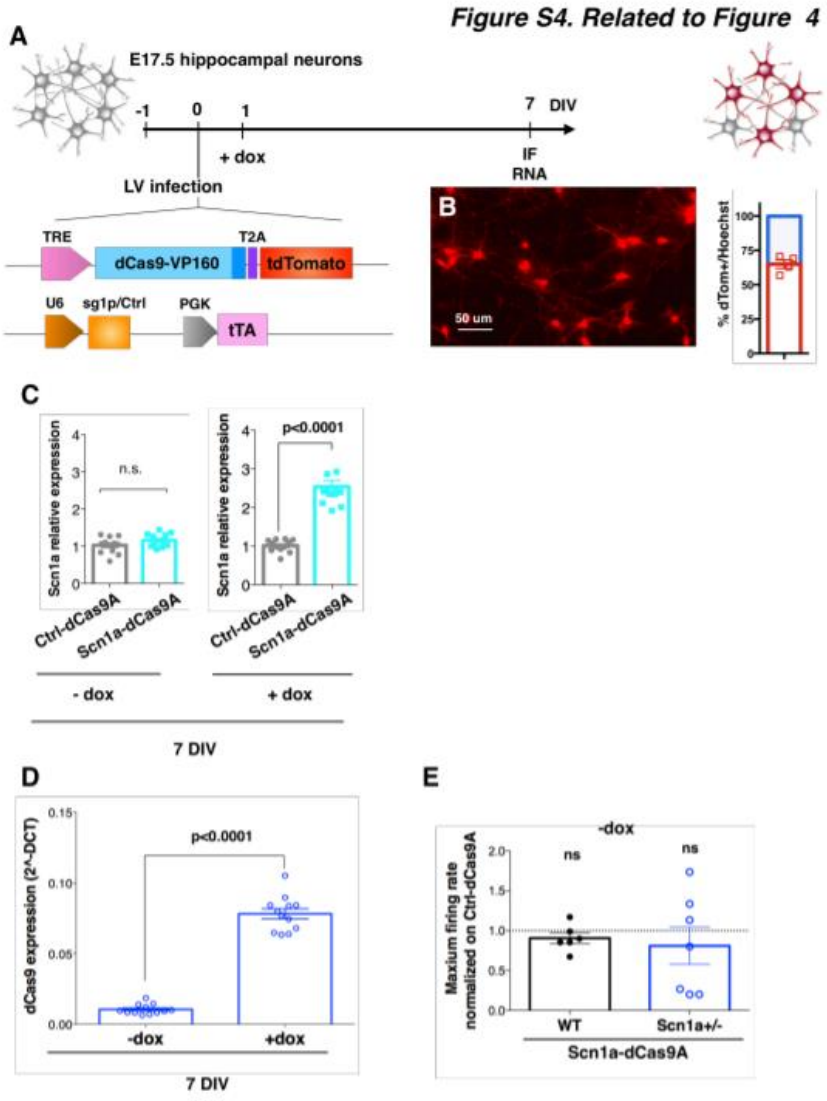

Figure S4 | Assessing the leakiness of the *Scn1a* gene activation by the *Scn1a*-dCas9A system. A, Illustration of the dual LV doxycycline (dox) inducible system set for patch-clamp experiments *in vitro*: a first LV carrying dCas9-VP160 regulated by the rtTA responsive element (TRE) and a second carrying the transactivator rtTA together with the sgRNA. Dox was administered or not at / DIV IF and RNA extraction were performed; B, anti-RFP immunofluorescence and

quantification of tdTomato+ transduced cells over total neurons. C, Relative RT-qPCR for Scn1a performed on RNA extracted from either Ctrl-dCas9A or Scn1a-dCasA in WT neurons at 7 DIV in the absence or presence of dox. Data are expressed as ratios relative to Ctrl-dCas9A. D, RT-qPCR for dCas9 (2^- DCt) in neurons transduced with Scn1a-dCas9A system in the absence or presence of dox (n=12, p<0.0001 Student's t test. E, Histogram plot of maximum firing rate in Scn1a-dCas9A treated wt and Scn1a+/- GAD67-GFP neurons relative to Ctrl-dCas9A in the absence of dox (n=7, Student's t test).

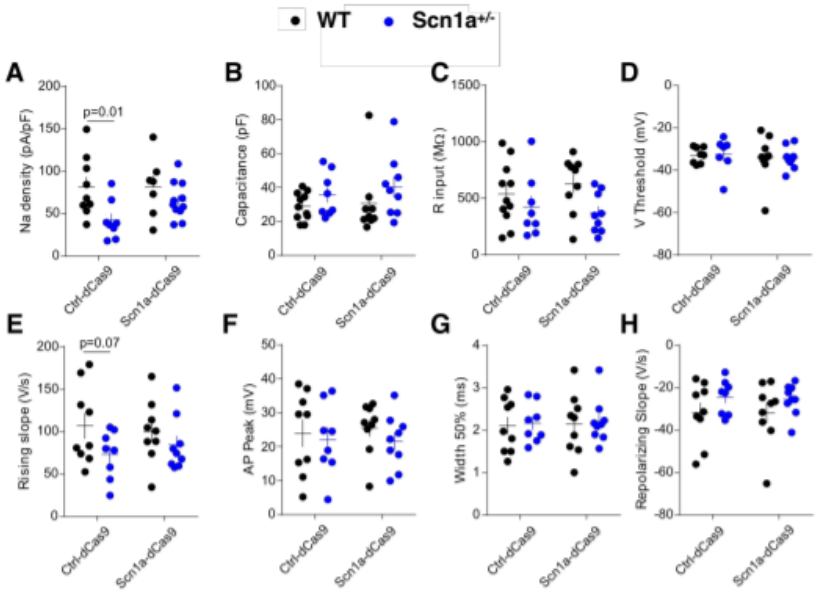

Figure S5| The Scn1a-dCas9 system corrects some functional impairments in 18-20 DIV primary *Scn1a*$^{+/-}$ neurons while is not altering activity in corresponding wild-type neurons. A-H, Analysis of passive properties, Na^+ current density and single AP shape in *Scn1a*$^{+/+}$ (black dots) and Scn1a$^{+/-}$ (blue dots) primary neurons transduced with either the Ctrl-dCas9A or the Scn1adCas9A system.

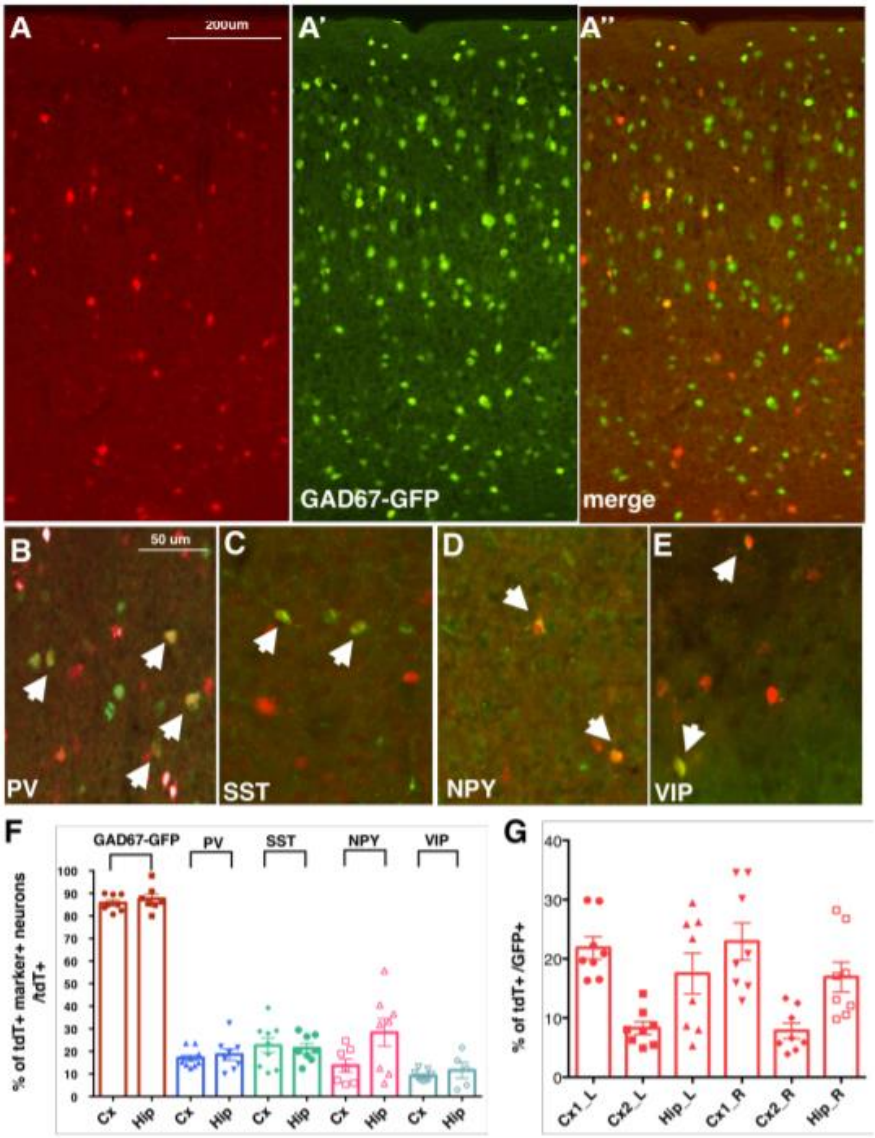

Figure S6 | AAVs packaged with the Scn1a-dCas9A system controlled by the Dlx5/6 enhancer direct tdTomato expression specifically in cortical interneuron subpopulations *in vivo*. A-A'', Anti-GFP and anti-RFP dual immunofluorescence in brain sections of P30 GAD67-GFP mice subjected to intracerebroventricular injections at P0 with AAVs carrying Scn1a-dCas9A elements, scale bars 200um.

B-E, Representative cortical areas of P30 mouse brain sections transduced at P0 with the Scn1a- dCas9A elements stained for anti-PV, -SST, -NPY and -VIP in association with antiRFP to reveal transduced neurons, scale bars 50 um. F, Quantification of the percentage of tdTomato+ cells co-expressing each of the interneuron markers listed above (GAD67-GFP, PV, SST, NPY and VIP) over the total number of tdTomato+ cells. G, Quantifications of the percentage of tdTomato+ cells over the total of GAD67-GFP+ cells in various areas (Cx1, Cx2 and Hip in each brain hemisphere). Data are shown as mean ± s.e.m., with dots representing individual quantifications.

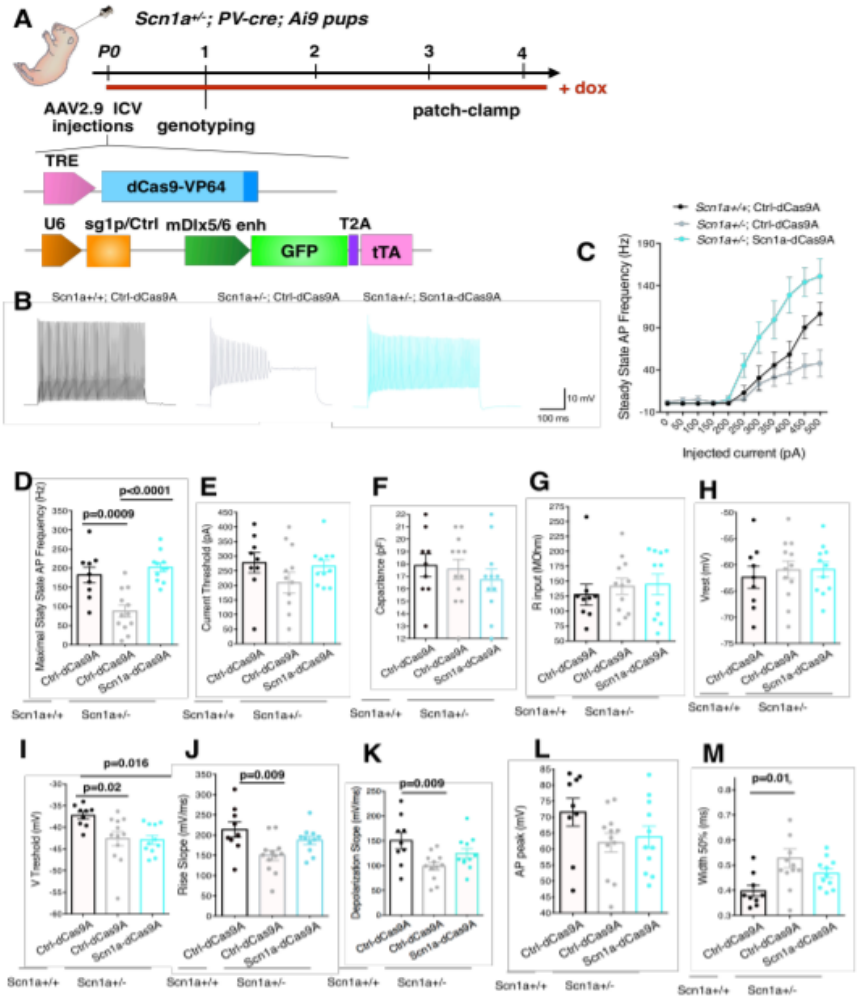

Figure S7 | Scn1a-dCas9A treatment ameliorates firing in *Scn1a*$^{+/-}$ PV interneurons. A, Schematic illustration showing the experimental setting for ICV injections of Ctrl and Scn1adCas9A with GFP reporter into *Scn1a*$^{+/+}$ and *Scn1a*$^{+/-}$; PV-Cre Ai9 P0 pups. Transduced PV interneurons appear GFP+ and tdTomato+. Dox was administered in drinking water until the final analysis. B, Representative traces recorded from GFP+/tdTomato PV+ interneurons in somatosensory cortex (SSC) (P21-28). C, I/O plot analysis show impaired functionality

in *Scn1a*$^{+/-}$ Ctrl-dCas9A compared to *Scn1a*$^{+/+}$; Ctrl-dCas9A interneurons which is recovered in *Scn1a*$^{+/-}$;Scn1a-dCas9A PV interneurons (p=0.003, two-way ANOVA/Bonferroni). D. Maximal steady state AP frequency and other passive and AP parameters of *Scn1a*$^{+/+}$; Ctrl-dCas9A and *Scn1a*$^{+/-}$; Ctrl-/ Scn1a-dCas9A transduced PV interneurons (one-way ANOVA/Bonferroni's multiple comparison tests).

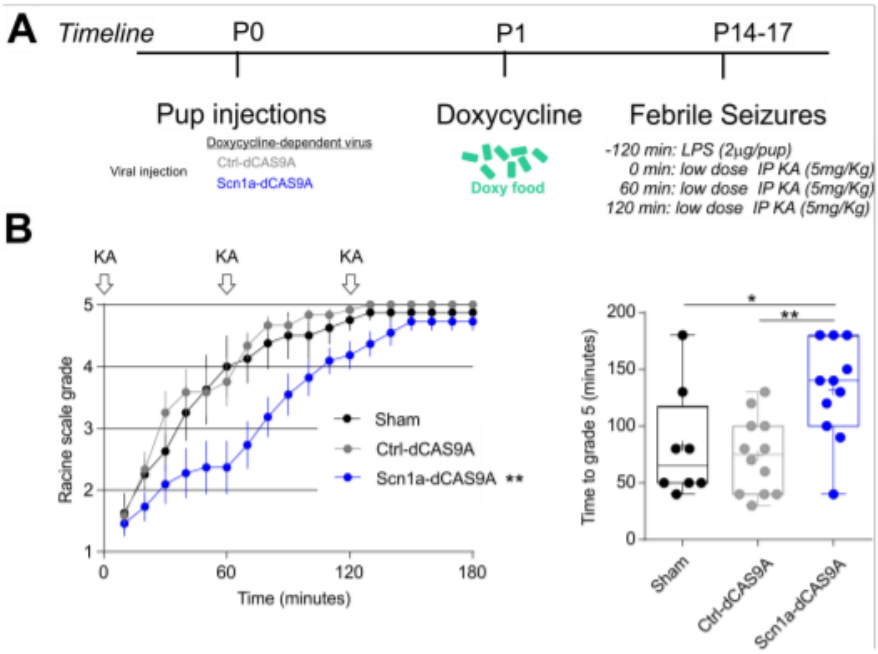

Figure S8 | Upregulation of $Na_v1.1$ during early development is protective against febrile seizures. A. Timeline of the experimental plan. B. Left. Racine scale scoring following low dose KA injections every hour over a 3-hour experimental time period with behavioural scoring every 10 minutes. ** p<0.01, two-way ANOVA, Sham or Ctrl-dCAS9A vs Scn1a-dCAS9A. Right. Box plots of the time taken to reach grade 5. Middle line represents the median, "+" the mean and the box,

the 10-90 percentile range. *p<0.05, **p<0.01, one-way ANOVA followed by Bonferroni multicomparison test.

sg1D	CGTTTTTGAAACGTTTTGGA AGG
sg4D	AGCATGAAAGCTAAATCTCC TGG
sg8D	ATAGGTCTCATTTTGTGGGT AGG
sg9D	TTGCATGGAAATCATGAACC AGG
sg11D	AAGTATTGGCAGCAGCAAGC AGG
sg8P	AATAAGCAAATTTCATTCAT GGG
sg6P	ATTGTTACTTTTACAGATTA CGG
sg7P	CCCCTTTGCTCTGCCTATCA TGG
sg1P	TAAGTCAATAGTTCCATGAT AGG
sg9P	CCCCTTTGCTCTGCCTATCA TGG
sg4P	CCATGATAGGCAGAGCAAAG TGG
sglacZ	TGCGAATACGCCCACGCGAT

Supplementary Table 1: Sequences of sgRNAs.

18s_F	GGTGAAATTCTTGGACCGGC
18s_R	GACTTTGGTTTCCCGGAAGC
Scn1a_F	CACCAACGCTTCCCTTGAGG
Scn1a_R	TGGACATTGGCCTGCATCAG
Scn1a_exA_F	GGTCCTGGTGGTACAAGCACT
Scn1a_exA_R	GAGGCTGCAGGAAGCTGAG
Scn2a_F	CCTCAGGAGGTCTATGCCAAA
Scn2a_R	GTGTCAGCTGGTTGCGAAAA
Scn3a_F	GCATTGCGTCCACGTAGATAA
Scn3a_R	GGAGCTGAAGACATGGGTCA
Scn4a_F	AGATCCCGCCTCCTGATTTA
Scn4a_R	ATCATGGGGGTGAGAGGAGT
Scn5a_F	TGGGAGAGGAGACAGTGTGG
Scn5a_R	CACGGGGATGATTGGACTTA
Scn7a_F	CCTTACCAACTTGCCTTGGA
Scn7a_R	ACCAACCAACCAACCAAACA
Scn8a_F	GCTTCTGCCATATCCCTCCA
Scn8a_R	GGCAGCTCCATCTTTCCATC
Scn9a_F	ATGGAAGATGCCAAGCAGTG
Scn9a_R	TGGATGTTTTGTGTGGCTCA
Scn10a_F	TCCCACCATCCTATGACAGC
Scn10a_R	ACTGAGGTCCAGGGCTCTTC
Scn11a_F	TTCATGGAGGCCAATCCTTT
Scn11a_R	TGACCTGCCTTTCAGCTTCA
Pde4b_F	TCAGCCAGGTCTAATCTGCCA
Prp4_F	GGTCCATGGTGACCTTCAAGA
Prp4_R	ATGTGGACTGTAGGTGGTGC
BC02_F	AGTGAGTGCAGGGGTCCT
BC02_R	GAAGGATGGTGGTTGGTGGG
Olfr919_F	CCTGGATGGTAGGTGGGGTA
Olfr919_R	GCAGGCAAGCTCCATCAATG
Plrg1_F	AGTTGCTACCGTGAGATGCC
Plrg1_R	TGGTTCGTCAGTGTCACTCG

Supplementary Table 2: Primers for RT-qPCRs

CHAPTER 4

CRISPR/dCas9 as a Therapeutic Approach for Neurodevelopmental Disorders: Innovations and Limitations Compared to Traditional Strategies

Ricci Raffaele[1,2], Colasante Gaia[1].

[1]Stem Cell and Neurogenesis Unit, Division of Neuroscience, San Raffaele Scientific Institute, 20132 Milan, Italy [2]Translational and Molecular Medicine PhD Program, DIMET, University of Milan-Bicocca, Milan, Italy

Published on Developmental Neuroscience

Abstract

Brain development is a complex process that requires a series of precise and coordinated events to take place. When alterations in some of those events occur, neurodevelopmental disorders (NDDs) may appear, with their characteristic symptoms, including cognitive, social motor deficits, and epilepsy. While pharmacologic treatments have been the only therapeutic options for many years, more recently the research is turning to the direct removal of the underlying genetic cause of each specific NDD. This is possible thanks to the increased knowledge of genetic basis of those diseases and the enormous advances

in genome-editing tools. Together with clustered regularly interspaced short palindromic repeats (CRISPR)/Cas9-based strategies, there is a great development also of nuclease defective Cas9 (dCas9) tools that, with an extreme flexibility, allow the recruitment of specific protein functions to the desired genomic sites. In this work, we review dCas9-based tools and discuss all the published applications in the setting of therapeutic approaches for NDDs at the preclinical level. In particular dCas9-based therapeutic strategies for Dravet syndrome, transcallosal dysconnectivity caused by mutations in C11orf46 gene, and Fragile X syndrome are presented and discussed. A direct comparison with other possible therapeutic strategies, such as classic gene replacement or CRISPR/Cas9-based strategies, is provided. We also highlight not only those aspects that constitute a clear advantage compared to previous strategies but also the main technical hurdles related to their applications that need to be overcome.

Introduction

The correct functionality of the brain is ensured by the accomplishment of complex processes occurring in both embryonic and postnatal life and tightly regulated and coordinated by transcriptional programs [1, 2]. Those processes, which in their entirety constitute the brain development, include proliferation of distinct cell types, differentiation into various fates, migration to their proper locations, and final maturation with

integration in local circuits. The final output of these impressive set of events is the brain acquisition of complex abilities like language, cognition, and emotion. Alterations or complete disruptions of those regulated events can ultimately lead to neurodevelopmental disorders (NDDs) that affect about 3% of children worldwide [3, 4]. Typical manifestations of NDDs are impairment in cognition, communication, behavior, and psychomotor abilities and include autism spectrum disorder, intellectual disability (ID), attention-deficit hyperactivity disorder, and epilepsy. From a genetic perspective, mutations in genes involved in very different developmental pathways are associated with NDDs, including transcriptional and epigenetic regulation, synaptic signaling and neuronal excitability, the signaling of growth factors, and aminoacid and protein synthesis [5, 6], evidencing a heterogeneous origin of these disorders. Different types of mutations can occur; not only chromosomal rearrangements, copy number variations, indels, and point mutations but also polygenic origin has been described for some of them [7]. The effect of those mutations may be a “gain of function” (GoF) that is characterized by an increased activity of the mutated gene product not necessarily carrying a dominant-negative effect, or a “loss of function” (LoF) effect, with a reduction of a cellular function. For a long time, the only therapeutic option for those disorders has been pharmacological treatments; for GoF mutations, they aim to neutralize the mutated protein and/or block its downstream deleterious effects, while in LoF mutations, they try to stimulate the protein function or inhibit

the opposite function. In recent years, the effort to define new therapeutic options is shifting toward the reduction of side effects with more specific disease-targeting treatment, that is, precision medicine [8]. This was possible thanks to a deeper understanding of genetic basis of the disease and also to the dramatic advances in DNA manipulation and editing tools. Classic gene therapy approaches based on gene replacement in cells lacking that specific gene function are the most suitable option for those disorders caused by LoF gene mutations. Nevertheless, it cannot be applied when the coding sequence of the gene exceeds the cargo capacity of currently used viral vectors for gene therapy in the central nervous system (CNS) or when the expression levels of the specific gene need to be carefully dosed as its overexpression may be detrimental [9, 10]. Furthermore, gene replacement is not an option in the case of GoF mutations, where instead strategies to reduce the expression of mutant target genes, such as antisense oligonucleotides or RNA interference, have been applied [11, 12]. The recent advent of clustered regularly interspaced short palindromic repeats (CRISPR)/Cas9 technology [13, 14] has revolutionized functional investigations of gene expression together with the optimization of gene therapy approaches [15]. In comparison to previous gene-editing tools (TALEN and zinc finger proteins), the simplicity of CRISPR/Cas9 tool manipulation has allowed its widespread usage in laboratories with minimal requirement of molecular biology skills and has pushed an enormous development and application of this technique. Cas9

can be employed to specifically inactivate alleles carrying GoF mutations by insertion of indels at sites where it is recruited by sgRNA to make double-stranded breaks (DSBs; [16–19]) or to directly correct gene mutations in both GoF and LoF mutations upon homology direct recombination (HDR) at DSB sites when a donor DNA is provided [20]. HDR works with high efficiency in dividing cells [21] but not in postmitotic cells like mature neurons. In this case, homology-independent targeted integration has been recently described as a promising option for gene targeting [22], although efficiency is still low to ensure widespread gene correction. Moreover, a major concern for the employment of Cas9-based technologies is that off-target editing may occur [23, 24] and may cause permanent DNA alterations with eventual disruption of gene function. Another possibility in the development of new treatments is in regard to the usage of nuclease defective Cas9 (dCas9), which can become an adaptor to which a variety of effector domains can be attached to address functions in the desired genomic site. In particular, it can be employed to enhance or repress transcription, making it suitable for GoF and LoF mutations, with a reduced risk of off-target compared to Cas9. dCas9 itself can bind target genomic DNA sequences, creating steric hindrance that prevents the activity of other DNA-binding proteins such as endogenous transcription factors and RNA polymerase II and therefore interfering with gene expression (CRISPR interference) [25]. The fusion of dCas9 to a strong repressor complex such as Kruppel-associated Box results in a stronger and more specific gene

repression [26]. Similarly, specific induction of gene expression has been achieved by fusing dCas9 to transcriptional activators in the activatory CRISPR (CRISPRa) [27–30]. dCas9 can also be exploited to recruit various epigenetic writers and erasers to a specific locus. Indeed, dCas9 has been fused to different epigenetic factors, such as the catalytic domain of eukaryotic DNA methyl transferase 3A (DNMT3A) [31–35] and ten-eleven translocation (TET) proteins to methylate and de-methylate DNA [36, 37]. dCas9 fusion to histone modifiers, like histone demethylase LSD1, that removes the active enhancer marker H3K4me2 mark [38], and histone acetyl transferase P300 [39] result in the reduction and increase of enhancer activity, respectively. dCas9-SunTag is a scaffold protein made of a repeated peptide array, which can recruit multiple copies (up to 24) of a desired regulatory protein to a genomic site, thanks to the fusion of the specific effector protein to an antibody with high affinity to that peptide array [40]. Finally, dCas9 fusion to an engineered reverse transcriptase makes it possible to rewrite new genetic information into a specified DNA site; in this case, the prime editing exploits a guide RNA (prime editing guide RNA) that both addresses the dCas9 to the specific target genomic region and encodes the edit to be introduced at the same time [41]. All these tools represent a gold mine in which many laboratories have dived to make the most of them. In the present work, we aimed to review all the therapeutic approaches selectively targeting NDDs based on CRISPR/ dCas9 that are being developed at the preclinical level (Table 1), highlighting

those aspects that could give them an advantage compared to previous strategies and main limitations. CRISPR/dCas9-Based Applications in Models of NDDs CRISPRa has been recently exploited to recover the haploinsufficiency of *Scn1a* gene [42, 43], a gene encoding for the alpha subunit of voltage-gated sodium channel $Na_v1.1$. LoF mutations in *SCN1A* determine a spectrum of disorders with different phenotypic severity, ranging from febrile seizures plus to generalized epilepsy with febrile seizures plus and Dravet syndrome (DS), a severe infantile epilepsy that begins during the first year of life and leads to severe motor, cognitive, and social interaction deficits [44]. A strong contribution of the genetic background on the phenotypic manifestations of the same mutation has been reported [45, 46]. $Na_v1.1$ is enriched at the axonal initial segment of GABAergic interneurons – although more and more evidences regarding its expression in glutamatergic neurons are emerging [47, 48] – where it plays a critical role in AP generation. As a consequence, *Scn1a* LoF mutations imply decreased excitability of inhibitory neurons, which appears to be the underlying cause of intractable epilepsy [49]. Different animal models of DS that well recapitulate both the epileptic phenotype and behavioral alterations are available [50, 51]. DS is the ideal candidate for the application of a gene therapy based on CRISPRa either because the underlying genetic mechanism is gene haploinsufficiency or because the coding sequence of *Scn1a* gene, which is longer than 6 kb, cannot be accommodated in adeno-associated viral vectors (AAVs), commonly employed for gene delivery in the

CNS. With these premises, increasing the expression of the healthy copy of *Scn1a* looks like a promising approach, and other strategies based on the same rationale have been developed [52, 53]. The two studies [42, 43] start with a screening of sgRNAs targeting *Scn1a* distal and proximal promoters in a cell line *in vitro*. Several sgRNAs were tested for their ability to increase basal levels of *Scn1a* in those cells in association with dCas9 fused to different transcriptional activators, specifically VP160 [42] and VP64-p65-Rta (VPR) [43]. Surprisingly, they came to different conclusions, as one laboratory defined efficacious sgRNAs targeting the distal promoter [43], while the other a unique upregulating sgRNA targeting *Scn1a* proximal promoter [42]. Interestingly, this latter *Scn1a* promoter (1b) has been recently described as a critical disease-relevant regulatory element. In fact, its ablation in a mouse model is sufficient to induce Dravet phenotype [54], suggesting that this region, before considered as a redundant promoter, can have instead a pivotal regulatory function for *Scn1a* gene. Colasante and colleagues [42] performed a complete characterization of the effect of CRISPRa in primary neurons *in vitro* before moving to test its effect *in vivo*, showing that the selected sgRNA was able to upregulate specifically *Scn1a* gene without any relevant effect on predicted off-target genes. The *Scn1a*-dCas9A treatment can increase $Na_v1.1$ protein level in Dravet primary neurons, and it is sufficient to induce a recovery of Dravet GAD67 + GABAergic interneuron firing rates [42]. Both studies also provide a proof of principle of their efficacy *in vivo*. The first study proposes an

approach based on the intracerebroventricular delivery in perinatal Dravet mice pups of *Scn1a*-dCas9A tool by a dual AAV system (as also activatory dCas9 is a large protein) [42]. Yamagata and colleagues [43] crossed Dravet mice with dCas9VPR mice, while sgRNAs were delivered by systemic injection of PhPeB.AAV [55] in juvenile mice at 4 weeks of age. Interestingly, taking into account that $Na_v1.1$ is expressed also in pyramidal neurons where its overexpression may be detrimental [47], both strategies restricted *Scn1a* gene upregulation to GABAergic inhibitory interneurons either by the choice of mDlx5/6 enhancer [56] to drive the dCas9 expression cassette [42] or by using a further genetic crossing to express dCas9VPR only in vesicular GABA aminoacid transporter neurons [43]. In both studies, *Scn1a*-dCas9A treatment of *Scn1a*$^{+/-}$ mice could ameliorate febrile seizures, increasing the temperature threshold for seizure induction [42, 43]. Yamagata and colleagues [43] expanded their *in vivo* analysis, showing a modest effect on non-epileptic alterations. Ultimately, both studies, each with their specific limitations – delivery in pups or poor phenotypic amelioration – do not answer the open question of symptomatic reversibility in DS. In fact, in one study *Scn1a*-dCas9A is conceived as a preventive treatment (perinatally in pups), while in the other it is delivered in 4-week-old mice, but poor effect on phenotypic manifestations was observed. Therefore, they leave still open the possibility that increasing *Scn1a* gene is not efficacious in treating the pathology in the chronic phase of the disease [57], when normalization of interneuron activity occurs

[58] but seizures are still present. An evolution of dCas9-SunTag [40] has been recently exploited to set a treatment in transcallosal dysconnectivity caused by mutations in C11orf46 gene [59]. As described above, the main advantage of the dCas9-SunTag is its ability to recruit multiple copies of the protein of interest onto a single sgRNA-target sequence, providing a stronger effect in comparison to “1:1” systems (one transcriptional regulator for each dCas9 molecule). Disrupted interhemispheric communication due to defects in the corpus callosum is the cause of some NDDs manifesting with ID, autism spectrum disorder, and schizophrenia [60–62]. Point mutation genes encoding for signaling molecules encoding regulators of neurite outgrowth and axon guidance, such as the Roundabout guidance receptor 1 (ROBO1) and the L1 cell adhesion molecule (L1CAM), have already been described as the cause of callosal connectivity [63, 64]. Peter and colleagues [59] first reported that the haploinsufficiency of the small nuclear protein C11orf46/ADP ribosylation factor like GTPase 14 effector protein (ARL14EP), encoded in the chr. 11p13 Wilms tumor, aniridia, genitourinary abnormalities, and ID risk locus, causes callosal hypoplasia in patients. In rodents, C11orf46 is primarily expressed in postmitotic and post-migratory glutamatergic cortical neurons, and its silencing in mouse embryonic brain development impairs the projection formation in cortical neurons and transcallosal connectivity [59]. Interestingly, they identified C11orf46 as a key binding partner of the repressor complex SET domain bifurcated histone lysine methyltransferase 1 (SETDB1)/KMT1E (SETDB2/

KMT1F) MBD-containing-associated factor histone lysine 9 (K9) methyltransferase (KMT-RC). Accordingly, RNA-seq data showed that the expression of some genes relevant for axon guidance, like Semaphorin 6a (Sema6a), was increased upon C11orf46 knockdown, supporting the pivotal role of this protein in the repressor complex KMT-RC [59]. Given this, C11orf46's affinity to the KMT-RC complex was then exploited to alter neuronal gene expression via a chromatin-associated mechanism. The dCas9-SunTag protein scaffold system was chosen to load 10 copies of C11orf46 and recruit KMT-RC on Sema6a gene locus and repress its expression. The modular dCas9-SunTag has been previously shown to be able to recruit multiple DNMT3A catalytic domains to a target site for editing DNA methylation in a way that is more tunable, specific (strong decrease of off-target methylation), and more efficient in providing DNA methylation at target sites than the direct fusion of dCas9 to DNMT3A [65]. Strikingly, this dCas9-SunTag-C11orf46 targeting the Sema6a promoter, when expressed during mouse brain development, rescued impaired midline crossing of callosal projections and axonal arborization deficit normally encountered upon C11orf46 knockdown [59]. While this study has the value to pose the basis for recruiting any protein function in a specific locus and setting future chromatin-based therapies to correct developmental alterations in the brain's connectome, the direct advantages of using an epigenomic approach instead of a classic gene therapy based on the re-expression of C11orf46 is not clearly highlighted. In fact, gene

replacement of C11orf46 would have been able to restore the normal expression for all the C11orf46/KMT-RC direct target genes, although probably with less efficiency. More straightforward is the application of a dCas9- based epigenetic approach to treat the fragile X chromosome syndrome (FXS). FXS is an X-linked NDD and produces a complex disorder with a range of neurological and psychiatric problems, including in most cases autistic features with intellectual, cognitive, and social alterations [66–69]. The underlying cause is the loss of expression of the fragile X mental retardation protein (FMRP) encoded by the FMR1 gene during neurodevelopment [70–72]. FMR1 gene silencing is caused by hypermethylation of its promoter [73], due to a CGG trinucleotide repeat expansion mutation at the 5′ UTR of FMR1, which in healthy individuals is made approximately of 6–44 repeats, whereas FXS patients show more than 200 repeats [74, 75]. FMRP is an RNA-binding protein in neurons that controls protein synthesis at developing synapses and has a key role in the maintenance of synaptic plasticity [68, 76, 77]. Interestingly, when knock-in mice carrying different lengths of CGG repeat expansions (even >300) were generated, no increased methylation of the Fmr1 gene was found, and these mice displayed increased mRNA level but decreased Fmrp protein with a phenotype that is accordingly more similar to fragile X premutation carriers (with expansion The first attempts of epigenetic editing were done with non-specific demethylating agents [80–83], but these drugs are usually too toxic to be employed as a therapy in FXS patients, as they are

not specific at all and demethylation is a universal method of regulating gene expression. Recently, Dr. Rudolf Jaenisch lab demonstrated that the recruitment of dCas9-TET fusions to CGG repeats caused robust loss of methylation at the FMR1 promoter in human cells, associated with almost complete restoration of FMRP protein expression [84]. Demethylation of the CGG expansion increased histone H3 lysine 27 (H3K27) acetylation and H3K4 trimethylation, and decreased H3K9 trimethylation at the FMR1 promoter region, which finally induced FMR1 gene reactivation. RNA sequencing and whole-genome bisulfite sequencing (to measure DNA methylation changes) demonstrated that transcriptional and epigenetic effects were highly specific to the targeted FMR1 locus. Interestingly, FMR1 expression and demethylation of its promoter were maintained, at least for 2 weeks, in the presence of AcrIIA4, an inhibitor of Cas9/dCas9 [85]. Epigenetic editing was maintained also in iPSC-derived neurons in which the increased firing rate was rescued [84]. Also, neurons transplanted in mouse brains maintained FMR1 reactivation up to 3 months [84]. When the demethylation of the FMR1 promoter was performed directly in iPSC-derived neurons, the reactivation of the FMR1 gene was less robust than that seen in iPSCs [84], probably because DNA demethylation mechanisms are less efficient in postmitotic cells [86, 87]. Despite the lack of a murine model to directly test the dCas9- TET efficacy on demethylating FMR1 locus *in vivo*, this analysis on the stability of demethylation on transplanted neurons is promising for a long-term effect of the treatment.

Finally, in comparison to the classic CRISPR/Cas9- editing system that had been successfully exploited to eliminate or shorten the CGG repeats in hiPSCs carrying FXS expansion [88, 89], the epigenetic strategy has some advantages that will be highlighted in the next section. CRISPR/dCas9 Approaches: Advantages and Limitations The extensive usage of CRISPR/dCas9 tools attests their attractivity and their potential for the treatment of NDDs. Indeed, they present some indisputable advantages in comparison to previously available therapeutic strategies. First, in comparison to classic gene replacement, CRISPRa/dCas9 tools can boost gene expression, acting directly on endogenous genes, without any limitation of gene size. In addition, as they allow the expression of the complete mRNA of the target gene, its physiological splicing dynamics remain unaltered. Also, the 3′UTR of the target genes, which has a well-established role in the nuclear export, subcellular targeting, and rates of translation and degradation of mRNA [90, 91], is maintained. This aspect is particularly relevant when significant alterations of gene dosage may be detrimental, such as for Mecp2 gene [92, 93]. In comparison to nucleasic CRISPR/Cas9, the dCas9 has the advantage of being able to modulate gene expression by non-permanent changes in the genome, making them more suitable in a translational perspective. Moreover, the effect of eventual off-target genes is potentially less dangerous with respect to DSBs that might occur at Cas9 off-target sites. This is particularly meaningful in light of recent evidence indicating that AAVs – carrying, for example,

Cas9 or donors for HDR – can integrate with a relatively high frequency into Cas9-generated DSB sites [94–96]. On the other hand, nucleasic Cas9-based systems induce permanent modification in the genome, implying that its restricted expression in a short time window is sufficient to induce the desired editing. Conversely, CRISPRa/dCas9 tools rely on the continuous expression of dCas9 in the cells, increasing the risk of neuronal toxicity [43] and of the potential immunogenic response to the Cas9 bacterial protein [97]. Epigenetic changes induced by dCas9 seem to be maintained also in the presence of Cas9 inhibitor [84], suggesting that constitutive presence of dCas9 may not be required. However, most of the studies lack a long-term effect of CRISPR/dCas9 epigenetic hit and the real maintenance of the epigenetic mark should be tested in each single case. A major technical hurdle related to *in vivo* application of CRISPR/dCas9-based tools for the treatment of NDDs is the delivery in the CNS. In fact, packaging in AAVs Streptococcus pyogenes SpdCas9 with its extra fused protein functions together with the sgRNA cassette is a real challenge, and there is no room to introduce any additional regulatory elements, such as neuronal subtype-specific promoters. The identification of the shorter ortholog derived from Staphylococcus aureus (SaCas9, 1,053 amino acids) [98] has only partially solved the AAV cargo issue. For this reason, many *in vivo* applications are still based on dual AAV systems, in which each of the two AAVs carries some of the elements that need to be delivered [42] or carries a “split dCas9” system based on an intein protein that can mediate

dCas9 trans-splicing [99, 100]. In both cases, cell co-transduction with the two AAVs is needed to achieve the CRISPR/dCas9 therapeutic effect, a requirement that decreases the efficiency of the treatment. In conclusion, while numerous hurdles still exist for the delivery of CRISPR tools to the CNS, there are more and more preclinical studies for NDDs that offer the hope that transcriptional CRISPR/dCas9 modulation or epigenetic editing could be used in human diseases that affect brain function in the next future. In the process of development of those therapies, the acquisition of more knowledge regarding the basic biology of the pathologies would be of help. Understanding if a specific NDD can be reverted after symptom onset, defining the ideal therapeutic window, and identifying the minimal region of the brain or the minimal number of cells/neuronal subtype to be corrected to achieve a significant phenotypic amelioration would produce an acceleration of therapeutic translation of those approaches.

Disease	dCas9 effector domain	Delivery	Outcomes	Ref.
Dravet syndrome	VP160	Intracerebroventricular dual AAV9 injection	Endogenous *Scn1a* gene upregulation rescues excitability in *Scn1a*$^{+/-}$ mutant cortical interneurons *in vitro* and improves febrile seizures phenotype *in vivo* in *Scn1a*$^{+/-}$ mice	[42]
	VP64-p65-Rta (VPR)	Intravenous PhPeB AAV injection	Endogenous *Scn1a* gene upregulation ameliorates febrile seizures and improves behavioral impairments in floxed-dCas9-VPR$^{VPR/+}$/*Vgat*-Cre$^{Cre/+}$ /*Scn1a*$^{RX/+}$ triple mutant mice	[43]
Transcallosal dysconnectivity	SunTag-C11orf46	In utero electroporation	Repression of *Sema6a* gene expression rescues impaired midline crossing of callosal projections and axonal arborization deficit *in vivo*	[59]
Fragile X syndrome	TET1	Lentiviral transduction *in vitro*	Demethylation of CGG expansion in FMR1 promoter region restores *FMR1* expression in Fragile X syndrome patient derived iPSCs and induced neurons	[84]

Table 1. dCas9-based therapeutic approaches to treat NDDs

Conflict of Interest Statement

The authors have no conflicts of interest to declare.

Funding sources

This work was supported by the “Associazione Gruppo Famiglie Dravet” to G.C.; CARIPLO Foundation (2016-0532) and the Italian Ministry of Health (GR-2016-02363972) to G.C.; and Telethon GGP19249 to G.C.

References

1. Silbereis JC, Pochareddy S, Zhu Y, Li M, Sestan N. The cellular and molecular landscapes of the developing human central nervous system. Physiol Behav. 2017;176(1):139–48.
2. Yap EL, Greenberg ME. Activity-regulated transcription: bridging the gap between neural activity and behavior. Neuron. 2018; 100(2):330–48.
3. Gilissen C, Hehir-Kwa JY, Thung DT, Van De Vorst M, Van Bon BW, Willemsen MH, et al. Genome sequencing identifies major causes of severe intellectual disability. Nature. 2014; 511(7509):344–7.
4. Ismail FY, Shapiro BK. What are neurodevelopmental disorders?. Curr Opin Neurol. 2019;32(4):611–6.
5. Parenti I, Rabaneda LG, Schoen H, Novarino G. Neurodevelopmental disorders: from genetics to functional pathways. Trends Neurosci. 2020;43(8):608–21.
6. Turner TJ, Zourray C, Schorge S, Lignani G. Recent advances in gene therapy for neurodevelopmental disorders with epilepsy. J Neurochem. 2020(June):1–34.
7. Hu WF, Chahrour MH, Walsh CA. The diverse genetic landscape of neurodevelopmental disorders. Annu Rev Genomics Hum Genet. 2014;15:195–213.
8. Ashley EA. Towards precision medicine. Nat Rev Genet. 2016;17(9):507–22.

9. Meins M, Lehmann J, Gerresheim F, Herchenbach J, Hagedorn M, Hameister K, et al. Submicroscopic duplication in Xq28 causes increased expression of the MECP2 gene in a boy with severe mental retardation and features of Rett syndrome. J Med Genet. 2005; 42(2):e12–6.
10. Oostra BA, Willemsen R. A fragile balance: FMR1 expression levels. Hum Mol Genet. 2003;12 Spec No 2(REV. ISS. 2):R249–57.
11. Rinaldi C, Wood MJA. Antisense oligonucleotides: the next frontier for treatment of neurological disorders. Nat Rev Neurol. 2018; 14(1):9–21.
12. Setten RL, Rossi JJ, Han SP. The current state and future directions of RNAi-based therapeutics. Nat Rev Drug Discov. 2019;18(6): 421–46.
13. Knott GJ, Doudna JA. CRISPR-Cas guides the future of genetic engineering. Science. 361(6405):866–9.
14. Zhang F. Development of CRISPR-Cas systems for genome editing and beyond. Quart Rev Biophys. 2019;52.
15. Doudna JA. The promise and challenge of therapeutic genome editing. Nature. 2020; 578(7794):229–36.
16. Dai WJ, Zhu LY, Yan ZY, Xu Y, Wang QL, Lu XJ. CRISPR-Cas9 for in vivo gene therapy: promise and hurdles. Mol Ther Nucleic Acids. 2016;5:e349.
17. Wang D, Zhang F, Gao G. CRISPR-based therapeutic genome editing: strategies and in vivo delivery by AAV vectors. Cell. 2020; 181(1):136–50.

18. Christie KA, Robertson LJ, Conway C, Blighe K, DeDionisio LA, Chao-Shern C, et al. Mutation-independent allele-specific editing by CRISPR-Cas9, a novel approach to treat autosomal dominant disease. Mol Ther. 2020; 28(8):1846–57.
19. Gao X, Tao Y, Lamas V, Huang M, Yeh WH, Pan B, et al. Treatment of autosomal dominant hearing loss by in vivo delivery of genome editing agents. Nature. 2018;553(7687): 217–21.
20. Pawelczak KS, Gavande NS, VanderVereCarozza PS, Turchi JJ. Modulating DNA repair pathways to improve precision genome engineering. ACS Chem Biol. 2018;13(2): 389–96.
21. Lin S, Staahl BT, Alla RK, Doudna JA. Enhanced homology-directed human genome engineering by controlled timing of CRISPR/ Cas9 delivery. Elife. 2014;3:e04766.
22. Suzuki K, Tsunekawa Y, Hernandez-Benitez R, Wu J, Zhu J, Kim EJ, et al. In vivo genome editing via CRISPR/Cas9 mediated homology-independent targeted integration. Nature. 2016;540(7631):144–9.
23. Fu Y, Foden JA, Khayter C, Maeder ML, Reyon D, Joung JK, et al. High-frequency offtarget mutagenesis induced by CRISPR-Cas nucleases in human cells. Nat Biotechnol. 2013;31(9):822–6.
24. Pattanayak V, Lin S, Guilinger JP, Ma E, Doudna JA, Liu DR. High-throughput profiling of off-target DNA cleavage

reveals RNAprogrammed Cas9 nuclease specificity. Nat Biotechnol. 2013;31(9):839–43.

25. Qi LS, Larson MH, Gilbert LA, Doudna JA, Weissman JS, Arkin AP, et al. Repurposing CRISPR as an RNA-guided platform for sequence-specific control of gene expression. Cell. 2013;152(5):1173–83.
26. Thakore PI, D'Ippolito AM, Song L, Safi A, Shivakumar NK, Kabadi AM, et al. Highly specific epigenome editing by CRISPR-Cas9 repressors for silencing of distal regulatory elements. Nat Methods. 2015;12(12):1143–9.
27. Mali P, Esvelt KM, Church GM. Cas9 as a versatile tool for engineering biology. Nat Methods. 2013;10(10):957–63.
28. Perez-Pinera P, Kocak DD, Vockley CM, Adler AF, Kabadi AM, Polstein LR, et al. RNA-guided gene activation by CRISPRCas9-based transcription factors. Nat Methods. 2013;10(10):973–6.
29. Chavez A, Scheiman J, Vora S, Pruitt BW, Tuttle M, P R Iyer EE, et al. Highly efficient Cas9-mediated transcriptional programming. Nat Methods. 2015;12(4):326–8.
30. Konermann S, Brigham MD, Trevino AE, Joung J, Abudayyeh OO, Barcena C, et al. Genome-scale transcriptional activation by an engineered CRISPR-Cas9 complex. Nature. 2015;517(7536):583–8.
31. Amabile A, Migliara A, Capasso P, Biffi M, Cittaro D, Naldini L, et al. Inheritable silencing of endogenous genes

by Hit-and-Run targeted epigenetic editing. Cell. 2016;167(1): 219–e14.

32. McDonald JI, Celik H, Rois LE, Fishberger G, Fowler T, Rees R, et al. Reprogrammable CRISPR/Cas9-based system for inducing sitespecific DNA methylation. Biol Open. 2016; 5(6):866–74.
33. Vojta A, Dobrinić P, Tadić V, Bočkor L, Korać P, Julg B, et al. Repurposing the CRISPR-Cas9 system for targeted DNA methylation. Nucleic Acids Res. 2016;44(12):5615–28.
34. Xiong T, Meister GE, Workman RE, Kato NC, Spellberg MJ, Turker F, et al. Targeted DNA methylation in human cells using engineered dCas9-methyltransferases. Sci Rep. 2017;7(1): 6732–14.
35. Liu XS, Wu H, Ji X, Stelzer Y, Wu X, Czauderna S, et al. Editing DNA methylation in the mammalian genome. Cell. 2016;167(1):233– e17.
36. Morita S, Noguchi H, Horii T, Nakabayashi K, Kimura M, Okamura K, et al. Targeted DNA demethylation in vivo using dCas9- peptide repeat and scFv-TET1 catalytic domain fusions. Nat Biotechnol. 2016;34(10): 1060–5.
37. Xu X, Tao Y, Gao X, Zhang L, Li X, Zou W, et al. A CRISPR-based approach for targeted DNA demethylation. Cell Discov. 2016;2: 16009.
38. Shi Y, Lan F, Matson C, Mulligan P, Whetstine JR, Cole PA, et al. Histone demethylation mediated by the nuclear amine oxidase homolog LSD1. Cell. 2004;119(7):941–53.

39. Hilton IB, D'Ippolito AM, Vockley CM, Thakore PI, Crawford GE, Reddy TE, et al. Epigenome editing by a CRISPR-Cas9-based acetyltransferase activates genes from promoters and enhancers. Nat Biotechnol. 2015; 33(5):510–7.
40. Tanenbaum ME, Gilbert LA, Qi LS, Weissman JS, Vale RD. A protein-tagging system for signal amplification in gene expression and fluorescence imaging. Cell. 2014;159(3): 635–46.
41. Anzalone AV, Randolph PB, Davis JR, Sousa AA, Koblan LW, Levy JM, et al. Search-andreplace genome editing without doublestrand breaks or donor DNA. Nature. 2019; 576(7785):149–57.
42. Colasante G, Lignani G, Brusco S, Di Berardino C, Carpenter J, Giannelli S, et al. dCas9- based *Scn1a* gene activation restores inhibitory interneuron excitability and attenuates seizures in Dravet syndrome mice. Mol Ther. 2020;28(1):235–53.
43. Yamagata T, Raveau M, Kobayashi K, Miyamoto H, Tatsukawa T, Ogiwara I, et al. CRISPR/ dCas9-based *Scn1a* gene activation in inhibitory neurons ameliorates epileptic and behavioral phenotypes of Dravet syndrome model mice. Neurobiol Dis. 2020;141(May):104954.
44. Catterall WA, Kalume F, Oakley JC. Nav1.1 channels and epilepsy. J Physiol. 2010; 588(11):1849–59.
45. Marini C, Scheffer IE, Nabbout R, Mei D, Cox K, Dibbens LM, et al. *SCN1A* duplications and deletions detected in

Dravet syndrome: implications for molecular diagnosis. Epilepsia. 2009;50(7):1670–8.

46. Cetica V, Chiari S, Mei D, Parrini E, Grisotto L, Marini C, et al. Clinical and genetic factors predicting Dravet syndrome in infants with *SCN1A* mutations. Neurology. 2017;88(11): 1037–44.
47. Ogiwara I, Iwasato T, Miyamoto H, Iwata R, Yamagata T, Mazaki E, et al. Nav1.1 haploinsufficiency in excitatory neurons ameliorates seizure-associated sudden death in a mouse model of dravet syndrome. Hum Mol Genet. 2013;22(23):4784–804.
48. Almog Y, Fadila S, Brusel M, Mavashov A, Anderson K, Rubinstein M. Developmental alterations in firing properties of hippocampal CA1 inhibitory and excitatory neurons in a mouse model of Dravet syndrome. Neurobiol Dis. 2021;148:105209.
49. Yu FH, Mantegazza M, Westenbroek RE, Robbins CA, Kalume F, Burton KA, et al. Reduced sodium current in GABAergic interneurons in a mouse model of severe myoclonic epilepsy in infancy. Nat Neurosci. 2006; 9(9):1142–9.
50. Griffin A, Hamling KR, Hong S, Anvar M, Lee LP, Baraban SC. Preclinical animal models for Dravet syndrome: seizure phenotypes, comorbidities and drug screening. Front Pharmacol. 2018;9(Jun):573.
51. Ricobaraza A, Mora-Jimenez L, Puerta E, Sanchez-Carpintero R, Mingorance A, Artieda J, et al. Epilepsy and

neuropsychiatric comorbidities in mice carrying a recurrent Dravet syndrome *SCN1A* missense mutation. Sci Rep. 2019;9(1):14172–15.

52. Hsiao J, Yuan TY, Tsai MS, Lu CY, Lin YC, Lee ML, et al. Upregulation of haploinsufficient gene expression in the brain by targeting a long non-coding RNA improves seizure phenotype in a model of Dravet syndrome. EBioMedicine. 2016;9:257–77.
53. Han Z, Chen C, Christiansen A, Ji S, Lin Q, Anumonwo C, et al. Antisense oligonucleotides increase *Scn1a* expression and reduce seizures and SUDEP incidence in a mouse model of Dravet syndrome. Sci Transl Med. 2020;12(558):eaaz6100.
54. Haigh JL, Adhikari A, Copping NA, Stradleigh T, Wade AA, Catta Preta R et al. Deletion of a non-canonical regulatory sequence causes loss of *Scn1a* expression and epileptic phenotypes in mice. bioRxiv. 2021.
55. Chan KY, Jang MJ, Yoo BB, Greenbaum A, Ravi N, Wu WL, et al. Engineered AAVs for efficient noninvasive gene delivery to the central and peripheral nervous systems. Nat Neurosci. 2017;20(8):1172–9.
56. Dimidschstein J, Chen Q, Tremblay R, Rogers SL, Saldi GA, Guo L, et al. A viral strategy for targeting and manipulating interneurons across vertebrate species. Nat Neurosci. 2016; 19(12):1743–9.

57. Goldberg EM. Gene therapy in models of severe epilepsy due to sodium channelopathy. Epilepsy Curr. 2020;20(4):214–7.
58. Favero M, Sotuyo NP, Lopez E, Kearney JA, Goldberg EM. A transient developmental window of fast-spiking interneuron dysfunction in a mouse model of dravet syndrome. J Neurosci. 2018;38(36):7912–27.
59. Peter CJ, Saito A, Hasegawa Y, Tanaka Y, Nagpal M, Perez G, et al. In vivo epigenetic editing of Sema6a promoter reverses transcallosal dysconnectivity caused by C11orf46/Arl14ep risk gene. Nat Commun. 2019;10(1):4112.
60. Peiker I, David N, Schneider TR, Nolte G, Schöttle D, Engel AK. Perceptual integration deficits in autism spectrum disorders are associated with reduced interhemispheric gamma-band coherence. J Neurosci. 2015;35(50): 16352–61.
61. Ribolsi M, Daskalakis ZJ, Siracusano A, Koch G. Abnormal asymmetry of brain connectivity in schizophrenia. Front Hum Neurosci. 2014;8(Dec):1010–1.
62. Margari L, Palumbi R, Campa MG, Operto FF, Buttiglione M, Craig F, et al. Clinical manifestations in children and adolescents with corpus callosum abnormalities. J Neurol. 2016;263(10):1939–45.
63. Calloni SF, Cohen JS, Meoded A, Juusola J, Triulzi FM, Huisman TAGM, et al. Compound heterozygous variants

in ROBO1 cause a neurodevelopmental disorder with absence of transverse pontine fibers and thinning of the anterior commissure and corpus callosum. Pediatr Neurol. 2017;70:70–4.

64. Shieh C, Moser F, Graham JM, Watiker V, Pierson TM. Mutation in the sixth immunoglobulin domain of L1CAM is associated with migrational brain anomalies. Neurol Genet. 2015;1(4):e34–6.
65. Pflueger C, Tan D, Swain T, Nguyen T, Pflueger J, Nefzger C, et al. A modular dCas9- SunTag DNMT3A epigenome editing system overcomes pervasive off-target activity of direct fusion dCas9-DNMT3A constructs. Genome Res. 2018;28(8):1193–206.
66. Pugin A, Faundes V, Santa María L, Curotto B, Aliaga S, Salas I, et al. Aspectos clínicos, moleculares y farmacológicos en los trastornos asociados a gen 1 del retraso mental del X frágil. Neurología. 2017;32(4):241–52.
67. Santoro MR, Bray SM, Warren ST. Molecular mechanisms of fragile X syndrome: a twentyyear perspective. Annu Rev Pathol. 2012;7: 219–45.
68. Sidorov MS, Auerbach BD, Bear MF. Fragile X mental retardation protein and synaptic plasticity. Mol Brain. 2013;6(1):15–1.
69. Contractor A, Klyachko VA, Portera-Cailliau C. Altered neuronal and circuit excitability in Fragile X syndrome. Neuron. 2015;87(4): 699–715.

70. Crawford DC, Acuña JM, Sherman SL, Med G. FMR1 and the Fragile X syndrome: human genome epidemiology review HHS public access author manuscript. Genet Med. 2001; 3(5):359–71. Available from: https://europepmc.org/backend/ptpmcrender.fcgi?accid=PMC4493892&blobtype=pdf.
71. O'Donnell WT, Warren ST. A decade of molecular studies of fragile X syndrome. Annu Rev Neurosci. 2002;25:315–38.
72. Penagarikano O, Mulle JG, Warren ST. The pathophysiology of fragile X syndrome. Annu Rev Genomics Hum Genet. 2007;8:109–29.
73. Kumari D, Gazy I, Usdin K. Pharmacological reactivation of the silenced FMR1 gene as a targeted therapeutic approach for fragile X syndrome. Brain Sci. 2019;9(2):39.
74. Fu YH, Kuhl DP, Pizzuti A, Pieretti M, Sutcliffe JS, Richards S, et al. Variation of the CGG repeat at the fragile X site results in genetic instability: resolution of the Sherman paradox. Cell. 1991;67(6):1047–58.
75. Verkerk AJ, Pieretti M, Sutcliffe JS, Fu YH, Kuhl DP, Pizzuti A, et al. Identification of a gene (FMR-1) containing a CGG repeat coincident with a breakpoint cluster region exhibiting length variation in fragile X syndrome. Cell. 1991;65(5):905–14.
76. Darnell JC, Van Driesche SJ, Zhang C, Hung KY, Mele A, Fraser CE, et al. FMRP stalls ribosomal translocation on

mRNAs linked to synaptic function and autism. Cell. 2011; 146(2):247–61.

77. Smith LN, Jedynak JP, Fontenot MR, Hale CF, Dietz KC, Taniguchi M, et al. Fragile X mental retardation protein regulates synaptic and behavioral plasticity to repeated cocaine administration. Neuron. 2014;82(3):645–58.
78. Berman RF, Buijsen RA, Usdin K, Pintado E, Kooy F, Pretto D, et al. Mouse models of the fragile X premutation and fragile X-associated tremor/ataxia syndrome. J Neurodev Disord. 2014;6(1):25–16.
79. Irwin SA, Galvez R, Greenough WT. Dendritic spine structural anomalies in fragile-X mental retardation syndrome. Cereb Cortex. 2000;10(10):1038–44.
80. Coffee B, Zhang F, Ceman S, Warren ST, Reines D. Histone modifications depict an aberrantly heterochromatinized FMR1 gene in fragile x syndrome. Am J Hum Genet. 2002; 71(4):923–32.
81. Chiurazzi P, Pomponi MG, Willemsen R, Oostra BA, Neri G. In vitro reactivation of the FMR1 gene involved in fragile X syndrome. Hum Mol Genet. 1998;7(1):109–13.
82. Coffee B, Zhang F, Warren ST, Reines D. Acetylated histones are associated with FMR1 in normal but not fragile X-syndrome cells. Nature Genet. 1999;22:98–101. Erratum in: Nat Genet. 1999;22(2):209.
83. Biacsi R, Kumari D, Usdin K. SIRT1 inhibition alleviates gene silencing in Fragile X mental retardation syndrome. PLoS Genet. 2008;4(3):e1000017–9.

84. Liu XS, Wu H, Krzisch M, Wu X, Graef J, Muffat J, et al. Rescue of Fragile X syndrome neurons by DNA methylation editing of the FMR1 gene. Cell. 2018;172(5):979–92.
85. Rauch BJ, Silvis MR, Hultquist JF, Waters CS, McGregor MJ, Krogan NJ, et al. Inhibition of CRISPR-Cas9 with Bacteriophage Proteins. Cell. 2017;168(1–2):150–e10.
86. Wu SC, Zhang Y. Active DNA demethylation: many roads lead to Rome. Nat Rev Mol Cell Biol. 2010;11(9):607–20.
87. Wu H, Zhang Y. Reversing DNA methylation: mechanisms, genomics, and biological functions. Cell. 2014;156(1–2):45–68.
88. Park CY, Halevy T, Lee DR, Sung JJ, Lee JS, Yanuka O, et al. Reversion of FMR1 methylation and silencing by editing the triplet repeats in Fragile X iPSC-derived neurons. Cell Rep. 2015;13(2):234–41.
89. Xie N, Gong H, Suhl JA, Chopra P, Wang T, Warren ST. Reactivation of FMR1 by CRISPR/Cas9-mediated deletion of the expanded CGG-repeat of the fragile X chromosome. PLoS One. 2016;11(10):e0165499–12.
90. Conne B, Stutz A, Vassalli JD. The 3' untranslated region of messenger RNA: a molecular "hotspot" for pathology?. Nat Med. 2000;6(6): 637–41.
91. Parker R, Sheth U. P bodies and the control of mRNA translation and degradation. Mol Cell. 2007;25(5):635–46.

92. Ramocki MB, Tavyev YJ, Peters SU. The MECP2 duplication syndrome. Am J Med Genet A. 2010;152A(5):1079–88.
93. Luoni M, Giannelli S, Indrigo M, Niro A, Massimino L, Iannielli A, et al. Whole brain delivery of an instability-prone Mecp2 transgene improves behavioral and molecular pathological defects in mouse models of Rett syndrome. eLife. 2020;9:e52629.
94. Hanlon KS, Kleinstiver BP, Garcia SP, Zaborowski MP, Volak A, Spirig SE, et al. High levels of AAV vector integration into CRISPR-induced DNA breaks. Nat Commun. 2019;10(1):4439–11.
95. Nelson CE, Wu Y, Gemberling MP, Oliver ML, Waller MA, Bohning JD, et al. Long-term evaluation of AAV-CRISPR genome editing for Duchenne muscular dystrophy. Nat Med. 2019;25(3):427–32.
96. Wolter JM, Mao H, Fragola G, Simon JM, Krantz JL, Bazick HO, et al. Cas9 gene therapy for Angelman syndrome traps Ube3a-ATS long non-coding RNA. Nature. 2020; 587(7833):281–4.
97. Wang D, Mou H, Li S, Li Y, Hough S, Tran K, et al. Adenovirus-mediated somatic genome editing of Pten by CRISPR/Cas9 in mouse liver in spite of Cas9-specific immune responses. Hum Gene Ther. 2015;26(7):432–42.
98. Ran FA, Cong L, Yan WX, Scott DA, Gootenberg JS, Kriz AJ, et al. In vivo genome editing using Staphylococcus aureus Cas9. Nature. 2015;520(7546):186–91.

99. Fine EJ, Appleton CM, White DE, Brown MT, Deshmukh H, Kemp ML, et al. Transspliced Cas9 allows cleavage of HBB and CCR5 genes in human cells using compact expression cassettes. Sci Rep. 2015;5(May): 10777–9.
100. Chew WL, Tabebordbar M, Cheng JK, Mali P, Wu EY, Ng AH, et al. A multifunctional AAV-CRISPR-Cas9 and its host response. Nat Methods. 2016;13(10):868–74.

CHAPTER 5
SUMMARY, CONCLUSIONS AND FUTURE PERSPECTIVES

Dravet syndrome (DS) is a catastrophic developmental and epileptic encephalopathy characterized by severe, pharmaco-resistant seizures and the highest risk of Sudden Unexpected Death in Epilepsy (SUDEP) of all epilepsy syndromes. To date, no cure is effective in controlling seizures. About 80% of the patients present heterozygous loss-of-function mutations in the *SCN1A* gene, indicating that a haploinsufficient mechanism underlies the onset of the pathology (Catterall, Kalume, and Oakley 2010; Escayg and Goldin 2010). This gene encodes for the voltage-gated sodium channel alpha-subunit $Na_v1.1$, essential to initiate action potentials (APs) in GABAergic interneurons (GINs) (Ogiwara et al. 2007). The analysis of different animal models pointed out that seizure development is due to a reduction of excitability of GINs, particularly of parvalbumin (PV), somatostatin (SST), and vasoactive intestinal peptide (VIP) subtypes (Yu et al. 2006; Ogiwara et al. 2007; Tai et al. 2014; Goff and Goldberg 2019), ultimately resulting in an over-excitation of neuronal network. However, other works also reported hyperexcitability in excitatory neurons (ExNs) during all stages of the pathology or only in the pre-epileptic stage, suggesting the involvement of this neuronal subtype in Dravet pathogenesis (Mistry et al. 2014; Almog et al. 2021).

Heterozygous loss-of-function mutations result from quantitative reduction of gene expression to 50% of normal levels. For this reason, we decided to employ a new strategy based on the activatory CRISPR-dCas9 to specifically raise the $Na_v1.1$ protein levels by stimulating the transcription of the *Scn1a* gene in a DS mouse model (Colasante et al. 2019) (Chapter 3). We identified a specific sgRNA, sg1p, which aligns in the proximal promoter of this gene, that together with dCas9 fused to VP160 transcriptional activator, increases *Scn1a* gene expression levels in cell lines and WT primary neurons. Also, we demonstrated that the activatory dCas9 system was able to induce upregulation of $Na_v1.1$ protein in DS primary neuronal culture, leading them to express comparable $Na_v1.1$ levels to WT neurons. Then, we performed functional characterization of DS dCas9-treated GINs revealing a rescue in their ability to fire APs. Furthermore, by packaging Scn1a-dCas9 system into an AAV vector, we showed the therapeutical relevance of this tool by injecting DS pups, reporting a rescue of adult PV+ interneurons functionality, together with attenuation of febrile seizures.

Considering these promising data, we aimed to move this approach closer to translation and to test the efficacy of the activatory CRISPR-dCas9 system in a human setting. For this reason, firstly, we worked to establish a proper DS human model. We optimized a neuronal differentiation protocol already published (Meganathan et al. 2017), which allows to generate human neuronal cultures enriched in GINs from iPSCs, to make it more reproducible in our hands. Then, we generated induced

pluripotent stem cells (iPSCs) from fibroblasts of two DS patients carrying different point mutations on *SCN1A* gene. We used the CRISPR-Cas9 gene editing tool to isolate isogenic clones, to avoid the necessity to use different control cell lines, introducing variability associated to the genetic background.

By generating GINs from our iPSC lines, we only highlihted a trend of hypoexcitable state in DS neurons compared to controls, derived from the analysis of the mean of maximal APs. While, by generating cortical excitatory neurons (ExNs), only patient 1 neurons displayed an hyperexcitable phenotype compared to its control, while no alteration was detected from functional analysis of ExNs derived from patient 2.

Then, considering that $Na_v1.1$ is normally expressed in a post-natal stage during development (Trimmer and Rhodes 2004; Wang et al. 2011; Cheah et al. 2013), we assumed that the mild phenotype we revealed could derive from an inappropriate maturation state of our neurons. Indeed, even if we reported sufficient levels of *SCN1A* mRNA, we could never reveal a $Na_v1.1$ band by western blot. Trying to ameliorate this condition, we explored the possibility to test two different states of neuronal maturation. First, we introduced in our differentiation protocol the usage of a specific medium (BrainPhys medium) which can help neuronal activity, also inducing maturation. Second, we set the basis to explore the functionality of transplanted GINs into mouse brain. Several works reported that human neurons when transplanted into mouse brain could join to mouse circuits,

showing to receive from mouse neurons and generate excitatory and inhibitory currents (Zhang et al. 2013; Cunningham et al. 2014; Qi et al. 2017; Meganathan et al. 2017), also displaying an advanced state of spine maturation, compared to neurons growth *in vitro* in 2D condition, that is an index of improved maturation (Linaro et al. 2019). For this reason, to verify if transplanted neurons could display an amelioration in the maturation state, taking advantage from the mouse brain environment with all its stimuli, we performed the first experiments of transplantation of our vNPCs, transduced with LV GABAergic reporter, in immunodeficient mouse brains. Both strategies lead to interesting data. By introducing BrainPhys medium in our protocol to generate GINs we could reveal in patient 1 derived neurons a significant decrease in the mean of maximal APs, denoting a hypoexcitability state. By injecting vNPCs in the hippocampus of P30 immunodeficient mice, we could see that, after 5 months from the injection, time required to verify neuronal migration and integration in mouse cortex (Cunningham et al. 2014), human cells didn't lose their neuronal fate maintaining NEUN expression, differentiated into GINs also *in vivo*, and a part of them, ~25%, migrated towards mouse cortex. Further experiments will focus on the functional analysis of these migrated cells, to verify if this condition could help us in selecting a group of neurons which could display an advanced state of maturation compared to neurons growth *in vitro*.

Concurrently, to explore the potential role of the activatory CRISPR-dCas9 system in a human context, we started

performing an sgRNAs screening, targeting three different regions upstream *SCN1A* gene (A, B and C) very close to the the TSS, in SH-SY5Y cell line. We identified specific sgRNAs targeting region A and B able to boost *SCN1A* gene expression. Interestingly, we confirmed their efficiency also in human neurons, obtaining important functional results. Indeed, by patch clamp, we revealed a significant increase in the amount of Na^+ currents in dCas9-treated neurons compared to controls. These experiments constitute the proof of principle indicating that this approach can also be employed in DS patients carrying loss-of-function mutations on *SCN1A* gene. Considering that neurodegeneration was never reported in DS patients (Catarino et al. 2011), dysfunctional interneurons can potentially recover their activity whenever the right amount of wild-type $Na_v1.1$ channel will be available. Some DS pathological defects could be reverted.

However, to demonstrate the true efficiency of this tool, some improvements must be done in the setting of the human model. For this reason, we will perform some experiments to verify if the amelioration in the maturation state of our neuronal cultures due to the strategies mentioned before could be appropriated. We will characterize the functional properties of transplanted neurons and in all the *in vitro* experiments we will analyze $Na_v1.1$ protein levels as marker of maturatio, to verify if treatment with BrainPhys medium could enhance maturation and $Na_v1.1$ protein synthesis. At the same time, we will continue to perform functional assays in order to increase the number of cells studied,

trying to establish all the alterations carried by patients' derived neurons compared to their controls. In this setting, activatory CRISPR-dCas9 will be introduced to verify its real role as potential cure in reverting DS phenotype. These experiments could also introduce different therapeutical approaches working in a similar way, upregulating *SCN1A* wild type allele of patients to ameliorate their conditions. Also, a proper DS human model could be used to test all therapeutical strategies that reported interesting results *in vivo* in mouse models.

References

Almog, Yael, Saja Fadila, Marina Brusel, Anat Mavashov, Karen Anderson, and Moran Rubinstein. 2021. "Developmental Alterations in Firing Properties of Hippocampal CA1 Inhibitory and Excitatory Neurons in a Mouse Model of Dravet Syndrome." *Neurobiology of Disease* 148: 105209. https://doi.org/10.1016/j.nbd.2020.105209.

Catarino, Claudia B., Joan Y.W. Liu, Ioannis Liagkouras, Vaneesha S. Gibbons, Robyn W. Labrum, Rachael Ellis, Cathy Woodward, et al. 2011. "Dravet Syndrome as Epileptic Encephalopathy: Evidence from Long-Term Course and Neuropathology." *Brain* 134 (10): 2982–3010. https://doi.org/10.1093/brain/awr129.

Catterall, William A., Franck Kalume, and John C. Oakley. 2010. "NaV1.1 Channels and Epilepsy." *Journal of Physiology* 588

(11): 1849–59. https://doi.org/10.1113/jphysiol.2010.187484.

Cheah, Christine S., Ruth E. Westenbroek, William H. Roden, Franck Kalume, John C. Oakley, Laura A. Jansen, and William A. Catterall. 2013. “Correlations in Timing of Sodium Channel Expression, Epilepsy, and Sudden Death in Dravet Syndrome.” *Channels* 7 (6): 468–72. https://doi.org/10.4161/chan.26023.

Colasante, Gaia, Gabriele Lignani, Simone Brusco, Claudia Di Berardino, Jenna Carpenter, Serena Giannelli, Nicholas Valassina, et al. 2019. “DCas9-Based Scn1a Gene Activation Restores Inhibitory Interneuron Excitability and Attenuates Seizures in Dravet Syndrome Mice.” *Molecular Therapy* 28 (1): 235–53. https://doi.org/10.1016/j.ymthe.2019.08.018.

Cunningham, Miles, Jun-Hyeongf Chod, Amanda Leunga, George Savvidisa, Sandra Ahna, Minho Moona, Paula KJ Leea, et al. 2014. “Human PSC-Derived Maturing GABAergic Interneurons Ameliorate Seizures and Abnormal Behavior in Epileptic Mice.” *Cell Stem Cell* 15 (5): 559–73. https://doi.org/10.1016/j.stem.2014.10.006.

Escayg, Andrew, and Alan L Goldin. 2010. “Sodium Channel SCN1A and Epilepsy: Mutations and Mechanisms.” *Epilepsia* 51 (9): 16. https://doi.org/10.1111/j.1528-1167.2010.02640.x.Sodium.

Goff, Kevin M., and Ethan M. Goldberg. 2019. “Vasoactive Intestinal Peptide-Expressing Interneurons Are Impaired in a Mouse Model of Dravet Syndrome.” *ELife* 8: 1–28. https://doi.org/10.7554/eLife.46846.

Linaro, Daniele, Vermaercke, Ben, Iwata, Ryohei, Ramaswamy, Arjun, Libé-Philippot, Baptiste, Boubakar, Leila et al. 2019. Xenotransplanted Human Cortical Neurons Reveal Species-Specific Development and Functional Integration into Mouse Visual Circuits. Neuron 104 (5); 972-986

Meganathan, Kesavan, Emily M.A. Lewis, Paul Gontarz, Shaopeng Liu, Edouard G. Stanley, Andrew G. Elefanty, James E. Huettner, Bo Zhang, and Kristen L. Kroll. 2017. “Regulatory Networks Specifying Cortical Interneurons from Human Embryonic Stem Cells Reveal Roles for CHD2 in Interneuron Development.” *Proceedings of the National Academy of Sciences of the United States of America* 114 (52): E11180–89. https://doi.org/10.1073/pnas.1712365115.

Mistry, Akshitkumar M, Christopher H Thompson, Alison R Miller, Carlos G Vanoye1, Alfred L George Jr, and Jennifer A Kearney. 2014. “Strain- and Age-Dependent Hippocampal Neuron Sodium Currents Correlate with Epilepsy Severity in Dravet Syndrome Mice.” *Neurobiology of Disease* 65: 1–11. https://doi.org/10.1016/j.nbd.2014.01.006.

Ogiwara, Ikuo, Hiroyuki Miyamoto, Noriyuki Morita, Nafiseh Atapour, Emi Mazaki, Ikuyo Inoue, Tamaki Takeuchi, et al.

2007. “Nav1.1 Localizes to Axons of Parvalbumin-Positive Inhibitory Interneurons: A Circuit Basis for Epileptic Seizures in Mice Carrying an Scn1a Gene Mutation.” *Journal of Neuroscience* 27 (22): 5903–14. https://doi.org/10.1523/JNEUROSCI.5270-06.2007.

Qi, Yuchen, Xin-jun Zhang, Nicolas Renier, Zhuhao Wu, Talia Atkin, Ziyi Sun, Zeeshan Ozair, et al. 2017. “Accelerated Cortical Neuron Differentiation Protocol” 35 (2): 154–63. https://doi.org/10.1038/nbt.3777.Combined.

Tai, Chao, Yasuyuki Abe, Ruth E. Westenbroek, Todd Scheuer, and William A. Catterall. 2014. “Impaired Excitability of Somatostatin- and Parvalbumin-Expressing Cortical Interneurons in a Mouse Model of Dravet Syndrome.” *Proceedings of the National Academy of Sciences of the United States of America* 111 (30): 3139–48. https://doi.org/10.1073/pnas.1411131111.

Trimmer, James S., and Kenneth J. Rhodes. 2004. “Localization of Voltage-Gated Ion Channels in Mammalian Brain.” *Annual Review of Physiology* 66 (1): 477–519. https://doi.org/10.1146/annurev.physiol.66.032102.113328.

Wang, Wenze, Sachio Takashima, Yoshie Segawa, Masayuki Itoh, Xiuyu Shi, Su Kyeong Hwang, Kazuki Nabeshima, Morishige Takeshita, and Shinichi Hirose. 2011. “The Developmental Changes of Nav1.1 and Nav1.2 Expression in the Human Hippocampus and Temporal Lobe.” *Brain Research* 1389: 61–70.

https://doi.org/10.1016/j.brainres.2011.02.083.

Yu, Frank H., Massimo Mantegazza, Ruth E. Westenbroek, Carol A. Robbins, Franck Kalume, Kimberly A. Burton, William J. Spain, G. Stanley McKnight, Todd Scheuer, and William A. Catterall. 2006. “Reduced Sodium Current in GABAergic Interneurons in a Mouse Model of Severe Myoclonic Epilepsy in Infancy.” *Nature Neuroscience* 9 (9): 1142–49. https://doi.org/10.1038/nn1754.

Zhang, Yingsha, Changhui Pak, Yan Han, Henrik Ahlenius, Zhenjie Zhang, Soham Chanda, Samuele Marro, et al. 2013. “Rapid Single-Step Induction of Functional Neurons from Human Pluripotent Stem Cells” 78 (5): 785–98. https://doi.org/10.1016/j.neuron.2013.05.029.